UNIVERSITY OF SOUTHAMPTON

FACULTY OF ENGINEERING, SCIENCE & MATHEMATICS

School of Engineering Sciences

Structural Health Monitoring of Sandwich Beam and Application of Grid Technologies

by

Manoj Kumar

Thesis for the degree of Doctor of Philosophy

November, 2007

UNIVERSITY OF SOUTHAMPTON

ABSTRACT

FACULTY OF ENGINEERING, SCIENCE & MATHEMATICS
SCHOOL OF ENGINEERING SCIENCES

Doctor of Philosophy

STRUCTURAL HEALTH MONITORING OF SANDWICH BEAM AND APPLICATION OF GRID TECHNOLOGIES

by

Manoj Kumar

A damage occurs in a structure as a result of any adverse change in its mechanical and geometrical properties. If not identified at its early stage of propagation, it may cause catastrophic failure, which could be followed by significant economical, human and environmental losses. Therefore, a system which can timely identify damages in a structure must be developed to avoid these losses. The development of such a system requires a multi-disciplinary approach, which is investigated in this thesis.

In this work, the development and implementation approach, for a real-time structural health monitoring and control system, is presented. The process for development of this system is undertaken in three stages. In the first stage, a damage identification method, based on the changes in modal strain energies is developed and extensively examined, for various damage cases, by using numerical simulations. The sensitivity of this method is investigated for various parameters, such as the location, level and extent of the damage in a sandwich beam. In the second stage, this developed method is validated, with the experimental measurements obtained from the sandwich beam specimens, which have single and multiple damages. In the final stage, a system architecture is designed for transmission, pre-processing and analysis of the free vibration responses, recorded from the sandwich beam specimen. These responses are used for damage identification and to assess the criticality of damage by using the control method, which may also be used in the control system.

The results presented in this work indicate that the proposed methodology can be used for damage identification and to assess the criticality of damage in a sandwich beam. Guidelines and recommendations drawn from this research can be used for design and development of the system architecture for a real-time structural health monitoring and control system, by using toolkits based on the grid technologies.

Contents

List of Figures

List of Tables

Acknowledgements

There are many people I would like to acknowledge for their valuable help and support with my research. I would like to thank Prof. R. A. Shenoi and Prof. S. J. Cox for their supervision, guidance, encouragement, support and patience in the completion of this thesis. I would like to thank Dr. J. M. Dulieu-Barton and Dr. K. Djidjeli for their valuable suggestions during the M.Phil./Ph.D. transfer viva.

Next, I would like to thank everyone who provided technical support for this work. Thanks to Prof. A. J. Keane for his permission to use the resources of Computational Engineering and Design Centre and co-operation of Dr. N. W. Bressloff and Mr. Tony Scurr in solving numerous computer problems. My thanks go to Eric, Melin and Tariq for helping me in fabrication of sandwich beam specimens in the Transportation laboratory. I am grateful to Dr. G. Aglietti for his permission to use the experimental equipments and help from Christoph with testings in the Astronautics laboratory. Help and suggestions provided by Graeme, Jasmine, Jiao, Trevor from e-Science Centre proved invaluable for application of grid technologies in this work. In particular, the financial support provided by the School of Engineering Sciences, University of Southampton, is highly appreciated.

Special thanks to Prof. M. Mukhopadhyay of Indian Institute of Technology Kharagpur (India) for his constant motivation and encouragement for this research work.

The work carried out in this thesis has only been possible due to the great help and support from my friends and housemates: Sankalp Modi, Abheejeet, Rupa, Jadu, Puja, Berni, Kishore, Mandar, Matt, Alfred, Prasanth Nair, Ajay and many more.

Finally, and most importantly, I thank my grand parents and parents for encouraging me to value education and attend higher studies. I want to thank my wife Madhumita for her constant support and encouragement.

Chapter 1

Introduction

All structural systems are damaged at some phase of their operational life. These systems are expected to operate safely within this period; hence they require regular maintenance and repair for any existing damages. A maintenance schedule is usually planned at a fixed time interval, which involves necessary repairing of their structural components after assessment of their damage. Increasing use of light weight materials, i.e. composite and sandwich materials in structural systems require, a damage assessment technique, sensitive enough for low amount of damages. In sandwich structures, the anisotropy of the constituent materials and their layered construction with a soft core poses a challenging task for the damage assessment, which is further complicated by its damage mechanisms, i.e. damage generally propagates internally without showing any visible sign leading to catastrophic failure. Since, a sandwich structure is made of more than one type of materials, more than one modes of damage occur. As a result of the damage mechanism and the structural configuration, more than one types of damage occur simultaneously in sandwich structures. The complete process of damage assessment and subsequent maintenance scheduling for a structure can be termed as life-cycle management [Hall, 1999].

Over the last few decades, the problem of damage assessment in structural systems has been a subject of numerous research. Traditional non-destructive evaluation (NDE) techniques, such as visual inspection, coin-tap testing, ultrasonic testing, laser shearography, eddy current, etc., can detect small-scale flaws over a small area, but usually require the structure under inspection to be taken out of service for a certain time and to be placed under controlled environment. These techniques can be very expensive and time consuming, especially if the structural components are at inaccessible locations. These techniques are based on the propagation and reflection of waves

through the constituent structural material. It is well known that the velocity of a wave through a material largely depend on its properties. Also, the amount and intensity of reflected and transmitted waves are governed by the properties of material. If these waves pass through an isotropic materials, then it is easy to intrpret the results. However, if these waves are passed through more than one layer of different anisotropic materials then interpretation of results not only become difficult but also less reliable. Use of layered anisotropic materials and soft core in sandwich structures further complicates the interpretations of the results; hence making damage assessment by these techniques less reliabile. Therefore, NDE techniques could be unreliable for composite and sandwich structures compared to metallic structures. This has motivated further research in new damage assessment methods that can be applied to in-service composite and sandwich structures, reducing their maintenance cost, improving their life cycle management, safety and system performance. This requires the development of a damage assessment method that could preserve and possibly improve the current safety & reliability levels, concurrently reduce downtime & labour related costs; hence improving their life cycle management. Further, this process is complicated by the lack of development in a data management system specific to damage assessment of structures. In summary, the demands for an innovative life cycle management system is evident. However, the current level of maturity of this system is still evolving and several basic questions remain to be answered. Recent technological advances have renewed the interest in damage assessment research and the required data management system. Innovative sensing technologies, increased computational power, improvements in signal processing, better data management system and increased network bandwidth can all be combined together, to create a real-time structural health monitoring and control system, with a broad range of potential applications.

This work presents a methodology for the development and implementation of a real-time structural health monitoring and control system for a sandwich beam. To this end, the damage identification method for a sandwich beam and the potential applications of the Grid technologies, in a real-time Structural Health Monitoring (SHM) and control system are investigated. Novel features of this work can be outlined as follows,

- Formulation of a new two-stage damage identification method, by using vibration responses, for the multiple damage in a sandwich beam,

- At the first stage, formulation of the model-based damage identification method, by using modal strain energies, for the interactive damage modes in a sandwich beam,
- At the second stage, the damage quantification capabilities for a sandwich beam is improved by using model updating method based on non-linear optimisation technique,
- Innovative approach for the development of a real-time structural health monitoring and control system by using the grid technologies.

1.1 Objectives

The important objectives of this work are firstly to develop a damage identification method, and secondaly to provide guidelines towards the development of a real-time structural health monitoring and control system for a sandwich beam. This research work initiates with the development of damage identification method by using vibration responses of the sandwich beam. Salkind [Salkind, 1972] suggested that changes in stiffness might be an appropriate measure of damage. In case of a sandwich structure, the presence of damage directly reduces its stiffness modulus, i.e., Young and shear modulus of the faces and core respectively. Hence, vibration responses of the sandwich beam will be used to derive a damage parameter for predicting the presence, location and extent of damage. Further, feasibilities of applying grid technologies in the development of a real-time structural health monitoring and control system are investigated.

The following steps are a breakdown of the proposed work in order to achieve the novelties outlined in the previous section:

- To develop a model-based method for damage identification for a sandwich beam, by using their vibration responses.
- To study the effectiveness of the damage identification method for interacting damage modes in a sandwich beam.
- To investigate the effectiveness of the damage identification method for various damage cases in a sandwich beam.

- To validate the damage identification method, by using numerical simulations and experimental measurements, for single and multiple damages in a sandwich beam.
- To develop a control method for determining the criticality of damages in a sandwich beam.
- To develop the methodology for the development of a real-time structural health monitoring and control system.
- To demonstrate the feasibility of using grid technologies for development of a real-time structural health monitoring and control system.

These objectives will be achieved by developing methods in the present work.

1.2 Structure of the thesis

The first step in damage assessment of a structure is to characterise its damage modes and mechanism, which is discussed in Section 2.1. These damages continue to accumulate in a structure, which is predicted by using a cumulative damage model as discussed in Section 2.2. Non-destructive evaluation techniques for damage assessment in a structure are discussed in Section 2.3. This is followed by an extensive review of vibration-based damage identification methods in Section 2.4. Typical components of a SHM system and their role are described in Section 2.5. At the end of Chapter 2, the limitations of published works are identified in Section 2.7. Chapter 3 reviews the evolution in computing from legacy distributed systems to the emerging grid technologies. The state-of-the-art in grid technologies and their applications are described in Chapter 3, which concludes with identifying the role of grid technologies, in the development of a real-time structural health monitoring and control system. Based on the conclusions from literature review in previous chapters, the research methodology for the present work is outlined in Chapter 4. A model-based damage identification method is developed in Chapter 5, which is examined by using numerical simulations in Chapter 6. The experimental programme in Chapter 7 presents the fabrication procedure of the undamaged and damaged sandwich beam specimens; along with their experimental testings programme & signal processing of measured data. The proposed damage identification method is validated by using experimental measurements in Chapter 8. The components of the proposed real-time structural health monitoring and control

system are discussed in Chapter 9, which describes the implementation strategies, required technologies, and their testing. Finally, contributions of the present work are reviewed and future work are suggested in Chapter 10.

Chapter 2

Literature Review of Damage Assessment

This chapter reviews state-of-the-art techniques in damage assessment for sandwich structures. Damage modes in sandwich structures are characterised and models for predicting the accumulation of damage, are surveyed in Sections 2.1 and 2.2 respectively. An extensive review of damage assessment methods, including NDE and vibration-based techniques, are presented and discussed. Several NDE techniques are discussed and evaluated on the basis of their advantages and disadvantages for in-service structures in Section 2.3. Similarly, the approaches in vibration-based damage identification methods, are reviewed and their suitability for different levels of damage identification, in sandwich structures, are discussed in Section 2.4. These vibration-based methods are implemented in a structural health monitoring system. A survey of these systems and their components are presented in Section 2.5, which are used to identify their desirable characteristics in Section 2.6. Limitations of the vibration-based damage identification methods for sandwich structures and SHM systems are identified, in Section 2.7, which provides a foundation for the present work. Finally, conclusions from literature review and future works are outlined in Section 2.8.

2.1 Damage characterisation of sandwich structures

Damage is defined as intentional or un-intentional changes in a structure, resulting from the changes in its micro-structures, boundary conditions and system connectivity, which adversely affect its current and future performance. This thesis is primarily concerned with the damage occuring due to micro-structural changes in the faces and core of a sandwich beam, which govern its damage mechanism and mode. Figure 2.1

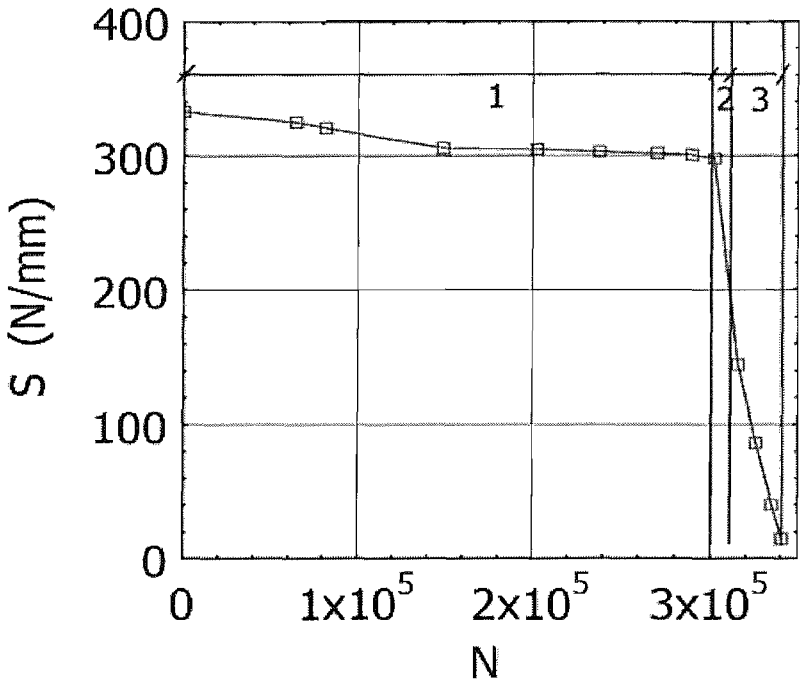

Figure 2.1: Variation of shear stiffness of a sandwich beam under fatigue load with numbers of cycles [Kulkarni *et al.*, 2003].

shows the variation of shear stiffness in the core of a sandwich beam with numbers of fatigue load cycles, which remains relatively constant during most part of its fatigue life. However, at the end of its fatigue life, there is a sharp reduction in shear stiffness of the core in a sandwich beam leading to catastrophic failure [Burman & Zenkert, 1997; Clark, 1997].

It is shown in Fig. 2.1 that damage in a sandwich beam initiates in the early phase of operational life, which continues to propagate until failure. This observation implies that damage and failure are two distinct events during the operational life of a sandwich structure. Difference between these two events are classified according to the quality of service during operation. After occurrence of damage, the structure is no longer operating as per the designed capacity, but still function satisfactorly. At this stage, safety of the structure is not compromised, but it needs repair. At failure, performance of the structure is much below the designed capacity, i.e., there is an unacceptable degradation in the quality of service. It means that the safety of the structure is severely compromised and it is not fit for meeting user requirements.

A sandwich structure, made of Poly Vinyl Chloride (PVC) foam as the core and

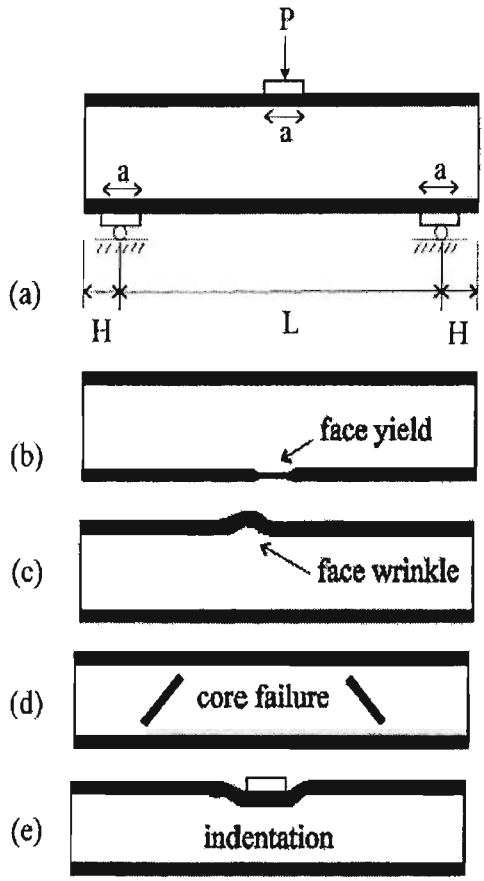

Figure 2.2: Damage modes of a sandwich beam under flexural loading [Zenkert, 1995].

composite materials as the faces, may damage in one or more modes [Zenkert, 1995], as shown in Figs. 2.2 - 2.4. The major damage modes are,

1. Core crushing,
2. Face damage,
3. Delamination,
4. Face wrinkling,
5. Global buckling,
6. Shear crimping, and

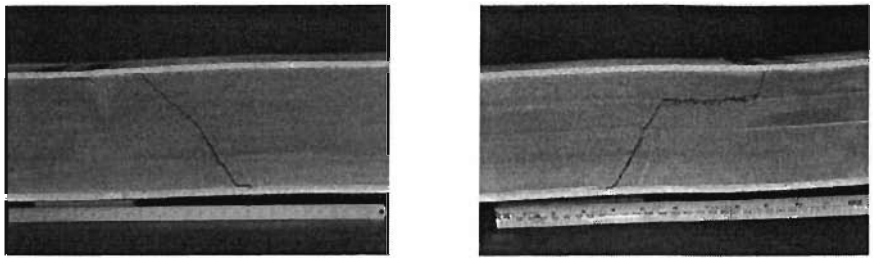

Figure 2.3: Core shear cracking (a) Mode : A, and (b) Mode : B. [Clark *et al.*, 1999].

7. Core indentation.

The damage mechanism in a sandwich beam is dominated by one of the above mentioned damage modes, often called critical damage mode. Critical damage mode depends on the mechanical and geometrical properties of the sandwich beam for a given loading condition.

One of common damage mode in a foam-cored sandwich beam is core shear, which is generally followed by other damage modes. It may be caused by impact, local indentation and/or excessive through-thickness loading. This damage mode can affect all types of foam core materials and results in the localised delamination and lack of support to the composite faces, leading to complete damage. A linear polymer foam core exhibits core shear yielding [Clark, 1997; Clark *et al.*, 1999], whereas, a cross-linked foam shows core cracking [Burman & Zenkert, 1997]. Figure 2.3 shows shear cracking of the core under fatigue load [Clark *et al.*, 1999]. Under four-points bending load, excessive internal heating in the core may cause thermal damage, slightly off near the mid-plane of a sandwich beam [Burman & Zenkert, 1997]. The thermal damage in the core occurs as a result of high repetitive shear stress in a zone, called *fracture process zone*. As a result of rising temperature, micro-cracks initiate in this zone and their cell walls rupture everywhere leading to the interaction among these micro-cracks. This process continues for most part of the operational life [Burman & Zenkert, 1997; Clark, 1997], depending on the mechanical and geometrical properties and the stress intensification. After saturation in the formation of micro-cracks, it converts into a crack and propagates rapidly towards the face causing a catastrophic failure. This crack propagation starts in the last 10 % of the fatigue life [Clark, 1997].

Under compression, faces are damaged in various modes as shown in Fig. 2.4. This damage occurs when the maximum stress in the face reaches to its ultimate value. It

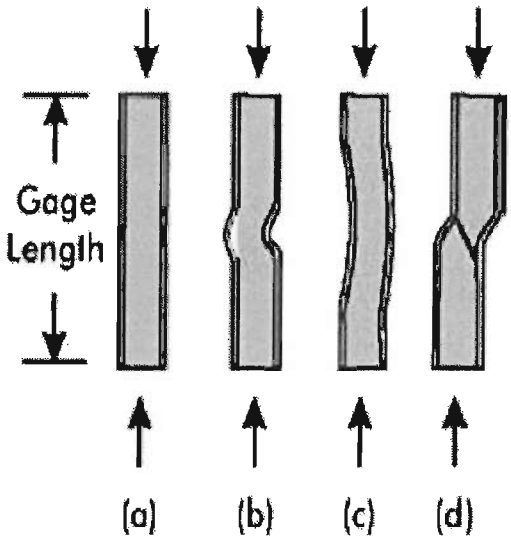

Figure 2.4: Damage modes of the compression loaded sandwich specimens : (a) Damage due to compression failure of face sheet, (b) Face wrinkling, (c) Global Buckling, and (d) Shear Crimping [Vadakke & Carlsson, 2004].

is caused by microbuckling of fibers inside the composite faces [Vadakke & Carlsson, 2004]. However, face yielding occurs in the tensile face under flexural loading as shown in Fig 2.2(b). Under low velocity impact, the front face is significantly damaged and virtually no damage is observed in the bottom face [Wu & Sun, 1996]. Resulting damages are mainly matrix cracking, delamination and local crushing of the foam core. At higher velocity, impact creates a cavity between the top face laminate and core.

Delaminations or de-bonds are one of the principal defects that can occur during manufacturing, machining and in-service condition. They may be caused by contamination at ply interfaces, insufficient cure and inclusions. The concept of a sandwich structure largely depends on the bonding between the faces and core. Thus, the strength of interface between the faces and core plays a vital role in the structural integrity of a sandwich structure. Any damage at the interface is known as *delamination/de-bonding*. De-bonding initiates slightly below the interface when a sandwich beam is subjected to three-points bending load [Burman & Zenkert, 1997; Kulkarni *et al.*, 2003; Noury *et al.*, 1998; Thomson *et al.*, 1998]. This depth is usually equal to the depth of resin penetration in the core, which is usually the size of the cell wall. De-bonding runs parallel to the beam axis as shown by damage event 1 in Fig.

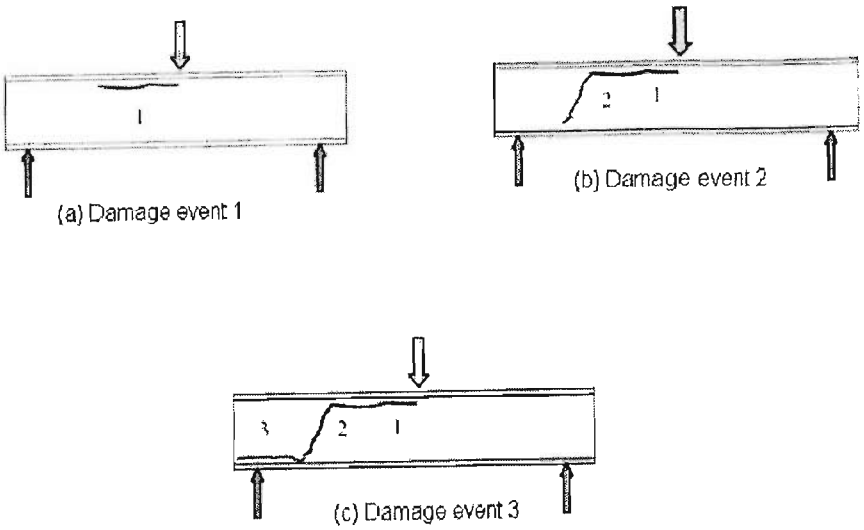

Figure 2.5: Damage sequence in a sandwich beam subjected to cyclic load under three-points bending test [Kulkarni *et al.*, 2003].

2.5 and causes initiation of crack in the core as shown by Fig. 2.5. Under moderate loading condition, fatigue strength of the interface is excellent. However, under extreme loading conditions, such as slamming, impact and explosive shocks, de-bonding has severe detrimental effects on their structural integrity and life expectancy.

De-bonding may also lead to the development of *face wrinkling*, which is a local elastic instability involving a short wavelength elastic buckling of the face, resisted by the underlying elastic core. The length of a half-wave is usually in order of the core thickness. As a result of local buckling, the core is either stretched or compressed, which is often referred as *symmetrical wrinkling mode*. In *asymmetrical wrinkling mode*, the faces and core do not exhibit any transverse extension through the thickness of the sandwich structure [Rose *et al.*, 2002]. It is a predominant damage mode for a sandwich structure made of a low density core. The damage mode transits to the face compression from the wrinkling with increasing core density [Fagerberg, 2004], which is schematically shown in Fig. 2.6.

The global buckling may occur for a long unsupported length under compression, as shown in Fig. 2.4. This damage mode can be classified as a global elastic instability,

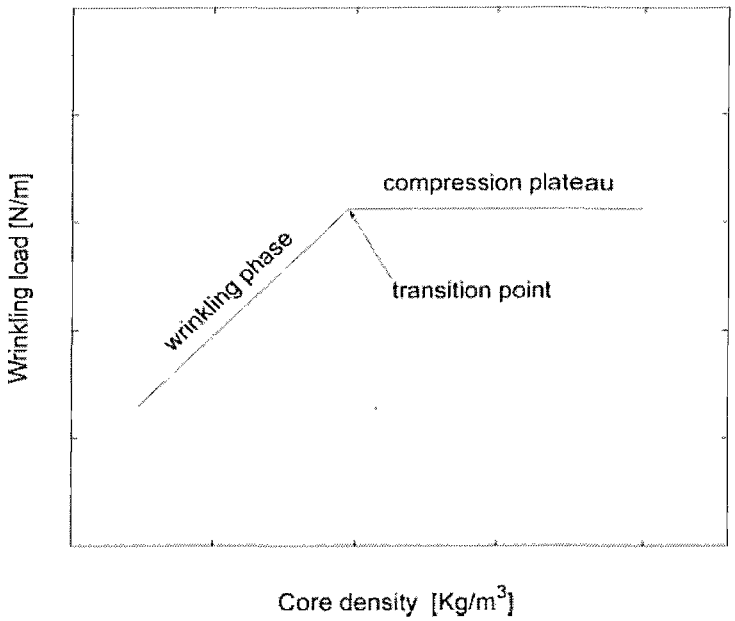

Figure 2.6: Transition between wrinkling and compression[Fagerberg, 2004].

where the faces and core buckle together into a long wavelength buckle. Generally, the length of a half-wave is equal to one of the planar dimensions of the sandwich structure.

Shear crimping is often considered as a special case of global buckling [Léotoing *et al.*, 2002]. It may occur in a post buckled state of a sandwich structure, as a result of the transverse shear load acting on the core in deformed state, which causes localised shear deformation. It occurs in the region of weak core where the transverse shear stress is maximum.

The core indentation is a local elastic instability of compressive face, which is accompanied by the local compressive yielding of the core. This damage mode is a particular problem for a sandwich structure made of a core having low transverse flexibility. The damage is characterised by plastic yield of the core with the faces deforming either elastically or plastically [Steeves & Fleck, 2004]. Triantafillou and Gibson [Triantafillou & Gibson, 1987] assumed that the core indentation is dictated by plastic yield of the core by neglecting the strength of the faces.

2.2 Cumulative damage models

A cumulative damage model predicts the accumulation of damage in a structure until its failure. It is based on the assumption that failure will occur when damage in a

structure exceeds its critical limit. Damage in a sandwich structure reaches to its final or critical limit, as a result of its continuous propagation from the initial undamaged state to critical damage state as described in Section 2.1. Their accumulation in a structure is usually expressed in the normalised form of cumulative damage parameter, i.e. D from zero at undamaged stage to unit value at final failure.

Under fatigue load, material performance is commonly characterised by the S-N curve, which plots the amplitude of a cyclic stress (S) against the number of cycles to failure (N). Normally, millions of cycles might be required to cause failure at lower loading levels, so the abscissa is usually plotted logarithmically. This curve is plotted using the test data of the material's sample subjected to a regular sinusoidal stress applied by a testing machine which also counts the number of cycles until failure.

The most simple cumulative damage model is frequently referred as 'Miner's rule' based on energy consideration [Miner & Calif, 1945]. This damage model is widely used and has been successful for metals. In this model, D is simply expressed as a function of the normalised number of load cycles,

$$D = \sum_{i=1}^{m} \frac{n_i}{N}, \tag{2.1}$$

where n_i is the number of load cycles at stress, σ_i, and N is the number of cycles to failure at stress level σ_i. Linear concept of 'Miner's rule' can be applied by considering the situation where a material is subected to n_1 cycles at alternating stress σ_1, n_2 cycles at stress σ_2,....,n_N cycles at σ_N. From the *S-N curve* of the material, we can find the number of cycles to failure, N_1 at σ_1, N_2 at σ_2,....,N_N at σ_N. In order to apply Eqn. 2.1, it is reasonable to assume the fractional damage at stress level σ_i be simply n_i/N_i.

For composite materials, the Miner's rule is generally conservative [Lee & Liu, 1994; Yang & Jones, 1980]. A non-linear version of this rule was later developed, which shows improved correlation for some materials such as graphite/glass epoxy cross-ply laminates [Gao, 1994]. This model is often referred as the 'modified Miner's rule', expressed as,

$$D = \left(\frac{n}{N_f}\right)^C, \tag{2.2}$$

where n is the applied number of cycles, N_f is the number of cycles to failure. C is a constant, which is determined from the experimental data.

Another improvement in the Miner's rule was made by Hashin [Hashin, 1985] by assuming accumulation of damage logarithmically rather than linearly with number of cycles,

$$D = \left[\frac{\mathtt{log(n)/log(N_e)}}{\mathtt{log(N_f)/log(N_e)}}\right], \tag{2.3}$$

where N_e is a parameter defining the fatigue limit of the material.

Hashin [Hashin, 1985] also defined the damage model as a function of the applied stress, residual strength and ultimate stress. The model is expressed as,

$$D = \left[\frac{(\sigma_u - \sigma_r)}{(\sigma_u - \sigma_a)}\right], \tag{2.4}$$

where σ_u is the ultimate strength, σ_r is the residual strength and σ_a is the applied stress. Residual strength is defined as the strength of the structure after damage. This model is restrictive in the sense that many fatigue tests are required to determine the static and fatigue strength and other required experimental parameters.

In order to determine the residual strength of sandwich beams, Dai and Hahn [Dai & Hahn, 2004] proposed a wear-out model, relating the ultimate strength (σ_u), the residual strength (σ_r) and the applied stress (σ_a). This model is represented by the following equation,

$$\sigma_u = \sigma_a \left[\left(\frac{\sigma_r}{\sigma_a}\right)^{1/s} + (n-1)f\right]^s, \tag{2.5}$$

where s and f are the experimentally obtained parameters. The parameter s is the absolute value of the asymptotic slope at long life on a log-log plot of S-N curve and describes the rate of strength degradation. Other parameter, f, scales the fatigue life in such a way that a small value of f, indicates a longer fatigue life at the same normalised applied stress. f is also known as the fatigue life scaling parameter. Eqn. 2.5 can be used to determine the residual strength (σ_r) of the sandwich beam. This value of σ_r can be substituted in Eqn. 2.4, to obtain the cumulative damage parameter.

Clark [Clark, 1997] assumed that damage initiates when fatigue damage is first observed, which implies that the cumulative damage parameter remains at zero, until initation of damage. Based on this assumption, four models were evaluated.

Clark [Clark, 1997; Clark *et al.*, 1999] modified Miner's rule to develop four cumulative damage models.

Model I was defined as,

$$D = \frac{(n - n_{if})}{(N_f - n_{if}} \qquad where \quad n \geq n_{if}, \tag{2.6}$$

Model II was defined as,

$$D = \frac{G_f(0) - G_f(n)}{G_f(0) - G_f(N_f)}, \qquad where \quad n \geq n_{if}, \tag{2.7}$$

where $G(0)$, $G(n)$ and $G(N_f)$ are fatigue modulus of a sandwich beam at undamaged state, at n number of cycle and at failure respectively.

Model III was defined as,

$$D = \frac{\gamma(n)}{\gamma(N_f)}, \tag{2.8}$$

where $\gamma(n)$ and $\gamma(N_f)$ are the shear strain at n number of cycle and at failure respectively.

Model IV was defined as,

$$D = \frac{\gamma(n) - \gamma(0)}{\gamma(N_f) - \gamma(0)}, \qquad where \quad n \geq n_{if}, \tag{2.9}$$

where $\gamma(0)$, $\gamma(n)$ and $\gamma(N_f)$ are shear strain in the core of a sandwich beam at undamaged state, at number of cycle (n) and at failure respectively.

2.3 Non-destructive evaluation techniques

Damage modes discussed in Section 2.1 must be identified at the early stage of their development to ensure safety of the structure. One such identification approach is Non-Destructive Evaluation (NDE) technique, which is extensively used for local damage assessment in a structure. NDE techniques provide improved damage assessment, but are still expensive, time consuming, need skilled personnel and often require special instruments and environmental conditions [Aktan *et al.*, 2000]. The pre-requisites for the application of these NDE techniques, except, for acoustic emission are that the vicinity of the damaged portion should be known in advance and the part of structure to be inspected, should be readly accessible. In this section, some of the most common NDE techniques are briefly described.

2.3.1 Visual Inspection

Visual inspection is the most common form of NDE technique for structural systems. This may be termed as 'enhanced or close visual inspection', if assisted by magnifying glasses, microscope, lighting or other tools. Increasingly, cameras are also used either for monitoring or to provide a permanent record of the inspection.

The best quality of visual inspection for transparent/translucent composite materials is where access is possible from both sides with backlighting. In this case, internal defects such as delaminations, fabrication defects and cracks may be found. Their effectiveness depends on wall thickness, resin type and coating of the composite structure. If access is limited to one side then only surface apparent or obvious defects can be seen. Users often have great confidence on visual inspection, which belies the limited data available on actual reliability. Identifiable damages include delamination, external cracks, localised deformation, impact damage, inclusions, air entrapments, excessive adhesive in joints, environmental damage, and wear damage. This method provides some useful data for damage assessment, but it may be inefficient and ineffective for a large structure.

2.3.2 Impact testing/Coin-Tap testing

Impact testing is a method which has been used for many years and covers a vast range, including coin tapping, the traditional method of testing aircraft flying surfaces, railway wheel tapping, to concrete testing using a hammer and vibration sensors. In its traditional form, the hammer is applied on the part of a structure by the tester, who also then listens to the generated ringing sounds. Anamolies in the structure are then recognised by an experienced tester, based on the differences in the characteristics of the ringing sound. Identifiable defects include regions of poor cure, delaminations, coating de-bonding or thickness variations. This method is not suitable for thick structures. This method is very subjective and its limitations include the possibility of impact damage and difficulties in applying to constrained structure, where its acoustic response will differ. Tap testing is a relatively low cost option and its reliability depends on the hearing ability and experience of the tester.

2.3.3 Acoustic emission

Formation, growth or loading of cracks in a structure may produce an Acoustic Emission (AE), which refers to a phenomenon of generating transient elastic waves releasing

high amount of energy suddenly from a crack in a structure. AE can be used on the whole structure and works by picking these transient elastic waves. This technique can be categorised as conventional analysis and wave-based modal analysis. In conventional analysis, parameters such as time of arrival, amplitude, counts, duration, energy and rise time are measured by using resonant AE sensors. In a wave-based modal analysis, broadband AE sensors are used to capture the wide range of frequencies in a given wave. Acoustic waves are generated from propagating/sliding crack tips in a high stress zone. Crack tips located in the low stress regions are static and do not produce acoustic waves [Beattie, 1998]. Hence, acoustic waves are generated as a result of high stress at the crack tips in the material. These waves are generated in the form of a sudden burst of acoustic energy for a short time and continue to propagate until they reache the surfaces.

Okafor *et al.* [Okafor *et al.*, 2001] used broadband AE sensors to characterise high velocity impact damage in a laminated composite plate. However, due to different damage modes in a laminated structure, damage mode identification also became important. Wevers [Wevers, 1997] created a filter, using light microscopy and penetrant enhanced radiography, to analyse AE signal characteristics for identification of the damage mode in a carbon reinforced composite. Extending this principle, Surgeon and Wevers [Surgeon & Wevers, 1999] demonstrated an intelligent and efficient analysis technique of AE signals, for quantitative assessment of active damage mode such as source location and orientation, in a CFRP laminate. AE signals were processed by using Wavelet Transform to identify the sequence of damage and their interaction in a composite. AE signals in conjunction with Neural Network were used to identify damage modes in a unidirectional glass/polyester composite [Godin *et al.*, 2004; Huguet *et al.*, 2002]. Similarly, Ramirez-Jimenez *et al.* [Ramirez-Jimenez *et al.*, 2004] established a relationship between micro mechanical events and frequency of AE signals, to differentiate damage mode in a glass/polypropylene composite specimen. Grondel *et al.* [Grondel *et al.*, 2004] used acoustic emission signature, to detect impact and fatigue damage between stiffeners and composite skins in an aircraft wing structure. They showed the sensitivity of AE signals for both types of damages.

AE historically, has had difficulty in application to large structures and false damage identifications. Widespread use of this technique require further development of data interpretation methods.

2.3.4 Ultrasonic testing

Another important NDE technique is Ultrasonic Testing (UT) used to assess the state of damage in sandwich structures. In this technique, Ultrasound is introduced into the structure by using a transducer and then reflections from the damaged interfaces, attenuation or diffraction signals are recorded. This technique is often termed as 'A, B, and C scans'. It is based on the principle of changes in energy, to identify defects in a structure, as mechanical wave propagates through it. These tests are usually conducted with two coupled water-jet heads moving in tandem on either side of the specimen surface, sending ultrasonic waves through the water stream on one side, and measuring the transmitted waves on the other side. A-scan refers to a single point measurement of density, B-scan measures the variation along a line and C-scan is a collection of B-scans forming a surface contour plot. C-scan testing is the most commonly used for composites and can be used to scan a large part of structure in a relatively short time. Apart from the size and cost of equipments, these testings also require both sides of the structure to be accessible; hence, parts of the structure may need to be dismantled for testing.

One of the main drawback of this method is the requirement to calibrate equipment for different lay-ups, coupling and the need for different probe types. Sound waves can be attenuated rapidly in certain materials, thereby making it difficult to perform pulse/echo measurements on thick parts. This method is also sensitive to surface roughness. A high scan of large parts and scans of parts with odd shapes or a complex surface can take many hours.

2.3.5 Thermo-elastic measurements

Thermography refers to the detection of defects in a structure, by evaluating the difference in its thermal responses, usually done by monitoring infra-red emissions using a thermal imaging camera. This technique is based on the thermo-elastic effects of a structure. It uses a Stress Pattern Analysis by Thermal Emission (SPATE) system, which is a highly sensitive infra-red detector to measure small temperature changes, caused by the change in stress in an elastic solid. In most cases, the structure to be assessed is subjected to cyclic loading at a particular frequency, in order to maintain adiabatic thermal conditions. The surface temperature changes are monitored and stress variations due to a cyclic loading are deduced.

To detect and image real defects with a reasonable sensitivity, it is necessary to apply a pulse of heat (or cooling) into the component and monitor their variation with time. This technique is also termed as 'pulsed or transient thermography'. The time at which temperature variations take place is often more important than the amplitude of the temperature change, which is usually a few degrees centigrade. Heating methods include excitation, a hot air gun, flash tubes, electromagnetic induction, hot and cold water and acoustic. Selection of the most suitable heating method depends on the thermal responses and the thickness of the structure.

Infrared thermography is an alternative thermo-elastic NDE technique to obtain rapid colour-coded results in realtime. However, this technique is not suitable for low extent of damage and further image processing is required to interpret the results.

2.3.6 Laser shearography

In recent years, laser shearography is increasingly being used for detection of delaminations, de-bonding, poor adhesion and other damages in composites and sandwich structures. This is due to the advent of advanced, portable devices and innovation in their data processing.

Shearography, a real-time NDE technique, is based on the idea that fringe patterns are produced, when interference occurs between coherent waves of light having different path lengths. This fringe pattern represents the changes in the surface strain field, from the difference in displacements between unloaded and loaded states, using a scanning laser system. Defects in the structure under test raise strain concentration under load, which is produced by a number of methods including vacuum loading, heating, and internal pressurisation. Thus, the fringe pattern can be used to identify damage. It involves a qualitative assessment of the fringe pattern, produced by using an image shearing camera to capture video images of surface displacement, illuminated by a coherent laser source, which is reflected from the specimen. These images are then stored digitally for future analysis. The main limitation of the technique is accessibility and it provides the indirect surface measurement.

2.3.7 X-ray computed tomography

Tomography refers to the cross-sectional imaging of an object, from either transmitted or reflected data, collected by illuminating the object from many different directions. This technique is widely used in medical applications. Recently, this technique is being used for damage assesment in structures. X-ray computed tomography is

Table 2.1: Key NDE techniques for damage assessment.

Feature	Ultrasonics	X-ray Computed Tomography	Acoustic Emission
Principles	Sound Transmission	X-ray transmission	Stress wave emission
Parameters	Scattering attentuation, and velocity	absorption and attentuation coefficients	Amplitude, counts and number of events
Advantages	Suitable for thick materials; relatively quick testing time	Creates cross-sectional view of the entire transmitted thickness	Real-time monitoring
Limitations	Requires water immersion or acoustic coupling	Expensive, limited specimen size, radiation hazard	requires a prehistory of stress for flaw detection
Detecteble damage	Voids, delaminations, porosity and inclusions.	Voids, delaminations, porosity and inclusions.	Delaminations and inclusions

a non-destructive technique that is used to obtain images of the interior of micro-heterogeneous materials, such as composites. Although, this technique can also be applied to any material, through which a beam of X-ray may be transmitted and reflected. Application of this technique to composite materials is mainly limited to metal-matrix and ceramic-matrix composites. The principal advantage of this method is that it provides densitometric (i.e. radiological density and geometry) images of thin cross sections through an object. In this technique, a beam of X-rays is fired at a rotating sample, which produces 2-D projections of the sample, to be recorded by a detector behind the sample. Then, these 2-D projections are stacked to provide 3-D data through out the entire object or section of the object. These 3-D images can be virtually sectioned by displaying part of the reconstructed volume, which create a "virtual" cutting plane.

As the X-ray pass through the object, the signal is attentuated by scattering and absorption. The ability to differentiate materials depend on their respective linear attentuation coefficient. Intensity and energy spectrum of X-ray are the important parameter for effectiveness of this technique. The energy spectrum defines the penetrative ability of the X-rays, as well as their expected relative attentuation as they pass through materials of different density. High energy X-ray penetrate more effectively than low energy, but also less sensitive to changes in material density and composition.

Intensity of X-ray controls the signal-to-noise ratio, hence image clarity. The major difficulties with this technique are the portability of equipment and access to structural members also limit field application.

2.3.8 Limitations

Non-destructive evaluation techniques, which are discussed in this section, play an important role in damage assessment of a structure. However, these conventional methods, especially ultrasonic methods, are difficult to be used successfully for sandwich structures [Wei *et al.*, 2004b]. The main reason behind this observation is that these methods use waves for damage assessment. These techniques are based on pulse bulk waves such as longitudinal and transient elastic waves, which are reflected or transmitted to be measured in realtime. Due to orthotropic nature of sandwich structures, the incident pulse waves may not be measured due to their low intensity; hence making the damage assessment unreliable.

2.4 Vibration-based methods

Structures are often subjected to vibration by ambient energy, an external shaker or an embedded actuator. Their vibration responses are usually measured by using sensors such as accelerometers. It is well known that the existence of damage modifies the vibration responses of a structure, which provides the foundation for vibration-based damage identification. The basic principle in this method assumes that the changes in vibration responses, correlate with the loss of stiffness in any or whole part of a structure. This is usually predicted by using a damage identification method, which holds more potential in a real-time structural health monitoring and control system compared to NDE techniques discussed in Section 2.3.

Damage identification in a structure can be divided into four levels [Rytter, 1993],

Level 1 : Identifying the presence of damage in a structure,

Level 2 : Level 1 plus determination of the geometric location of damage,

Level 3 : Level 2 plus quantification of the damage extent in the constituents of the structure, and

Level 4 : Level 3 plus prediction of the remaining service life of the structure.

The literatures reviewed in this section are for Level 1, 2 and 3. Level 1 and 2 of damage identification does not require any structural model; whereas, it is desirable for Level 3. Level 4 prediction is generally associated with the fields of fracture mechanics and fatigue life analysis, which is beyond the scope of vibration-based damage identification [Doebling *et al.*, 1996].

In this section, a review of the vibration-based damage identification methods applicable to any stuctures is presented. Here, reviewed damage identification methods are classified into two approaches, i.e. pattern recognition and model-based approaches.

2.4.1 Pattern recognition-based approaches

The basis of this damage identification approach is to recognise the changes in the "patterns" of vibration responses of a structure, by comparing with the patterns for the undamaged and damaged states of the same structure.

The simplest pattern recognition approach compares the natural frequencies of the undamaged and damaged structure. In 1963, Housner and Brady [Housner & Brady, 1963] used the changes in the natural frequencies of a building damaged by an earthquake, to estimate the degree of deformation after the earthquake. Doebling *et al.* [Doebling *et al.*, 1998] refers to Lifshitz and Rotem [Lifshitz & Rotem, 1969] as the author of presumably the first journal article to suggest the usage of vibration data for damage identification. However, the systematic study of the damage identification methods started in the late 1970's by Adams *et al.* [Adams *et al.*, 1978], and Cawley and Adams [Cawley & Adams, 1979], who used the sensitivity of the natural frequencies to detect and locate damage in an aluminium and a carbon reinforced fibre plastic plate. They used the ratio of frequency changes in two different modes to locate a single damage. Friswell *et al.* [Friswell *et al.*, 1994] extended Cawly and Adam's approach by introducing statistical analysis for identification of the best damage scenario. Chondros and Dimarogonas [Chondros & Dimarogonas, 1980] used the ratio of the natural frequencies of the undamaged and the damaged structure, to predict the damage severity of a cantilevered beam with the crack at the cantilevered end. Stubbs and Osegueda [Stubbs & Osegueda, 1990a,b] further developed the method based on sensitivity analysis of fractional changes in natural frequency, for better estimation of damage severity. Armon *et al.* [Armon *et al.*, 1994] introduced a rank-ordering procedure based on fractional eigenfrequency shift to overcome the requirements of high accuracy for the sensitivities and to provide a robust method for measurement errors and model uncertainties. Irretier [Irretier, 1993] and Irretier *et al.* [Irretier *et al.*,

1993] experimentally investigated the effects of the changes in damping and natural frequencies for a composite driving shaft. Based on their results, they concluded that the changes in the bending natural frequencies are more sensitive damage indicators. Valdes and Soutis [Valdes & Soutis, 1999] detected delamination in composite laminates by comparing natural frequencies of undamaged and delaminated composite beam, measured by using piezoceramic patches and piezoelectric film sensors, where higher natural frequencies were found to be more sensitive than those of lower.

The use of spatial information to improve damage detection was introduced by West [West, 1984], who suggested the use of a parameter called 'Modal Assurance Criterion (MAC)', for the correlation of mode shapes of the undamaged and damaged beam. Yoo *et al.* [Yoo *et al.*, 1999] compared several damage indicators derived from MAC, by using numerical simulations for a cracked plate and concluded that the absolute values of their difference is the best damage index for predicting the existence of damage. Yuen *et al.* [Yuen, 1985] suggested the use of rotational mode shapes to characterise the presence of damage. Rizos *et al.* [Rizos *et al.*, 1990] suggested to use the mode shapes information measured at two locations. Recognising the insensitivity of displacement mode shapes to damage, Pandey *et al.* [Pandey *et al.*, 1991] proposed that the absolute changes in the mode shape curvatures, can be a good indicator of damage and its location. Chance *et al.* [Chance *et al.*, 1994], Swamidas and Chen [Swamidas & Chen, 1995] and Yam *et al.* [Yam *et al.*, 1996] used strain mode shapes for damage identification, which could be directly obtained from strain gauge measurements. Ratcliffe and Bagaria [Ratcfliffe & Bagaria, 1998] used the changes in the curvature mode shapes for delamination localisation in a flat glass-reinforced epoxy beam. The curvature values were computed from the displacement mode shapes using the central difference approximation. Pandey and Biswas [Pandey & Biswas, 1994] compared the changes in the measured flexibility of a beam, to detect and locate a damage using vibration responses. Yang and Liu [Yang & Liu, 2006] applied the method based on using difference of flexibility matrix for locating single and multiple damages in a steel beam. Oh and Jung [Oh & Jung, 1998] used the curvature of mode shapes and static deflections to localise a damage in a multi-span beam and a truss structure made of steel. Hamey *et al.* [Hamey *et al.*, 2004] used the changes in curvature of mode shapes to locate delamination and impact damage in the carbon/epoxy composite beams. The concept of flexibility and curvature calculation is combined, to find the change in flexibility curvature of a reinforced concrete beam [Lu *et al.*, 2002] to locate single and multiple damages. Ratcliffe [Ratcliffe, 1997] used finite difference approximation of a

Laplacian operator on the mode shapes data to locate a damage in a beam. Santos *et al.* [Santos *et al.*, 2000] used the orthogonal properties of the mode shapes to locate a damage in a laminated plate.

Recently, there is an increasing trend of using pattern-recognition based approach in conjunction with a feature discrimination method, such as Artificial Neural Network (ANN), wavelet analysis, optimisation and genetic algorithms. Lopes *et al.* [Jr *et al.*, 1997] developed a damage identification method based on artificial neural network, in which numerical simulations were used during the training phase and experimentally validated the approach, by identifying damage in the welded joint of a metallic structure. Rytter and Kirkegaard [Rytter & Kirkegaard, 1997] evaluated the two three-layers neural networks, the multi-Layer Perception(MLP) network with back propagation and the Radial Basis Function (RBF) network, for damage assessment of a four-storied building. Yun and Bahng [Yun & Bahng, 2000] used the natural frequencies and the mode shapes as the input parameters for estimation of the stiffness coefficients of a complex structural system. Sahin and Shenoi [Sahin & Shenoi, 2003b] used feed-forward back-propagation ANN for damage identification of a laminated beam-like structure, using simulated curvature mode shapes. Their results show that the selection of the input parameters and the associated noise levels are crucial for the accuracy of damage assessment. However, noise polluted data provides robust prediction of the damage location compared to that of damage severity [Sahin & Shenoi, 2003b]. This approach was verified with experimental curvature mode shapes of a cantilevered steel beam [Sahin & Shenoi, 2003a]. Worden and Manson [Worden & Manson, 2003a] developed and validated a structural health monitoring methodology, for a laboratory stiffened panel made of aluminium, by using a standard feed-forward multi-layer perception neural network, where outlier analysis was used for novelty detection. Subsequently, Worden and Manson validated the methodology for identifying detectable damages on realistic structure such as wing panel of GNAT trainer aircraft [Worden & Manson, 2003b,c]. Kesavan *et al.* [Kesavan *et al.*, 2006] developed an approach for real-time damage assessment in a GFRP T-joint by using ANN and validated the approach with numerical and experimental results. Todoroki *et al.* [Todoroki *et al.*, 2006] used changes in electrical resistance with ANN to detect matrix cracks in a cryogenic tank made of carbon fibre laminates. They validated this method in laboratory condition for a small scale specimen.

The wavelet transform methods are based on the principle that the presence of damage causes singularities in the vibration responses. The main parameter in a

wavelet-based analysis is the Lipshitz or Holder exponent. The Lipschitz or Holder exponent characterises the level of singularities in the vibration signal of a structure. Robertson *et al.* [Robertson *et al.*, 2003] used the Holder exponent to identify the presence of a loose part in a machinery, by analysing acceleration measurements. Dawood *et al.* [Dawood *et al.*, 2003] used the wavelet-based multifractal approach for damage detection in a composite beam. This approach was extended for delamination identification in a GFRP sandwich beam using experimental data [Dawood *et al.*, 2004b]. Dawood *et al.* [Dawood *et al.*, 2004a] demonstrated that the multifractal approach has the capability to identify low level of damage in an aluminium and FRP sandwich beam. Yam *et al.* [Yam *et al.*, 2003b] and Wu *et al.* [Wu *et al.*, 2000] used wavelet transform in conjunction with artificial neural networks for damage identification in a composite structure. Rucka and Wilde [Rucka & Wilde, 2006] used continuous wavelet transform method for locating damage in a cracked cantilever plexiglas beam and steel plate, by measuring their mode shapes. In this approach, Gaussian wavelet and reverse bi-orthogonal wavelet were used for the cracked isotropic beam and plate respectively. Kim and Melhem [Kim & Melhem, 2004] presented the overview of the applications of the wavelet analysis for damage identification.

2.4.2 Model-based approaches

The model-based approaches differ from the pattern recognition-based approaches, because of the use of a numerical model. Model updating technique is one of the simplest model-based approach used for damage identification. This is based on the principle of minimising the residuals of the natural frequencies and/or the mode shapes. Ricles and Kosmatka [Ricles & Kosmatka, 1992] developed a method based on residual forces to locate a damage and a separated weighted sensitivity analysis was then used to predict the changes in the mass and stiffness matrices. Banks *et al* [Banks *et al.*, 1996b] used enhanced least-square error minimisation, to detect holes of different sizes in a cantilevered aluminium beam. Mannan and Richardson [Mannan & Richardson, 1990] proposed the usage of mass, stiffness and damping matrices estimated from the measured model data and used the differences to the corresponding undamaged matrices, for damage identification. Zimmerman and Kaouk [Zimmerman & Kaouk, 1994] proposed a minimum rank perturbation theory that gave perturbation matrices the same rank as the number of modes used for the analysis. Zimmerman *et al* [Zimmerman *et al.*, 2001] minimised the dynamic residuals of the NASA 8-bay truss to locate damage, using the numerical and experimental mode shapes. Similar approach is used by

Thyagarajan *et al* [Thyagarajan *et al.*, 1998] to locate damage in a truss bridge using FRF data. Teughels *et al* [Teughels *et al.*, 2002] minimised the residuals of the natural frequencies and the mode shapes of a concrete beam, to localise and quantify damage. In order to reduce the number of variables, they used a damage function based on *legendre polynomial*. These methods use a FE/numerical model in conjunction with an optimisation technique for damage identification. Since, it is based on an optimisation technique, it requires a good initial guess for satisfactory convergence and optimum results. This assumes of paramount importance for damage severity predictions. This problem can be solved by using a model-based damage identification method.

The most commonly used methods are based on the changes of strain energy. Kam and Lee [Kam & Lee, 1992] used natural frequencies and mode shapes of a structure to evaluate crack size. An energy balance is performed by equating the maximum strain energy of the damaged structure with that of the undamaged structure. Shi and Law [Shi & Law, 1998] developed a method based on the changes in strain energy for damage identification of a truss structure. Damage is localised by calculating the ratio of change in elemental modal strain energy to undamaged elemental modal strain energy. Subsequently, Shi *et al.* [Shi *et al.*, 2000, 2002] extended the changes in modal strain energy method for damage identification of simply supported and continuous isotropic beam, where the damage severity of the damaged element was calculated by an iterative procedure. Cornwell *et al.* [Cornwell *et al.*, 1999] proposed an analytical method for damage identification of an isotropic beam and a plate structure, which was verified with experimental data. Damage was localised by calculating the ratio of strain energy of an element to total strain energy of the structure. Worden and Fieller [Worden & Fieller, 1999; Worden *et al.*, 2001] presented a strain energy-based theory for damage localisation in an aluminium plate stiffened with stringer. Park *et al.* [Park *et al.*, 2001] used damage index method for damage localisation in a concrete girder bridge. The damage index method is used for damage identification of a deteriorated timber bridge [Peterson *et al.*, 2001a,b] and concrete bridge [Farrar & Jauregui, 1998a,b]. Recently, Hu *et al.* [Hu *et al.*, 2006] used strain energy based damage index method, to locate surface crack in a carbon/epoxy laminated plate with uni-directional fibre orientation. The strain energy-based approach in conjunction with improved mode selection criteria was developed for improved damage location of a frame structure [Doebling *et al.*, 1997]. Doebling *et al.* [Doebling *et al.*, 1997] developed a maximum strain energy criterion to select the mode shape, which significantly affects the damage

identification procedure. Sampaio [Sampaio, 2000] compared the FRF based damage identification methods and suggested to use a strain energy-based method.

2.4.3 Pattern recognition Vs. model-based approaches

It has been demonstrated in previous sub-sections that an extensive amount of research work has been undertaken for vibration-based damage identification, specially for isotropic and composite structures. These methods are based on either pattern recognition approaches or model-based approaches, which compare the vibration responses of the undamaged and damaged structures. Some of the related references are tabulated in Table 2.5. These methods have been developed because of relatively less sensitivity of the natural frequencies and mode shapes towards damage [Farrar & Jauregui, 1998a,b]. Thus, a damage index which sensitive enough for low extent of damage must be developed from the vibration responses of the damaged structure. There have been many such damage indices proposed in literature, which were discussed in previous sub-sections and recent literature review papers [Doebling *et al.*, 1996; Sohn *et al.*, 2003]. Farrar & Jauregui [Farrar & Jauregui, 1998a,b] and Alvandi & Cremona [Alvandi & Cremona, 2006] compared different damage identification methods, for damage identification in a multi-span bridge and a simply supported beam respectively. Studies by Farrar and Jauregui include the experimental [Farrar & Jauregui, 1998a] and numerical [Farrar & Jauregui, 1998b] data for comparison. Alvandi and Cremona [Alvandi & Cremona, 2006] also investigated the role of statistical theory in damage identification. These methods were, damage index method, change of mode shape curvature method [Pandey *et al.*, 1991], change in flexibility method [Pandey & Biswas, 1994], change in flexibility curvature [Zhang & Aktan, 1995], change in uniform load surface curvature, change in stiffness method, and strain energy method [Cornwell *et al.*, 1999]. Other comparative studies of different vibration-based damage identification methods by using FRFs are performed by Sampaio [Sampaio, 2000]. These methods are used for Level 1 and 2 of damage identification. Out of these methods, only damage index method and strain energy method are model-based approaches, hence these require the numerical model in damage identification. Based on the discussion so far, the performances of pattern recognition-based approaches and model-based approaches are compared with the amount of data in Fig. 2.7. This is also supported by their results, in which methods based on strain energy have successfully located damage in the most damage cases and have performed better than those of the pattern recognition approaches.

The two approaches for vibration-based damage identification methods discussed in Section 2.4 have their own intrinsic advantages and limitations, which are summarised in Table 2.2. Pattern recognition approaches have the advantage of avoiding modelling errors and computational costs, which can be a severe limitation for an iterative damage identification method. However, most pattern recognition approaches provide Level 1 and 2 damage identification. Furthermore, remaining Levels, i.e. 3 & 4 by means of pattern recognition approach, requires a considerable increase in number of sensors and a significant amount of signal and data processing [Farrar *et al.*, 2003] as shown in Fig. 2.7. This indicates that, in order to achieve Level 3 and 4, a model-based approach is necessary [Farrar *et al.*, 2003]. Model-based approaches can be advantageous in many aspects. For example,

- The use of a mathematical model describing the dynamic system permits the application of model-based damage identification methods, possibly reducing the amount of experimental data required.
- It allows numerical simulations for slight variations in the structural system, such as changes in physical parameters, boundary conditions, external influences, etc.
- The model can be used in the test design phase to optimise the number and location of sensors and excitation/measurement techniques.
- The model can be used to easily generate extensive amounts of data, as needed to study the sensitivity of damage on the structure.

It is shown in this section that there are many advantages of the model-based damage identification method. However, there are also few limitations of this method. These are as follows,

- Role of the mathematical model is important in the model-based damage identification method. Hence, it requires availability of an accurate mathematical model of the structure.
- This method is computationally expensive. In case of an iterative method, the computational cost becomes very high.

Table 2.2: Comparison of pattern recognition approach with model-based approach for damage identification.

	Pattern recognition approach	Model-based approach
Level of identification	1 and 2, and 3 for isotropic structure	All levels
Incomplete measurements	No	Yes
damage mode identification	No	Yes
Numerical model required	No	Yes
Computational cost	Inexpensive	Expensive

Table 2.3: Comparison of damage identification approaches.

Damage identification method	Inputs required	Damage identification approach	Levels of damage identification
Dynamic residual method	Mode shapes and stiffness matrix	Model-based approach	1,2, and 3
Change in mode shape curvature	Mode shapes	Pattern recognition approach	1 and 2
Change in flexibility method	Natural frequencies and mode shapes	Pattern recognition approach	1 and 2
Changes in flexibility curvature method	Mode shapes	Pattern recognition approach	1 and 2
Change in stiffness matrix	Natural frequencies and mode shapes	Pattern recognition approach	1 and 2
Change in modal strain energy	Natural frequencies, mode shapes and elemental stiffness matrix	Model-based approach	1,2, and 3
Damage index method	mode shapes and stiffness modulus	Model-based approach	1 and 2

Table 2.4: Comparing vibration-based damage identification methods for structure's materials and topology.

Damage identification parameter	Materials used and structural topology
Natural frequencies and/or Damping	Composite beams[Kyriazoglou *et al.*, 2004; Valdes & Soutis, 2000] [Kim, 2003; Lee *et al.*, 1987; Okafor *et al.*, 1996; Wu *et al.*, 2000] [Islam & Craig, 1994] Composite plate[Adams *et al.*, 1978; Cawley & Adams, 1979]
Residual mode shapes forces	Steel Truss[Thyagarajan *et al.*, 1998; Zimmerman *et al.*, 2001] Aluminium beam[Banks *et al.*, 1996b] Reinforced concrete beam [Teughels *et al.*, 2002] Composite beam[Cunha & Perreux, 1998; Nag *et al.*, 2002] Composite plate[Santos *et al.*, 2000]
Mode shape curvature	Steel beam[Oh & Jung, 1998; Pandey *et al.*, 1991] Concrete bridge[Wahab & Roeck, 1999] Composite beam[Hamey *et al.*, 2004; Sahin & Shenoi, 2003b] [Ratcfliffe & Bagaria, 1998] Concrete bridge[Farrar & Jauregui, 1998a]
Flexibility	Steel beam [Pandey & Biswas, 1994] Concrete bridge [Farrar & Jauregui, 1998a]
Stiffness matrix	Concrete bridge[Farrar & Jauregui, 1998a] Steel truss[Doebling *et al.*, 1997]
Modal strain energy	Steel beam and frame[Shi *et al.*, 2000, 2002] Steel beam and plate[Cornwell *et al.*, 1999; Worden *et al.*, 2001] , Composite plate[Wei *et al.*, 2004b; Yan & Yam, 2004]
Damage index method	Concrete girder bridge [Farrar & Jauregui, 1998a; Park *et al.*, 2001] Timber beam [Peterson *et al.*, 2001a,b] Composite beam[Ratcfliffe & Bagaria, 1998]

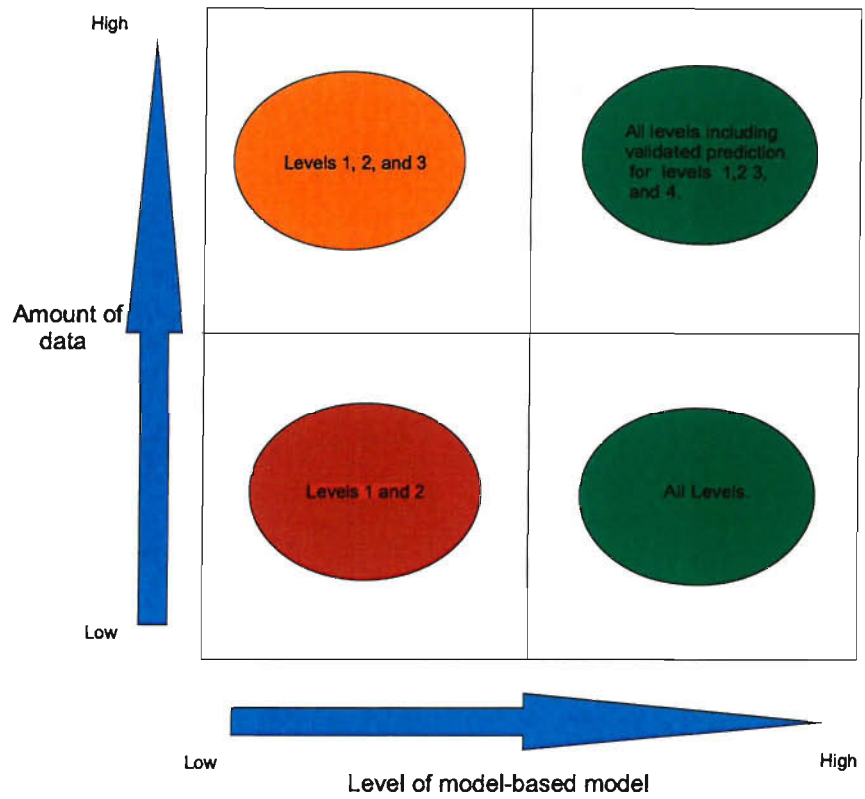

Figure 2.7: A comparison of regimens appropriate for model-based approach and pattern recognition approach.

Table 2.5: Damage identification approaches.

Pattern recognition approach	Model-based approach
[Kim, 2003],[Dawood *et al.*, 2003]	[Liu & Chen, 2001]
[Dawood *et al.*, 2004b],[Dawood *et al.*, 2004a]	[Liu & Chen, 2002]
[Adams *et al.*, 1978],[Cawley & Adams, 1979]	[Zimmerman *et al.*, 2001]
[Chondros & Dimarogonas, 1980]	[Thyagarajan *et al.*, 1998]
[Pandey *et al.*, 1991],[Pandey & Biswas, 1994]	[Teughels *et al.*, 2002]
[Ratcliffe, 1997],[Santos *et al.*, 2000]	[Shi & Law, 1998]
[Yun & Bahng, 2000]	[Shi *et al.*, 2000, 2002]
[Sahin & Shenoi, 2003a]	[Cornwell *et al.*, 1999]
[Sahin & Shenoi, 2003b]	[Worden & Fieller, 1999]
[Robertson *et al.*, 2003],[Yam *et al.*, 2003a]	[Worden *et al.*, 2001]
[Kim & Melhem, 2004],[Rizos *et al.*, 1990]	[Park *et al.*, 2001]
[Rytter & Kirkegaard, 1997]	[Wang *et al.*, 1996]

Table 2.6: Approaches and damage types in vibration-based damage identification of sandwich structure.

Reference	Technique(s) used	Damage identification approach	Type of damage
[Wang *et al.*, 1996]	Strip element method	Model based	Core flaws
[Liu & Chen, 2001] [Liu & Chen, 2002]	Genetic algorithm	Model based	Core damage
[Kim, 2003]		Pattern recognition	Delamination
[Yam *et al.*, 2003a] [Yam *et al.*, 2003b]	Wavelet transform and ANN		Crack
[Dawood *et al.*, 2003] [Dawood *et al.*, 2004b] [Dawood *et al.*, 2004a]	Wavelet transform	Pattern recognition	Delamination

2.5 Structural health monitoring systems

Structural Health Monitoring (SHM) is the process of implementing a damage identification method for structures by using their responses, measured over time. These measurements are mostly time-series vibration responses such as accelerations, strains, etc., which are pre-processed and analysed by using a damage identification method, to extract damage sensitive features. Thus, the primary objective of a SHM system is to assess the ability of a structure to perform its intended function in view of inevitable ageing and degradation under the operational conditions. Development of reliable and robust SHM systems are still evolving with development in new technologies. Some of these systems are reviewed in this section.

Goranson [Goranson, 1997] described the SHM system to assess the structural integrity of aging jet transport system. A similar SHM system to perform real-time fatigue calculation of the airframe in Eurofighter Typhoon was developed and validated [Hunt & Hedben, 2000]. These systems were used to record the structural events and flight performance data, which were stored in a bulk storage device. Iglesias and Palomino [Iglesias & Palomino, 2000] described working of the SHM system for Eurofighter-18 and provided the design guidelines for Eurofighter 2000. These two systems differ because of different sampling rates. The system for Eurofighter-18 was restricted by low sampling upto 20 Hz for strain measurements, due to limitation in onboard storage capacity of magnetic tapes; whereas, the system for Eurofighter 2000 was designed for higher sampling rates. These systems for Eurofighter were designed for fleet management to plan their maintenance schedule and manpower management. Kabashima *et al.* [Kabashima *et al.*, 2000] presented the requirements of a health monitoring system for a satellite structure during all stages of the life cycle. Hall [Hall, 1999] highlighted the need for data management systems to be incorporated during the design of a SHM system for aircrafts. Lynch *et al.* [Lynch *et al.*, 2002b] designed a wireless structural health monitoring system capable of acquiring measurement data, interrogating the data and their real-time transmission to a data management system. In this system, an additional software layer was then designed to execute an algorithm for computation. Data management system was implemented in this system and tested with data obtained from a bridge testing [Lynch *et al.*, 2002a]. Kottapalli *et al.* [Kottapalli *et al.*, 2003] presented the requirements of a structural monitoring system for civil infrastructures, such as buildings and defined key issues for design of appropriate wireless monitoring strategy. Their study was focussed on the design

of data acquisition system and communication protocols, which were verified in the laboratory testings. Giurgiutiu *et al.* [Giurgiutiu *et al.*, 2002] proposed the conceptual design of a SHM system for monitoring fatigue cracks and corrosion in the ageing aircraft structure in the laboratory environment.

2.5.1 Instrumentations and measurements

The damage sensitive features are extracted from the measured vibration responses, using a damage identification method discussed in Section 2.4. Therefore, physical quantities most relevant and sensitive to damage in a structure must be selected for monitoring purposes. These are typically accelerations, strains and displacements [Sohn *et al.*, 2003]. Advantages and disadvantages of each of these quantities have to be put in accordance with the specific situation of monitoring.

Accelerometers are extensively used to measure the vibration responses of the test structures in a SHM system [Doebling *et al.*, 1996]. These accelerometers measure time series acceleration responses, which are used to extract the natural frequencies and mode shapes using Fast Fourier Transform described in Appendix F. The measured acceleration values are converted into the mode shapes by using a suitable numerical integration technique as described in Appendix G.

Strain, other physical quantity used in a SHM system, is measured by using strain gauges and fibre-optic sensors. Strain is locally quite sensitive to damage. It may be used when the damage location is known and their allowable limit for damage is relatively large [Boller, 2000]. However, a large number of strain gauges would be required to monitor a large structure, resulting in a complex and bulky system with many wires. This situation can be avoided by placing strain gauges at few selected locations or a wireless sensor network. The strain measurements are subsequently processed by techniques discussed in Section 2.4 such as Artificial Neural Network (ANN) [Sahin & Shenoi, 2003a,b], and Wavelet Transform [Dawood *et al.*, 2003, 2004a,b] to obtain damage information.

Other measured quantity of interest in a SHM system is direct displacement measurement. Many SHM systems measure displacement of the test structure directly by using displacement sensing devices such as Laser Doppler Vibrometry (LDV) [Zak *et al.*, 1999; Zimmerman, 1999], Continuously Scanning Laser Doppler Vibrometry (CSLDV) and Piezoelectric transducers [Martin *et al.*, 1999]. These are a non-contact vibration measurement techniques, which focus the laser beam on the structure and scattered back to these equipments. Typically, these reflected waves are measured by

the equipments, which may need to be positioned in a certain way. Another restrictions are the weight and cost of the equipments. Hence, the requirement to position the equipment in a certain manner and their weight restrict their use in a real-time SHM system. Sometimes, specimens also need special surface preparation. These limitations restrict their use in the real-time SHM system.

Sensing technology is one of the most rapidly evolving technology in SHM. Therefore, one must always be aware of new technologies that are applicable in SHM applications. These include Micro-electro-mechanical Systems (MEMS), piezoelectric (PZT) actuators/sensors and fibre optic strain sensors.

2.5.2 Data pre-processing and feature extraction

Generally, measured signals, discussed in Sub-section 2.5.1, are processed to be used by damage identification methods reviewed in Section 2.4. Signal processing relevant to a SHM system are noise reduction, data normalisation and features extraction. The simplest method for noise reduction is local and/or global averaging. However, this area of signal processing uses a variety of different techniques. Most of these techniques are used for data smoothing and de-noising. Smoothing can be implemented by using filtering or fitting techniques. The best fit polynomial of a data set is a smoothing process, in which the number of fitted coefficients is usually much less than the number of analysed data. Also, there exists a number of low pass filters to smooth the data. These are Weiener filter, based on the Fourier Analysis and Savitzky-Golay [Press *et al.*, 1992], least-squares [Hamming, 1989] and digital smoothing polynomial [Press *et al.*, 1992] filters. Recently high pass filters such as a wavelet analysis is used to find the coefficients related to undesired features from the signals [Staszewski, 2002].

A structure is often subjected to changing environmental and operational conditions often caused by the changes in loading, boundary conditions, temperature, and moisture. These variations may introduce noise in the signals, which are minimised by a noise reduction technique. Feature extraction is the other important step in signal processing in a SHM system, which refers to the process to obtain information from measured data through signal processing. There are different methods for feature extraction [Staszewski, 2000]. Simple extraction methods are based on a data condensation process.

2.6 Characteristics of real-time SHM and control systems

Some of the structural health monitoring systems reviewed in Section 2.5 monitor responses of the structures continuously and autonomously; however, these are still based on the "black-box" concept. This implies that the measurements are not used to make decisions during normal operation and are typically available and analysed during a scheduled inspection or after an accident. Hence, there is a need to improve these SHM systems with improved performance characteristics. In this section, the characteristics of such a system are identified.

A real-time SHM and control system needs to perform various tasks such as data acquisition, data pre-processing, data fusion, data analysis, and visualisation for damage identification in a structure. The importance of these tasks in structural health monitoring are highlighted by Staszewski [Staszewski, 2002] and suggested further investigation by developing a system architecture. This requires a well planned system architecture to integrate all the components performing various tasks in a pre-defined sequence. Based on these tasks, desirable characteristics of a real-time SHM system can be identified as follows:

- Sensor network for data acquisition from sensors such as acceleremoters must be designed, to acquire measurements and should be scalable to incorporate any future requirements.
- It should have a reliable communication system to transmit sensors' data to a data management system. A reliable communication system will ensure that the sensor data will be stored, even if a part of communication system failed due to any fault in the communication network.
- It should have a data management system to manage the data measured from the data acquisition system.
- It should have a well defined strategy to meet the computational power required for signal processing, such as pre-processing of accelerometers' data for estimation of vibration responses such as natural frequencies and mode shapes of a structure.
- There should be automated mechanism for data fusion into the damage identification calculation after signal processing tasks.

- It must have an in-built control system to raise the alarm if damage severity exceeds a pre-defined critical limit and to send a control signal to the users and data management system.

2.7 Limitations of published work

The literature review in Section 2.4 reveals the existence of a huge amount of literature for damage identification in different types of structural materials and topologies. However, there are few published works relevant to sandwich structures. In this section, the limitations of the published work relevant to sandwich structures will be identified in Sub-section 2.7.1, followed by limitations of a SHM system in Sub-section 2.7.2. The limitations of SHM systems gain significance for development of a real-time system, as it can severly affect the efficiency of the system. These limitations are concerned with the transfer of data to a data management system, data analysis and alerting the concerned authority/person towards the critical level of damage.

2.7.1 Limitations of damage identification methods

As per the discussion in the previous sections, it appears that development in the damage identification methods have been generally focussed towards isotropic and composite structures; mainly for Levels 1 and 2 as tabulated in Tables 2.3 and 2.4. Usually, these methods are developed for single damage identification with exception of a few for multiple damage identification [Lu *et al.*, 2002; Shi & Law, 1998; Shi *et al.*, 2000, 2002] in isotropic structures. Despite extensive amount of research in vibration-based damage identification [Doebling *et al.*, 1996, 1998; Sohn *et al.*, 2003], there are few research works reported in public domain for a sandwich structure as evident in Table 2.6. These methods have been developed for identification of only one damage mode among few more discussed in Section 2.1. Hence, damage identification of a sandwich beam with interacting damage modes is yet to be addressed. Moreover, most of these methods only identify existence and location of damage except for few, which also quantify the extent of damage [Dawood *et al.*, 2003, 2004a,b]. The quantification of damage gains significance for the identification of the damage mode. This helps in early prediction of the damage as initiation of another damage mode indicates an imminent failure [Renard & Thionnet, 2006]. This can be achieved by predicting the damage severity of the constituents. To this end, there is an apparent lack of literature in public domain for damage severity prediction of a sandwich structure.

2.7.2 Limitations of structural health monitoring systems

In this section, some of the limitations of existing SHM system reviewed in Section 2.5, in context of characteristics outlined in Section 2.6 are identified. These limitations are as follows:

1. The measured vibration data are first stored into the local data acquisition system during the testing. Later on, these data are manually transferred as files to a computational system for their analysis. These files may be transferred through internet or storage media, but both require human intervention. This means that the measured data are not available for immediate analysis, hence restraining real-time damage identification and collaboration among users.

2. There is no focussed approach for an efficient and reliable data management for sensors' data and damage identification results. This limitation restrains future analysis and monitoring of the development of damage.

3. Signal processing and data fusion requires human intervention, which constrains monitoring and control in real-time.

4. Unreliable and insecure communication infrastructure, leading to potential unauthorised access of data and intended attempt to misuse/corrupt data/information.

5. Very little collaboration exists among the users in the decision making process leading to delay in making the decision.

6. No automated control system for raising an alarm after occurrence of a critical damage in the structure.

7. There are very few systematic approaches regarding the integration of various components for a real-time structural health monitoring and control.

These limitations significantly affect the effectiveness and efficiency of the system. The computational and data management aspects in engineering application, are discussed in Chapter 3 and those specific to a real-time SHM and control system, are identified in Section 3.6.

2.8 Conclusions

In this chapter, a brief literature review on different aspects of damage in a sandwich beam was presented. These were mainly damage modes, cumulative damage model, damage identification methods and structural health monitoring system. The following conclusions can be drawn from this review.

- It is shown in Section 2.1 that there are more than one damage modes in a sandwich beam. After initiation of the first damage mode, it continues to propagate causing initiation of the second damage mode as shown in Fig. 2.5. Hence, it is very likely that there will be more than one mode of damage present in a damaged sandwich beam. This phenomenon is also known as interactive damage. It is recognised in Sub-section 2.7.1 that the methods reviewed in this chapter are developed for predicting extent of only one damage mode in a sandwich structure. It appears that there is not any damage identification method published in public domain, which deals with interactive damage mode in a sandwich beam. Therefore, there is a need to develop a damage identification method, which can identify interactive damage in a sandwich beam.

- Natural frequency shift is extensively used for the prediction of damage existence in a structure, i.e. Level 1 of damage identification. Shift in natural frequencies mainly depends on the location, amount and type of damage in a structure. However, it is also true that the natural frequencies of two different damaged beams with damage at the different locations may be same. This is because of the fact that the natural frequencies are the global parameters, representing dynamic characteristics of a sandwich beam. In case of a sandwich beam, occurrence of interactive damage mode further complicates the damage identification procedure by using the shift in natural frequencies. Therefore, in order to perform higher levels of damage identification, parameters measuring local structural responses must be used in damage identification method.

- Displacement mode shapes measure local structural responses of a structure. It is observed in literature review that the mode shapes of the higher modes are more capable of capturing local damage than those of the lower one. However, it is very difficult to measure mode shapes from higher modes. Hence, mode shapes from the first few lower modes will be used for damage identification.

- It is learnt in Sub-section 2.4.3 that the model-based damage identification methods perform better than those of the pattern recognition methods for the higher levels of damage identification. It is specially useful for Level 3 of damage identification in the sandwich beam. Hence, a model-based damage identification method will be formulated in this work. It is proved that modal strain energies are good damage parameter.

From the discussion so far, it is clear that there is a need to develop a novel damage identification method having the features outlined in Chapter 1. This is because of the fact that there is not any damage identification method published in public domain, which deals with interactive damage mode and multiple damage in a sandwich beam. Hence, a model-based damage identification method will be developed for identification of interactive damage mode and multiple damage in a sandwich beam. It is shown in this chapter that modal strain energy is a good parameter for higher levels of damage identification in the isotropic structures. In the first stage, modal strain energy will be used as the damage parameter, to develop the modal-based damage identification method for sandwich beams. At the first stage, damages' extent in the faces and core of the sandwich beam will be approximated. These approximated values will be used as the initial guesses at the second stage. In the second stage, the predictions of damages' extent, obtained from the first stage will be further improved by using the model updating method. Currently, there is no literature available in public domain, which predicts damages' extent in the sandwich beam for interactive damage.

Chapter 3

Grid Technologies : Introduction and Literature Review

Inspired by the electrical power grid's pervasiness and reliability, computer scientists in the mid-1990s began exploring the design and development of a new infrastructure for sharing available distributed computing-related resources. Their efforts lead to the development of a new paradigm in computing, known as grid technologies. Grid technologies enable to harness the power of distributed computing-related resources into a single large virtual system for delivering seamless and reliable access at a single user point to solve specific problems. The available resources may be computing/processing power, data storage, networked file system, application software and scientific instruments. Moreover, in many cases these resources may be shared by large communities of users, pooling these resources from different sites in a single organisation or many institutions. The problems to be solved can involve data processing, network bandwidth, or data storage. From user perspective, this system appears to be a single enormous virtual computing system accessible via a single interface. It implies that the individual resources will not be visible to the user. Here, focus is on sharing the available resources rather than only information as in internet. Sharing of these resources is not constrained by their locations and ownership, i.e. they might be in the same room or distributed around the world at different organisations. They might be running different operating systems on many hardware platforms. In this way, Grid technologies improve resource utilisation and reduce costs, while maintaining a flexible computing infrastructure to cope with changing requirements, yet remain reliable, resilient and secure. Hence, grid technologies enable users to access and/or aggregate potentially large number of powerful and heterogeneous resources, available within and outside of the organisation via a single interface.

Technically, the term "grid" refers to a distributed "cyberinfrastructure" for problem solving in science and engineering, by using a set of computing technologies and infrastructure. These technologies and infratructure enable *flexible, secure and coordinated resource sharing and problem solving in dynamic, multi-institutional virtual organisations* [Foster & Kesseleman, 1999]. In grid technologies applications, the resource sharing is primarily focussed on direct access to computational resources, application software, data and other resources as required in a range of collaborative problem-solving environments. The sharing is made possible by using a set of continuously evolving grid technologies and infrastructure. In such environments, major challenges are user authentication, authorisation, resource access, resource discovery and data management. The chronological evolution of these computing technologies are reviewed in Section 3.1, which is followed by an overview of grid technologies in Section 3.2. The toolkits required for implementing grid applications are presented in Section 3.3, which can be used with a pure Java program by using the commodity toolkits described in Section 3.4. Their usage in science and engineering applications are reviewed in Section 3.5. Finally, the justifications for application of grid technologies in the present work is presented in Section 3.6.

Table 3.1: The generations of computing.

Generation	Characteristics
First (Host-based computing)	1. Dumb terminal. 2. Single server. 3. Monolithic applications.
Second (Remote access)	1. Single client supporting only terminal emulation functions. 2. Single server.
Third (client/server)	1. Single client supporting rules processing as well as user interface. 2. Up to two server.
Fourth (Multitier)	1. Single client supporting rules processing as well as user interface. 2. More than two server tiers.
Fifth (Grid computing)	1. Virtual environment where all systems are considered a pool of resources. 2. N-tier. 3. Service-oriented architectures.

3.1 Evolution in computing

The role of computation is always important in any scientific and engineering application. In past several years, its role has been increasing for solving complex problems, resulting in its continuous development and evolution, motivated by needs to share the available resources for more efficiently and economically. In recent years, computing technologies have evolved rapidly as a result of developments in the Internet technologies, available network bandwidth and inter-connected resources. Their evolution can be classified into five generations, which are summarised in Table 3.1. This section reviews the important technological developments towards internet-based computing and resources sharing.

3.1.1 Distributed computing

The most important objective of a distributed system is sharing of resources efficiently and effectively across one or more organisations. Earlier distributed systems were intended to share computational resources in a local area network by using a simple architecture. Developments in Internet-related technologies enabled the sharing of computational resources beyond a network, spanning across multiple organisations. In order to achieve this, an architecture based on multiple layers is used. Figure 3.1 shows one such architecture having protocol stacks conforming a seven-layer reference model for *open system interconnection (OSI)* adopted by International Standard Organisation (ISO) [Coulouris *et al.*, 2001]. The purpose of each layer of Fig. 3.1 is summarised in Table 3.2. The layering scheme simplifies and generalises the interface between each layer, but at a significant performance cost. In order to minimise the performance cost, a simplified protocol layering scheme as shown in Fig. 3.2 is used in internet-based distributed computing. Each layer provides a service to the layer above it and extends its service to the layer below it. Interaction with/within the n-tier distributed systems are generally based on distributed object technologies with Remote Method Invocation (RMI). RMI is an object-oriented Remote Procedure Call (RPC), with a target method associated with the application components that are registered, identified and invoked as remote objects. Example of such technologies include the Distributed Common Object Model (DCOM), Common Object Request Broker (CORBA) and Java/RMI.

A distributed system shares the computational resources at a limited scale, as few limitations of this technology prevent its scaling to a large scale. Typical problems in this system are lack of inter-operability among resources and their heterogeneity.

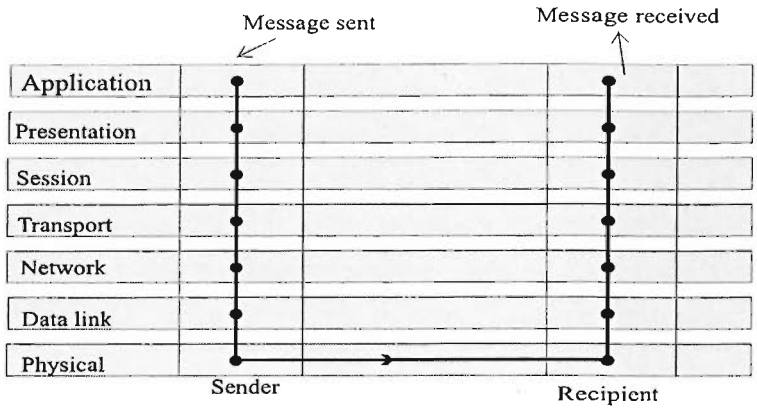

Figure 3.1: Protocol layers in the ISO open system interconnection (ISO) protocol model.

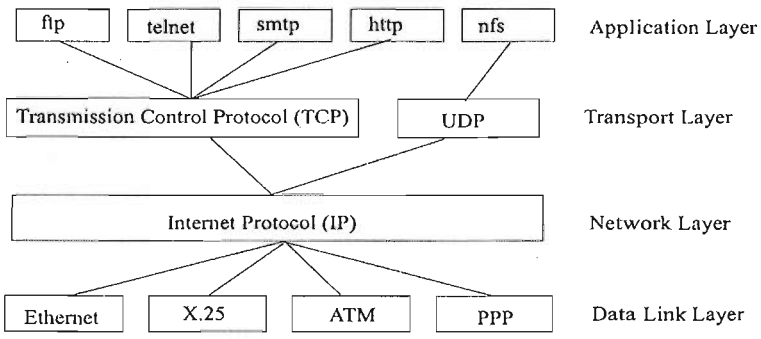

Figure 3.2: TCP/IP architecture in the OSI layer model [Boger,2001].

Table 3.2: OSI Protocol summary[Coulouris *et al.*, 2001].

Layer	Description	Example
Application	Protocols are designed to meet the communication requirements of specific application often defining the interface to a service.	HTTP,FTP, SMTP, CORBA, IIOP.
Presentation	Protocols at this level transmit data in a network representation that is independent of the representations used in individual computers, which may differ. Encryption is also performed in this layer, if required.	Secure Sockets (SSL), CORBA, Data Rep.
Session	All this level reliability and adaption are performed, such as detection of failure and automatic recovery.	NetBIOS, RPC
Transport	This is the lowest level at which messages (rather than packets) are handled. Messages are addressed to communication ports attached to process. Protocols in this layer may be connection oriented or connectionless.	TCP, UDP.
Network	Transfer data packets between computers in a specific networks. In a WAN or an internetwork, this involves generation of a route passing through routers. In a single LAN, no routing is required.	IP, ATM, Virtual circuits.
Data link	Responsible for transmission of packets between nodes that are directly connected by a physical link. In a WAN, transmission is between pairs of routers or between routers and hosts. In a LAN, it is between any pair of hosts.	Ethernet MAC, ATM Cell transfer ,PPP

Problem of inter-operability arises due to the different platforms of implementation and the programming environments. In many cases, the proprietary hardwares and softwares do not inter-operate and collaborate among themselves.

3.1.2 Large scale web-based resources sharing

The emergence of World Wide Web (WWW) facilitated the large scale sharing of information and resources. The WWW is an evolving system for publishing and accessing information/services over the internet. The web provides "a shared information space through which people and computers communicate", where hypermedia resources, such as texts, audios, videos, photographs and computer graphics can be shared among geographically distributed users and heterogeneous computer systems. This feature is of great importance in the development of the Grid technologies. Over time, the web has developed beyond simple data resources sharing, without changing the basic system architecture. The web is based on three main technological standards, namely, HyperText Markup Language (HTML), Uniform Resource Locators (URL) and HyperText Transfer Protocol (HTTP).

3.1.3 Peer to Peer (P2P) resources sharing

P2P networks are well-known for the use of content sharing, which allow internet users to share files of their choice among P2P communities. A notable limitation with this technology is that the availability of resources is not always guaranteed, as sharing is totally under the control of an individual participant. Architecture of P2P is client-oriented, which means that the operations are mainly carried out by clients (peers); whereas, servers are in a subservient position, or not needed at all. This architecture makes a P2P network loosely coupled. An advantage is that participants in the P2P network can join or leave the network at any time of their choice, without affecting the overall system. Another advantage of P2P networks is collaborative computing, which enables the users to work together for a joint project across geographical boundaries. The technologies used in this network are TCP/IP, HTTP and URL. Thus, the technologies, enabling P2P network, can be used for sharing of hardware resources, such as idle CPU cycles.

3.2 Overview of Grid technologies

Distributed technologies as described in Section 3.1 provided foundation for the development of grid technologies, which are often termed as latest generation of distributed computing environments. The grid technologies are a set of computing technologies used for the co-ordinated collaboration and resources sharing environment. The differences between a conventional distributed system and grid technologies are summarised in Table 3.4, which shows that grid technologies offer more advantages than any single technology refered in Section 3.1. Table 3.3 compares the technologies discussed in Section 3.1 with respect to the features of the grid technologies. In the words of Foster *et al.* [Foster *et al.*, 2001], the term Grid is defined as *"Flexible, seamless, and secure resource sharing and co-ordinated problem-solving within and across organisation."* A grid is characterised by heterogeneous environment, diverse application models, vast system scale and co-ordination among the resources.

Table 3.3: Comparison of the computing technologies with respect to requirements for the Grid.

	Distributed computing	Internet	Peer to peer computing
Flexibility	No	Yes	Yes
Seamless	No	Yes	Yes
Security	Yes	No	No
co-ordination	Yes	No	Yes
Centralised control	Yes	No	No

To simplify and clarify the definition of a grid, a three point checklist is proposed to distinguish it from other distributed computing system [Foster, 2002b]. These three criteria are,

1. Co-ordinate resources that are not subjected to centralised control,
2. Using standard, open, general-purpose protocols and interfaces,
3. Deliver nontrivial qualities of service.

The first two criteria in the above checklist are self explanatory. The third criterion specifies the various qualities of service delivered by the grid system to the users. These qualities of service are response time, throughput, availability, security and co-allocation of mutiple grid resource types to meet complex user requirements. These

Table 3.4: Comparison of conventional distributed environments and Grids [Németh & Sunderam, 2003].

	Conventional distributed environments	Grids
1	A virtual pool of computational nodes.	A virtual pool of resources.
2	A user has access to all the nodes in the pool.	A user has access to the pool but not to individual nodes.
3	Access to a node means access to all resources on the node.	Access a to resource may be restricted.
4	The user is aware of the capabilities and features of the nodes.	The user has little or no knowledge about each resource.
5	Nodes belong to a single trust domain.	Resources span multiple trust domain.
6	Elements in the pool 10-100, more or less static.	Elements in the pool $\gg$ 100, dynamic

qulities of service are delivered in such a manner that the utility of the combined grid system is significantly greater than that of the sum of its constituent system [Foster, 2002b].

Continuous research and development in grid technologies will continue to evolve. But it can be assumed that the essential features described in the above checklist is expected to remain same.

3.2.1 The Grid architecture

Grid architecture can be thought of as a stack of layers, similar to that of a distributed system. These layers are based on the standard protocols, which form the core of the grid and are essential for inter-operability of resources as shown in Fig. 3.3. At the lowest level, i.e. the fabric layer in Fig. 3.3, various grid resources that grid users want to share are connected. These resources may be computational, storage, network, instruments and sensors. Their implementation is specific to the resource only. The minimum implementation requirements in a grid application are enquiry mechanisms and resources management mechanisms [Foster, 2002a]. Enquiry mechanisms enable a user to discover structure, state and capabilities of resources; whereas, resource

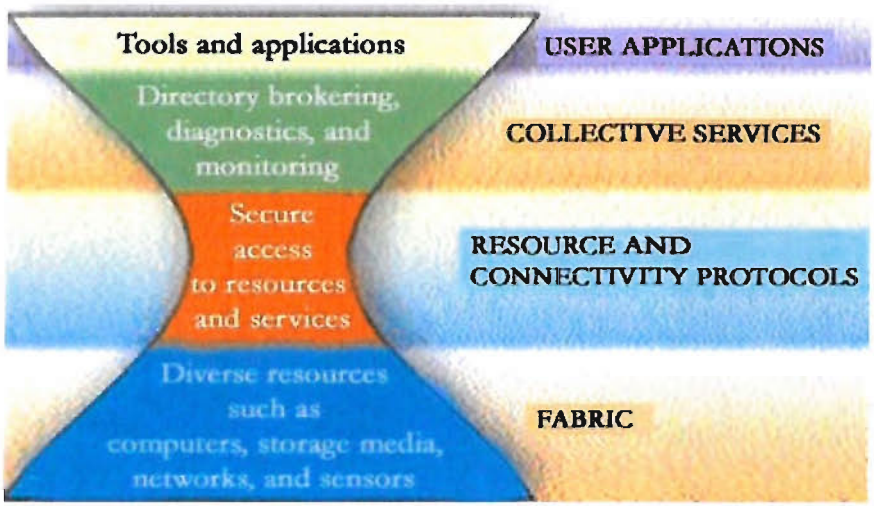

Figure 3.3: Layers in Grid architecture [Foster, 2002a].

mechanisms provide some control over the delivered quality of service. The fabric layer is connected to the next higher layer through the resources and connectivity protocols. Combination of these protocols forms a layer for secure access to the resources and services, which is also termed as *hour glass mode.* Resources are accessed by using the communication protocols; whereas, security is implemented by using the authentication and authorisation protocols. Authentication protocols provide cryptographic secure mechanisms to verify the identity of a user and permission to access resources. The next higher layer provides the collective services, which are global in nature and capture interaction among the collection of resources. Protocols used in these layers range from general purpose to highly application/domain specific. The final layer in a grid architecture comprises of the user applications. Functions of each layer in Fig. 3.3 is summarised in Table 3.5. The features of a grid architecture can be summarised as follows,

- Inter-operability at all levels among the heterogeneous resources.
- Future scalability and adaptability.
- Decentralised and loosely-coupled system structure.
- Rapid deployment and participation.

Table 3.5: The function of each layer in a Grid architecture.

Collective	Resource discovery, resource brokering, system monitoring, community authorisation, certificate revocation.
Resource	Access to resources connected at the fabric layer. access to information about system structure, state, perfomance.
Connectivity	Communication, service discovery, authentication, authorisation, delegation.
Fabric	Storage systems, computers, networks, code repositories, catalogs.

3.2.2 Open grid service architecture

The reason for the development of Open Grid Service Architecture (OGSA) is the need to define standards for integration and inter-operability among the resources in grid applications. To achieve this, OGSA defines the grid service concept, based on the principles and technologies from both the grid computing and Web services communities. In recent years, various toolkits and software environments for deployment of grid applications have been developed. Some of these are Legion(www.legion.virginia.edu), Condor(www.cs.wisc.edu/condor), Unicore(www.unicore.org), and Globus(www.globus.org). Among these, the Globus toolkits are the most widely used in scientific and engineering grid applications, and are becoming a de facto standard for implementation around the world. The toolkits provide security, information discovery, resources and data management, communication, fault detection and portability services, which are based on the framework of OGSA [Foster *et al.*, 2001].

Web services describe the software components to be accessed, methods for accessing the components and a discovery method that inform users and applications to identify relevant service providers. Web services are independent of programming languages and system software. The objective of web services and OGSA is to enable inter-operability among loosely coupled services independent of implementation, location or platform. OGSA defines standard mechanisms for creating, naming, and discovering the grid services; provides location transparency and multiple protocol bindings for service; and supports integration with underlying native platform facilities. Hence, OGSA aims to define a common resource sharing model that is an abstract representation of resources, such as computers; data storage & file system; and logical resources. It provides some common operations and supports multiple underlying resource models representing resources as a service.

Web services are implemented by using a number of open standard or industry standard technologies, which are summarised in Table 3.6.

Table 3.6: Technologies used in Web services and their functions.

Technology	Function
Extensive Markup Language (XML) and its schema	To structure documents and data for data storage, database access, and exchange.
Service-Oriented Architecture Protocol(SOAP)	Exchange structured data between two end points in a distributed environment.
Web Services Description Language (WSDL)	Used to describe the characteristics of web services.
Universal Description, Discovery and Integration (UDDI)	Enable publication and retrieval of information about web services.

3.3 Grid middleware - Globus Toolkit

Based on OGSA, various toolkits for deployment of grid applications are developed. The most popular among them is the Globus Toolkit (GT), which provides protocols and services for the development of grid applications. GT offers core grid services for communication, security, resource access, information management and brokering, which are built around standard protocols and services, to allow their seamless integration with an existing network. A Globus-based grid application can be spread over several administrative domains and may span multiple organisations.

The GT is released under a public license permitting the distribution and use of the binary and source code of the toolkit. Partly due to the open license, but also due to the other characteristics, the Globus Toolkit has a large tools and user base. It is used in the majority of grid applications across the world. The wide acceptence and use of the GT makes it a de-facto standard for grid computing.

3.3.1 Toolkit architecture and components

GT provides middleware services at the neck of the hourglass model shown in Fig. 3.3. This architecture enables secure access to heterogeneous underlying grid resources. GT provides following services,

1. Security : the Grid Security Infrastructure (GSI),
2. Resource Management : the Grid Resource Allocation Manager (GRAM),
3. Data Management : the Globus Access to Secondary Storage (GASS),
4. Information Infrastructure : the Metacomputing Directory Service (MDS).

Globus Toolkit can be installed on a wide variety of operating systems such as Linux, AIX, Solaris, and Irix.

3.3.2 Security services

The core component of GT is Grid Security Infrastructure (GSI). All other Globus services use GSI for authentication and authorisation to use available resources. However, GSI can be deployed independently from the other toolkit components. GSI is also being used in a GSI-enabled secure-shell implementation. GSI uses a Public Key Infrastructure (PKI) for mutual authentication among users, services and resources, based on X.509 public key certificates. An access request is authorised, if a resource has an entry in its grid map file for the authenticated global identity presented with a request by an user, which is then mapped to a corresponding local user-id and finer grain authorisation is left to the local resource operating system mechanisms. This enables GSI to be embedded seamlessly on top of existing systems, to provide uniform credentials and certification infrastructure, without compromising local security mechanisms.

GSI also offers single sign-on capability through the use of proxy certificates (PC) [Welch *et al.*, 2004]. A proxy certificate is derived from a user certificate or another PC, which is then used to delegate the user authority to resources for a limited time period. The proxy certificate is then used to authenticate a user to remote resources. Access to the confidential user credentials is only required at initial log-on, i.e. at the time of proxy creation. A short life span of the proxy certificate ensures the protection against the misuse of user credentials.

3.3.3 Resource management

Resource management services in a grid application are provided by the Globus Resource Allocation Manager (GRAM), which consists of a "gatekeeper" and a "jobmanager" module executing on a resource's job scheduling system. GRAM is a fundamental

$(count = 5)$
$(jobType = MPI)$
$(directory = /home/manojk/testapp)$
$(executable = /home/manojk/bin/myexecutable)$
$(arguments = -finput.dat)$
$(stdout = testout.dat)$

Figure 3.4: A Sample RSL description.

GT service enabling remote users to instantiate, manage and monitor the computational jobs on remote resources securely. User instantiates a job by describing details, such as the name of the executable, the working directory to store input and output and the job manager, by defining a set of "attribute-value" pairs in the the Globus Resource Specification Language (RSL) script. A sample RSL job description for a parallel job using five nodes on a grid resource is shown in Fig. 3.4. This job is submitted by the user with the authentication proxy credential having authorisation to use the resource. This task is performed by saving the RSL script in a file (e.g. MyJob.rsl) and submitting it to the resource's GRAM using command,

```
globusrun -r pacifica.iridis.soton.ac.uk/jobmanager-pbs MyJob.rsl
```

Apart from job submission, GRAM also provides services to monitor and control the overall job life cycle. Two higher-level components that also fall into the resource management category are the General-purpose Architecture for Reservation and Allocation (GARA) and the Dynamically Updated Request Online Co-allocator (DUROC).

3.3.4 Data management

Access to remote data is an important requirement for many grid applications. Existing technologies like standard FTP, can neither efficiently provide the desired functionality nor the security required by grid applications that access large volume of data

on remote resources. Furthermore, data transfers may need to be performed across institutional boundaries and their firewalls. To support these types of applications, GT provides protocols built on by extending existing Internet protocols, which are described in the following paragraph.

Globus Access to Secondary Storage (GASS) provides data transfer capabilities based on the HTTP and HTTPS protocol. GASS clients and servers are used when executables and data files have to be staged to remote grid resources and for the redirection of input and output streams to remote processes. GridFTP, a grid enabled FTP protocol includes features for efficient data grid operations like parallel data transfers, partial file transfers, stripping across several grid nodes and third-party data transfers with data channel authentication (DCAU). Both GASS and GridFTP use the GSI as described in Sub-section 3.3.2 for authentication and authorisation.

3.4 Commodity Grid toolkit - Java CoG

Commodity toolkits emphasise use and reuse of the existing software codes/applications in user (especially desktop) environments. One of such existing software/application is application based on grid technologies, i.e. Globus as described in Section 3.3. The user environments in the present work are distributed computing frameworks, industry standard database management system, object-oriented programming languages & frameworks. Hence, commodity toolkits enable application of Globus in user environments without its installation. A Commodity Grid Toolkit (CoG Kit) defines and implements a set of components that map grid services available in Globus to a commodity environment, i.e. Java CoG [Laszewski *et al.*, 2001]. Their combination of commodity environment with grid technologies, have potentials to enable a whole range of exciting new applications, to connect advanced network-enabled resources into commodity desktop. A CoG kit maps the grid services as described in Section 3.3 into specific commodity environments and frameworks. Here, *mapping* is concerned with not only an interface definition but also the way in which grid concepts and services are best expressed in terms of concepts and services of a particular commodity framework.

In Java CoG toolkits, the capabilities of Globus toolkits described in Section 3.3 are provided via Job objects and Java events. A large number of packages and classes are required to access the necessary functionality of the Globus toolkit. However, only a subset of all available packages and their general functionalities that is useful in this work will be described. These packages provide the interface to the low level grid

services and application interfaces, which are used to develop the Java program in the present work.

RSL: The package `org.globus.rsl` provides methods for creating, manipulating and checking the validity of the RSL expressions used in Globus to describe resource requirements. The argument to a new call includes parameters specifying the characteristics of the required resources and the properties of the computation. An example of embedding RSL in a Java program is given as,

```
RSL rsl = new RSL("(executable=FFTanalyse.exe)
(directory=/manojk/temp)")
```

GRAM: This service is available in the package `org.globus.gram` to map the Globus GRAM services, which is used to schedule and manage remote computations. Various classes and methods are used to submit jobs, manage already submitted jobs and cancel jobs on the computational resources. Some methods also control access of users to specific resources by using a Globus gatekeeper and a monitor of the job status (*pending, active, failed, finished and suspended*). A job is submitted to computational resources by issuing command through the runtime method of Java. This method provides an easy way to utilise grid technologies by using pure Java program.

GASS: GASS stands for Global Access to Secondary Storage service, which simplifies the porting and running of applications that use file I/O, without the need to manually log into the storage resources and files [Bester *et al.*, 1999]. This service is available in the package `org.globus.gass` to support the copy and transfer of files between computers on which Grid services are installed. The Java CoG command `globus-url-copy` copies a file from one file server to another. It can also be used to stage data to a computational resource prior to job execution.

GSI: This service provides a secure method for accessing remote grid resources [Butler *et al.*, 2000]. It enables secure and single sign-on capabilities, while maintaining local control over access control policies and local security mechanism. This service is included in the package `org.globus.security` to develop client- and server-side applications requiring access to GSI-enabled resources.

GSI-FTP: This service securely transfers files in a grid application [Butler *et al.*, 2000]. It is an extension of the standard FTP protocol and supports third party file transfer, i.e. files can be transferred directly between servers while the user controls the transfer from a third machine. The package `org.globus.io.ftp` provides all the necessary functions such as copying and getting files and listing directories. This method is executed by using a Java CoG command `cog-file-transfer`.

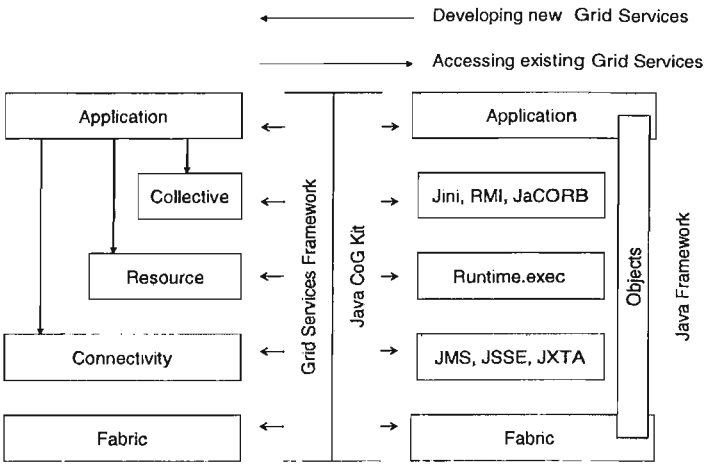

Figure 3.5: Relationship between grid services and Java CoG kit [Laszewski *et al.*, 2002].

The Java CoG Kit is general enough for the design of various advanced grid applications with different user requirements. Java CoG toolkit enables the rapid deployment of grid applications by bridging the gap between grid technologies and commodity development environments; hence, enabling each to use the other's services to develop grid applications based on Java technology and to expose higher-level frameworks to the grid community while providing inter-operability [Laszewski *et al.*, 2002]. This is achieved by providing a rich set of classes, libraries and frameworks in Java programming language, for development of middleware to access the basic grid services, without compromising their capabilities. Some of the classes and libraries in pure Java are shown on the right side of Fig. 3.5. On the left side, the grid services available in Globus are depicted. The middle column shows the Java CoG toolkit and framework required to access the grid services using Java. In this middle column, Java classes and libraries embedding Grid services framework are implemented. These classes and libraries are integrated with pure Java, so that these can be used with the other Java's classes and libraries in user environmets. Hence, Fig. 3.5 shows the manner in which the the grid services described in Section 3.3 are accessed by using Java CoG toolkit. The relationship between the grid services and Java CoG is shown in Fig. 3.5. Thus, Java CoG toolkit will be used to deploy the real-time structural health monitoring and control system having characteristics identified in Section 2.6.

3.5 Literature review of applications

Grid technologies differ from conventional distributed technologies in the sense that these focus on the large-scale resource sharing and problem solving in dynamic networked environment spanning across multiple organisations. This implies that the resources owned by multiple organisations can be pooled seamlessly for large scale resources sharing. Thus, grid technologies can be used as an effective infrastructure in applications requiring high-performance computing and data processing capabilities. Typical grid applications include [Talia, 2002],

1. Intensive simulations on a single high throughput remote supercomputers,
2. Co-operative visualisation of very large scientific data sets,
3. Distributed processing for computationally demanding data analysis using globally distributed computers, and
4. Coupling of scientific instruments with remote computers and data archives.

First and third applications are related to the use of the computational resources for data analysis in the grid applications. However, there is a fundamental difference in their management and access control. In case of the first application, a high throughput remote supercomputer is completely under control of one organisation. Its access and use are completely managed by one organisation. However, the third application uses the heterogeneous computational resources spread across several organisations. Their access and use are managed by the concerned organisation.

Their application areas include high-energy physics research, earth system modelling, drug discovery and design, multi-disciplinary optimisations, condition monitoring, etc. A list of application areas and the name of related grid projects are given in Table 3.7. The projects listed in Table 3.7 are indicative only and does not include all the undergoing projects around the world. An exhaustive list of the grid projects can be found at the Globus website, www.globus.org/alliance/projects.php.

High energy physics research generates petabytes of experimental/numerical data for analysis. It is expected that Large Hadron Collider (LHC) experiments will start generating approximately 40 TB/sec of experimental data for 10-15 years from 2006 [Avery, 2002]. These data need to be stored at very high rates (from 100Mb/sec to 1GB/sec). Although, a large fraction of data will be redundant, but there will be still few petabytes of data per day. Existing data storage and processing facilities at CERN

Table 3.7: The major grid projects and its application areas.

Project	Application areas
EUROGRID (EU) www.eurogrid.org	Bioinformatics, climate modelling, computer aided engineering, high performance computing
NEESgrid (USA) www.neesgrid.org	Earthquake engineering simulation and structural dynamics
Particle Physics Data Grid(USA) www.ppdg.net	Particle physics research
NASA's Information Power Grid (USA) www.ipg.nasa.gov	Various engineering disciplines
Grid Physics Network (GriPhyN, USA) www.griphyn.org	High-energy physics research
Grid Particle Physics (GridPP,UK) www.gridpp.ac.uk	Particle physics research
AstroGrid(UK) www.astrogrid.org	Astro physics and Astronomy research
DOE Science Grid (USA) www.doesciencegrid.org	Large scale scientific simulations
TeraGrid (USA) www.teragrid.org	Large scale scientific and engineering simulations
Biomedical Informatics Research Network (USA) www.nbirn.net	Biomedical and bioinformatics research

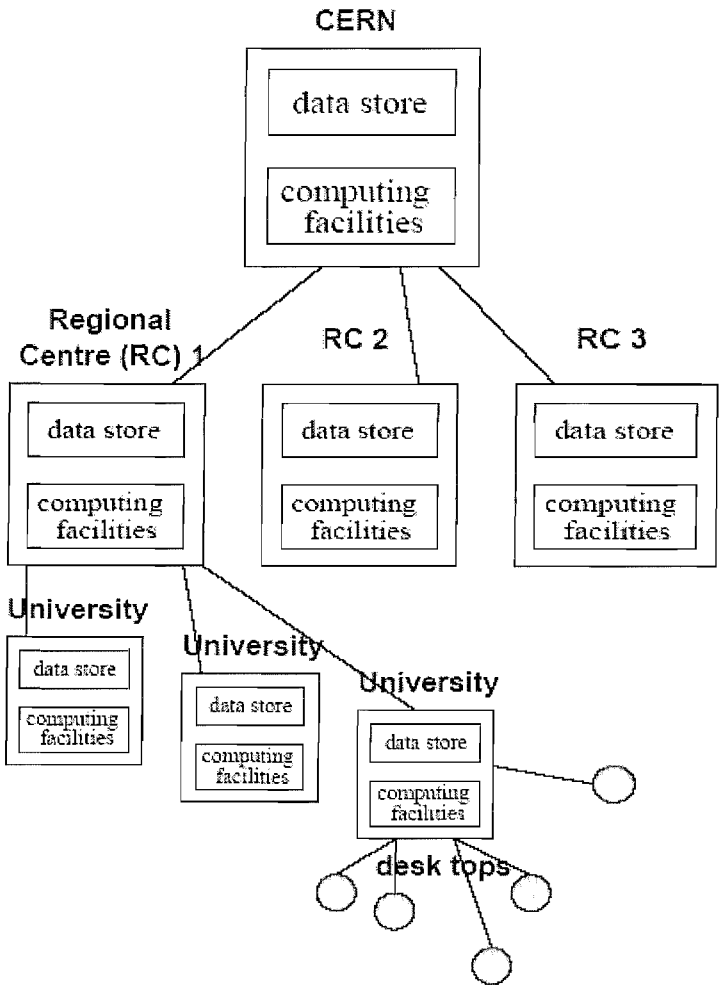

Figure 3.6: Scheme for sharing of data and computational resources in LHC experiment [Hoschek *et al.*, 2000].

can handle at most a third of the requirements, while remaining requirements shall be fulfilled from partner's resources termed as Regional Centres (RCs) [Avery, 2002] as shown in Fig. 3.6. This architecture not only provides computing and data resources, but also enables analysis of the data outside CERN, with a reasonable response time rather than accessing all data at CERN. The proposed architecture is implemented by using Globus and forms a part of International Data Grid Project [Avery, 2002; Hoschek *et al.*, 2000]. Storage Resource Broker (SRB) is used to access data stored in the heterogeneous data storage system at CERN and RCs. Another similar project using grid technologies is being implemented at Stanford Linear Accelerator [Keahey *et al.*, 2002].

Earth system modelling is also a data and compute intensive application. One such project is Grid ENabled Integrated Earth (GENIE) system modelling, which aims to share distributed data from simulations and provides a high-level access to the system by creating and supporting virtual organisations [Gulamali *et al.*, 2003; Price *et al.*, 2004]. The computational requirements are fulfilled by using Condor. The large volume of data generated from the simulations are managed by a MATLAB^{TM} based data management toolkit, named Geodise Database Toolkit. This toolkit is based on the web services, which uses database technology to allow additional information (metadata) to be associated with the produced data. The grid technologies are also applied by other researchers for earth system and climate modelling [Ananthanarayan *et al.*, 2003; Chervenak *et al.*, 2003].

Engineering design search and optimisation is another computationally intensive application, which is well suited to grid technologies. This application extensively uses the analyses involving Finite Element Analysis (FEA) and Computational Fluid Dynamics (CFD) applications. It involves a number of variables and iterative calculations requiring significant computational resources. The various low-level functionalities such as authentication, resource management, job submission, etc., are provided by using Globus [Song *et al.*, 2003]. These functionalities are interfaced to end users via commodity technologies such as Java CoG, Python, Perl, etc. Access to the database in GEODISE is provided through the web services by using SOAP for transfer of data between the end points. Other similar engineering applications include FE simulation of a mechanical device [Wei *et al.*, 2004a] and structural dynamics simulation for earthquake engineering research [Kesselman *et al.*, 2003], as a part of the consortium called NEESgrid (www.neesgrid.org). NEESgrid is developed for collaboration among researchers of earthquake engineering research communities. Using NEESgrid,

an architecture for hybrid experiments using earthquake engineering simulations is developed [Spencer *et al.*, 2004].

Fault identification and diagnosis are applicable across various application domains such as transport, marine, aerospace and mechanical. All these applications share similar characteristics such as sensors' measurements, high volume of data for analysis, distributed sensors placement and are often business critical. These characteristics make the applications suitable for grid technologies. Monitoring of an aero-engine may generate up to 1 Gigabyte of data per flight and if scaled up to fleet level, it will be in Terabyte [Jackson *et al.*, 2003]. These data must be analysed within a reasonable time frame to meet the operational demands. A step further, modelling of the entire commercial airspace of the USA is being carried out by using the grid technologies [Johnston, 2002]. In this project, aircraft sub-systems are modelled and combined with the sytem simulations of the aircraft, and then integrated into an operational air space [Johnston, 2002].

3.6 Why use Grid technologies in the present application?

In this section, justifications behind the application of grid technologies, in the development of a real-time structural health monitoring and control system will be presented. Objective of this innovative approach is to improve the functionalities of a SHM system, described in Section 2.5 for an efficient operation and maintenance of a structure.

A SHM system monitors the responses of a structure to assess its current status of damage, using procedures and methods described in Chapter 2. However, capabilities of a SHM system needs to be enhanced in order to overcome the limitations identified in Sub-section 2.7.2, to incorporate the desirable characteristics outlined in Section 2.6. These limitations are of similar nature like those faced by applications reviewed in Section 3.5. Foremost among these limitations in a SHM system are existence of the large amount of experimental measurements, which remain near the monitoring location. If a structure is located at remote location then these measurements are unavailable for real-time analysis by the damage identification method. Apparently, this limitation is because of the lack of effort to integrate instruments and sensors on a structure with the communication network and computational resources. Real-time unavailabilities of experimental measurements restrict real-time damage identification calculation, hence the real-time capabilities in a SHM system. This limitation can be partly attributed

to the lack of any concentrated effort to transfer these data in real-time to a database management system, which significantly improved many applications as discussed in Section 3.5. In the present application, the database management system will also provide an innovative solution for reliable and secure transmission of data across network and also facilitate collaboration among users. The amount of data may vary widely across different SHM systems depending on the number of sensors, but it may be approximately a Giga Bytes per day [Hall, 1999], posing challenges for processing and managing these data. In a real-time system, the time required for processing and analysis to extract the desired information such as damage information in the present system, is the most important task; hence, it demands a high performance computing system.

It can be concluded that a real-time SHM and control system is a computation and data intensive problem. It is shown in Section 3.5 that similar type of problems were solved by using grid technologies, providing an attractive approach to overcome the limitations in Sub-section 2.7.2. Some of these limitations are attributed to the lack of technologies [Worden & Dulieu-Barton, 2004]. Solution to these limitations can be provided by grid technologies based approaches, which relate to computation, data transfer and data management in a real-time SHM and control system and directly influence its efficiency. Hence, it is decided to use the toolkits based on grid technologies in the following ways in the present work,

1. Available network bandwidth can be used to transfer large amount of sensors' measurements, i.e. accelerometers' readings from the test specimens in the laboratory to a control station in real-time, for processing by damage identification method.

2. Distributed data storage resources can be used to store the data generated from accelerometers on the structure, at an affordable cost. A proper data management system is probably the most important requirement of a real-time SHM and control system, as these data contain all the information regarding existence, location, extent and level of damage.

3. Distributed data storage is aimed to enhance the collaboration among users in decision-making procedure and provide backup against any form of failure or accident at one site. In this case, the security of information is crucial, which is essential in order to prevent unauthorised access to data and corruption of the

data, eventually making these data useless. Security service provided by grid technologies such as certificate based security discussed in Section 3.3, can be used to make data secure by controlling access.

4. In a real-time system, the efficiency and robustness depend on the time required for processing and analysis of resulting data, for extraction of damage information. Here, computational resources across a grid can be exploited by using grid technologies, as described in Section 3.3 to perform data pre-processing related damage identification calculation, at an affordable cost in near real-time.

5. In view of continuous damage progression in a sandwich beam, it is desirable to perform damage identification calculation periodically without any human intervention. This requires automated processing of data and damage identification computation, which can be achieved by the scheduler technologies available in a database system.

6. A control system in a real-time SHM and control system can be activated automatically if a damage endangers safety of the structure. This is an important task requiring reliable, secure and high-speed communication network, which are provided by grid technologies and are being used by researchers in many applications as explained in Section 3.5.

These capabilities can be achieved by developing and implementing a system, by using the grid technologies discussed in Sections 3.3 and 3.4. The system architecture for this purpose will be developed in Chapter 8.

Chapter 4

Research Methodology

This work presents the development of damage identification method for a sandwich beam and implementation strategies for a real-time structural health monitoring and control system, by using a toolkit based on grid technologies. The basic components of this system are damage identification method, data acquisition and signal processing unit, data management system and control system. In a vibration-based damage identification method, it is essential to have an accurate numerical model of the undamaged beam. This model is used to simulate different damage scenarios, for investigation of their effects, on the vibration responses of a sandwich beam. These responses are used to extract the current damage status of a sandwich beam and compare with those of the undamaged beam model. At the same time, it also enables the numerical verification of the damage identification method for many damage scenarios. This method is validated with the experimental measurements obtained from monitoring the vibration responses, by using vibration sensors such as accelerometers. For a better and efficient damage assessment, a system architecture of real-time structural health monitoring and control system needs to be outlined and implemented. It would include the methods for monitoring, acquiring, transferring to remote location and processing of sensors' measurements, to predict the current status of damage by using the damage identification method. The predictions of damage identification method are used as the inputs in the control system to assess their current status of damage. Finally, these components of system architecture are tested to verify their designed objective.

4.1 The proposed methodology

The proposed methodology can be divided into three main parts: development and numerical verification of the damage identification method, experimental validation of

the damage identification method, and implementation of the components in real-time structural health monitoring and control system.

In the first part, methodologies for the predictions of existence, location, extent and level of damage in a sandwich beam are developed and verified, by using numerical simulations. To achieve these, a cantilever sandwich beam model is created by using the Finite Element (FE) beam formulation. Subsequently, this model is used for the modal analysis, to obtain their natural frequencies and mode shapes. The natural frequencies obtained from the undamaged beam model are compared with the experimental natural frequencies, to validate the model. The validated undamaged beam model is then used to simulate the damage scenarios, to create the damaged model of the sandwich beam and obtain their natural frequencies and mode shapes. These natural frequencies and mode shapes of the beam models are used as inputs in the damage identification method. Their outputs are the predictions of existence, location, level and extent of damage in the beam models. Their accuracies are verified by comparing these predictions with the values of the simulated damage cases. After obtaining these predictions, sensitivity analysis of these predictions with respect to location and extent of damage in the beam models is performed. The inputs and steps used for different levels of damage identification are listed in Table 4.1.

In the second part, the sandwich beam specimens with real structural damage are fabricated for experimental vibration testings, to validate the damage identification method. The cantilever boundary condition in the experiments is achieved by clamping one end of the beam specimen in the fixture and then it is excited by using the electrodynamic shaker over a range of frequency. Miniature piezoelectric accelerometers are glued at regular intervals along the centre line of the beam specimen. These accelerometers measure accelerations, from which their natural frequencies and mode shapes are extracted. After processing and normalisation, the mode shapes of the damaged specimen are used for the prediction of existence, location, extent and level of damage in the beam specimen.

In the final part, different components of the real-time structural health monitoring and control system are developed and their implementation techniques based on grid technologies are outlined. These components include the systems to monitor the beam specimen using accelerometers, transfer and storage of these measurements to the remote data storage system along with the analysis of the measured data. In Fig. 4.1, these components are named as data acquisition system, data management system, computational system and control system, which will be developed by using the toolkits

based on grid technologies. Figure 4.1 also shows their role in the overall system, as well as displays how these components are linked with the steps of damage identification and control methods. These components will be tested individually and also as a cohesive system. Control method is numerically characterised and recommendations for its implementation and integration in the real-time structural health monitoring and control system are discussed. Based on the numerical characterisation of the control method, the threshold values are determined to assess the criticality of damage affecting performance of the structure. Finally, the potential applications of this system are outlined.

Table 4.1: The levels of damage identification and method proposed.

Level	Inputs	Method used
1	Natural frequencies Modal strain energy	Reduction in natural frequencies Variation of strain energies
2	Modal strain energies	Comparison of modal strain energies of the undamaged and damaged sandwich beam
3	Modal strain energies.	Processing modal strain energies using damage identification method
4	Predicted location and extent of damage in the face and core	Analysis of these predictions using control method

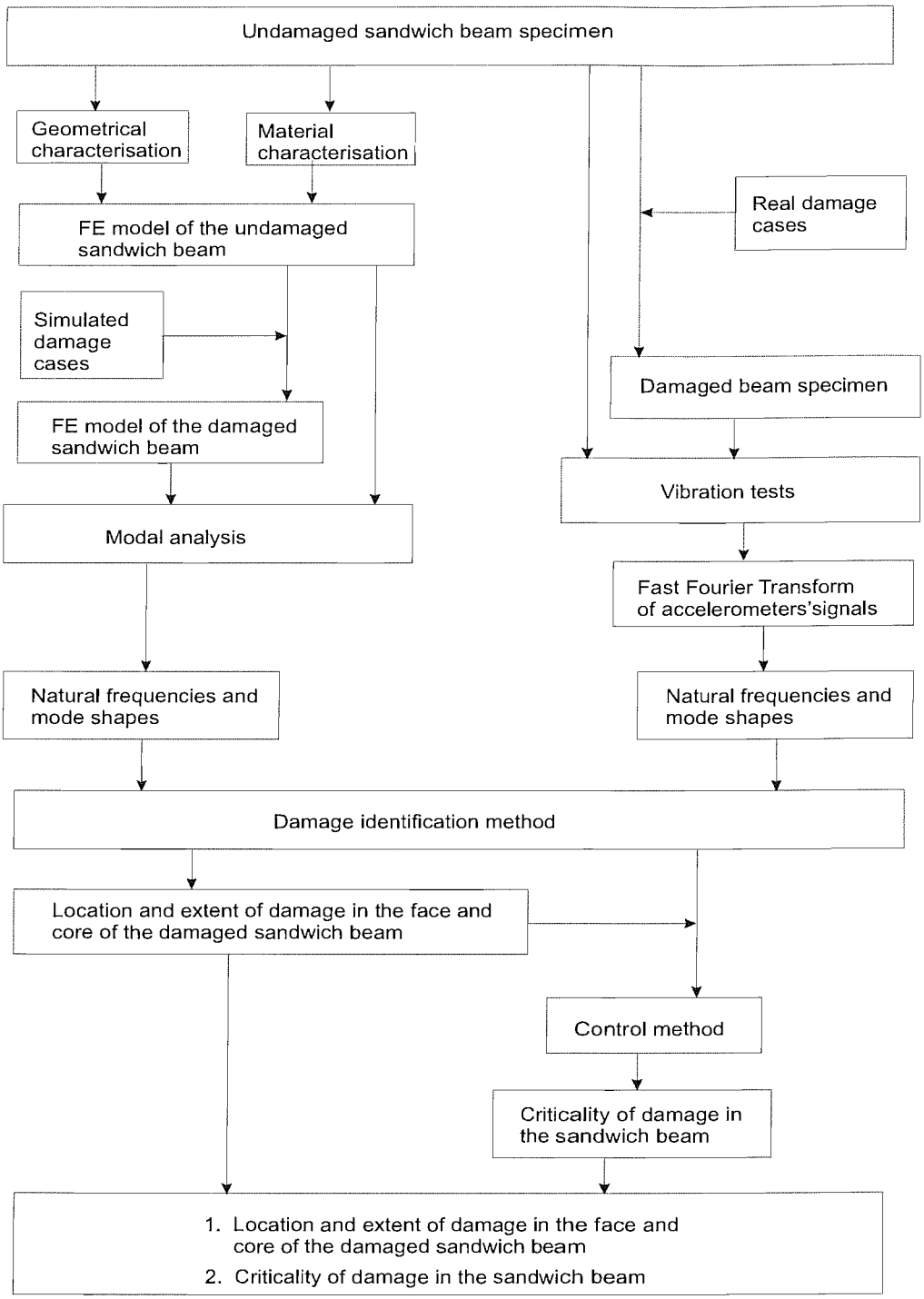

Figure 4.1: Outline of the methods and procedures in the real-time structural health monitoring and control system.

Chapter 5

Proposed Approach

In order to identify the structural damage in a sandwich beam, the development of a vibration-based damage identification method, as identified in Fig. 4.1, is of primary importance. Hence, in this chapter, a vibration-based damage identification method, based on using the natural frequencies and mode shapes of a sandwich beam is developed. Analytical and numerical solutions for the natural frequencies and mode shapes of a sandwich beam, are presented in Section 5.1. Analytical close form solution is derived for cantilever boundary condition only. Numerical solutions are obtained by using the FE models. After developing the damage identification method, in Section 5.2, the theoretical background of the control method is also discussed in Section 5.3.

5.1 Analysis of sandwich beam

Vibration problems are frequently formulated by using the mathematical models based on the differential equations. A mathematical model of a beam describing certain specific characteristics may be obtained by using different approaches. Depending on the approach, a sandwich beam can be modelled as either a continuous or a discrete model. Simple beam theory, based on partial differential equations, may be used for the analysis of a simple and continuous beam. For a complex and discontinous structure, a discrete model is needed for its analysis. Hence, a discrete model such as a FE model, is used for modelling a structure, which may contain geometrical and mechanical discontinuities. In this section, both approaches for modelling a sandwich beam are described.

5.1.1 Simple beam theory

The theory for free vibration analysis of a sandwich beam is virtually same as the simple beam theory, except that the sandwich beam theory must include shear deformation of the core. One such beam theory is 'Timoshenko beam theory', which includes shear deformation in entire cross-section of a beam by using shear correction factor. However, in a sandwich beam only core is assumed to carry shear load. This means that only shear deformation of the core should be included in theory. Hence, Timoshenko beam theory is modified for a sandwich beam and is described in details in standard text books [Allen, 1969; Zenkert, 1995] related to sandwich construction. In this sub-section, the Timoshenko beam theory is described first and a solution for a cantilever sandwich beam is derived. Subsequently, Zenkert's formula for natural frequencies of a cantilever sandwich beam is outlined.

The equation of motion for an isotropic beam vibrating in transverse direction is well established [Timoshenko *et al.*, 1974] and given as,

$$EI\frac{\partial^4 w}{\partial x^4} + m\ \frac{\partial^2 w}{\partial t^2} - mR_g^2\left(1 + \frac{E}{k'G}\right)\frac{\partial^4 w}{\partial x^2 \partial t^2} = 0, \tag{5.1}$$

where EI, G and m are flexural rigidity, shear modulus and mass per unit length of the beam respectively. $k^{'}$ is the shear coefficient/shape factor for the of cross section, which accounts for shear deformation in the beam.

For a sandwich beam, it is assumed that outer layers, i.e. the faces carry bending load whereas the inner part, i.e. core carries shear load only. This assumption is analogous to that of the Timoshenko beam, which carries both bending and shear load. This implies that the parameters accounting for the bending and shear load must be identified in Eqn. 5.1 for the sandwich beam. These parameters are flexural rigidity (EI) and shear coefficient ($k^{'}$) in Eqn. 5.1. For the sandwich beam, the methods for calculating these parameters are different from those of an isotropic Timoshenko beam. These methods are based on the assumptions made for the sandwich beam. Since, the faces carry bending load and and separated by the core, flexural rigidities of the faces are calculated about the neutral axis of the sandwich beam. The values of $k^{'}$ is the ratio of the centre to centre distance between the faces and total depth of the sandwich beam.

Assuming that the beam is vibrating harmonically at frequency ω, the solution of Eqn. 5.1 is given as,

$$w(x,t) = W(x)sin\omega t. \tag{5.2}$$

Substituting Eqn. 5.2 into Eqn. 5.1 gives the following equation,

$$\frac{\partial^4 W(x)}{\partial x^4} + \Omega^2(r^2 + c^2)\frac{\partial^2 W(x)}{\partial t^2} - \Omega^2 W(x) = 0 \tag{5.3}$$

where

$$\Omega^2 = \frac{\omega^2 m L^4}{EI} \qquad r^2 = (R_g/L)^2 \tag{5.4}$$
$$R_g = \sqrt{\frac{I}{A}} \qquad c^2 = \frac{EI}{k'AGL^2}$$

The general solution of Eqn. 5.3 can be easily verified to be,

$$W(x) = C_1\, cosh\Omega S_1 x + C_2\, sinh\Omega S_1 x + C_3\, sin\Omega S_2 x + C_4\, cos\omega S_2 x \tag{5.5}$$

where

$$S_{1,2} = \left\{ \mp\frac{r^2 + c^2}{2} + \frac{1}{2}\left[\left(r^2 + c^2\right)^2 + \frac{4}{\omega^2} \right]^{1/2} \right\}^{1/2} \tag{5.6}$$

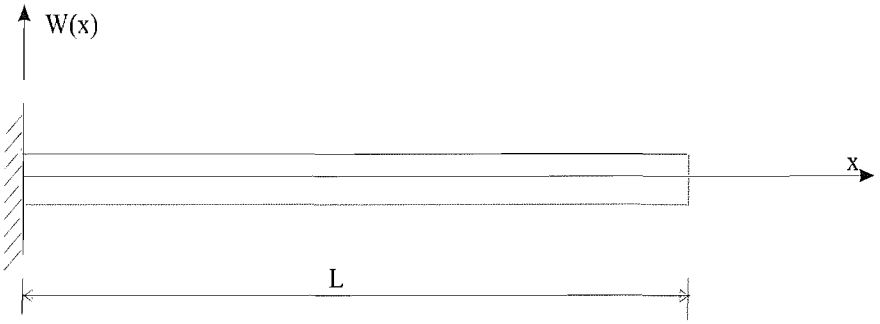

Figure 5.1: Boundary condition of beam.

The value of constants are obtained by applying suitable boundary conditions as shown in Fig. 5.1. For fixed-free boundary condition at the fixed end i.e. $x = 0$,

$$W(0) = 0 \qquad \frac{dW(x)}{dx}|_x = 0 \tag{5.7}$$

On the other hand, at the free end i.e. $x = L$, the boundary condition is given as,

$$\frac{d^2 W(x)}{dx^2}|_{x=L} = 0 \qquad \frac{d^3 W(x)}{dx^3}|_{x=L} = 0 \tag{5.8}$$

Using the boundary condition given by Eqn. 5.7 in Eqn. 5.5 leads to $C_2 + C_4 = 0$ and $C_1 + C_3 = 0$ respectively. Thus, the solution given by Eqn. 5.5 can be written as,

$$W(x) = C_1\, (cos\omega S_2 x - cosh\omega S_1 x) + C_2\, (sin\omega S_2 x - sinh\omega S_1 x)\,. \tag{5.9}$$

Using boundary condition given by Eqn. 5.8 in Eqn. 5.9, two simultaneous equations are obtained as,

$$C_1\ (cos\omega S_2 L + coshh\omega S_1 L) + C_2\ (sin\omega S_2 L + sinh\omega S_1 L) = 0, \tag{5.10}$$

$$C_1\ (sin\omega S_2 L + sinh\omega S_1 L) - C_2\ (cos\omega S_2 L - cosh\omega S_1 L) = 0. \tag{5.11}$$

Relationship given by Eqn. 5.11 is used to find C_2 in terms of C_1,

$$C_2 = C_1 \frac{sin\omega S_2 L - sinh\omega S_1 L}{cos\omega S_2 l + cosh\omega S_1 L}, \tag{5.12}$$

$$C_1 [cos\omega S_2 L + cosh\omega S_1 L] + C_1 \frac{sin\omega S_2 L + sinh\omega S_1 L}{cos\omega S_2 L + cosh\omega S_1 L} \times [sin\omega S_2 L - sinh\omega S_1 L] = 0$$

$$C_1 [cos\omega S_2 L + cosh\omega S_1 L]^2 + C_1 \left[sin^2\omega S_2 L - sinh^2\omega S_1 L\right] = 0 \tag{5.13}$$

For non-trivial solution $C_1 \neq 0$, then the expression inside the brackets in Eqn. 5.13 must be zero. After simplification, this leads to the equation,

$$cos\omega S_2 L \times cosh\omega S_1 L = -1. \tag{5.14}$$

Eqn. 5.14 is solved for the natural frequencies. The constants, S_1 and S_2, are functions of mechanical and geometrical properties of the beam. Thus, Eqn. 5.14 is solved to calculate the natural frequencies of the given beam.

5.1.2 Finite element modelling

Analytical solution described in Sub-section 5.1.1 is used to predict free vibration responses of a continuous sandwich beam, which cannot include damage in the modelling. In order to include damage, the damaged sandwich beam is modelled as a discrete model by using FE formulation. A discrete model is thought to be made of finite number of elements having finite number of nodes, where responses are calculated for a given boundary condition. The FE model is used at many steps in Fig. 4.1.

In this section, the FE formulation based on the classical beam theory is described. This formulation is based on the three-layer concept. A sandwich beam is made of three layers [Zenkert, 1995] and can be modelled as a three layered structure [Vinson, 1999] irrespective of the core thickness. These three layers are two outer stiff layers known as the faces and the inner soft layer known as the core. This concept assumes that the

deflection of the upper and lower faces are same because no transverse flexibility of the core layer occurs. Also, the longitudinal displacement distribution through the height of the core is linear. Hence, the total displacement of a sandwich beam is split into two parts, i.e. primary and secondary deformation. Primary deformation is as a result of normal behaviour of the sandwich beam without shear deformation, i.e. bending occurs about the neutral axis of the beam. In secondary deformation, the faces bend about their own neutral axis and the core deforms under shear. Therefore, it is assumed that faces carry bending load only whereas core carries shear load [Zenkert, 1995]. In the FE model, the stiffness matrix of a sandwich beam include the contribution of its bending and shear stiffness of the faces and core respectively. This means that elements used in the FE model must account for the bending and shear stiffness matrices of the faces and core respectively. However, there is no standard sandwich beam element available in the commercial software such as ABAQUS. Hence, the FE formulation for the sandwich beam described in this section is adopted in this work.

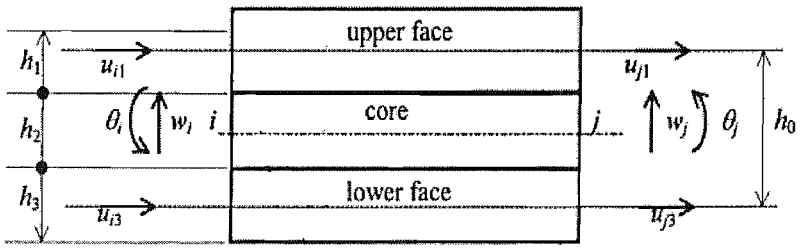

Figure 5.2: Element description.

In the present work, a simple FE beam formulation described by Sainsbury and Zhang [Sainsbury & Zhang, 1999] and based on the above assumptions for a sandwich beam is adopted. In this formulation, faces are modelled by using integral method [Wu *et al.*, 2003], which treats each laminate face as one equivalent quasi-isotropic layer. It means that there are three layers, i.e., two outer layers of the faces and one inner core layer, in the element. Also, the element is 2-dimensional, i.e., 2-D. The finite element of a three-layer beam, in the present formulation, is shown in Fig 5.2. At each node, there are four degree of freedoms, namely, the transverse displacement w, the rotation

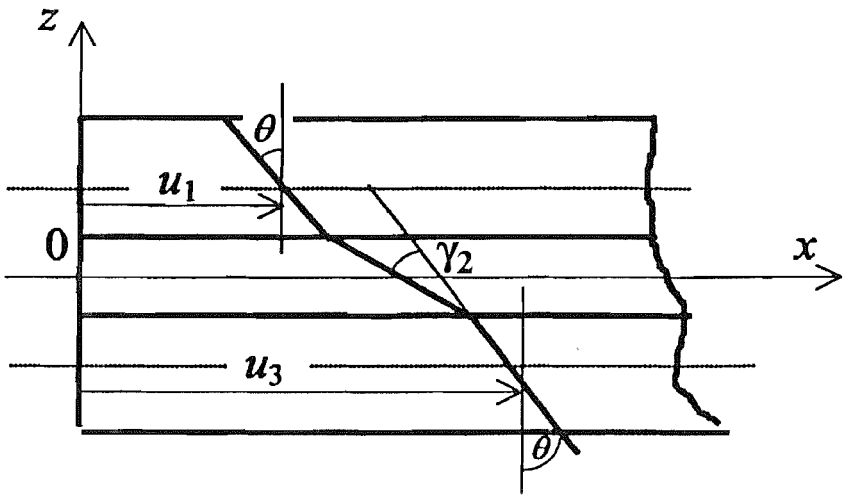

Figure 5.3: Shear strain description [Sainsbury & Zhang, 1999].

θ of the elastic layers (or faces), and the axial displacements u_1, u_3 of the middle planes of these faces. The total set of displacements for the element is,

$$\{\Phi\} = \left\{ \begin{array}{c} \phi_i \\ \phi_j \end{array} \right\} = \left\{ \begin{array}{cccccccc} w_i & \theta_i & u_{i1} & u_{i3} & w_j & \theta_j & u_{j1} & u_{j3} \end{array} \right\}^T \tag{5.15}$$

Using the traditional shape functions of the beam formulation, the displacement vector $\{\delta\}$ may be written as

$$\left\{ \begin{array}{c} w \\ \theta \\ u_1 \\ u_3 \end{array} \right\} = \left[\begin{array}{c} N_f \\ N_f' \\ N_1 \\ N_3 \end{array} \right] \{\Phi\} \tag{5.16}$$

where

$$[N_1] = \left\{ \begin{array}{cccccccc} 0 & 0 & 1-\xi & 0 & 0 & 0 & \xi & 0 \end{array} \right\}$$

$$[N_3] = \left\{ \begin{array}{cccccccc} 0 & 0 & 0 & 1-\xi & 0 & 0 & 0 & \xi \end{array} \right\}$$

$$[N_f] = \left\{ \begin{array}{cccccccc} (1-3\xi^2+2\xi^3) & (\xi-2\xi^2+\xi^3)l & 0 & 0 & (3\xi^2-2\xi^3) & (-\xi^2+\xi^3)l & 0 & 0 \end{array} \right\}$$

$$[N_f'] = \left[\frac{\delta \mathbf{N_f}}{\delta x} \right] = \left[\frac{1}{l} \frac{\delta \mathbf{N_f}}{\delta \xi} \right] \tag{5.17}$$

ξ=x/l, l is element length.

The stiffness matrix for the elastic faces can be obtained from their extensional and the bending strain energies as follow,

$$\begin{aligned} U_b &= \frac{1}{2}\int_V (\sigma_e\epsilon_e + \sigma_b\epsilon_b)dV, \\ &= \frac{1}{2}\int_0^L \left(E_f A_f \left(\frac{\partial u_1}{\partial x}\right)^2 + E_f A_f \left(\frac{\partial u_3}{\partial x}\right)^2 + E_f I_f \left(\frac{\partial^2 w}{\partial x^2}\right)\right), \\ &= \frac{1}{2}\{\Phi\}\int_0^1 \left(\frac{E_f A_f}{l}[N_1']^T[N_1'] + \frac{E_f A_f}{l}[N_3']^T[N_3'] + \frac{E_f I_f}{l^3}[N_f''']^T[N_f'''] \right) d\xi\{\Phi\} \\ &= \frac{1}{2}\{\Phi\}^T[K_b]\{\Phi\}, \end{aligned} \tag{5.18}$$

where $I_f = I_{f,l} + I_{f,u}$. $I_{f,l}$ and $I_{f,u}$ are the moment of area of the lower and upper face about its own neutral axis.

The elements of bending stiffness matrix $[K_b]$ are obtained by solving eqn. 5.18 and given as follows,

$$K_b = E_f \begin{bmatrix} \frac{12I_f}{l^3} & & & & & & & \\ \frac{6I_f}{l^2} & \frac{4I_f}{l} & & & & & & \\ 0 & 0 & \frac{A_f}{l} & & & & & \\ 0 & 0 & 0 & \frac{A_f}{l} & & & & \\ -\frac{12I_f}{l^3} & -\frac{6I_f}{l^2} & 0 & 0 & \frac{12I_f}{l^3} & & & \\ \frac{6I_f}{l^3} & \frac{2I_f}{l} & 0 & 0 & -\frac{6I_f}{l^2} & \frac{4I_f}{l} & & \\ 0 & 0 & -\frac{A_f}{l} & 0 & 0 & 0 & \frac{A_f}{l} & \\ 0 & 0 & 0 & -\frac{A_f}{l} & 0 & 0 & 0 & \frac{A_f}{l} \end{bmatrix} \tag{5.19}$$

The stiffness for the core layer can be obtained from its shear strain energy. Here the bending and extensional strain energies are ignored due to their second order smallness compared with the shear strain energy.

From Fig. 5.3, it is clear that shear strain is given by

$$-\gamma_c = \frac{u_1 - u_3}{h_2} + \frac{h_0}{h_2}\theta = \frac{u_1 - u_3}{h_2} + \frac{h_0}{h_2}\frac{dw}{dx} \tag{5.20}$$

Substituting Eqn. 5.15 and 5.16 into Eqn. 5.20, we have

$$\gamma_c = -\left[\frac{N_1 - N_3}{h_2} + \frac{h_0}{h_2}\frac{d\mathbf{N_f}}{dx} \right]\{\Phi\} \tag{5.21}$$

Based on the energy approach, the stiffness matrix for the viscoelastic layer can be deduced as

$$
\begin{aligned}
U_s &= \frac{1}{2}\int_V G_c\gamma_c^2 dV \\
&= \frac{1}{2}\frac{G_c A_c l}{h_2^2}\{\Phi\}^T \int_0^1 \left[\ N_1 - N_3 + \tfrac{h_0}{L}N_f'\ \right]^T \left[\ N_1 - N_3 + \tfrac{h_0}{L}N_f'\ \right] d\xi\{\Phi\} \\
&= \frac{1}{2}\{\Phi\}^T[K_s]\{\Phi\} \qquad (5.22)
\end{aligned}
$$

The elements of the shear stiffness matrix, $[K_s]$, are given by Eqn. 5.23.

$$
K_s = \frac{G_c b l}{t_c}\begin{bmatrix}
\frac{6h_0^2}{5l^2} & & & & & & & \\
\frac{h_0^2}{10l} & \frac{2h_0^2}{15} & & & & & & \\
-\frac{h_0}{2l} & \frac{h_0}{12} & \frac{1}{3} & & & & & \\
\frac{h_0}{2l} & -\frac{h_0}{12} & -\frac{1}{3} & \frac{1}{3} & & & & \\
-\frac{6h_0^2}{5l^2} & -\frac{h_0^2}{10l} & \frac{h_0}{2l} & -\frac{h_0}{2l} & \frac{6h_0^2}{5l^2} & & & \\
\frac{h_0^2}{10l} & -\frac{h_0^2}{30} & -\frac{h_0}{12} & \frac{h_0}{12} & -\frac{h_0^2}{10l} & \frac{2h_0^2}{15} & & \\
-\frac{h_0}{2l} & -\frac{h_0}{12} & \frac{1}{6} & -\frac{1}{6} & -\frac{h_0}{2l} & \frac{h_0}{12} & \frac{1}{3} & \\
\frac{h_0}{2l} & \frac{h_0}{12} & -\frac{1}{6} & \frac{1}{6} & -\frac{h_0}{2l} & -\frac{h_0}{12} & -\frac{1}{3} & \frac{1}{3}
\end{bmatrix} \qquad (5.23)
$$

$$
h_0 = t_c + t_f \qquad (5.24)
$$

The elemental stiffness matrix for the sandwich beam element is obtained from Eqn. 5.18 and 5.22.

$$
K_j = K_b + K_s \qquad (5.25)
$$

Following similar procedure in the last paragraph for the stiffness matrix, the mass matrix for the sandwich beam element is obtained from the kinetic energy as follows:

$$
\begin{aligned}
T &= \frac{1}{2}\int_0^L (m\dot{w}^2 + m_f\dot{u}_1^2 + m_f\dot{u}_3^2)dx \\
&= \frac{L}{2}\{\dot{\Phi}\}^T \int_0^L (m[N_f]^T[N_f] + m_f[N_1]^T[N_1] + m_f[N_3]^T[N_3])d\xi\{\dot{\Phi}\} \\
&= \frac{1}{2}\{\dot{\Phi}\}^T[M_j]\{\dot{\Phi}\} \qquad (5.26)
\end{aligned}
$$

The present formulation yields a consistent mass matrix and its elements are given by Eqn. 5.27.

$$M_j = \begin{bmatrix} \frac{13ml}{35} & & & & & & & \\ \frac{11ml^2}{210} & \frac{ml^3}{105} & & & & & & \\ 0 & 0 & \frac{m_f l}{3} & & & & & \\ 0 & 0 & 0 & \frac{m_f l}{3} & & & & \\ \frac{9ml}{70} & \frac{13ml^2}{140} & 0 & 0 & \frac{13ml}{35} & & & \\ -\frac{13ml^2}{420} & -\frac{ml^3}{140} & 0 & 0 & -\frac{11ml^2}{210} & \frac{ml^3}{105} & & \\ 0 & 0 & \frac{m_f l}{6} & 0 & 0 & 0 & \frac{m_f l}{3} & \\ 0 & 0 & 0 & \frac{m_f l}{6} & 0 & 0 & 0 & \frac{m_f l}{3} \end{bmatrix} \tag{5.27}$$

where $m = 2 \times m_f + m_c$, m_f and m_c are the mass per unit length of the face and the core respectively. The elemental stiffness and mass matrix of a sandwich beam given by Eqns. 5.25 and 5.27 respectively are used to assemble the stiffness and mass matrix of a beam as follow,

$$[K] = \sum_{j=1}^{m} K_j, \tag{5.28}$$

$$[M] = \sum_{j=1}^{m} M_j, \tag{5.29}$$

where m is the number of element in the sandwich beam model.

Stiffness and mass matrix given by Eqns. 5.28 and 5.29 are used to solve the well established equation of motion for undamped vibration [Cook *et al.*, 1989] given by,

$$[M]\{\ddot{d}\} + [K]\{d\} = 0 \tag{5.30}$$

Solution of Eqn. 5.30 is similar to that of given by Eqn. 5.2 and can be written as,

$$\{d_n\} = \{\Phi_n\} sin\omega_n t \qquad and \qquad \{\ddot{d_n}\} = -\omega_n^2 \{\Phi_n\} sin\omega_n t \tag{5.31}$$

where $\{\phi_n\}$ is the vector of amplitudes of nodal d.o.f. vibration also known as mode shapes and ω_n is the natural frequency in nth mode of vibration.

Combining eqn. 5.30 and 5.31 gives,

$$([K] - \lambda_n[M])\{\Phi_n\}) = \{0\} \qquad where \qquad \lambda_n = \omega_n^2. \tag{5.32}$$

In order to get the non-trivial solution of Eqn. 5.32, eigenvalues λ is determined by finding roots of the following equation,

$$| ([K] - \lambda_n[M]) | = 0 \tag{5.33}$$

Finally the natural frequencies are calculated from the eigenvalues using relationship given in Eqn. 5.32.

In this section, mathematical models for estimating the vibration responses of a sandwich beam were presented. The solution methods used in solving these models and behaviour of the beam responses may be used to develop damage identification method in next section.

5.2 Damage identification method

In this section, a model-based damage identification method is developed which uses the geometrical properties, virgin mechanical properties, natural frequencies and mode shapes of the given sandwich beam to predict the damage. The predictions include existence, location, level and extent of damage in the sandwich beam. The flowchart of the proposed damage identification method is shown in Fig. 5.4, which is the part of research methodology shown in Fig. 4.1.

5.2.1 Theoretical basis of damage

Structural damage causes a loss of stiffness in damaged element(s) of a structure without affecting its mass. Hence, damage is assumed to affect only the stiffness matrix in Eqn. 5.28 for a structural system, which can be represented as a small perturbation in the stiffness matrix [Ostachowicz & Krawczuk, 2001; Shi & Law, 1998]. In a sandwich beam, the stiffness matrix is the sum of bending and shear stiffness matrices as given by Eqn. 5.25. Thus, damage in a sandwich beam can be represented as the perturbation in the bending (K_b) and shear (K_s) matrices as given by Eqn. 5.34. The global stiffness matrix of the damaged sandwich beam K^d, the nth eigenvalue λ_{n_d}, and the nth mode shapes Φ_n^d of the damaged sandwich beam are expressed as

$$K^d = K + \sum_{j=1}^{m}(1 - \alpha_{j,b})K_j^b + \sum_{j=1}^{m}(1 - \alpha_{j,s})K_j^s, \tag{5.34}$$

$$\lambda_{n,d} = \lambda_n + \Delta\lambda_n, \qquad \Phi_n^d = \Phi_n + \Delta\Phi_n. \tag{5.35}$$

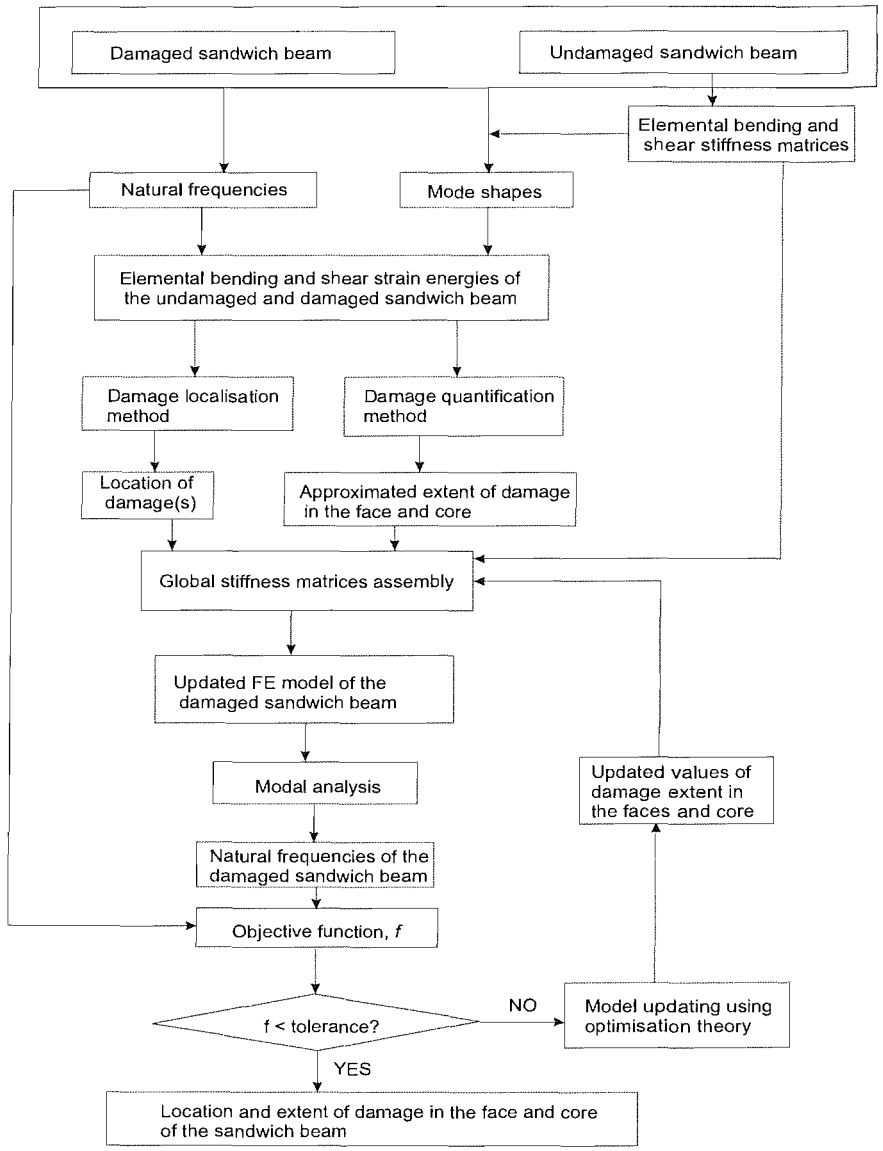

Figure 5.4: Flow chart for the damage identification method.

where damage in an element is represented as a fractional change of the elemental stiffness matrix; the super-script d denotes the damage case, K_j^b & K_j^s are the bending and shearing elemental stiffness matrix respectively, $\alpha_{j,b}$ & $\alpha_{j,s}$ are the fractional damage in the faces and core of the jth sandwich beam element respectively, K is the global stiffness matrix of the undamaged sandwich beam, and m is the total number of elements in the FE model. Φ_n is the nth mode shapes of the undamaged sandwich beam.

5.2.2 Estimation of strain energy

The changes in the vibration properties are also reflected in derived quantities such as Modal Strain Energy (MSE), which is defined as the product of the elemental stiffness matrix and second power of the mode shapes [Meirovitch, 1986]. For the jth element and the nth mode, the MSE before and after occurrence of damage are given as,

$$MSE_{n,j} = \frac{1}{2}\Phi_{n,j}^T K_j \Phi_{n,j}, \tag{5.36}$$

$$MSE_{n,j}^d = \frac{1}{2}\Phi_{n,j}^{d^T} K_j \Phi_{n,j}^d, \tag{5.37}$$

where $\text{MSE}_{n,j}$ and $\text{MSE}_{n,j}^d$ are the modal strain energies of the jth undamaged and the damaged element in nth mode of vibration. $\Phi_{n,j}$ and $\Phi_{n,j}^d$ are the vectors containing the elements of Φ_n and Φ_n^d corresponding to the jth element respectively. Since, the location and extent of damage in the sandwich beam are unknown, $\text{MSE}_{n,j}^d$ is approximated by using elemental stiffness matrix (K_j) of the undamaged element rather than that of the damaged element.

Similar to the expression of modal strain energy given by eqn. 5.36, the bending strain energies of the undamaged and damaged elements, $\text{MSE}_{n,j}^b$ and $\text{MSE}_{n,j}^{b,d}$ respectively, can be given as the product of the elemental bending stiffness matrix and the second power of the bending component of the mode shapes. Since, the bending components in the mode shapes of the sandwich beam are unknown, the total mode shapes are used as an approximation. Thus, the bending strain energies of the jth element in the nth mode are approximated as,

$$MSE_{n,j}^b = \frac{1}{2}\Phi_{n,j}^T K_j^b \Phi_{n,j}, \tag{5.38}$$

$$\begin{aligned} MSE_{n,j}^{b,d} &= \tfrac{1}{2}\Phi_{n,j}^{d^T} K_j^{b,d} \Phi_{n,j}^d, \\ &= \frac{1}{2}\ (1-\alpha_{j,b})\Phi_{n,j}^{d^T} K_j^b \Phi_{n,j}^d, \end{aligned} \tag{5.39}$$

where K_j^b and $\alpha_{j,b}$ are the bending elemental stiffness matrix and the fractional reduction in bending stiffness respectively for the jth element. Similarly, the shear strain energies of the jth undamaged and damaged element in nth mode, $\text{MSE}_{n,j}^s$ and $\text{MSE}_{n,j}^{s,d}$ respectively, are approximated as,

$$MSE_{n,j}^s = \frac{1}{2}\Phi_{n,j}^T K_j^s \Phi_{n,j}, \tag{5.40}$$

$$\begin{aligned} MSE_{n,j}^{s,d} &= \tfrac{1}{2}\Phi_{n,j}^{d^T} K_j^{s,d} \Phi_{n,j}^d. \\ &= \frac{1}{2}\ (1-\alpha_{j,s})\Phi_{n,j}^{d^T} K_j^s \Phi_{n,j}^d, \end{aligned} \tag{5.41}$$

where K_j^s and $\alpha_{j,s}$ are the shearing elemental stiffness matrix and the fractional reduction in shearing stiffness respectively, for the jth element.

5.2.3 Damage localisation method

To localise damage in a composite sandwich beam, a damage localisation method previously developed and validated [Shi & Law, 1998; Shi *et al.*, 2000, 2002] for isotropic structures is extended. This method is based on comparison of modal strain energies of undamaged and damaged composite sandwich beams. Since, the location of damage is unknown, the $\text{MSE}_{n,j}^d$ is approximated by using the undamaged elemental stiffness matrix (K_j) rather than the damaged one.

The elemental $\text{MSE}_{n,j}$ and $\text{MSE}_{n,j}^d$ are compared by defining a new parameter Modal Strain Energy Change Ratio (MSECR) for jth element in the nth mode as follows,

$$MSECR_{n,j} = \frac{MSE_{n,j}^d - MSE_{n,j}}{MSE_{n,j}}. \tag{5.42}$$

Damage is localised by calculating the MSECR of each element for the first few modes. Subsequently, the summation $MSECR_j$ of all modes are averaged and normalised with respect to the largest value of $MSECR_j$ in the respective mode. $MSECR_j$ can be defined as,

$$MSECR_j = \frac{1}{m}\sum_{n=1}^{M} \frac{MSECR_{n,j}}{MSECR_{n,max}}, \tag{5.43}$$

where M is the number of mode shapes used. MSECR_j is used as the damage indicator for damage localisation. The unit value of MSECR_j indicates presence of damage in the jth element. This method requires only the first few lower modes since

the contribution of the higher modes are insignificant[Shi & Law, 1998; Shi *et al.*, 2000, 2002].

5.2.4 Damage quantification method

In this section, the bending and shear strain energy given by Eqn. 5.39 and 5.41 respectively, are used to derive the expressions for damage extent in the face and core respectively. The proposed damage quantification approach is based on the following assumptions,

1. Damage reduces the stiffness matrices only.
2. The fractional bending and shear strain energies before and after occurrence of damage, are relatively constant for each element i.e. $F^{b}_{n,j} \approx F^{b,d}_{n,j}$ and $F^{s}_{n,j} \approx F^{s,d}_{n,j}$.

The first assumption is widely used for damage identification in a structure [Doebling *et al.*, 1998], whereas the second assumption has been proved to be effective for an aluminium plate [Cornwell *et al.*, 1999]. Expression of fractional strain energy given by Stubbs and Kim [Stubbs & Kim, 1996] and Kim *et al.* [Kim *et al.*, 2003] for an isotropic beam is extended for a sandwich beam. These derived expressions will then be used to approximate damage extent of the face and core, in the first stage of damage extent prediction.

In case of a sandwich beam, the fractional energies are the bending and shearing fractional energies of the jth element in the nth mode, which are expressed as follows,

$$F^{b}_{n,j} = \frac{MSE^{b}_{n,j}}{SE_n}, \tag{5.44}$$

$$F^{b,d}_{n,j} = \frac{MSE^{b,d}_{n,j}}{SE_n}, \tag{5.45}$$

$$F^{s}_{n,j} = \frac{MSE^{s}_{n,j}}{SE_n}, \tag{5.46}$$

$$F^{s,d}_{n,j} = \frac{MSE^{s,d}_{n,j}}{SE_n}, \tag{5.47}$$

where SE_n & SE^{d}_{n} are the strain energies of the undamaged and damaged sandwich beam respectively, $F^{b}_{n,j}\&F^{s}_{n,j}$ are the bending and the shearing fractional energies for the jth undamaged sandwich beam element respectively, and $F^{b,d}_{n,j}\&F^{s,d}_{n,j}$ are the bending and shearing fractional energies for the jth damaged sandwich beam element respectively in the nth mode.

In order to improve the accuracy of damage quantification method, the vibrational properties from more than one mode are used. Thus, the weighted average of fractional bending and shearing strain energies given by Eqn. 5.44 - 5.47 with respect to the natural frequencies are used to incorporate more than one mode. The weighted average of the fractional energies are given as follows,

$$F_j^b = \frac{1}{\sum_{n=1}^{N} \omega_n} \sum_{n=1}^{N} \frac{\omega_n \times MSE_{n,j}^b}{SE_n}, \tag{5.48}$$

$$F_j^{b,d} = \frac{1}{\sum_{n=1}^{N} \omega_{n,d}} \sum_{n=1}^{N} \frac{\omega_{n,d} \times MSE_{n,j}^{b,d}}{SE_{n,d}}, \tag{5.49}$$

$$F_j^s = \frac{1}{\sum_{n=1}^{N} \omega_n} \sum_{n=1}^{N} \frac{\omega_n \times MSE_{n,j}^s}{SE_n}, \tag{5.50}$$

$$F_j^{s,d} = \frac{1}{\sum_{n=1}^{N} \omega_{n,d}} \sum_{n=1}^{N} \frac{\omega_{n,d} \times MSE_{n,j}^{s,d}}{SE_{n,d}}. \tag{5.51}$$

Comparing the weighted average bending and shearing fractional energies of the undamaged and damaged sandwich beam element given by Eqn. 5.48-5.51 and using the bending and shearing modal strain energy given by Eqn. 5.39 & 5.41 respectively, the damage extent of the face and core respectively, are given as follows,

$$1 - \alpha_{j,b} = \left(\frac{\sum_{n=1}^{N} \omega_{n,d}}{\sum_{n=1}^{N} \omega_n} \right) \times \left(\sum_{n=1}^{N} \frac{MSE_{n,j}^b}{\omega_n} / \sum_{n=1}^{N} \frac{\Phi_n^{d^T} K_j^b \Phi_n^d}{\omega_{n,d}} \right) \tag{5.52}$$

$$1 - \alpha_{j,s} = \left(\frac{\sum_{n=1}^{N} \omega_{n,d}}{\sum_{n=1}^{N} \omega_n} \right) \times \left(\sum_{n=1}^{N} \frac{MSE_{n,j}^s}{\omega_n} / \sum_{n=1}^{N} \frac{\Phi_n^{d^T} K_j^s \Phi_n^d}{\omega_{n,d}} \right) \tag{5.53}$$

Since, there is very little influence of low extent damage on the natural frequencies, the first part of the Eqn. 5.52 and 5.53 remains close to unity. In order to simplify, these terms are considered to be unity and thus the damage extent expressions for the face and core can be given as follows,

$$\alpha_{j,b} = 1 - \left(\sum_{n=1}^{N} \frac{MSE_{n,j}^b}{\omega_n} / \sum_{n=1}^{N} \frac{\Phi_n^{d^T} K_j^b \Phi_n^d}{\omega_{n,d}} \right) \tag{5.54}$$

$$\alpha_{j,s} = 1 - \left(\sum_{n=1}^{N} \frac{MSE_{n,j}^s}{\omega_n} / \sum_{n=1}^{N} \frac{\Phi_n^{d^T} K_j^s \Phi_n^d}{\omega_{n,d}} \right) \tag{5.55}$$

Eqn. 5.54 and 5.55 approximate the fractional reduction in the Young's modulus of the face and the shear modulus of the core respectively, i.e. the fractional damage

in the face and core respectively. Any negative values of the $\alpha_{j,b}$ and $\alpha_{j,s}$ are made equal to zero. These approximations are caused by the following assumptions,

1. The elemental strain energies are approximated in the calculation.

2. It is assumed that the fractional energies are relatively constant, i.e. the changes in their values are negligible.

As a result of the approximation of the modal strain energies and assumptions in deriving Eqns. 5.54 and 5.55, the damage extent predictions in the first stage are also approximated. The approximation in the prediction of the damage extent values ($\alpha_{j,b}$ & $\alpha_{j,s}$) can be refined in the second stage by an optimisation technique such as Nelder-Mead method, a multi-dimensional unconstrained nonlinear optimisation algorithm. The theoretical background of the Nelder-Mead method can be found in any standard text book [Fletcher, 1987].

In an optimisation method, the roles of the objective function, the starting point for the searches of the optimum or the initial guess, and the number of optimisation variables are important. Since, the damaged element is already located by the method presented in Sub-section 5.2.3, it will reduce the number of variables by selecting only the damaged element. In the present work, an objective function based on the residuals of the natural frequencies is used. The choice of the initial guess directly affects the convergence of the optimisation variables. Generally, initial guesses closer to the optimum values ensure better convergence. Here, the approximated values of $\alpha_{j,b}$ and $\alpha_{j,s}$ are used as intial guesses, to obtain the optimum values of these predictions. The objective function used in this study is expressed as follows,

$$f = \sum_{n=1}^{N} \left(\frac{\omega_n^u - \omega_n^t}{\omega_n^u} \right)^2, \tag{5.56}$$

where ω_n^t is the target natural frequency in the nth mode, which is the natural frequency of the damaged composite sandwich beam. ω_n^u is the natural frequency updated at each iteration of the optimisation process.

Thus, the damage quantification method is performed in two stages as given below,

1. The prediction of the damage severity in the faces and the core of the damaged sandwich beam, using Eqn. 5.54 and 5.55 respectively.

2. The refinement of the damage severity prediction of the first stage by an optimisation method, using the objective function based on the frequency-error criterion given by Eqn. 5.56.

5.3 Control method

Once the existence, location and extent of damage have been predicted, the final step is determining their criticality and severity, by using a control method based on a cumulative damage model, like those reviewed in Section 2.2. Role of the control method in the proposed system is shown in Fig. 4.1. In this section, the theoretical basis of the control method in the proposed system is presented, by defining and calculating a parameter to represent the criticality and severity of damages in a structure. Criticallity and severity of damage are defined by determing the threshold values for the parameter, which can be used to activate the control system. The input for the control method must be the results obtained from the damage identification method developed in the previous Section 5.2. Since, the damage can be in face and/or core at any location in the beam, the parameter must include their effects such as their location, extent and level in the beam. At the same time, their value must be in a close range from zero to one, which is proved to be effective for accounting cumulative damage in the sandwich beams [Clark, 1997; Clark *et al.*, 1999; Mahi *et al.*, 2004]. The cumulative damage models reviewed in Section 2.2, consider accumulation of damage in the core only. However, damage may start propagating in the core after its occurrence in the face. Hence, it is essential to include the effects of interacting damage modes in the parameter, to account the damage mechanism in a sandwich beam as discussed in Section 2.1.

In Sub-section 5.2.1, it is shown that the global stiffness matrix of a damaged sandwich beam can be assembled by knowing the location, extent and level of damage, apart from the stiffness matrix of the undamaged element. Since, the location, extent and level of damage are calculated by the methods in Section 5.2, the global stiffness matrix of the damaged sandwich beam is now known; hence, their difference with the global stiffness matrix of the undamaged sandwich beam is estimated. This difference in the global stiffness matrix of the undamaged and damaged sandwich beam must be indicated by a number, which can be given by the value of `determinant` of the respective global stiffness matrix. Based on the presented theory, the parameter can be calculated as follows,

$$D = \frac{\Delta(K) - \Delta(K_d)}{\Delta(K)}. \tag{5.57}$$

In Eqn. 5.57, K and K_d are the global stiffness matrices of the undamaged and damaged sandwich beam whereas $\Delta(K)$ and $\Delta(K_d)$ are their determinant value respectively.

It is expected that for the undamaged sandwich beam, the value of D will be zero whereas at failure, it will be equal to unity. Hence, any value between zero and unity indicates the presence of damage and its severity. Higher the value of D, more severe and critical is the damage [Clark, 1997; Clark *et al.*, 1999; Mahi *et al.*, 2004]. A detailed numerical characterisation of the presented control method for the selected beam specimens, with various damage scenarios will be presented in Sub-section 9.3.5 and the threshold values of D, will be determined to indicate safety of the beam specimens, in Sub-section 9.3.5.

5.4 Summary

In this chapter, a model-based approach for the damage identification in a sandwich beam was developed, which uses the natural frequencies and mode shapes to identify the existence, location and extent of damage. The damage quantification method can be distinctly divided into two stages as given below,

1. The prediction of the damage extent in the faces and core of the damaged sandwich beam, using Eqn. 5.54 and 5.55 respectively.

2. The refinement of the damage extent prediction of the first stage was performed by using an optimisation technique. In this technique, the predictions of the first stage were used as the initial guesses and the frequency error criterion given by Eqn. 5.56, was used as the objective function.

Figure 5.4 shows the steps used in the damage identification method, in which the results of the first stage, are used as the initial guesses in the optimisation technique at the second stage of damage identification. This allows fast convergence of damage extent in the faces and core in the second stage. It is noted that the first stage is a model-based approach and the effectiveness of the proposed damage identification method, will be verified by using numerical simulations in Chapter 6.

Chapter 6

Damage Identification using Numerical Simulations

In this chapter, numerical simulations will be used for examining the damage identification method developed in the previous chapter. Numerical simulations offer opportunities to benchmark the damage identification method against various damage cases. For this purpose, a beam example is selected to examine the sensitivities of the damage identification method, for different extent and types of damage, at various locations. The beam is modelled by using the numerical model described in Sub-section 5.1.2.

Theoretically, objectives of damage identification are achieved by the method developed in Chapter 5. However, the development of damage identification method in Chapter 5, followed an analytical and logical line of reasoning in which many assumptions were made. Numerical testing of the method is intended to check the legitimacy of these assumptions in a controlled manner. The most critical claim of the proposed damage identification is that the elemental modal strain energy, is sensitive towards the presence of damage in a structure. Establishing the validity of this claim is the main focus of this chapter. Numerical simulations are used to generate the inputs for the damage identification method, namely the natural frequencies and mode shapes of the beam model, for the selected damage scenarios. Outputs of the damage identification method in terms of existence, locations and extent of damage are compared with the simulated damage cases, to verify the accuracy of predictions.

6.1 Description of the numerical beam model

The composite sandwich beam chosen for this study is shown in Fig. 6.1. The faces of the beam model are made of glass fibres whereas the core is made of Poly Vinyl

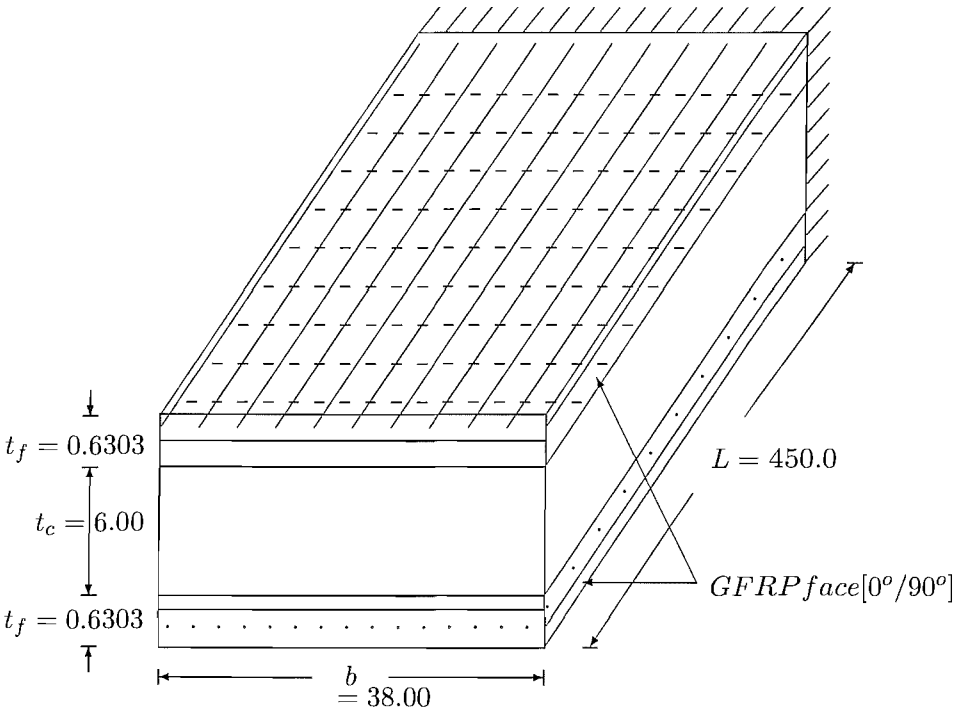

Figure 6.1: Geometrical properties of the sandwich beam (All dimensions are in *mm*).

Chloride (PVC) foam (CoreCell A400). The geometrical properties of the beam are chosen such that the specimen behaves like a thin beam structure. Thickness of core is 6.00 *mm*, which requires thickness of each face to be less than 1.04 *mm* for thin beam behaviour [Zenkert, 1995]. The detailed calculations for design of the composite sandwich beam are presented in Appendix A. The calculation presented in Appendix A will be used to fabricate the sandwich beam specimens as per procedure described in Section 7.1. Based on calculations in Appendix A, selected lay-up for the sandwich beam specimen is $[0^o/90^o/\text{Core}/90^o/0^o]$ and geometrical properties are shown in Fig. 6.1. The mechanical properties are calculated in Appendix A and are given in Table 6.1.

6.2 Validation of the numerical beam model

The most critical phase in numerical simulations is the selection of an appropriate numerical model for the generation of numerical results. Before using these numerical

results, the selected FE beam model must be validated with the other approaches. Here, the FE beam model is validated with other approaches such as ABAQUS, Timoshenko beam theory and Zenkert model. First, the sandwich beam described in Section 6.1 is modelled as a cantilever beam using the FE beam formulation presented in Sub-section 5.1.2. The beam model is discretised into 15 equal size of two-dimensional elements as shown in Fig. 6.2. The geometrical and mechanical properties of the beam model are same as those in Section 6.1 and used in all selected approaches as listed in Table 6.2. In other approach based on ABAQUS, the sandwich beam is modelled by using 2-dimensional 4 nodes shell elements. In this approach, it is assumed that the faces and core are quasi-isotropic and isotropic respectively. These assumptions in the ABAQUS approach is consistent with those of the FE beam model of Sub-section 5.1.2. Cantilever boundary condition in the both FE approaches, is modelled by making all translations and rotations at the cantilever end equal to zero. Next, the FE beam model is also validated with two close form solutions based on Timoshenko beam theory and Zenkert approach. Timoshenko beam theory is a generic beam theory, which includes shear deformation of the beam in the solution as explained in Sub-section 5.1.1. Zenkert proposed the close form solution for the cantilever sandwich beam. In this approach, the Timoshenko beam theory was modified for the sandwich beam.

The first five natural frequencies of the undamaged sandwich beam using the FE beam model are compared with the other approaches in Table 6.2. In Table 6.2, it can be observed that there is a good correlation between results from the FE beam model with those of the other approaches specifically Zenkert's approach. It can be seen in the Table 6.2 that there is a significant difference in the first natural frequency given by Zenkert's approach with that of the FE beam model. On the other hand, the higher modes natural frequencies obtained from the FE beam model and Zenkert's approach show good correlation i.e. maximum difference between them is 3.30%. Then, the first natural frequency obtained from the FE beam model is compared with that of the Timoshenko beam theory and ABAQUS model, which shows a better correlation. Further investigation reveals that the difference between the first natural frequencies given by the Zenkert approach and the Timoshenko beam theory is because of the different value of the co-efficient used in the both approaches. The co-efficient for the Timoshenko beam theory is obtained by solving Eqn. 5.14. These co-efficients are 3.4551 and 2.4674 for the Timoshenko beam theory and Zenkert's approach respectively, which shows significant difference. These values indicates that the co-efficient obtained for the first natural frequency in the Zenkert approach is an approximation of

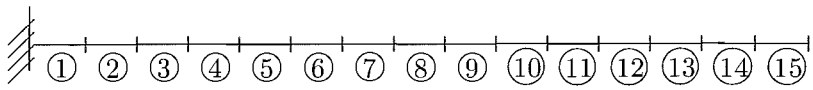

Figure 6.2: The FE discretisation of the cantilever composite sandwich beam.

the value obtained by solving the Timoshenko beam theory. Based on discussion here, it can be concluded that the FE beam model compare well with the Zenkert approach.

Table 6.1: Mechanical properties of the beam model.

E_1 (GPa)	G_{core} (MPa)	ρ_{face} (kg/m^3)	ρ_{core} (kg/m^3)
20.14	18.20	1353.92	69.00

6.3 Modelling damage in the beam model

A sandwich structure is a composite configuration made of high strength composite faces bonded to a lightweight foam core. Load transfer between them is accomplished by bonding between the faces and core. Any degradation in their stiffness properties and bonding between them, affect the load transfer capabilities; hence, reducing their contribution towards the stiffness of a sandwich beam as shown in Sub-section 5.2.1. Reduction in these stiffness properties can be mapped to several damage modes in a sandwich beam. The main damage modes considered here are face fracture/buckling,

Table 6.2: Natural frequencies (Hz) of the undamaged beam model.

Mode no.	Present	ABAQUS	Timoshenko	Zenkert
1	23.42	23.42	23.20	16.52
2	136.14	134.32	129.05	140.64
3	345.10	335.91	315.25	355.08
4	602.32	579.63	535.34	619.78
5	885.55	845.58	775.54	907.04

core shear, and face-core debonding for a foam-cored sandwich beam, as a result of micro-structural changes in one or more constituents [Zenkert, 1995]. In case of core shear, these micro-structural changes in the core develop into multiple micro-cracks. Finally, these micro-cracks saturate into a single crack propagating outward in the core towards the face leading to the development of debonding. For tougher adhesive between the faces and the core, debonding first develops slightly below the interface and then the crack enters into the relatively soft core. Under fatigue load, the propagating crack terminates with catastrophic failure of sandwich beam by face failure. Generally, these damage types develop when the relevant stress exceeds their respective threshold value, as indicated by Zenkert [Zenkert, 1995].

Local damage in a structure always causes reduction in local structural stiffness, which can be included in the model by changing stiffness matrices [Talreja, 1994]. In a sandwich beam, these stiffness matrices are bending and shear stiffness matrices, which contribute to the total stiffness matrix. These matrices are modified at structural damage location using modification coefficients ($\alpha_{j,b}$ & $\alpha_{j,s}$) for Young's modulus and shear modulus of the faces and core respectively, as given by Eqn. 5.34. Hence, damage modes considered in this study are simulated by reducing the respective modification coefficients. In case of face fracture/buckling, a part of the face at the damage location is removed, resulting in the reduction of their Young's modulus and thickness. This means that the contribution of the bending stiffness of the damaged face into total stiffness matrix is reduced, which is incorporated into the model by changing the value of modification coefficient ($\alpha_{j,b}$). The value of $\alpha_{j,b}$ can be calculated by using the remaining thickness of the damaged face into the elemental bending stiffness matrix. Since, the thickness of the face is also reduced, the contribution of the mass matrix of the faces into total mass matrix is also reduced, which will change the mass matrix as given in Sub-section 5.1.2. After disbonding between the faces and the core, load transfer capabilities between the face and the core is lost without changing their mass. This is modelled by reducing the contribution of the bending stiffness into the total stiffness matrix, to a certain extent at the disbonded location [Ostachowicz & Krawczuk, 2001]. For core damage, part of the core throughout the width is cracked leading to reduction in its load carrying capability, hence changing its responses [Wang *et al.*, 1996]. In terms of numerical modelling, shear modulus of the core is reduced by changing the modification coefficient ($\alpha_{j,s}$ to simulate core damage. The value of $\alpha_{j,s}$ for a length of crack in the core can be calculated by using a polynomial formula, proposed and numerically characterised by Wang *et al.* [Wang *et al.*, 1996]. The outlined

Table 6.3: Relationship between damage types and reduction in the stiffness matrices.

Damage types	Bending	Shearing	Mass
Face fracture/buckling	Yes	No	Yes
Core shear	No	Yes	No
Disbond	Yes	No	No

approach to model damage is also verified by other researchers [Banks *et al.*, 1996a; Gagel *et al.*, 2006; Luo & Hanagud, 1997; Ostachowicz & Krawczuk, 2001; Yan & Yam, 2004; Yuen, 1985]. The appropriate value of modification coefficient for the faces and the core depends on the extent of damage and can be calculated by using FE analysis [Yan & Yam, 2004]. The summary of damage types and the affected stiffness matrices are listed in Table 6.3.

6.4 Simulated damage cases

In this section, simulated damage cases are selected on the basis of damage characteristics of a composite sandwich beam. It is well established that propagation of damage in one constituent of a composite sandwich beam, is followed by the initiation of damage in an other constituent [Renard & Thionnet, 2006]. This implies that the resulting failure pattern causes damage in both, the faces and the core, and can be simulated by introducing different extents of damage in the face and/or the core. It is argued in Section 6.3 that any type of damage reduces the contribution of bending and/or shear stiffness matrix into the global stiffness matrix. Thus, damage cases consisting of varying damage extent in the face and the core, are considered to benchmark the abilities of the proposed damage identification method. Similarly, damage can occur anywhere along the length of the sandwich beam, depending upon the boundary and the loading conditions. Thus, the selected damage cases are simulated at the fixed-end, mid-span and free-end of the beam model, which are indicated by the element number 1, 8, and 15 respectively, in Fig. 6.2.

Damage of different extents are simulated by reducing the respective stiffness of the face and the core by 5%, 10%, 25%, and 50% in both the face and the core, resulting in 24 damage cases for each damage location. Thus, a total of 72 damage cases are simulated for all damage locations. These damage cases are designated in a way, to represent the percentage damage in the face and the core. The adopted scheme in Table

Table 6.4: Simulated damage scenarios (DF-DC) at the fixed-end, the mid-span, and the free-end of the composite sandwich beam.(DF and DC are % damage in the face and the core respectively).

Damage Location	% Damage in Face (DF)	% Damage in Core (DC)				
		00	05	10	25	50
Fixed-end	00		00-05	00-10	00-25	00-50
	05	05-00	05-05	05-10	05-25	05-50
	10	10-00	10-05	10-10	10-25	10-50
	25	25-00	25-05	25-10	25-25	25-50
	50	50-00	50-05	50-10	50-25	50-50
Mid-span	00		00-05	00-10	00-25	00-50
	05	05-00	05-05	05-10	05-25	05-50
	10	10-00	10-05	10-10	10-25	10-50
	25	25-00	25-05	25-10	25-25	25-50
	50	50-00	50-05	50-10	50-25	50-50
Free-end	00		00-05	00-10	00-25	00-50
	05	05-00	05-05	05-10	05-25	05-50
	10	10-00	10-05	10-10	10-25	10-50
	25	25-00	25-05	25-10	25-25	25-50
	50	50-00	50-05	50-10	50-25	50-50

6.4 is in the format of **DF-DC**, where **DF** and **DC** are the percentage reduction in the Young's and shear modulus of the face and the core respectively. For example, 5% and 10% damage in the face and the core respectively, is represented by (05-10) in Table 6.4 for each damage location. The complete list of the identified damage cases at each location is given in Table 6.4.

6.5 Sensitivity of mode shapes for damage

The vibration-based damage identification method proposed in Chapter 5, is based on the premise that the presence of damage changes the vibration responses, such as the natural frequencies and the mode shapes of a structure. Theoretically, this concept is described in Section 5.2. In this section, the sensitivity of the mode shapes of the numerical sandwich beam model towards the location, and extent of damage for damage cases outlined in Table 6.4, will be examined by using the FE model presented in Section 5.1.2. The damage in the beam model is simulated by using the techniques described in Section 6.3.

6.5.1 Varying of damage location

In this sub-section, effects of damage at different locations on the mode shapes of the numerical beam model are investigated. It is shown in Sub-section 5.2.1 that presence of damage at any location in a numerical model, affects the overall mode shapes of a beam. Hence, it is desirable to study the changes in mode shapes of the beam model, in the context of damage identification for the selected damage cases of Table 6.4, at various locations. Therefore, the extent of simulated damage at all locations is kept constant, i.e. 50% damage in the face of the selected location in the numerical beam model of Section 6.1. The mode shapes of the damaged beam model for damage at fixed-end, mid-span and free-end, are compared with those of the undamaged beam model, in Figs. 6.3, 6.4, and 6.5 respectively. It is observed that the magnitude of changes vary in each mode for different damage cases. It is also seen that the first mode shape for all cases, show the largest variation at the mid-span of the beam model, for damage at the fixed-end and mid-span. As the damage location shifts towards the free-end of the beam model, the changes in the first two mode shapes tends to reduce. This can be observed in Fig. 6.5, where changes in the first two mode shapes are almost invisible. The damage location at the mid-span of the beam model in Fig. 6.4, shows the largest changes in the mode shape; whereas, damage at free-end in Fig. 6.5 shows the least variation. Thus, it can be concluded that the magnitude of changes in the mode shapes, depend on the location of the damage but the mode shapes alone are insufficient to locate the damage in the given beam.

6.5.2 Varying of damage extent

In this sub-section, the effects of varying damage extent on the mode shapes of the numerical beam model of Section 6.1 are investigated. The location of damage in the numerical beam model, is selected in such a way that the influence of damage on the changes in the mode shapes, are maximum. This decision is crucial, as there might be some cases where changes in the mode shapes of the damaged beam model, are almost negligible, as shown in previous Sub-section 6.5.1. Comparison of Figs. 6.3 - 6.5 and following discussion in Sub-section 6.5.1, reveals that the maximum changes in the mode shapes are observed for damage located at the mid-span, as shown in Fig. 6.4. Hence, the influence of varying damage extent on the face of the element, at the mid-span of the beam model, is investigated.

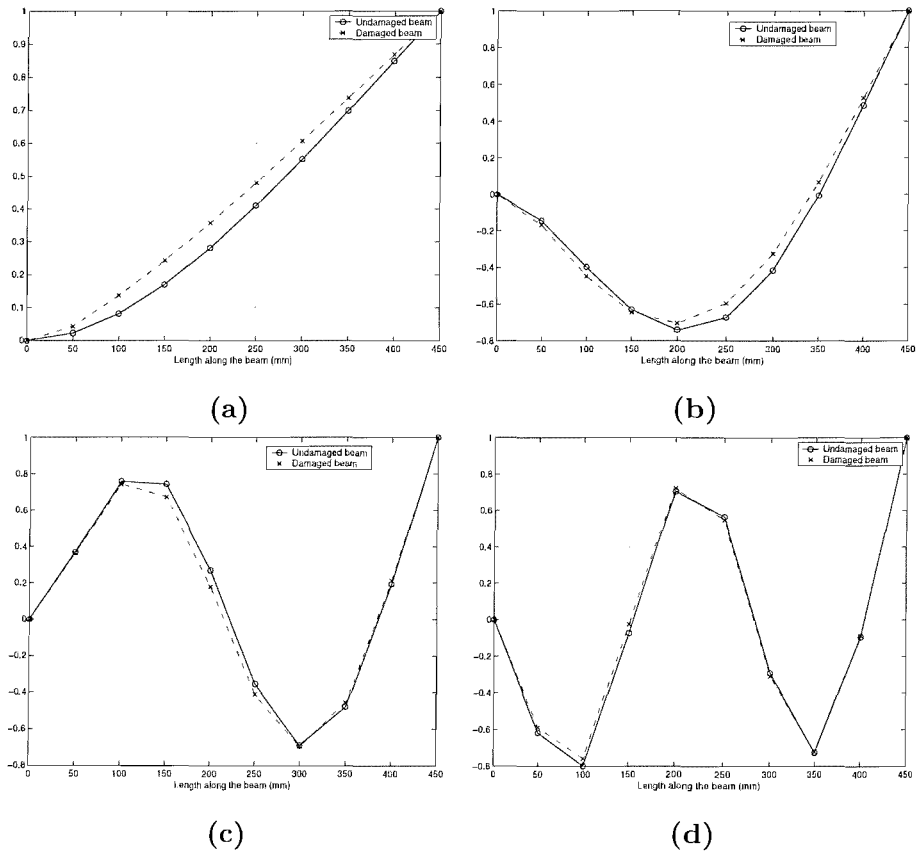

Figure 6.3: Mode shapes of undamaged and damaged sandwich beam model for 50% face damage at the fixed end : (a) First mode, (b) Second mode , (c) Third mode, and (d) Fourth mode.

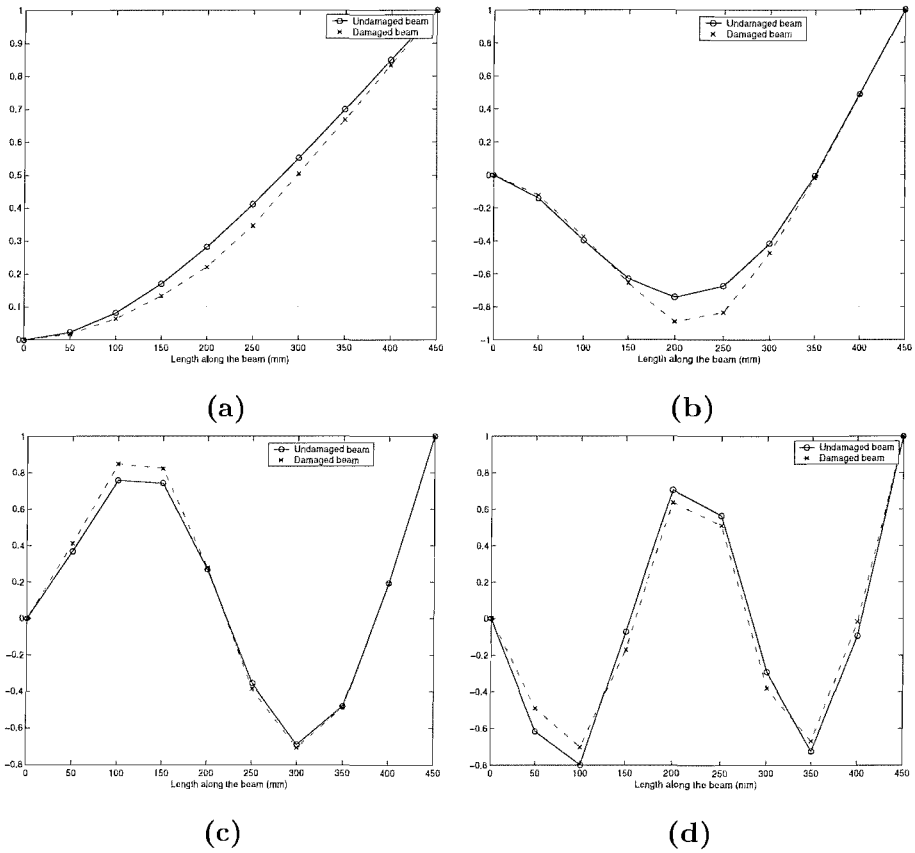

Figure 6.4: Mode shapes of undamaged and damaged sandwich beam for 50% face damage at the mid span : (a) First mode, (b) Second mode , (c) Third mode, and (d) Fourth mode.

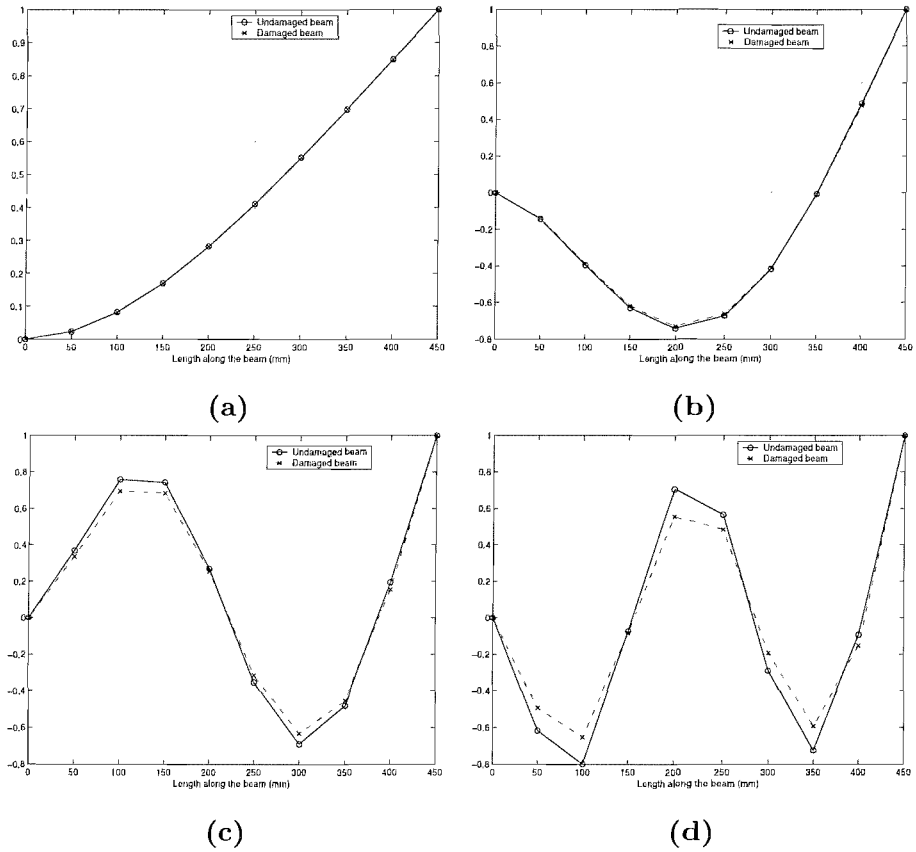

Figure 6.5: Mode shapes of undamaged and damaged sandwich beam for 50% face damage at the free end : (a) First mode, (b) Second mode , (c) Third mode, and (d) Fourth mode.

Damage is simulated in the face of the element at mid-span of the beam model. The extent of damages are chosen from Table 6.4, i.e. 5%, 25%, and 50%. As seen in Fig. 6.6, for the lower value of damage extent (5%) in the face at the mid-span, the changes in the mode shapes of the damaged beam model with respect to those of the undamaged beam model, are almost negligible. As the extent of damage increases, the changes in the mode shapes of the damaged beam model also increase, which are shown in Fig. 6.7 and 6.4, for the damage extent of 25% and 50% in the face, respectively. In all cases, the similar trend in the variations of mode shapes are observed. As shown in this and previous sub-sections, a strong correlation is observed between the changes in the mode shapes and the location and extent of damage in the beam; however, these changes are insufficient to draw any conclusion about the location and the extent of damage in the beam model. This limitation also applies for other damage cases in Table 6.4. Based on these results, it is likely that an observer can discern whether a structure has been damaged or not. However, higher level of damage identification would be unreliable, without analysing these mode shapes, using a damage identification method such as the method proposed in Section 5.2.

6.6 Damage identification calculations and analysis

In Section 6.2 and 6.5, it is shown that the numerical beam model of Section 6.1 is capable of modelling the behavior of the undamaged and damaged beam. This gives the confidence in using the numerical beam model, to generate their natural frequencies and mode shapes, for damage cases referred in Section 6.4. Damage is simulated as per using techniques described in Section 6.3. Results in Section 6.5 reveal that the mode shapes of the damaged beam model are sensitive to the presence of damage. However, the degree of sensitivity depends on the location and the extent of damage. For a relatively lower extent of damage such as 5% in the face of selected element, sensitivity of the mode shapes towards damage is almost negligible as shown in Fig. 6.6. Similarly, for a relatively higher value of damage extent (50%) at the free-end of the beam model, variation in the mode shapes as shown in Fig. 6.5, are negligible for the first two lowest mode. The variation in the mode shapes of the damaged beam model indicates the presence of damage, i.e. level 1 of damage identification as referred in Section 2.4, but by no means useful for higher level of damage identification, i.e. its location, extent and level. The inability of the mode shapes to locate damage in the numerical beam model, highlights the limitation of the changes in mode shapes

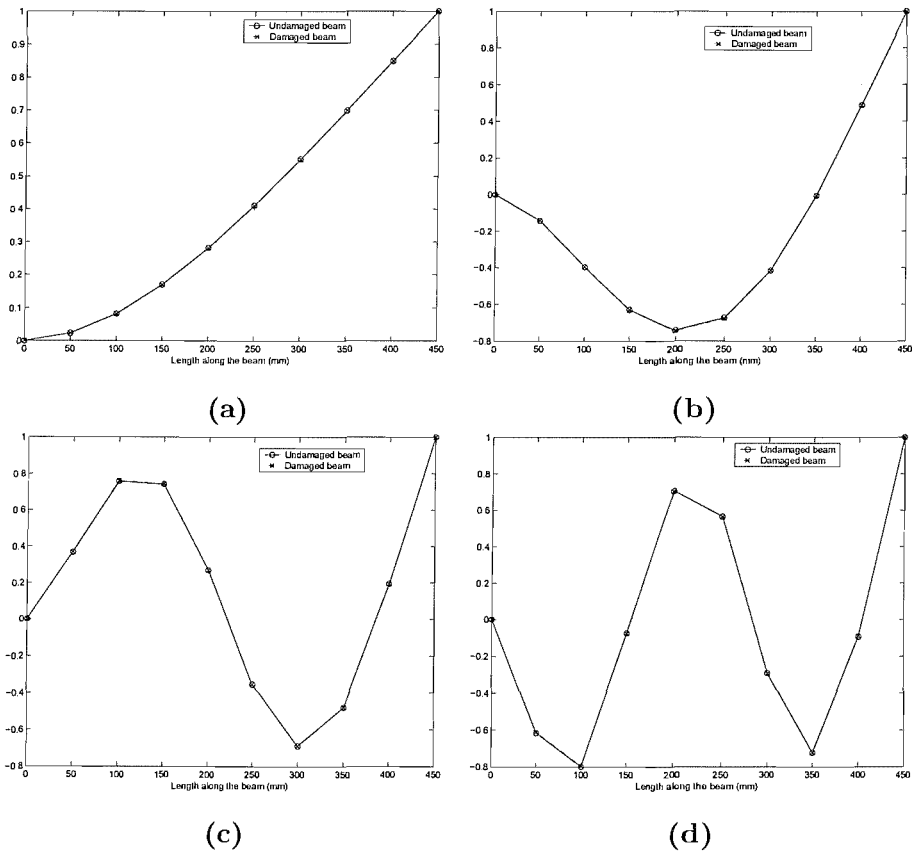

Figure 6.6: Mode shapes of undamaged and damaged sandwich beam for 5% face damage at the mid span : (a) First mode, (b) Second mode , (c) Third mode, and (d) Fourth mode.

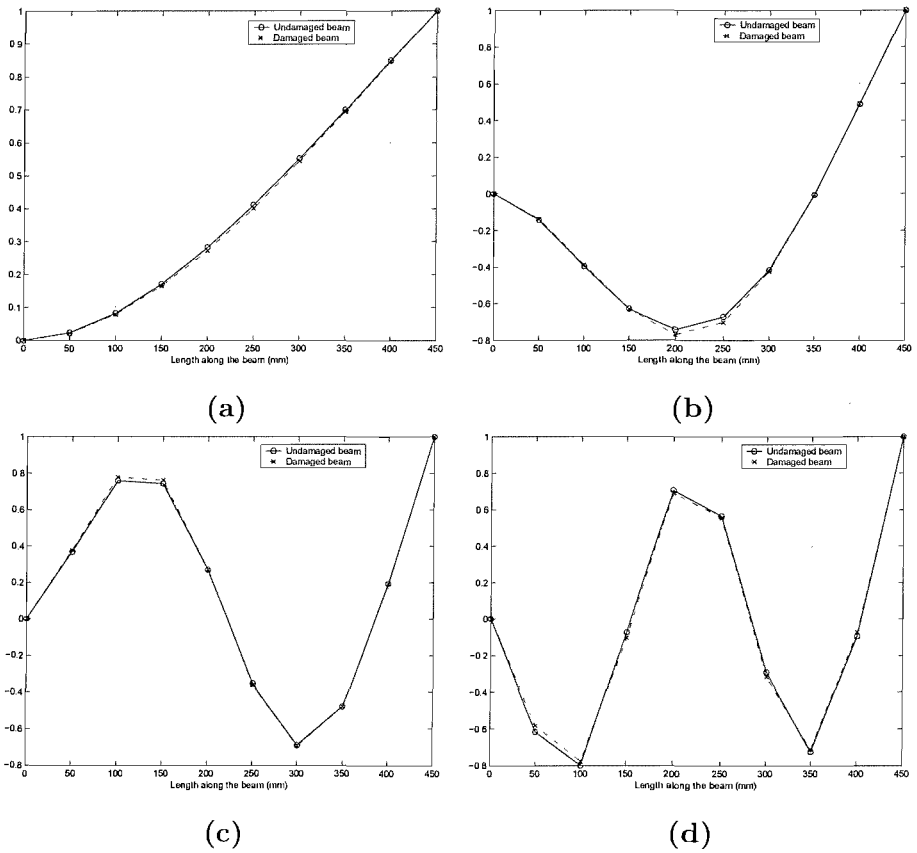

Figure 6.7: Mode shapes of undamaged and damaged sandwich beam for 25% face damage at the mid span : (a) First mode, (b) Second mode , (c) Third mode, and (d) Fourth mode.

for damage localisation. Thus, the damage identification method for identification of location and extent of damage in the beam model is required. In this section, the damage identification method proposed Chapter 4 and developed in Section 5.2 will be examined, for the damage scenarios presented in Table 6.4, to assess the abilities of the method to identify location and extent of damage, using the numerical beam model.

6.6.1 Prediction of damage location

The objective of this sub-section, is to examine the capability of the damage identification method, for locating a single damage in the numerical beam model for the selected damage cases. The damage localisation method described in Sub-section 5.2.3 is used to locate damage for the damage cases as in Table 6.4. The first four mode shapes of the undamaged and damaged sandwich beam model are used to calculate MSECR_j of the jth element, using Eqn. 5.43. MSECR_j values are then normalised with respect to the largest value, $\text{MSECR}_{j,max}$, to obtain a damage index. It is expected that the unit value of damage index will simply indicate the presence of damage at that element in the beam.

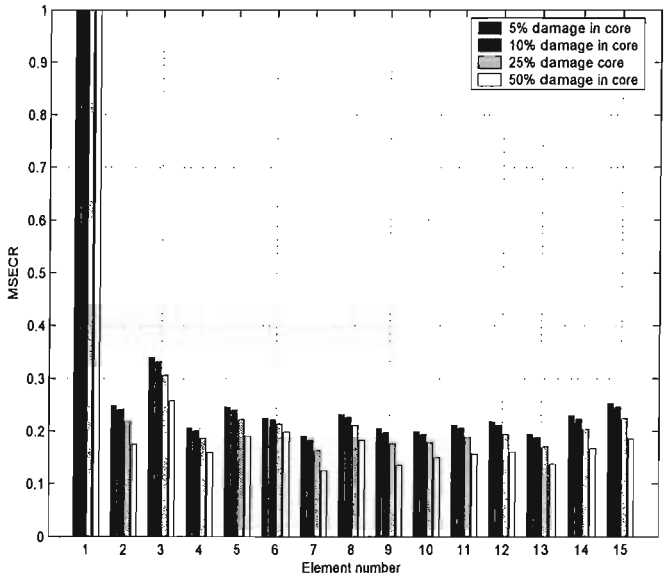

Figure 6.8: Damage localisation at the fixed-end (element 1) : undamaged face and 5%, 10%, 25%, and 50% of damage in the core.

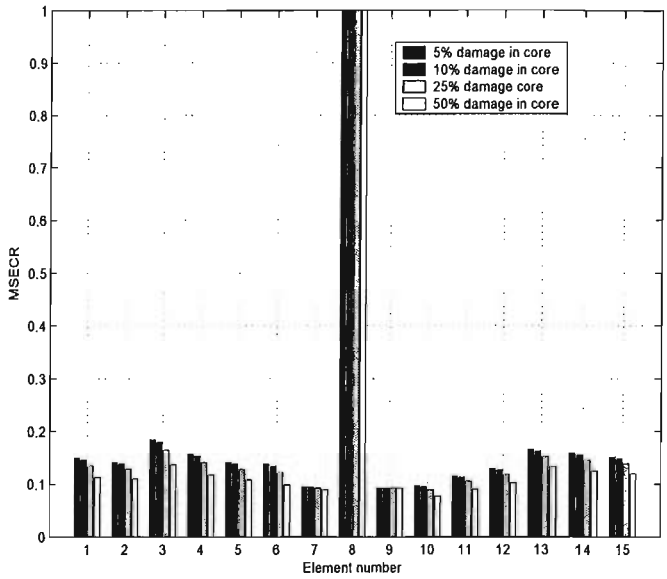

Figure 6.9: Damage localisation at the mid-span (element 8) : undamaged face and 5%, 10%, 25%, and 50% damage in the core.

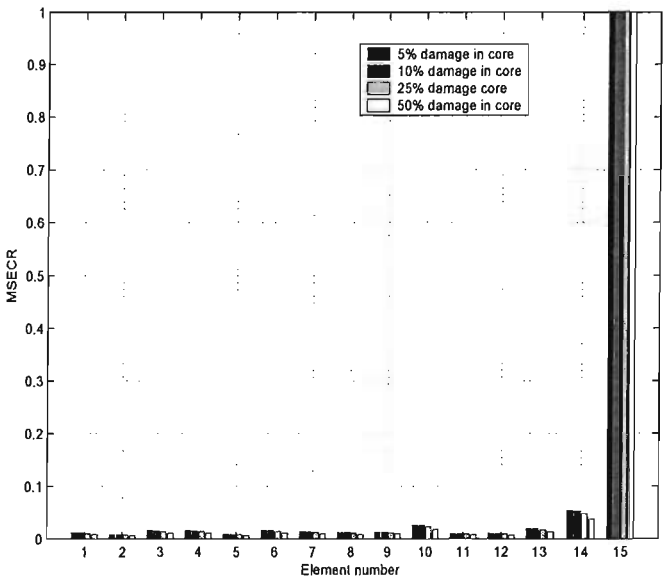

Figure 6.10: Damage localisation at the free end (element 15) : undamaged face and 5%, 10%, 25%, and 50% damage in the core.

Results indicate that MSECR of the damaged element is most sensitive towards the presence of damage, as indicated by their unit value for the damaged element and much higher than those of the other undamaged elements. Results for few damage cases are plotted in Figs. 6.8 - 6.13 and these show similar trends for other damage cases. In all selected damage cases, damage is successfully indicated by unit value of $MSECR_j$. The results indicate that the modal strain energy changes, in the element adjacent to the damaged element, are relatively higher than those of the elements far away, validating the assumptions made for the damage localisation formulation in Sub-section 5.2.3. The changes in the modal strain energy in the element adjacent to the damaged element, also depends on the location of the damage, which corraborates the observation made in Section 6.5. The difference between the MSECR for the damaged and its adjacent elements is the largest for the damage at the free-end; this reduces as the damage location moves inward and becomes the lowest for the damage at the fixed-end of the beam model. This leads to the conclusion that the damage localisation method performs better if the damage is located towards the free-end. It is interesting to note that the $MSCER_j$ for undamaged elements, reduces by more than 70% in most of the damage cases, which proves the sensitivity of modal strain energy towards the damage. Similar trends were also observed by Shi *et al* [Shi *et al.*, 2000, 2002] in a simply supported steel beam and truss structure.

The results presented in this sub-section, indicate that the modal strain energy change in the damaged element of the numerical sandwich beam model, is maximum compared to those of other undamaged elements, which proves the sensitivity of elemental modal strain energy towards the presence of damage. This is supported by the fact that the normalised MSECR value for the damaged element is much higher compared to those of the other elements. Thus, the results and subsequent discussion indicate that the proposed damage localisation method in Sub-section 5.2.3 successfully achieves its objective of locating damage for the selected damage cases, in the numerical beam model.

6.6.2 Predictions of damage extent

In Sub-section 6.6.1, it was shown that the elemental modal strain energy estimated by using the formulae of Sub-section 5.2.4, was sensitive towards the presence of damage in the element and was successfully applied for damage localisation. The successful application of the elemental modal strain energy for the damage localisation, makes this concept an attractive choice for prediction of damage extent. In this section, changes

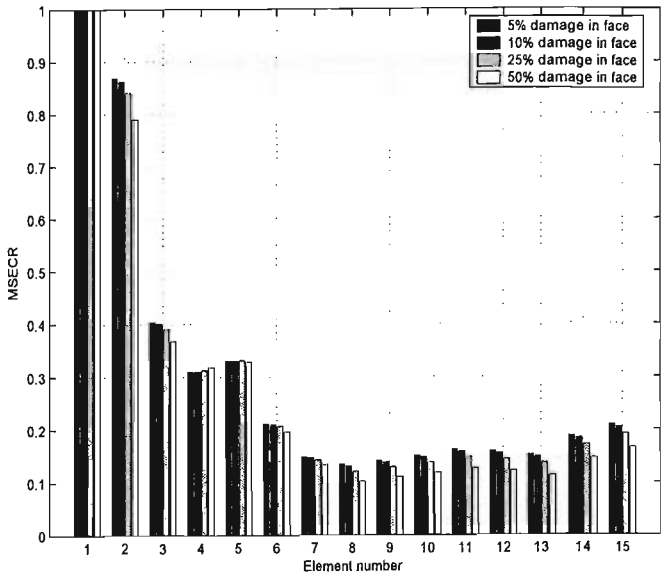

Figure 6.11: Damage localisation at the fixed-end (element 1) : undamaged core and 5%, 10%, 25%, and 50% of damage in the face.

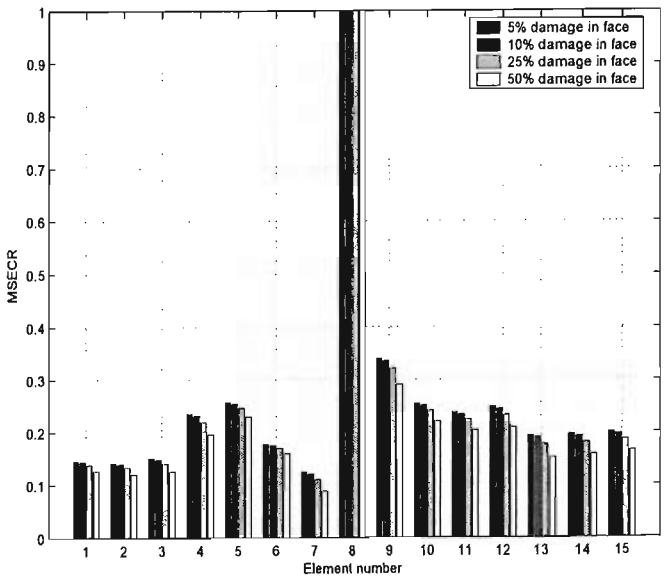

Figure 6.12: Damage localisation at the mid-span (element 8) : undamaged core and 5%, 10%, 25%, and 50% damage in the face.

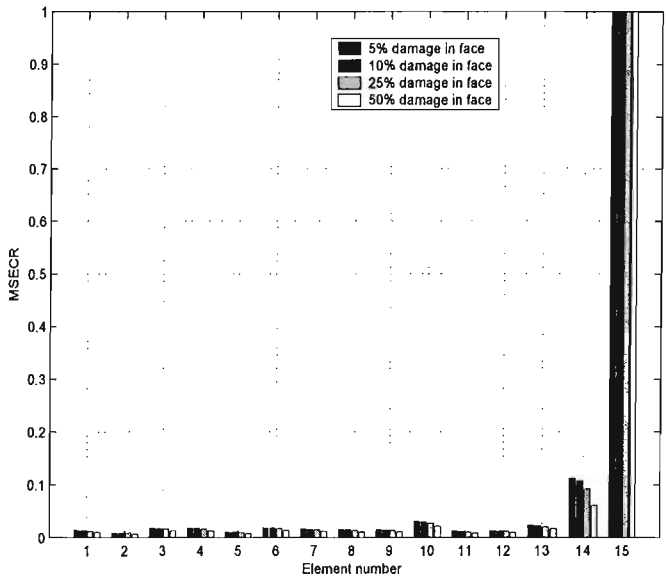

Figure 6.13: Damage localisation at the free-end (element 15) : undamaged core and 5%, 10%, 25%, and 50% damage in the face.

in the elemental modal strain energies are used for the prediction of damage extent, for different damage cases, using the method outlined in Chapter 4 and developed in Sub-section 5.2.4. Simulated damage cases and the numerical beam model in this sub-section are same as those of Sub-section 6.6.1.

The inputs for damage quantification in the methodology proposed in Chapter 4 are the natural frquencies and mode shapes of the damaged sandwich beam. Using these inputs, damage extents in the face and core of the given sandwich beam model are calculated by using the derived Eqn. 5.54 and 5.55 respectively, in Section 5.2. The resulting prediction of the damage extent using these equations are presented in Tables 6.5, 6.6, and 6.7 for the damage at the fixed-end, mid-span, and free-end of the beam model respectively. Their accuracies are examined by comparing with the simulated values in Table 6.4 and also are indicated within parenthesis in Tables 6.5 - 6.7, for convenience in comparison. Thus, the predicted values of damage extent for the damage case of (00-05)%, at the fixed-end of the beam model, are represented as (4.28-5.43)% in Table 6.5. Comparisons in Tables 6.5 - 6.7 reveal the overestimation in the predicted values of damage extent, after the first stage of damage quantification in most of the damage cases. However, there are a few instances, where the damage extents are underestimated for the damage in the faces, specially at the ends of the beam model

Table 6.5: Damage extent predictions (DF-DC : % damage in the face and the core respectively) after the first stage of the damage quantification for the damage at the fixed-end (element 1) of the composite sandwich beam.(Numbers in the parenthesis are the simulated values of DF-DC)

% Damage in face (DF)	% Damage in core (DC)				
	00	05	10	25	50
00		3.08-5.13 (00-05)	8.01-10.42 (00-10)	19.06-24.93 (00-25)	45.28-46.11 (00-50)
05	4.63-0.21 (05-00)	5.92-5.48 (05-05)	8.43-10.89 (05-10)	19.91-25.54 (05-25)	48.81-46.43 (05-50)
10	5.32-0.43 (10-00)	9.04-5.91 (10-05)	12.71-10.96 (10-10)	22.12-25.17 (10-25)	45.86-45.02 (10-50)
25	13.82-1.12 (25-00)	17.07-6.51 (25-05)	20.39-12.82 (25-10)	29.21-26.81 (25-25)	51.02-47.78 (25-50)
50	30.43-3.56 (50-00)	30.91-9.90 (50-05)	31.12-14.81 (50-10)	45.73-31.67 (50-25)	60.33-50.15 (50-50)

for a lower extent of damage, such as 5% and 10% in the core and as given in Tables 6.5 and 6.7. The overestimation/underestimation of these predictions are attributed to the assumptions made in Section 5.2, which have affected the results. Assumptions in Subsection 5.2.2 result in the approximation of the elemental modal strain energies, which are used as inputs for predicting the damage extent, using approximate expressions derived in Section 5.2. This results in further approximating the predictions of damage extent in the faces and the core. The approximation may be an overestimation or an underestimation of the predictions. However, the results in this section after the first stage of damage identification, are indicative of the damage extent in most of the damage cases, specially for the core damage. The difference between the predicted values in Tables 6.5 - 6.7 and their simulated values in Table 6.4, varies widely for different damage cases, but show similar trends for each damage location. Hence, for improved results, there is a need to optimise these predicted values of damage extent.

The objective of the second stage of damage quantification is to optimise the approximated damage extent values, obtained at the first stage, to the target values, i.e., the simulated damage extent. Also, the modelling errors inherent to the model-based damage identification method can be greatly reduced by using well-established model updating techniques [Carneiro, 2000] as outlined in Chapter 4. This is essential as the elemental modal strain energies used in the first stage of damage quantification are

Table 6.6: Damage extent predictions (DF-DC : % damage in the face and the core respectively) after the first stage of the damage quantification for the damage at the mid-span (element 8) of the composite sandwich beam.(Numbers in the parenthesis are the simulated values of DF-DC)

% Damage in face (DF)	% Damage in core (DC)				
	00	05	10	25	50
00		0.72-6.58 (00-05)	1.02-13.28 (00-10)	5.87-32.63 (00-25)	23.34-58.78 (00-50)
05	7.29-0.08 (05-00)	8.14-6.84 (05-05)	8.58-13.34 (05-10)	12.42-32.62 (05-25)	25.47-58.87 (05-50)
10	12.34-0.21 (10-00)	14.79-7.58 (10-05)	15.22-14.75 (10-10)	20.72-33.88 (10-25)	36.17-59.28 (10-50)
25	35.86-0.37 (25-00)	36.76-8.12 (25-05)	38.12-15.09 (25-10)	40.58-33.81 (25-25)	50.52-60.21 (25-50)
50	64.78-0.53 (50-00)	64.68-8.12 (50-05)	64.87-16.07 (50-10)	65.61-34.81 (50-25)	69.51-62.61 (50-50)

Table 6.7: Damage extents predictions (DF-DC : % damage in the face and the core respectively) after the first stage of the damage quantification for the damage at the free-end (element 15) of the composite sandwich beam.(Numbers in the parenthesis are the simulated values for DF-DC)

% Damage in face (DF)	% Damage in core (DC)				
	00	05	10	25	50
00		3.21-8.41 (00-05)	7.06-16.71 (00-10)	17.96-38.98 (00-25)	42.67-69.25 (00-50)
05	4.56-0.97 (05-00)	7.87-8.60 (05-05)	11.04-17.01 (05-10)	21.58-38.91 (05-25)	48.11-69.24 (05-50)
10	9.09-0.18 (10-00)	11.29-9.05 (10-05)	14.14-16.91 (10-10)	25.81-38.79 (10-25)	50.13-71.05 (10-50)
25	24.03-1.09 (25-00)	26.01-8.18 (25-05)	28.68-16.92 (25-10)	38.81-41.02 (25-25)	60.27-72.25 (25-50)
50	51.24-1.69 (50-00)	54.08-9.86 (50-05)	54.81-19.16 (50-10)	60.73-41.02 (50-25)	76.01-73.07 (50-50)

Table 6.8: Damage extents predictions (DF-DC : % damage in the face and the core respectively) after the second stage of the damage quantification for the damage at the fixed-end (element 1) of the composite sandwich beam.(Numbers in the parenthesis are simulated values for DF-DC).

% Damage in face (DF)	% Damage in core (DC)				
	00	05	10	25	50
00		2.56-3.19 (00-05)	0.00-5.26 (00-10)	0.00-16.70 (00-25)	0.00-21.12 (00-50)
05	4.78-0.02 (05-00)	3.68-3.11 (05-05)	4.78-5.66 (05-10)	4.79-18.81 (05-25)	4.82-44.71 (05-50)
10	9.82-0.00 (10-00)	8.24-4.78 (10-05)	8.21-4.88 (10-10)	9.01-17.23 (10-25)	8.71-42.81 (10-50)
25	23.87-0.01 (25-00)	19.31-4.21 (25-05)	21.81-9.32 (25-10)	23.89-21.82 (25-25)	19.26-40.82 (25-50)
50	49.82-0.00 (50-00)	48.22-3.91 (50-05)	46.71-4.81 (50-10)	46.62-22.36 (50-25)	49.21-35.01 (50-50)

Table 6.9: Damage extents predictions (DF-DC : % damage in the face and the core respectively) after the second stage of the damage quantification for the damage at the mid-span (element 8) of the composite sandwich beam.(Numbers in the parenthesis are the simulated values for DF-DC)

% Damage in face (DF)	% Damage in core (DC)				
	00	05	10	25	50
00		0.00-4.88 (00-05)	0.92-9.22 (00-10)	0.00-23.75 (00-25)	1.01-49.78 (00-50)
05	4.99-0.00 (05-00)	4.67-4.71 (05-05)	4.64-9.86 (05-10)	4.37-24.16 (05-25)	0.00-48.91 (05-50)
10	9.86-0.00 (10-00)	9.66-4.84 (10-05)	8.78-8.42 (10-10)	8.02-23.21 (10-25)	5.03-45.06 (10-50)
25	24.87-0.00 (25-00)	22.78-4.80 (25-05)	21.89-8.07 (25-10)	20.01-17.06 (25-25)	19.63-45.81 (25-50)
50	49.87-0.00 (50-00)	49.01-4.66 (50-05)	48.81-5.06 (50-10)	46.18-16.26 (50-25)	46.21-43.28 (50-50)

Table 6.10: Damage extents predictions (DF-DC : % damage in the face and the core respectively) after the second stage of the damage quantification for the damage at the free-end (element 15) of the composite sandwich beam.(Numbers in the parenthesis are the simulated values for DF-DC)

% Damage in face (DF)	% Damage in core (DC)				
	00	05	10	25	50
00		1.71-3.97 (00-05)	1.05-9.01 (00-10)	1.21-17.24 (00-25)	0.70-32.97 (00-50)
05	11.12-4.13 (05-00)	11.02-4.81 (05-05)	15.07-9.21 (05-10)	15.01-22.19 (05-25)	16.19-31.18 (05-50)
10	9.72-0.04 (10-00)	13.86-4.89 (10-05)	18.97-9.03 (10-10)	21.78-22.48 (10-25)	24.29-30.06 (10-50)
25	24.29-0.01 (25-00)	27.92-4.57 (25-05)	37.78-8.98 (25-10)	37.12-18.91 (25-25)	38.12-42.28 (25-50)
50	50.00-0.00 (50-00)	52.81-3.45 (50-05)	53.05-9.01 (50-10)	56.12-17.17 (50-25)	60.21-41.12 (50-50)

approximated, as evident from the results in Tables 6.5 - 6.7. Thus, the FE model updating procedure, described in Section 5.2, is used for optimising the predictions from the first stage. This is done in order to minimise the large difference between the predictions from the first stage of damage identification with those of the simulated values of damage extent. Therefore, the predictions of damage extents after the first stage in Tables 6.5 - 6.7 are used as the inputs for the second stage, i.e., FE model updating stage as shown in Fig. 5.4. Since, location of damage is predicted in the previous sub-section, the updated FE model of the sandwich beam is created by using the outputs from the first stage of damage quantification. Hence, starting step at the second stage is the creation of the updated FE model of the damaged sandwich beam using the predictions of the first stage. This model is used to calcuate the updated natural frequencies, which are compared with the measured natural frequencies of the damaged sandwich beam using the objective function defined in Sub-section 5.2.4. If the output of the objective function is more than the pre-determined tolerance limit, then, the extent of damage in the face and core is updated by using the non-linear optimisation method known as Nelder-Mead method. This part of damage quantification is known as model updating procedure. This cycle continues until the output of the objective function is under the tolerance limit. Once this convergence condition is achieved, the model updating procedure is terminated. Hence, the damage extents in

the face and core are updated at each iteration. The final values of damage extents after the model updating are the damage extent in the face and core. These predictions of damage extent in the face and core of the sandwich beam model after the FE model updating, are presented in Tables 6.8, 6.9, and 6.10 for damage at the fixed-end, mid-span, and free-end of the beam model. The improvements in the predicted damage extent values after the FE model updating procedure, are assessed by comparing the results in Tables 6.5 and 6.8, for damage at the fixed-end of the beam model. It can be observed that a better convergence is achieved after the second stage of damage extent prediction. This is specially true where the damage extent is higher than 5 % in the face of the beam model for all damage cases. The damage extent of the core tends to be underestimated after the second stage. Similar trends are observed for the predicted values of damage extent in the core for other damage locations. It is observed that the damage extent predicted by the second stage tends to converge better where the damage extent higher than 5 %.

6.6.3 Sensitivity for damage location

In this sub-section, the sensitivity of the damage identification method for different locations of damage, based on the results presented in Sub-sections 6.6.1 and 6.6.2, is discussed. In these sub-sections, the damage cases listed in Table 6.4 were simulated at the three different locations, namely, the fixed-end, the mid-span, and the free-end of the numerical beam model.

Analysis of the results in Figs. 6.8 - 6.13, reveals that the location of damage influences the changes in the elemental modal strain energy, hence the damage identification results. The changes are clearly distinguishable, compared to those of the changes in the mode shapes for the same damage cases, as in Section 6.5. However, magnitudes of the changes are sensitive to damage locations as seen in Figs. 6.8 - 6.13. In most of the cases, the normalised MSECR_j of the undamaged elements were about 70% less than that of the damaged element. The largest changes are observed for the damage at the free-end of the beam model, in Figs. 6.10 and 6.13, and the lowest for the damage at the fixed-end as shown in Figs 6.8 and 6.11. Hence, it can be inferred that the changes in the elemental modal strain energy, decreases as the damage location moves from the free-end to the fixed-end, for the same level and extent of damage. This observation implies that a relatively low extent of damage at the fixed-end in the beam model, may be difficult to locate.

Effects of damage location are more prominent for predictions of damage extents than those of damage location. Although predictions of damage extents after the first and second stage of damage quantification vary widely, their accuracies show dependency on the location, extent and type of damage. Generally, a better convergence is achieved for damage located at the mid-span and fixed-end of the beam model, than those at the free-end. This is believed to be because of the fact that changes in the mode shapes of the given beam model in damaged zone, are smooth and continuous, which result in a smooth and continuous profile for changes in the elemental modal strain energies, across the damaged zone in the beam model. For damage located at the free-end, a better convergence is achieved for a relatively lower extent of damage in the core. With increasing value of damage extent in the core, the difference between the predicted values and the simulated values increases, as seen in Table 6.7 and 6.10.

6.6.4 Sensitivity for damage type and extent

Next, sensitivity of the proposed damage identification method for remaining factors, i.e. extent and type of damage, is discussed in this sub-section. For this purpose, two sets of damage scenarios are considered. In the first set, only those damage scenarios are selected in which the faces remain undamaged and the core is damaged. Similarly, the second set of damage scenario includes cases where the core is undamaged and the faces are damaged. These results prove that the level of damage influences the changes in the elemental modal strain energies, as shown by the damage localisation results in Figs. 6.8 and 6.11, for damage at the fixed-end of the beam model. Different levels of damage at other locations, show similar trends but the changes are significantly less compared to that of the fixed-end, i.e. they show sensitivity for damage locations. Their results indicate that the proposed method predicts the extent of damage, as low as 5% in the face and the core of the sandwich beam model, with a fairly reasonable accuracy. For damage cases with damage in either faces or core, predictions of the damage extent after the second stage of damage quantification, have a better accuracy compared to the damage cases with interacting damage modes. It can be seen in Tables 6.5 - 6.10 that interacting damage modes adversely affect the prediction of the damage extent, specially for damage scenarios where damages in both the faces and the core are 25% or more. This is particularly significant for the faces, where predictions of the damage extent were adversely affected, by the presence of damage in the core. However, these predictions improved significantly after the second stage of damage quantification, for most of the damage cases, specially for damage at the mid-span of

the beam. It is interesting to note that in most of the damage cases, overestimated damage extent predictions for the core after the first stage, tend to be underestimated in the second stage of damage quantification. This trend in predictions of the damage extent in the core is also observed for interacting damage modes. Based on the trends in predictions of the damage extent for the core, it can be concluded that the average of damage extent predictions of the first stage and the second stage, may be a better indicator of the damage extent for a relatively low extent of damage in the core.

6.7 Conclusions

In this chapter, the proposed damage identification method, using the numerical beam model was examined, for the simulated damage cases identified in Table 6.4. This includes the study of the effectiveness of the proposed damage identification method for varying location, extent and level of damage, which comprised the focus of Section 6.6 and the results were indicative of the existence, location, extent and level of the damage. The damage extent predictions in Sub-section 6.6.2 enables to decide whether damage is in the face, core or in both. Thus, the objectives of the damage identification method were achieved, proving the legitimacy of the assumptions made in Section 5.2. It also gives the confidence to use the proposed damage identification method with the experimental measurements, which is objective of Chapter 8. For this purpose, the required experimental specimens, equipments and procedures will be systematically laid out in Chapter 7.

Chapter 7

Experimental Procedure and Specimens Fabrication

In this chapter, experimental procedures for the measurement of natural frequencies and mode shapes of the sandwich beam specimens are described, which will be used to validate the damage identification method. The natural frequencies and mode shapes of the beam specimens are obtained by performing two sets of vibration experiments. The first set measures and records the acceleration responses at one location of the specimen covering a certain range of frequencies, to obtain their natural frequencies. In the second set, nine accelerometers will be used to measure acceleration responses at nine different locations along the centre line of the beam specimen, to obtain its mode shapes. This chapter outlines firstly, the fabrication procedures for the undamaged and damaged sandwich beam specimens, secondly, the required experimental set-up, thirdly, the excitation techniques and experimental measurements and fourthly, their pre-processing techniques for the calculation of the free vibration properties of the beam specimens.

7.1 Fabrication of sandwich beam specimens

In this section, fabrication procedures for the undamaged and damaged beam specimens are presented. The geometrical and mechanical properties of the beam specimens are same as those of the numerical beam model in Chapter 6. The materials used for fabrication of the beam specimens are glass fibres and Poly Vinvyl Chloride (PVC) foam (CoreCell A400 [CoreCell©]) for the faces and the core, respectively. All these constituents are bonded together by an epoxy resin system (PRIME 20). Specimens are fabricated by using the *vacuum bagging* technique. In this technique, the glass

fibres and the PVC foam in the selected lay-up, are covered by plastic sheets to form an air-tight bag and sealed to prevent the entry of air bubbles. The sealed bag is vacuumed by using a suction pump from one end. The other end is tight enough to prevent the entry of any air bubbles. After vacuuming, the inlet is used to infuse low viscosity resin such as epoxy inside the bag. Excess amount of resin after infusion, is sucked by a suction pump to prevent accumulation of resin inside the bag; hence, it prevents the formation of resin rich pockets in the specimen. This technique is also used for the fabrication of damaged sandwich beam specimens.

Two type of damaged sandwich beam specimens are fabricated to introduce the damage modes discussed in Section 2.1. The following damage modes are introduced during the fabrication process,

1. Face-core debonding, and
2. Face damage/delamination.

Damage is introduced at the mid-span and one third distance from the fixed-end of the sandwich beam specimens. The face-core debonding is introduced by placing a thin teflon tape, across the width between the face and the core during their fabrication. The extent of debonding and face damage, is equal to the size of the teflon tape across the whole width of the sandwich beam specimens. The face damage is introduced by removing a part of the face along the length of the beam specimen.

7.2 Experimental set-up

The beam specimens fabricated in Section 7.1, must be tested to measure their natural frequencies and mode shapes, by using the available experimental set-up. This requires the beam specimens to be excited by using an external excitation source and recording their responses. The main components of the available experimental set-up are,

- Digital vibration controller with in-built data acquisition unit, for acceleration measurements from four in-built measurement channels.
- Electrodynamic shaker to apply excitation force to the specimen.
- Power amplifier to control the electrodynamic shaker.
- Signal-conditioning amplifier connected with external data acquisition system.

The beam specimens fabricated in Section 7.1, are excited by using the experimental set-up and their reponses are measured, by using miniature accelerometers. The excitation technique used to excite the beam specimen will be discussed in Section 7.3. The used experimental set-up for this purpose is shown in Fig. 7.1. The excitation source in the set-up is controlled by the digital vibration controller, which in conjunction with the power amplifier constitutes the main part of the set-up. The digital vibration controller has four measurement channels, one for measuring the input excitation force and the other three for measuring the acceleration responses of the beam specimen. The input channel measures the applied input excitation force to the specimen by the shaker; whereas, output channels measure the output responses of the specimen. Experimental readings obtained by these channels are processed, by using the in-built analyser and their power spectral density is plotted, to obtain the natural frequencies of the specimen. However, the natural frequencies alone are insufficient for damage identification in the beam specimen, using the method verified in Chapter 6, which also requires the mode shapes of the beam specimen to be measured.

In order to measure mode shapes of the beam specimen, the acceleration responses must be measured at various points along the centre line, at regular intervals as shown in Fig. 7.2. Miniature accelerometers used for these measurements were manufactured by PCB piezotronics (model 352A21), each having weight of 0.6 *gm*. These accelerometers sample analog signals at frequency of 1800 *Hz*, which then passes through the signal conditioning unit and Analog-to-Digital Converter (ADC), to data acquisition software for their storage and analysis, as discussed in Section 7.4.

7.3 Excitation techniques

In order to measure the vibration responses of the beam specimen, it must be excited by using an external excitation source, such as an electrodynamic shaker attached with the experimental setup of Section 7.2. The applied excitation forces are controlled by the digital vibration controller attached with the setup, as per the selected excitation technique. The available excitation techniques are sine frequency sweep excitation, fixed frequency excitation and random excitation.

Out of these three excitation techniques, sine frequency sweep excitation is used to excite the beam specimen, as it excites the specimen across a range of frequency. In this excitation, a sinewave is swept through the frequency range of interest, while output responses are measured and input signals are controlled, via a digital vibration

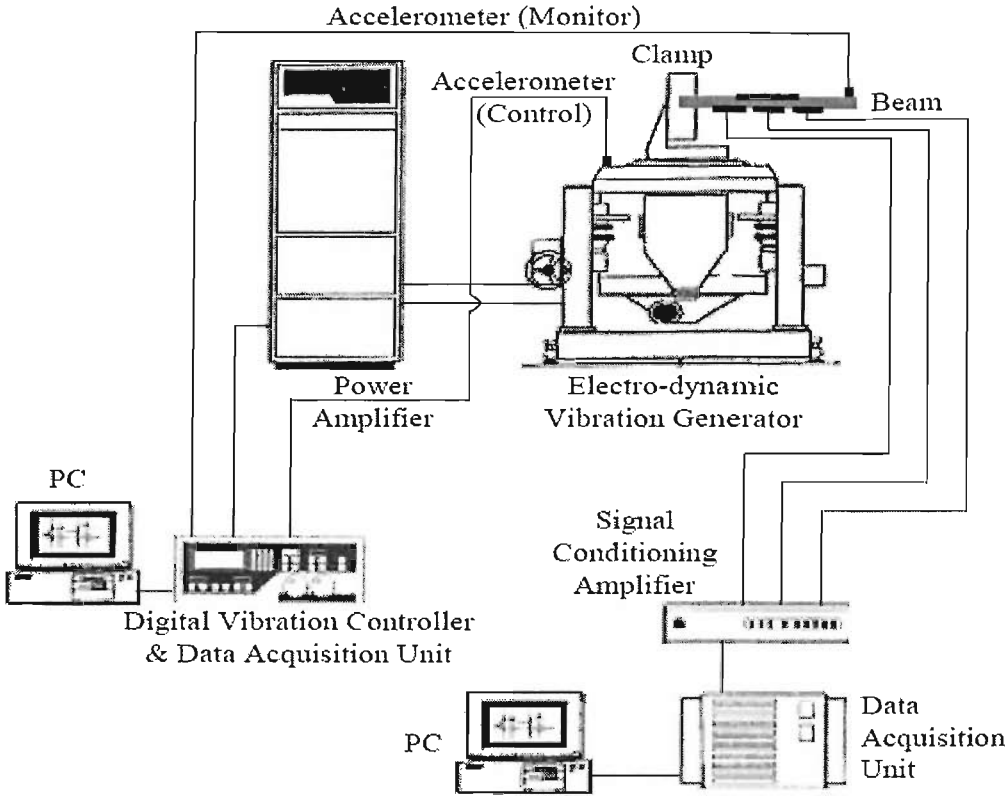

Figure 7.1: Experimental set-up for the vibration test.

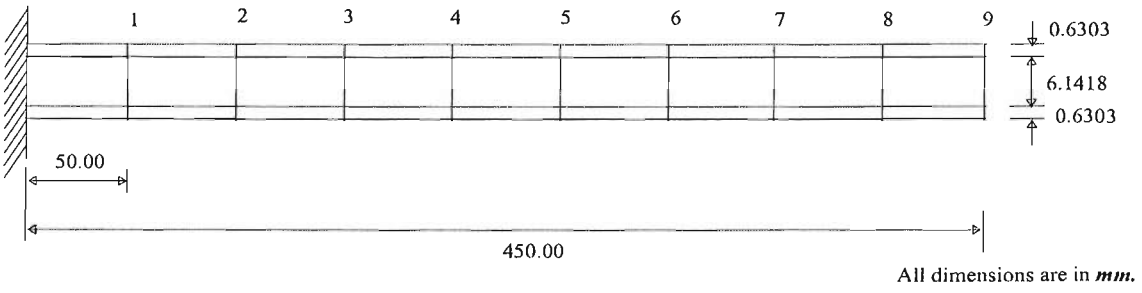

Figure 7.2: Accelerometers location of the beam specimen.

controller to maintain a constant sinusoidal input excitation force. In this way, the natural frequencies of the beam specimen are obtained. In this setup, sweep rate can be entered as time per complete frequency sweep or directly as a rate (Hz/s). Unidirectional, sine sweep with the linear incremental sweep rate from low frequency limit to higher frequency limit, is used for exciting the beam specimen.

Constant frequency excitation technique can be used to obtain the vibration responses at a single frequency. Usually, this is performed after identifying the natural frequencies of a specimen. In random excitation, a test specimen is subjected to vibration consisting of randomly (i.e. continuous random noise with Gaussian distribution) varying levels of frequencies, within a specified range. One of the important parameters in random excitation is the bandwidth value, which is used to determine the highest frequency that can be measured during the test. The bandwidth value can be set automatically and it accommodates the entire profile.

The excitation techniques presented in this section will be used to excite the beam specimens, to measure the acceleration responses at the locations shown in Fig. 7.2. These measurements will be processed to extract the natural frequencies and mode shapes of the beam specimen, by using the procedure presented in Section 7.4.

7.4 Experimental measurements and processing techniques

An accelerometer converts an acceleration signal to voltage signal that can be measured, analysed and recorded by a data acquisition system. Voltage signals from an accelerometer are converted into digital signals using an Analog-to-Digital Converter (ADC). The digital signals are converted into measurement values by the data acquisition software. The experimental setup in Section 7.1, measures the time series acceleration responses of the beam specimen at locations shown in Fig. 7.2, which must be converted into the frequency domain, in order to extract the natural frequencies and mode shapes.

The first step in processing the measured time series accelerations, is their transformation into the frequency domain, by using Fast Fourier Transformation (FFT). The basic mathematical background of FFT is given in Appendix F. The input forces and the output responses in frequency domain, are used to calculate the complex valued Frequency Response Function (FRF), which is simply the ratio of the output responses of the beam specimen to the applied input force. Similarly, the FRFs are calculated for all measurement locations shown in Fig. 7.2. The collection of FRFs is also known

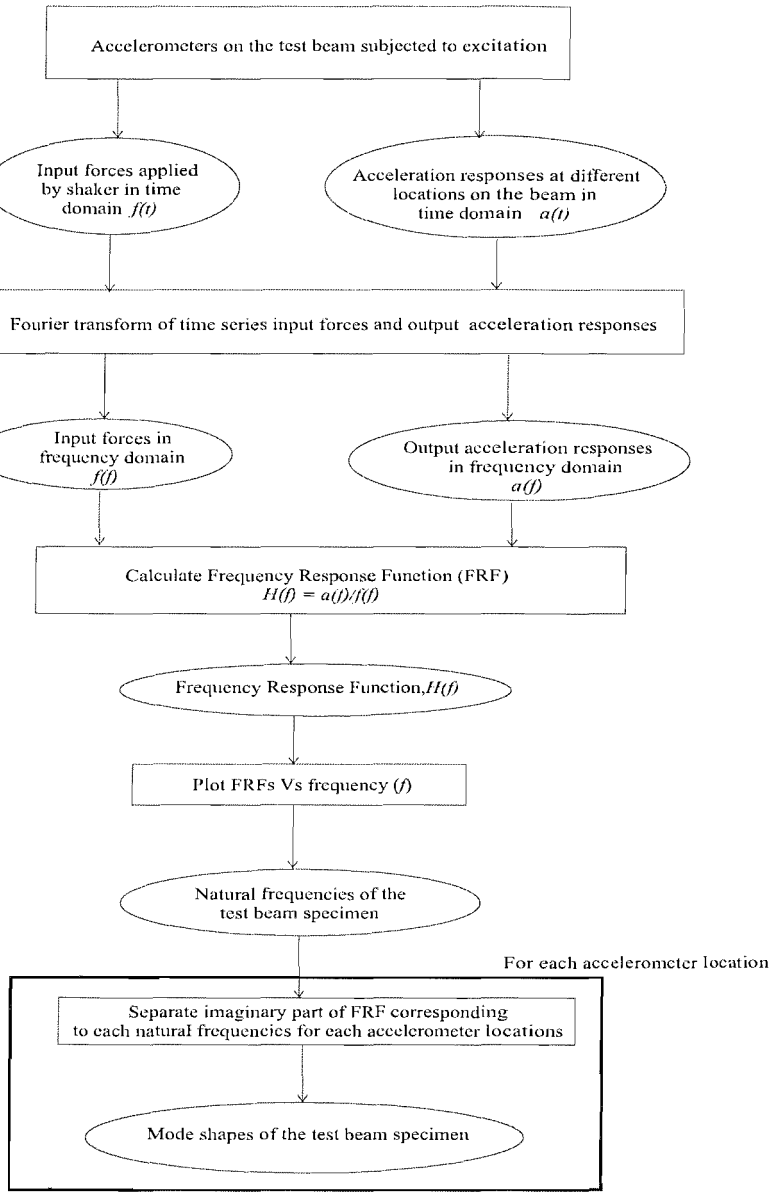

Figure 7.3: Signal processing steps for estimation of natural frequencies and mode shapes.

as Transfer matrix [Ewins, 2000], which is a symmetric matrix. In the present case, only the columns of the FRF matrix are measured. Values of the imaginary part of each FRF, at each frequency, are then used to extract the mode shapes of the beam specimen. The complete processing steps are depicted in Fig. 7.3, which will be used in Chapter 8, to obtain the natural frequencies and mode shapes of the beam specimen.

7.5 Summary

The experimental programme outlined in this chapter, will be used to obtain the vibration responses in Chapter 8. The measured reponses will be processed, as per the procedures discussed in Section 7.4, to extract the natural frequencies and mode shapes of the specimens, which are used as the inputs in the damage identification method, presented in Chapter 5. Hence, the focus of the next chapter is experimental validation of the damage identification method.

Chapter 8

Damage Identification using Experimental Measurements

In this chapter, the damage identification method proposed in Chapter 5 is validated, by using experimental measurements of the face delaminated sandwich beam specimens. Each damaged beam specimen has face delamination, located at mid-span and at a distance of one-third from the fixed-end. The beam specimens were manufactured as per the design calculations for the beam model used in Chapter 6. The geometrical dimensions of the beam specimens are measured by using a macro-scope. Acceleration responses at the various locations of the sandwich beam specimens, are measured and pre-processed as per the procedures outlined in Chapter 7, to extract their natural frequencies and mode shapes.

8.1 Description of the beam specimens

The sandwich beam specimens were fabricated by using the procedure described in Section 7.1. The faces and the core of the beam specimens were made of glass fibre and Poly Vinyl Chloride (PVC) foam respectively. The geometrical dimensions of the beam specimens were same as those in Chapter 6. In order to achieve the required thickness of each face in the design calculation, it is fabricated by using two layers of glass fibres. The selected lay-up in the face was $[0^o/90^o]$. The introduced damage type in the damaged beam specimen was face damage, i.e. face delamination. Face delamination in the beam specimen was introduced, by removing a part of the upper face across the width as shown in Fig 8.1 and 8.2. The extent of damage was 40 *mm* along the length of the beam. The specimens are cut by using a diamond wet saw in the desired dimensions, as shown in Fig. 8.1 and 8.2. After cutting, the

geometrical dimensions of the fabricated beam specimens are measured at various locations, by using a macro-scope. These macro-scopic measurements were averaged and their values are as shown in Fig. 8.1. The averaged measured width of the beam specimens is 38.00 *mm*. The mechanical properties of the beam specimens are given in Table 8.2 and their calculation procedures are described in Appendix A. The face delamination in the damaged sandwich beam specimen was introduced only in one face. The core of the beam specimens is left undamaged because the reduction in its stiffness is negligible up to 90 % of their service life as shown in Fig. 2.1. This damage type was introduced at different locations as shown in Fig. 8.1 and 8.2, in each beam specimen. Thus, two damage cases were considered for the experimental validations in this chapter, which are listed in Table 8.1.

Table 8.1: Location and extent of damage in the beam specimens.

Damage case	Extent (mm)	Location (mm)
1	40.00	150
2	40.00	225

Table 8.2: Mechanical properties of the composite sandwich beam specimen.

E_1 (GPa)	G_{core} (MPa)	ρ_{face} (kg/m^3)	ρ_{core} (kg/m^3)
20.14	18.20	1353.92	69.00

8.2 Experimental measurements and processing

The undamaged and damaged sandwich beam specimens, were fixed in the cantilever configuration and excited by using the experimental set-up as described in Section 7.2, for the measurement of acceleration responses at the locations shown in Fig. 8.3. The cantilever configuration was realised by clamping one end of the beam specimen on the shaker, using the fixture as shown in Fig. 8.4. The fixture was designed to ensure adequate clamping of the specimen without crushing the core. The sandwich specimen was attached to the fixture at the root section, using the four bolts as shown in Fig. 8.4. In order to prevent the core crushing, these bolts were tightened enough, so that the gap between the metallic plates on the top of the beam specimen and fixture

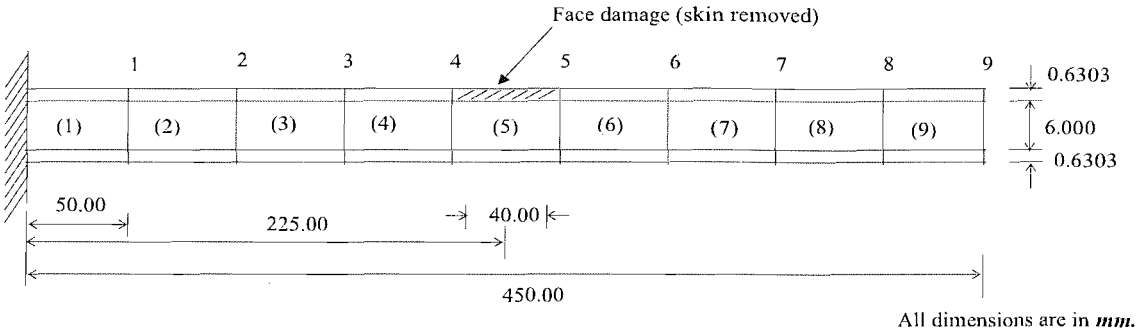

Figure 8.1: Geometrical dimensions of composite sandwich beam specimen and damage location.

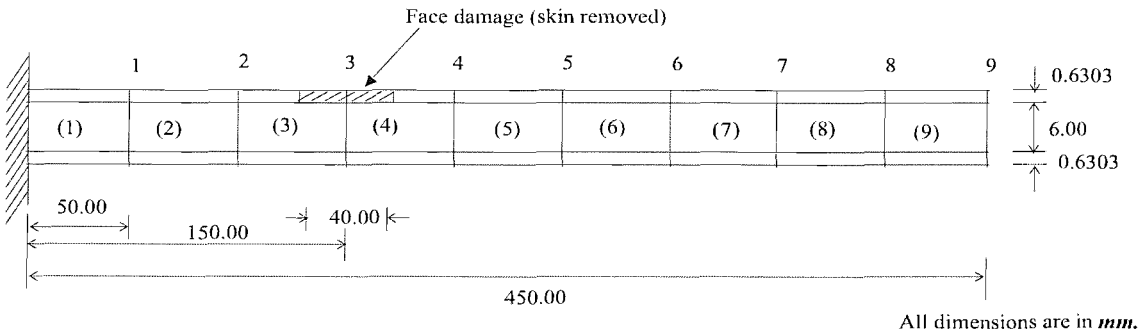

Figure 8.2: Geometrical dimensions of the beam specimen for damage located at 150 mm from the fixed end.

was slightly less than that of thickness of the sandwich beam specimen. Using this clamping arrangement, the natural frequencies of the beam specimen were measured to check their repeatability. The applied clamping force was adjusted, until repeatability in the measurements of the natural frquencies was achieved. Subsequently, much care was taken to apply same clamping pressure consistently for other experiments. Next, the signal processing of acceleration measurements were performed by using the steps shown in Fig. 7.3. The applied excitation technique was sine sweep excitation in the frequency range of 10-900 Hz. The time-series acceleration measurements in this frequency range are plotted in Fig. 8.5, where four distinct peaks corresponding to the respective bending natural frequencies can be distinguished. In order to validate the accelerometer's readings, these measurements were taken repetitively, which were found to be similar, i.e., the natural frequencies of the specimen showed very little variation in all the testings. Similarly, other accelerometers' readings were also validated.

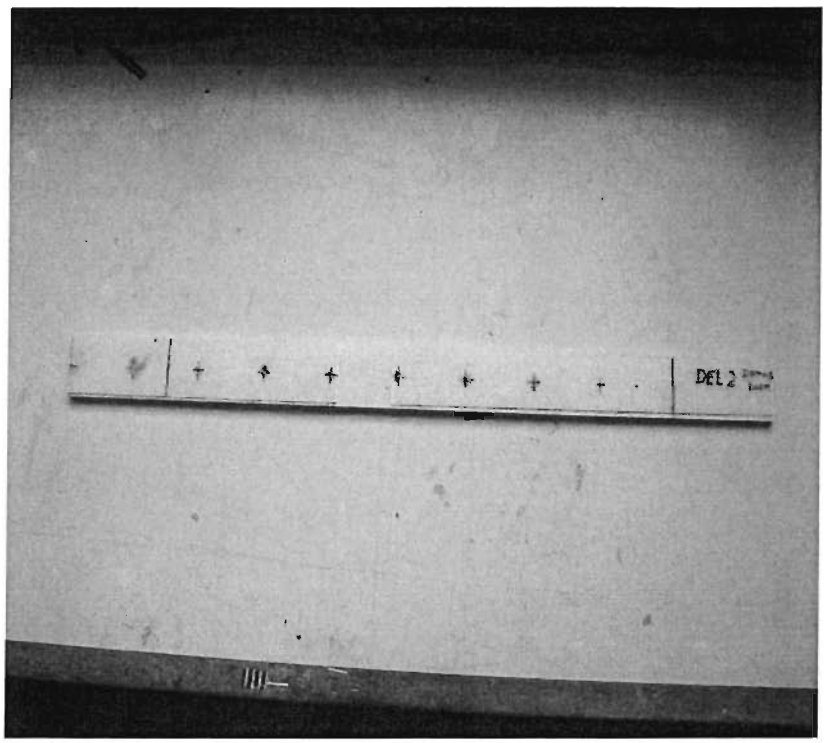

Figure 8.3: Accelerometer location on the beam specimens for mode shape measurements.

In order to measure mode shapes of the beam specimen, nine accelerometers were

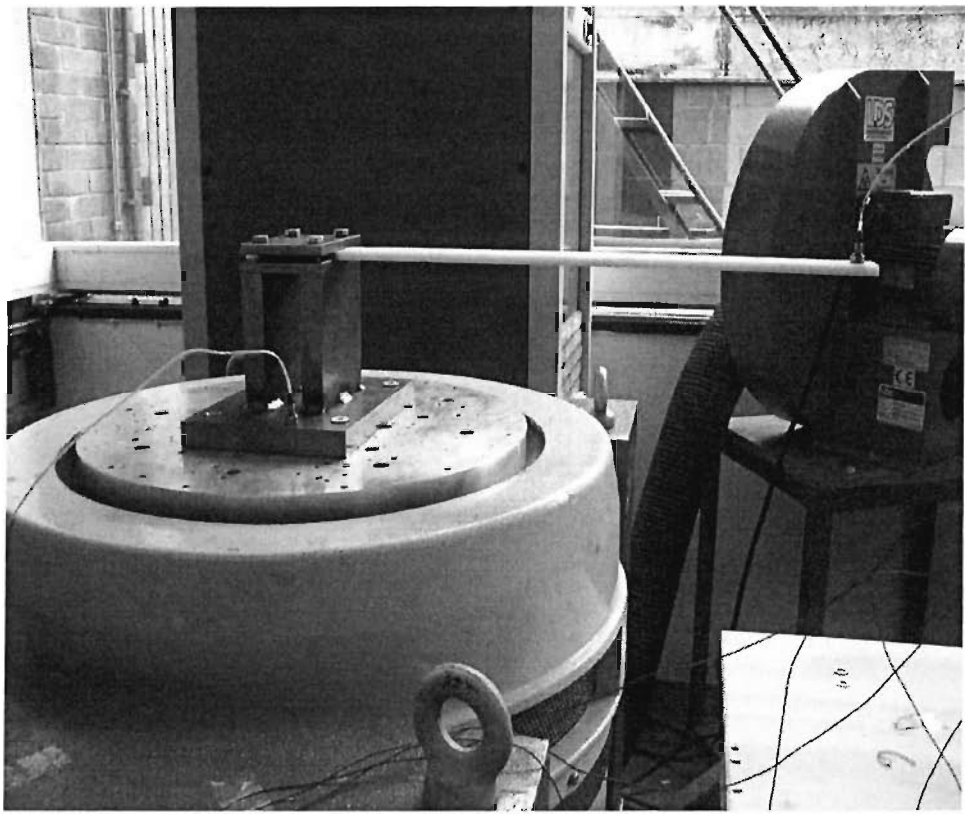

Figure 8.4: Placement of the beam specimen on the experimental set-up.

placed along the center line at regular intervals of 50 *mm* as shown in Fig. 8.3. One additional accelerometer was placed at the electrodynamic shaker as shown in Fig. 8.4, for measuring the input excitation forces. The sensitivitivities of the accelerometers used for monitoring input excitation forces and beam responses are 99.2 mV/g and 8.89 mV/g respectively. Each accelerometer samples the analog signals at a frequency of 1800 *Hz*, passes the signal through signal conditioning unit and analog-to-digital converter (ADC) to the data acquisition system for conversion, storage and analysis. In order to measure FRFs, the data acquisition system was configured to measure time series acceleration responses, at the accelerometer locations and input forces from the electrodynamic shaker, as shown in Fig. 8.3 and 8.4 respectively. The vibration responses, namely the natural frequencies and mode shapes of the beam specimen are extracted from the FRFs, which are calculated from the time series acceleration responses and input forces, using the steps shown in Fig. 7.3. The imaginary part of the FRFs were obtained to extract the mode shapes. Finally, these extracted values of mode shapes of the beam specimen were normalised, with respect to their maximum values in the respective mode.

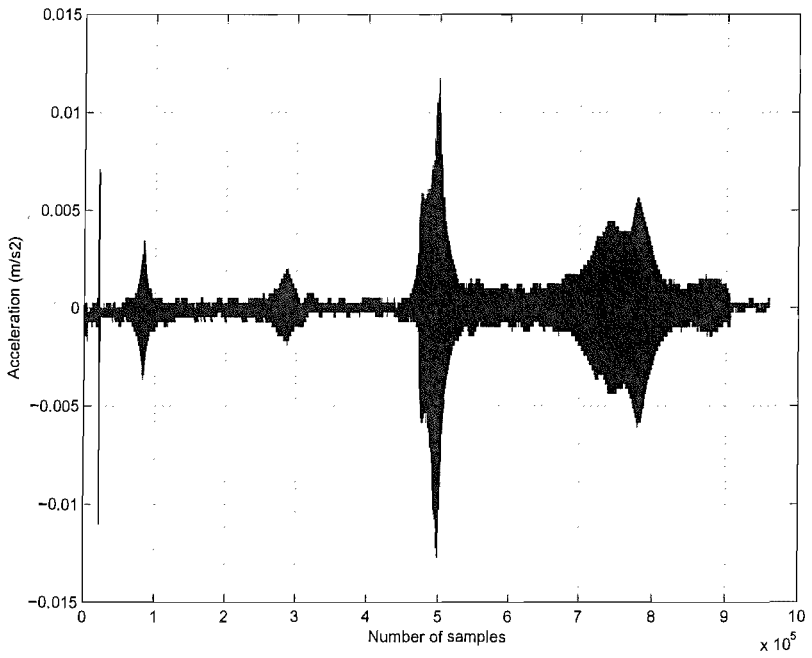

Figure 8.5: Output acceleration measurements of the sandwich beam specimen.

8.3 Damage identification calculations and analysis

Figure 8.5, shows the existence of first four lowest bending natural frequencies, in frequency range of 10 - 900 Hz, at which the mode shapes will be extracted. Sandwich beam specimens were tested several times and their Frequency Response Function (FRFs) were calculated, which were averaged to identify their mode shapes. FRF for the undamaged beam specimen is shown in Fig. 8.6. The natural frequencies of the undamaged and damaged sandwich beam specimens, for both damage cases, are compared in Table 8.3. In this table, the experimental natural frequencies of the undamaged and given sandwich beam specimens, are also compared with those of the FE beam models used in Chapter 6. The FE models were used to simulate damages, by using the techniques described in Section 6.3, for the damage cases referred in Table 8.1.

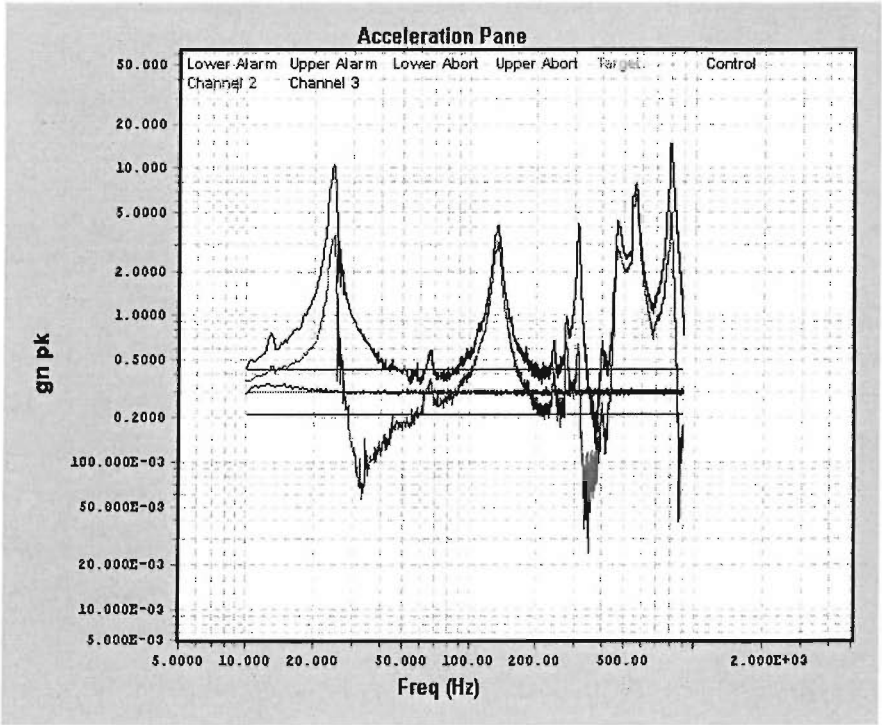

Figure 8.6: FRF measurements for the undamaged composite sandwich beam specimen.

The comparison of the natural frequencies of the beam specimens in Table 8.3, clearly indicate the existence of damage, by showing the reduction in the natural

Table 8.3: Natural frequencies of the undamaged and damaged sandwich beam.

Mode	Undamaged beam (Hz)		Damaged beam (Hz) at Mid-span : Case 1		Damaged beam At one-third : Case 2	
	Exp.	Beam Model	Exp.	Beam Model	Exp.	Beam Model
1	24.29	23.42	17.86	16.57	12.68	12.53
2	133.47	136.14	79.71	84.66	112.64	115.81
3	310.00	345.09	282.73	324.42	298.45	300.35
4	563.62	602.32	494.37	526.49	463.50	508.99

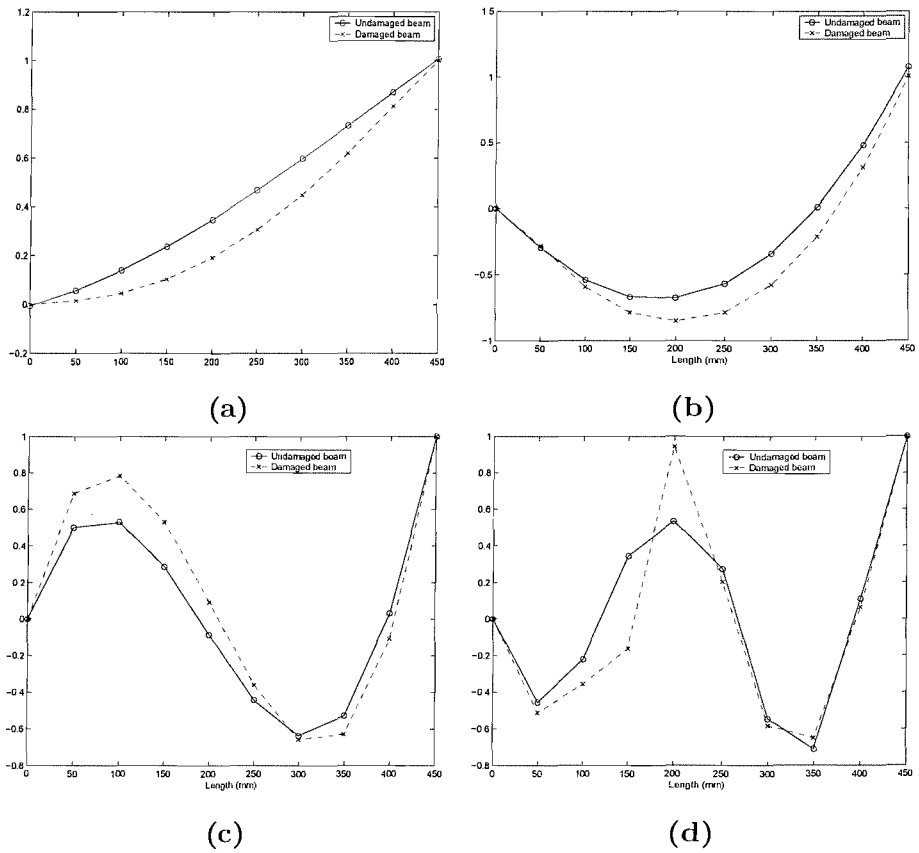

Figure 8.7: Mode shapes of undamaged and damaged sandwich beam : (a) First mode, (b) Second mode , (c) Third mode, and (d) Fourth mode.

frequencies of the damaged beam specimen, compared to those of the undamaged beam specimen. Reduction in natural frequencies vary for the different modes, with maximum reduction of 40.28%, in the second mode and minimum reduction of 1.88%, in the fifth mode. Reduction of the natural frequencies clearly show the effects of damage in the sandwich beam specimen, validating the theory in Section 5.2. So far, the reduction in the natural frequencies indicated only the existence of damage, but not their location. However, damage may be located, by comparing the changes in the mode shapes of the undamaged and tested beam specimens.

The first four mode shapes of the undamaged and damaged sandwich beam specimens, are plotted and compared in Fig. 8.7. The variations in the mode shapes of the undamaged and damaged beam specimens, are similar to those in Section 6.5. Comparison of the mode shapes of the undamaged and damaged beam specimens, indicates the probable damage location, verifying the findings in Section 6.5. However, the difference in their magnitudes varies consistently along the length. The changes of the mode shapes in the damaged part are significant for the first, second, and fourth mode; whereas, the third mode shape shows the least amount of changes. This can be attributed to the fact that in the third mode shape, the damaged part does not show larger deflection, compared to other parts of the beam specimen. In the second and fourth mode of vibration, the amplitudes of vibration in the damaged part, were significantly higher as compared to other parts. However, it is evident that these changes in mode shapes do not explicitly indicate damage location, hence there is a need to apply the damage identification method as developed in Section 5.2.

For locating damage, the first four mode shapes of the undamaged and damaged beam specimens, were used to calculate the elemental modal strain energies, by using the relevant equations in Section 5.2. These modal strain energies were compared by calculating $MSECR$ values, as described in Sub-section 5.2.3 and plotted against the element number, in Fig. 8.8 and 8.9 for damage case 1 and 2 respectively. Here, the element numbers correspond to the number shown in bracket of Fig. 8.1. In Fig. 8.8, it is clear that the elemental modal strain energy changes, are maximum for the damaged element, which is indicated by the unit value of $MSECR$, in element 5 for the damage case 1. This explicitly means that the damage is present in element 5, i.e., at the mid-span of the beam specimen. For damage case 2, the damage is distributed across two elements, i.e., 3 and 4 as shown in Fig. 8.2. This implies that damage is present in multiple elements. $MSECR$ values for the damage case 2 are plotted against the element number in Fig. 8.9, which clearly shows that the changes in modal strain

energy are maximum for two elements (3 & 4). These values are indicated by the unit and close to unit value of $MSECR$, in the element 3 and 4 respectively, for damage case 2. This explicitly means that damages are present in both elements, i.e., 3 and 4. However, for all other undamaged elements, the $MSECR$ values are less compared to that of the damaged element in both damage cases, which corraborate the observations in Sub-section 5.2.3. Similar to the trends observed for numerical simulations in Sub-section 5.2.3, the modal strain energy changes in the undamaged elements adjacent to the damaged element, are relatively higher than those of the undamaged elements far away, except for the element at the free-end. Here, it is interesting to note that the higher value of $MSECR$ at the free-end of the beam specimens compared to that of the adjacent element. These results can be attributed to the "end effects", geometrical and mechanical discontinuities at the free-end, which were also observed by Dawood *et al* [Dawood *et al.*, 2004a,b]. However, it can be observed that as damage moves towards the fixed-end, their effects reduce.

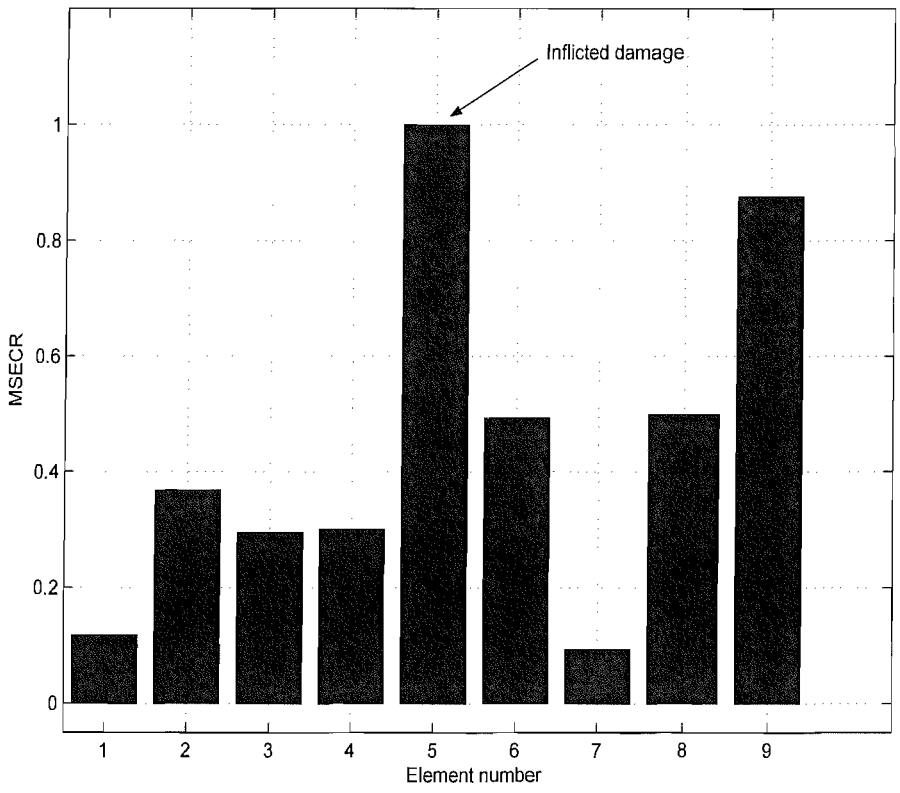

Figure 8.8: Damage localisation results for damage case 1.

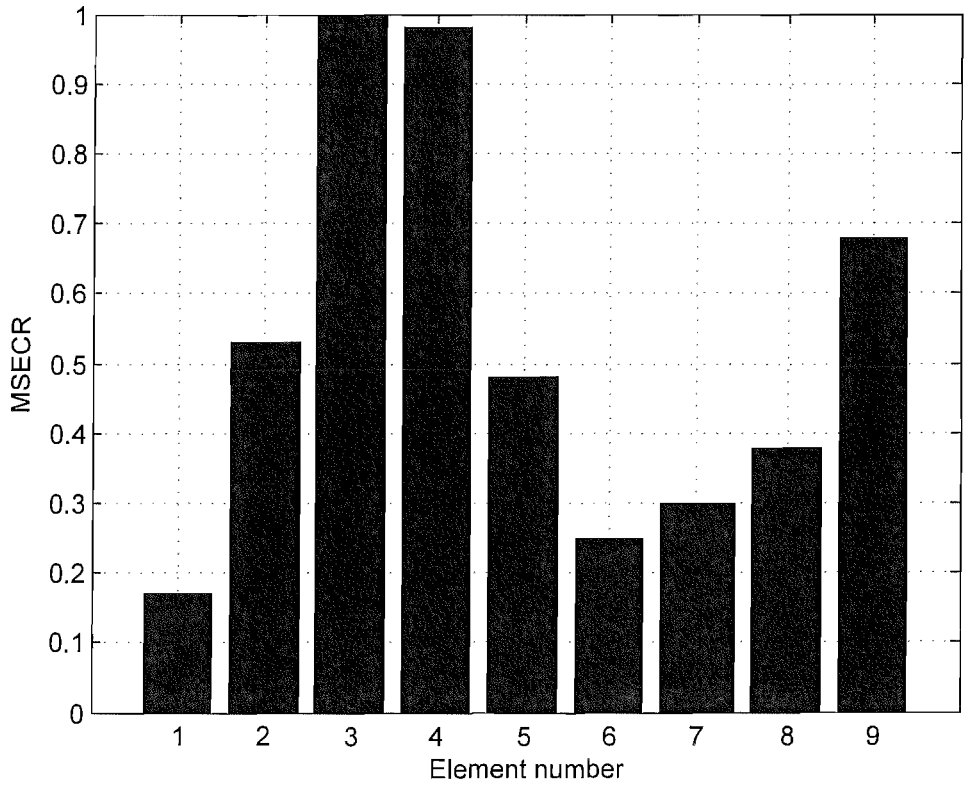

Figure 8.9: Damage localisation result for damage case 2.

Figures 8.8 and 8.9 clearly indicate the location of damages in the beam specimens but their level and extent are still unknown. In order to assess the criticality of damage in the beam specimens, their level and extent must be known by using the method as proposed in Sub-section 5.2.4. Hence, the next logical step after damage localisation, is predicting the level and extent of damage in the beam specimens. For this purpose, the natural frequencies and mode shapes of the beam specimens are used as the inputs. Since, location of damage is identified, the damage extents are calculated for the damaged elements only for both the damage cases. The first stage of damage identification predicts 77.12 % and 8.06 % of damage extent, in the face and core respectively, in element 5 for damage case 1. Similarly, these predictions are 48.23 % and 47.52 % in the faces and 6.17 % & 8.07 % in the core of the elements 3 and 4 respectively, for damage case 2. These damage extent predictions are then used as initial guesses in the optimisation process, to obtain their optimum values in the second stage. The second stage of damage quantification, predicts the damage extent 34.21% and 1.90 % in the face and core respectively, for damage case 1. For damage case 2, these predictions of damage extent converges to 18.38 % & 17.62 % in the faces and 1.16 % & 1.07 % in the core of elements 3 and 4 respectively. These predictions of damage extent after the second stage of damage quantification are, presented in Table 8.4. Comparing these predictions with the results of Table 6.9 in Sub-section 6.6.2, the low value of damage extent, i.e. 1.90% in the core indicates that there is no damage in it. This means that only the faces are damaged and the core is undamaged. In the damaged beam specimen, 80 % part of the upper face in element 5 is removed. This corresponds to the 40 % part of the sum of the upper and lower faces in the element 5 for damage case 1 and 20 % for the elements 3 and 4 in damage case 2. This leads to the conclusion that there is 40% damage in the face of element 5, which is close to the predicted damage extent of 34.21% in the face. The same trends are observed for damage case 2. Accuracies of these predictions of the damage extent are consistent with those of Sub-section 6.6.2. Thus, after the second stage of damage quantification, it can be concluded that damage is present only in the face and the predicted damage extent is close to the real damage.

8.4 Conclusions

Similar beam specimens used in Chapter 6 were fabricated in the laboratory and an FE model was created, by using the formulation presented in Sub-section 5.1.2, where the

Table 8.4: Damage extent prediction of the damaged sandwich beam specimens.

Damage case	Damaged element	Damage extent predictions	
		Face (%)	Core (%)
1	5	34.21	1.90
2	3	18.38	1.16
2	4	17.62	1.07

natural frequencies predictions closely matched with the experimental measurements. It is observed that there is close correlation between the predicted geometrical and mechanical properties of the designed beam, as given in Chapter 6 and the fabricated beam specimens. After the signal processing of measured acceleration responses, the processed data, namely, the natural frequencies and mode shapes of the beam specimen were used by the damage identification method to identify the existence, the location, the extent and the level of damage. The damage extents were predicted in terms of reduction in stiffness of the faces, in the damaged element.

Chapter 9

Real-time Structural Health Monitoring and Control System

Design, development and testing methodologies for the components of a real-time structural health monitoring and control system, is the main focus of this chapter. These components are developed by using grid technologies based toolkit, which can also be used to implement the damage identification method, as discussed in the previous chapters. This work offers a new and innovative application of grid technologies, in the development of a real-time structural health monitoring and control system, for real-time transfer of measured data, computation, data management, software applications and integration. Objectives of the system are identified in Section 9.1, which are used to design a scalable multi-layer system architecture in Section 9.2. The software layers in this system architecture are developed in Section 9.3, and their basic functionalities are tested in Section 9.4. Finally, this chapter also recommends the guidelines for implementing and integrating the control system in the overall system in Section 9.5 and briefly describes the vision of the system, by outlining various application scenarios in Section 9.6.

9.1 Objectives of the system

The main objective of this system is automation of the damage identification procedures used in Chapter 8 and their integration with the control method. These procedures are acquisition, processing and transmission of the data to a remote control station and their analysis. Data from the sensors must be transmitted to data management and computational systems, which analyse the data by using algorithms such as those used in Chapter 8 and the control method described in Section 5.3. All of

these components must act cohesively, in order to perform the procedures in Chapter 8, in an automated manner. The proposed system is designed to achieve the following objectives,

- Data acquisition and their local storage near the structure location, i.e., at the laboratory in the present work,
- Real-time transmission of these data to remote data management, computational and control systems,
- Automated data analysis to obtain damage information of the structure and their storage in the data management system,
- Assess criticality and severity of the existing damage in the structure by using the control system.

To achieve these objectives, the system architecture will be designed and developed in Section 9.2 and implemented in Section 9.3, which can be easily scaled up to meet any future requirements and improvements.

9.2 Architecture of the system

This section describes the design of the system architecture, which links the components of a real-time structural health monitoring and control system. This system architecture includes all the grid technologies related components shown in Fig. 4.1. This system architecture is based on the "hourglass model" shown in Fig. 3.3. The system architecture consists of logical middleware layers, to integrate the physical components like those used in Chapter 8. These physical components are interfaced with the computational resources by using software layer. In the system architecture, the physical resources are connected to the fabric layer as shown in Fig. 3.3 whereas users and grid applications accessing the resources are connected through the user application layer. Logical middleware are classified as per their distinct tasks, which are used in the damage identification procedure in Chapters 6 and 8. The analysis steps and procedures such as those used in Chapters 6 and 8, in conjunction with the advanced capabilities such as real-time monitoring and control, enhances the system to impart the characteristics as outlined in Section 2.6. The logical middleware required to achieve these characteristics, are developed in this section.

There are several types of questions that must be answered during the design of the system architecture. These questions include the following,

1. What is the topology of the structure to be monitored?
2. What material is being used in the structure?
3. What type of damage pattern can be expected?
4. What physical quantities are being monitored and which sensor is suitable for the measurement application?
5. Where should sensors be placed and their density?
6. How the data acquisition system is integrated with the system?
7. If the system is real-time, then how often will the sensors' measurement be transferred to a control station?
8. How reliable and secure is the data transfer?
9. How will these measurements be pre-processed and analysed to obtain the damage information for the structure?
10. How frequently will the measurements be pre-processed and analysed?
11. How will the calculated damage information be used to activate the control system?

Many of these questions are already answered in the previous chapters. Still, many questions concerned with the limitations identified in Sub-section 2.7.2, remain unanswered, which are addressed in this chapter, by using the technologies identified in Section 3.6. A solution is proposed by designing and developing a system architecture connecting the components as shown in Fig. 9.1, by using the software layers known as middlewares. These components interact among themselves to perform many actions as follows,

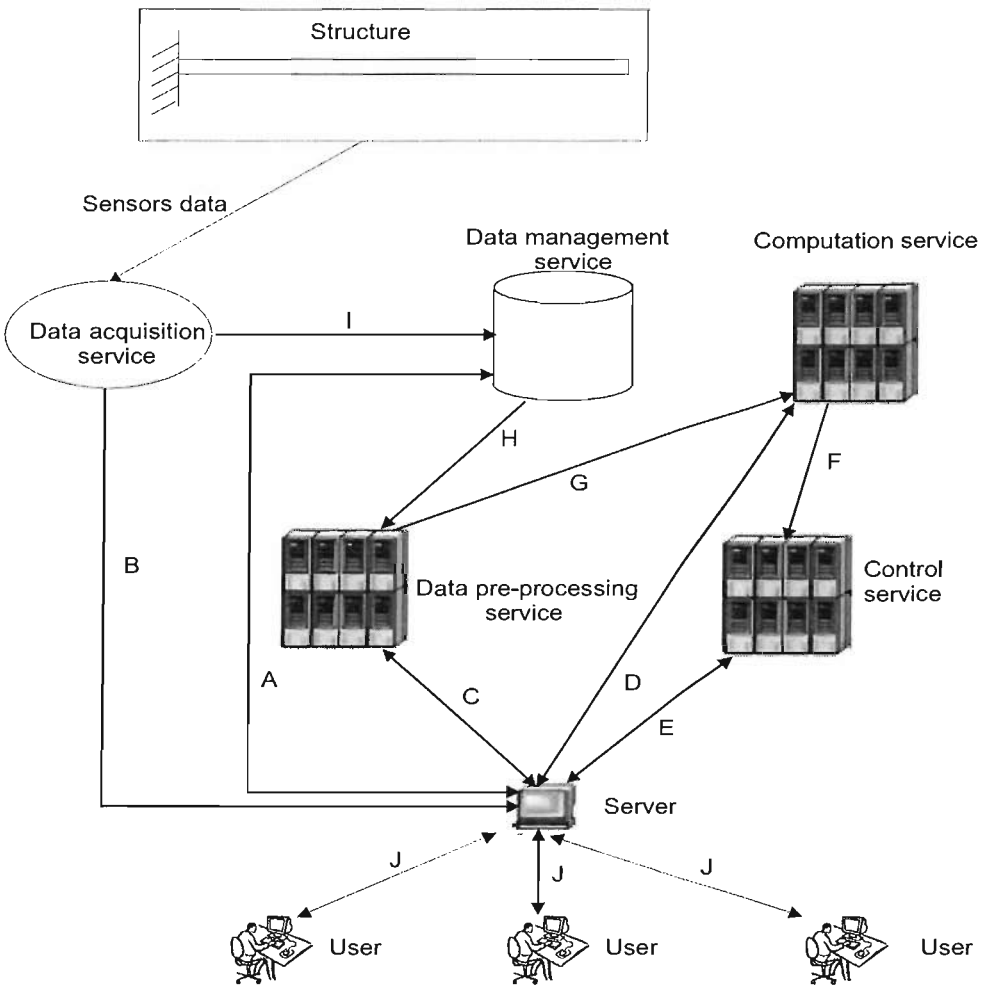

Figure 9.1: Grid service architecture for the real-time structural health monitoring and control system.

Table 9.1: Functions of each components of the system architecture.

Services	Functions
Data acquisition service	Acquires experimental signals from the structure and transmit to data management service and the users.
Data management service	Provide mechanisms for storage and retrieval of the vibration signals from the database.
Data pre-processing service	Pre-process the raw signal from the data acquisition service and the data management service to be used by computation service.
Computation service	Analyse the vibration mode shapes obtained from the data pre-processing service for the damage identification.
Control service	1. Retrieve the critical level of damage from data management service. 2. Compare the damage identification results to the critical damage.

A Request for historical vibration signals for visualisation.
B Request for real-time vibration signals from data acquisition service.
C Requesting to pre-process the raw vibration signals into mode shapes and their visualisation.
D Invoking damage identification service and receiving current structural health information.
E Invoking control service for information about safety of the structure.
F Receiving the current status of damage.
G Downloading the natural frequencies and the mode shapes to the damage identification service for damage assessment.
H Downloading the real-time and historical raw vibration signals for pre-processing.
I Uploading the raw vibration signals from the structure for storage.
J Secure login, access control, authorisation to the user(s).

In the system architecture shown in Fig. 9.1, access to the resources at all steps are managed by using "hourglass model" shown in Fig. 3.3. There can be two possible modes of access. In the first mode, the user creates the proxy manually by using the certificate and password, to access resources directly. In the second mode, the software program, stored in one resource, needs to access other resources by using the proxy. Step **J** implements the first mode of access control; whereas, other steps, except **I** and **J**, require access control mechanism for one resource to another resources, i.e. the second mode of access. In step **J**, the user log-in into the system manually by using the certificate and password to access the resources. However, when automated computing is required at other steps, then, the user's proxy is generated automatically by the

system. Then, this automatically generated user's proxy is delegated to the resources and used at all other steps. This proxy is used for authentication and authorisation by the resource and connectivity protocols in Fig. 3.3.

The summarised functions of each components is given in Table 9.1. The middlewares used in development of the system architecture are based on the Java CoG toolkit as discussed in Section 3.4. The novel aspect of the proposed system architecture is the application of the capabilities of generic grid toolkits such as Java CoG, Globus and a commercial database system, which add many advantages to the system in line with the desirable characteristics as outlined in Section 2.6 for a real-time structural health monitoring and control system. In the next section, individual components of the system architecture will be designed and developed.

9.3 Design and development of the system

The system architecture proposed for the real-time SHM and control system in the previous section has various interlinked components, as shown by Fig. 9.1. These components are namely, the data acquisition system, the data management system, and the computational system, which interact and communicate amongst themselves in a pre-defined manner, as described in the previous section. In this work, the grid technologies based toolkits are used for development purposes i.e., designing these components and interlinking them by using the middleware. These middlewares include communication protocols, streaming strategies for the measured data, real-time data transfer and its computation, as required in the proposed system.

9.3.1 Security and access control

The fundamental requirement in a resources sharing environment, spanning across organisations, is to ensure security of the system seamlessly, which is indicated by the step **J**, in Fig. 9.1. The security requirements are authentication and authorisation of the users for access to available resources, which is an essential feature in all grid applications. This system implements the resources and connectivity protocols of "hourglass model" shown in 3.3. In this section, one such scenario for their application, in a real-time structural health monitoring and control of a structure, is outlined by using the technologies as described in Sub-section 3.3.2.

A diverse community of users have interests in ensuring safety of the structures such as ships, aircrafts, bridges, etc. Each user has a different interest with the com-

mon goal of ensuring the safety and the productive use of a structure. This often demands collaboration and interaction among the users. For example, the collaboration may be in the form of sharing full structural health information or a part of it, with the individual user, a group of users, or all of the users, who require controlled but seamless access. These capabilities are provided by the core grid services for access, authentication and authorisation, such as Grid Security Infrastructure (GSI), by using state-of-the-art digital certificate technology. The digital certificate technology is based on the Public Key Infrastructure (PKI) single sign-on, authentication, communication protection, and some basic support for restricted delegation. GSI uses X.509 standard, a widely used standard for PKI certificate for the user authentication. GSI defines an X.509 proxy to leverage X.509 for support of single sign-on.

PKI is based on third-party trust. A third party essentially guarantes the identity of an individual user or other entity. The physical "identity proof" is then held within a digital certificate that has been digitally signed by this third party. In this way two unknown parties can trust each other's identity. A typical use of this technology in the present work is to authenticate the user to the computational and database resources. Hence, rather than presenting the password, the user (or software program) presents this certificate as the "proof" of identity.

The trust is established by having faith in the third party, which certifies a user identity. The third party is popularly known as Certificate Authority (CA). The trust is established through a certificate policy. This policy is written typically by the relying parties, who are taking the risk of accepting identities. The certificate policy states all policies related to how the CA establishes the identity and how the keys and certificate are managed.

The authorisation in GSI is managed by identity mapping where the GSI (X.509) subject names are mapped with the local user names. The access is controlled by granting access to these local login accounts. When a GSI-enabled server receives an authorisation request, the server matches user's credential with the subject name, which is stored in the mapping database, to find the local user name associated with the respective subject name and gives the remote user the same permission as the corresponding local user. Typically, the subject name of a user'a credential is as follows,

```
subject=/C=UK/O=eScience/OU=Southampton/L=SeSC/CN=manoj kumar
```

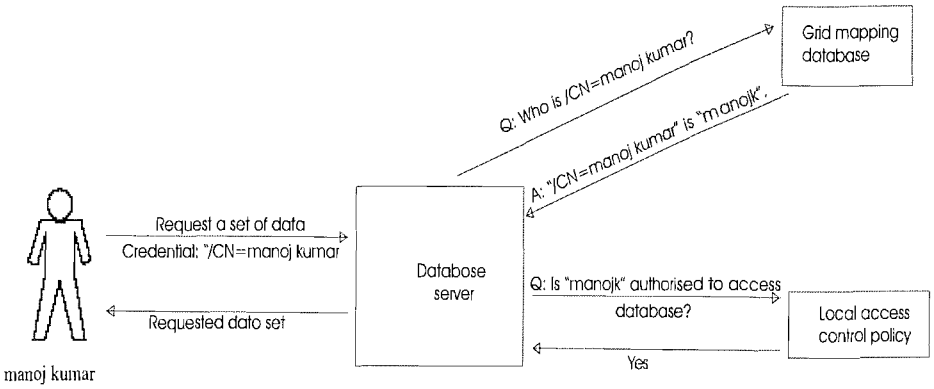

Figure 9.2: The basic steps in *authentication* and *authorisation* using PKI in the Grid environment.

In the subject line, a special convention is used to specify the identity of the issuer and the *subject*. The subject line shown above follows the convention with **C**(Country), **O**(Organisation), **OU**(Organisational unit), **L**(Locality), and **CN**(Common name). The authentication and authorisation scheme shown in Fig. 9.2 is used in the present work for access control to the resources.

9.3.2 Data acquisition system

In this section, an advanced data acquisition system as per the desired characteristics referred in Section 2.6 is designed, with an aim to integrate the accelerometers on the beam specimen, to the real-time structural health monitoring and control system. This function is indicated by step **I** in Fig. 9.1. In this way, measured signals are available for real-time processing and analysis. The schematic architecture of the data acquisition system is shown in Fig. 9.3.

In the scheme of Fig. 9.3, the data acquisition system samples the acceleration readings from the accelerometers and stores it into the local database system, for transmission to the remote data management system. These measurements are transmitted

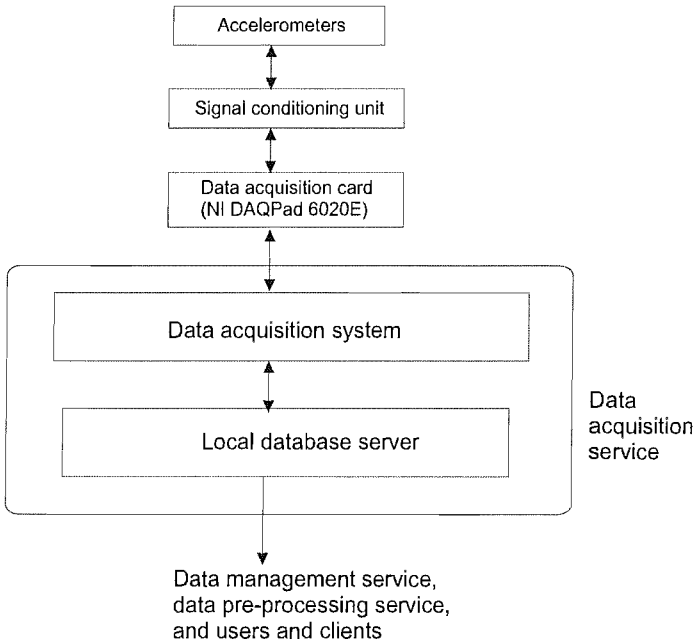

Figure 9.3: Architecture of the data acquisition service.

in real-time to the remote data management system, using the giga-byte ethernet connection.

Software used for the development of this system is Measurement Studio (http://www.ni.com/mstudio), which consists of three components, namely, LabWindows/CVI, Component Works and Component Works ++, which are compliant to ANSI C, Microsoft Visual Basic & C and add-in to Visual C++ respectively. It is decided to use Component Works to develop the data acquisition software because of its convenient interface to the database system. The data acquisition system has three basic modules as follows,

1. Hardware components such as accelerometers, signal conditioning unit and data acquisition card,

2. Data acquisition software,

3. Local database server (Oracle 10g).

These modules interact among themselves as shown in Fig. 9.3. The interface between two modules are provided by the software layer by using the code given in

Appendix D. There are several parameters such as the number of channels, their sampling frequency, the duration of scan and an anti-alias filter, which need to be set before acquiring the data. This task is performed by the code given in Appendix D.1. Hardwares are interfaced with the data acquisition system using the code given in D.2. The code in Appendix D.3 interface data acquisition system with the local database server.

The hardware used for data acquisition is NI DAQPad 6020E, which provides an interface between accelerometers and the data acquisition system, by using the code given in D.2. The next step is to provide an interface between the data acquisition system and the local database server as per the scheme presented in Fig. 9.3. This interface is provided by the in-built networking capabilities of the data acquisition software and the database server, using the client/server technology as described in Chapter 3. Here, the data acquisition system and the database server act as the client and the server respectively. This approach provides two-fold advantages, firstly it ensures zero data loss in transmisson and the secure delivery of data to the remote data management system, and secondly it provides improved performance by using the in-built optimised cache mechanism of the database system. In this way, the local database server is coupled with the data acquisition system, to store the readings and transmit them to the remote data management system in real-time.

The function used for interfacing the data acquisition software to the local database server in the data acquisition software, is given in Appendix D.3. The steps used in the function to upload the measurements in the database are as follows,

1. Logging into the database named `Oracledb` using the user name `manojk` and password.
2. Prepare the Structured Query Language (SQL) command (**INSERT**) to insert the data into the table (`list`) of the database `Oracledb`.
3. Open the connection to the database i.e. Oracledb.
4. Begin the transaction to upload the data into the database.
5. Prepare the transaction to insert the measured data and their time-stamp into the table.
6. Add the data into a queue and execute the command.

7. Commit the transaction to store the acquired data permanently in the table.

8. Close the connection.

The accelerometers' readings are uploaded into the local database server, by using the array binding and stored procedure features of Oracle10g. This approach allows faster uploading of acquired data in the local database server and hence, it results in faster transfer of data to the remote database system. The data acquisition system is connected to the local network and assigned an unique IP address with name in the network. Finally, the local database server is configured to propagate any changes in the table (`list`), to the remote data management system in real-time.

Every measured data has a time-stamp, which is unique to each measurement and is set as the primary key (`measuredtime`)in the table of the database. The primary key (`measuredtime`) is an integer, which gives the number of milli-seconds elapsed since 1^{st} January 1970, 00:00:00 GMT as measured by JAVA. This is selected because of the use of Java for the design of other components of the system. Hence, 1^{st} January 1970, 00:00:00 GMT is set as a reference date. The data acquisition system returns the current time in a SYSTEMTIME structure with fields for the year, month, day of the month, day of the week, hour, minute, second and milli-second. Duration between the current and the reference time is obtained and converted into number of milli-seconds elapsed, to obtain the `measuredtime`. Hence, at the beginning of each data acquisition, the Windows time-stamp is converted to a Java time-stamp for easy processing by the Java client in the system. Since, the number of measurements and the sampling frequency are known, the `measuredtime` is calculated.

9.3.3 Data management system

Data management system is the backbone of the system by being a server for all other components in the system architecture, designed in Section 9.2. It has been developed in a layered manner for a flexibile and a scalable design. At the front end, it accepts the experimental measurements being transferred from the laboratory, updates the stored data and accepts queries for the data. At the back end, it is currently using `Oracle 10g` as the database server. This system supports many steps in the system architecture, which are indicated by **A, B** and **F** in Fig. 9.1.

The data management system provides the functionality for the managing and processing capabilities in the system, to transfer the data from the data acquisition system, as designed in previous Sub-section 9.3.2. At the design level, this system

provides a number of capabilities to support the data management tasks in the system, as outlined in Section 2.6 such as,

1. Support for transferring and storing accelerometers' reading from the sandwich beam specimen by using data acquisition system.

2. Mechanisms for locating and accessing accelerometers' reading in the correct time sequence.

The data management system in the present work uses `Oracle10g` running on `Windows` platform and the database servers are located at two places, i.e., the Astronautics Laboratory and Southampton Regional e-Science Centre at the University of Southampton, Southampton (UK). The database servers are assigned an unique IP address and name and connected to the university network. The database system, `Oracle 10g`, located in the Astronautics Laboratory is coupled with the data acquisition system, which is designed and developed in Sub-section 9.3.2. It also provides an excellent opportunity to integrate two distributed database systems, by using *Oracle streaming technology*, in a real-time structural health monitoring and control application. `Oracle 10g` is selected because of its grid compatible design. It is claimed to be the first and most suitable database system for grid applications [Cyran & Lane, 2003]. It also provides an excellent opportunity to leverage the power of a mature relational database technology, for design of the data management system, in a real-time structural health monitoring and control system. In the current application, a number of design decisions were made that lead to the development of the prototype of the proposed real-time system. These key design issues were as follows,

1. Data granularity : The available approaches include *coarse grained* and *fine grained* approaches. A coarse grained approach makes the design of the system simpler by storing the data as a Binary Large Object (BLOB) or a Character Large Object (CLOB). Although this approach provides better performance and efficiency but BLOB and CLOB data can not be queried by the database and thus, slicing of data is not possible by using SQL queries, making the approach very similar to a conventional file system. Further, it requires an interface to convert the data into human readable format (ASCI), requiring an additional layer in the middleware. In contrast to the coarse grained approach, the fine grained approach offers the data to be explicitly stored in rows and columns of a table, which makes data extraction simple and flexible. This advantage makes

the fine grained approach suitable for storing data into the databases, hence adopted in the present application.

2. Table : In the present case, the accelerometers' sample time series data at the significantly high sampling rate is generating thousands of unique data identifier in proper sequence. Here, maintaining the sequence of reading across different database systems is the most important requirement, otherwise the data will be unable to provide any sensible information, after the signal processing in Section 7.4. Thus, an unique data identifier, i.e., time-stamp of each reading, is attached with every reading during data acquisition, in Sub-section 9.3.2. In order to improve the performance of the insert operations, readings are uploaded to the database system attached to the data acquisition system, in bulk, as an array.

In a database system, the data is stored in rows in an object called `Table`, which has number of columns. In the current work, a table named `list` is created in both the database systems. Based on the discussion in Sub-section 9.3.2, the primary key named `measuredtime` is defined, which is the value of elapsed time in milli-seconds since 1^{st} January 1970, 00:00:00 GMT. This scheme makes the values of `measuredtime` unique, thus, it provides an unique identifier. In rest of the columns, the accelerometers' readings are stored accordingly.

Based on the above design decisions, the remote database systems were connected and the accelerometers' readings were transmitted, in real-time, from the data acquisition system in the laboratory using *Oracle Streaming* technology [Urbano, 2003]. In this technology, two database systems, namely the laboratory and remote databases, are synchronised. This process is performed in three consecutive steps, namely, capturing the changes in the laboratory database after storing accelerometers reading, propagation of changes in the laboratory database to the remote database system, and applying the propagated changes from the laboratory database system to the remote database system. Internal state of the database system changes after making any changes such as modifying the stored database, saving and deleting data, modifying schemas, etc. These changes are recorded in the *redo* log of the database. In the first step, changes in the *redo* log of the laboratory database system are captured. Here, these changes are captured immediately after storing accelerometers readings in the laboratory database. In the second step, the captured changes in the *redo* log of the laboratory database are automatically propagated to the remote database system. In the third step, these propagated changes in the remote database system are applied so

that the remote database system is updated with the accelerometers readings. All these three steps are automatically performed one after each other in very short duration. In this way, the accelerometers readings are transferred to the remote data management system in real-time for their analysis by the computational system. The interface of this system with the computational system is provided by using the technologies, as discussed in Section 3.3.

9.3.4 Computational system

Because of a complex analysis, SQL by itself is insufficient for data analysis as performed in the previous Chapters 6 and 8. The analysis in the present work range from pre-processing of measured data, like in Section 7.4, to damage identification calculations as in the Chapters 6 and 8. These are indicated by steps **C, D, E, G** and **H** in Fig. 9.1. The computational tasks are mainly performed by using so called legacy codes, written in `FORTRAN` and `MATLAB`, as referred in Appendices C and E. Hence, a custom interface is developed to connect the remote database systems, the grid computational resource and the legacy codes. The interface communicates with the database system by using Java DataBase Connectivity (JDBC) in a Java program. The interface ensures the authentication of the user and authorisation to use the selected computational resources, by using the scheme described in Sub-section 9.3.1. In this interface, GRAM service of Globus, described in Section 3.3, is used, which is invoked by the user to submit the jobs. This service submits the jobs to the Globus gatekeeper after due authentication.

In the current work, it is decided to use the grid computational resource available at University of Southampton and named as `pacifica`. The `pacifica` is a RedHat Linux based computational cluster having 12 dual Intel Pentium Xeon Blades. The first step for use of the `pacifica` as a grid resource, is to create a local user account and map this local account with the user credential, given in Sub-section 9.3.1. This task was performed by the local administrator of `pacifica`. In order to submit a computational job at `pacifica`, the proxy containing the user credential is initiated at the client machine. This task can be performed by either using Java CoG toolkit, as presented in Section 3.4, or executing the pre-compiled Java class used in Globus, as discussed in Section 3.3. Initiation of the proxy using the former scheme requires the user intervention every time; whereas, the latter scheme does not require any user intervention, if used in conjunction with the database systems, designed in Sub-section 9.3.3. The automated proxy initiation by using the latter scheme, is essential to realise

a desirable feature of analysing the experimental reading periodically. Hence, the latter scheme for proxy initiation is adopted in the system, which is integrated with the database system of Sub-section 9.3.3.

After designing the interface and access mechanism to the computational resource, the next step is to pre-process the accelerometers' readings as per the scheme in Fig. 7.3. This requires two interfaces. The first is between the client/user machine and the database system of Sub-section 9.3.3, and the second is between the database system and the computational resource. These tasks must follow a pre-defined work flow, as in Fig. 7.3, for pre-processing and Fig. 5.4 for damage identification. The first interface is designed by using JDBC and Java. By using this interface, a SQL query is made to the database (`Oracledb`), to retrieve the accelerometers' readings arranged in order of `measuredtime`, which is stored in the database, as described in Sub-sections 9.3.2 and 9.3.3. The SQL command used for this purpose in the present application is as follows,

```
SELECT channel00,channel01 FROM list ORDER BY measuredtime;
```

The data retrieved from the above command, are stored in the local file of the machine running the remote database system. This file is subsequently transferred to the grid computational resource using GridFTP protocol, implemented in the second interface. Once the file containing the accelerometers' readings are completely transferred to the computational resource, the next step is to initiate the job submissions process. After data analysis, the results are returned back in the file to the user and the remote database system. In the present application, only transfer matrix as per steps in Fig. 7.3 are calculated. This scheme is designed to be scalable so it can be easily extended to accomodate any future requirements. The complete process in the computational system is shown in Fig. 9.4.

The adopted approach is developed to harness the capabilities of the grid technologies in the present application, as identified in Section 3.6. It is worth noting that the grid computational resource (`pacifica`) is Linux based; whereas, the remote database system at Southampton Regional e-Science centre and the data acquisition system in the Astronautics Laboratory at the University of Southampton are Windows XP machines. This successful implementation of the proposed system proves the claim made in Chapter 3 regarding the seamless integration of the heterogeneous resources using the grid technologies. The use of Java CoG in the present application ensure that the system is scalable and can continue to operate, despite any upgrade of the grid software at the remote grid resources [Laszewski *et al.*, 2001].

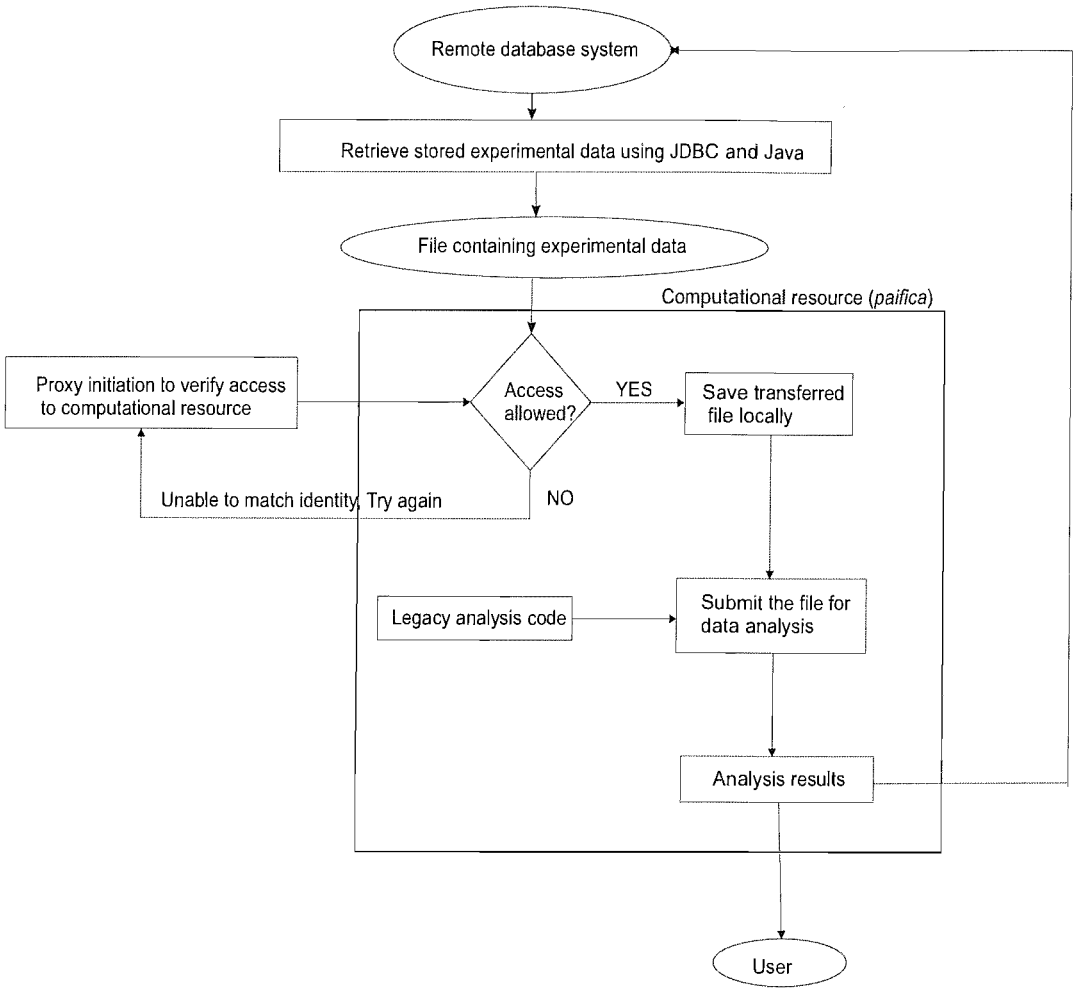

Figure 9.4: Steps and process in the computational system.

Table 9.2: Values of cumulative damage parameter for damage located at the fixed-end of the beam model

Damage in face (%)	% Damage in core					
	00	20	40	60	80	100
00	0.00	0.2768	0.5145	0.7131	0.8727	0.9931
20	0.3639	0.5405	0.6920	0.8185	0.9200	0.9965
40	0.6444	0.7434	0.8283	0.8991	0.9558	0.9985
60	0.8429	0.8868	0.9244	0.9557	0.9807	0.9995
80	0.9609	0.9719	0.9813	0.9890	0.9953	0.9999
100	1.0000	1.0000	1.0000	1.0000	1.0000	1.0000

9.3.5 Control system

The role of the control system is indicated as step **E** in the system architecture, shown in Fig. 9.1. For the application of the control method presented in Section 5.3, sensitivity of the cumulative damage parameter (D), as given by Eqn. 5.57, must be studied for different locations, the extent, and the level of damage in the sandwich beam used in Chapters 6 and 8. The effects of interacting multiple damage modes occuring in the sandwich beam will be also investigated. This will be used for determination of the threshold value of D in the control system, to raise the alarms as explained in this sub-section.

In order to use the control method presented in Section 5.3, its sensitivity for the different damage scenarios in the sandwich beam must be understood. Then, it will be used to determine the threshold values of D, for the sandwich beams used in Chapters 6 and 8 for the control application. The threshold values must be indicative of the different stages of damage and should warn the imminent catastrophic failure, observed in the sandwich beam at the end of fatigue life, as described in Section 2.1. This requires numerical simulations by using the model described in Section 6.1, for the various cases of damage in the selected beam configuration shown in Fig. 6.1 and calculation of D, as per procedure outlined in Section 5.3. Similar to the damage cases in Chapter 6, damages are simulated at three different locations. In this section, the extent of the damage in the faces and core start from zero, leading to complete failure, i.e., 100% damage in an increment of 20 %.

First, the variation of D for different extents of damage in the face and core of the sandwich beam at each damage locations, were calculated by using the theory

Table 9.3: Values of cumulative damage parameter for damage located at the mid-span of the beam model

Damage in face (%)	Damage in core (%)					
	00	20	40	60	80	100
00	0.0000	0.3446	0.6061	0.7948	0.9214	1.0000
20	0.3665	0.5854	0.7513	0.8708	0.9509	1.0000
40	0.6472	0.7695	0.8619	0.9286	0.9730	1.0000
60	0.8448	0.8987	0.9395	0.9688	0.9883	1.0000
80	0.9616	0.9749	0.9851	0.9923	0.9971	1.0000
100	1.0000	1.0000	1.0000	1.0000	1.0000	1.0000

Table 9.4: Values of cumulative damage parameter for damage located at the free end of the beam model

Damage in face (%)	% Damage in core					
	00	20	40	60	80	100
00	0.0000	0.4126	0.6976	0.8764	0.9710	1.0000
20	0.3690	0.6303	0.8105	0.9231	0.9817	1.0000
40	0.6501	0.7956	0.8957	0.9580	0.9902	1.0000
60	0.8467	0.9107	0.9546	0.9818	0.9959	1.0000
80	0.9622	0.9781	0.9889	0.9956	0.9990	1.0000
100	1.0000	1.0000	1.0000	1.0000	1.0000	1.0000

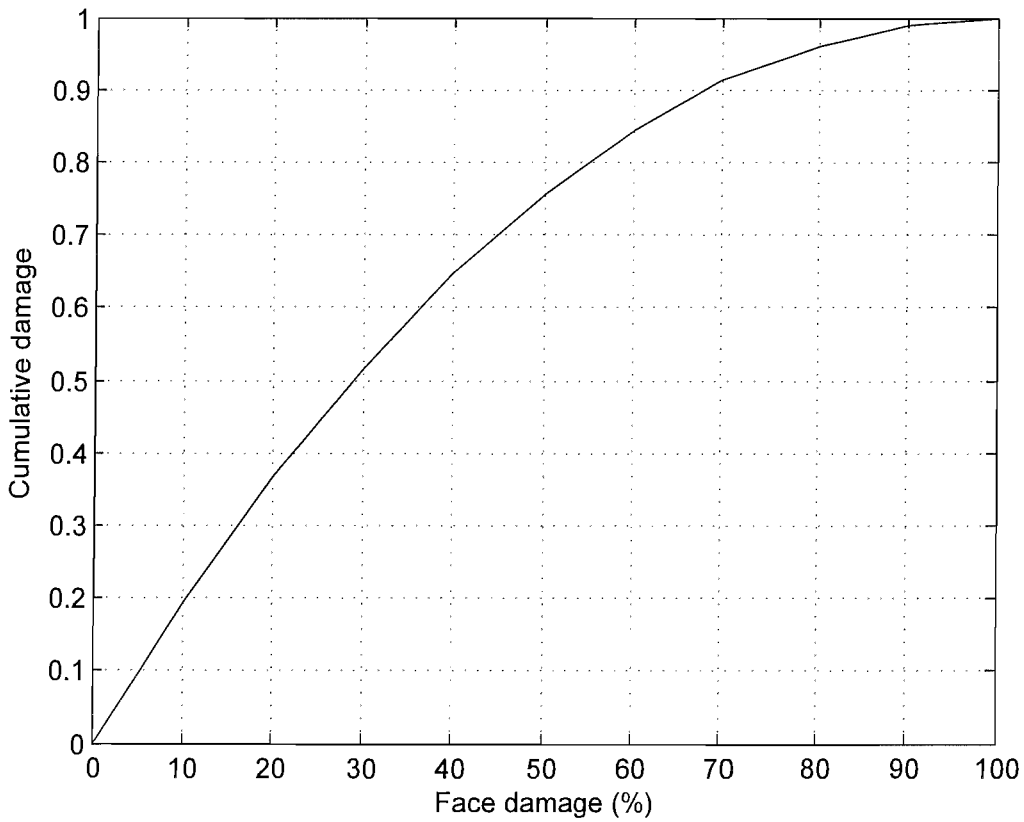

Figure 9.5: Variation of cumulative damage parameter for damage located at the mid-span of the beam in the face.

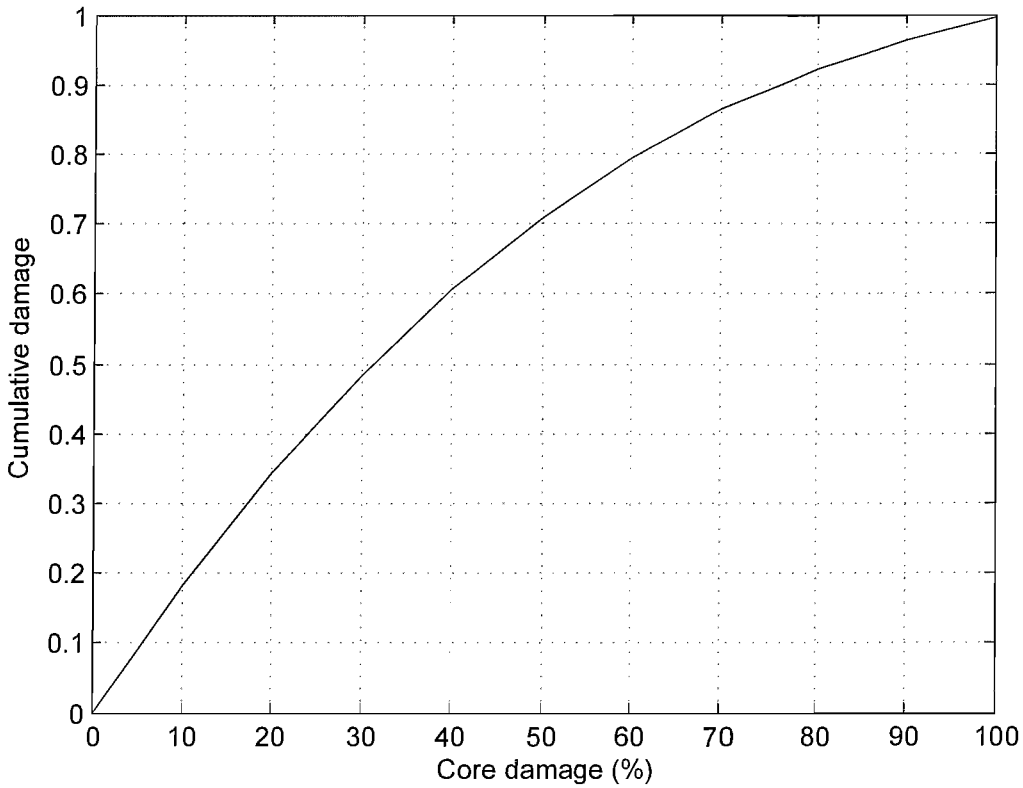

Figure 9.6: Variation of cumulative damage parameter for damage located at the mid-span of the beam in the core.

presented in Section 5.3. The variation of D for each location shows a similar trend and one such variation for damage in the face only at the mid-span of the beam model as used in Chapters 6 and 8, which is plotted in Fig. 9.5. It is evident from Fig. 9.5 that damage accumulates faster for lower extent of damage and relatively slower, for higher extent of damage in the face. A similar trend is observed for damage in the core only, as shown in Fig. 9.6. Further, the unit value of D confirms sudden collapse of the sandwich beam, as a result of complete failure, i.e., 100% damage at the end of fatigue life.

In view of the damage mechanisms presented in Section 2.1, the variations of D for different extents of damage in the face and the core of the beam model at each locations are investigated. Variation in D for varying extent of damage in the face and the core, located at the fixed-end, mid-span, and free-end of the beam model, are presented in Tables 9.2, 9.3, and 9.4 respectively. These results indicate the uniform increment in D with increasing damage in the face and the core. Analysis of results in Tables 9.2 - 9.4 reveal that the damage in the faces and the core has visible effects, on the cumulative damage parameter in the sandwich beam model, in the early period of damage development. Comparison of Figs. 9.5 and 9.6 reveal that trends in variation of D for face damage is almost similar to that of the core damage. This indicates that damage in the faces, accumulates rapidly during the initial period of life and slows down, as propagating damage approaches towards the complete collapse of the sandwich beam. The same trends are observed for damage located at other locations in the beam. This also confirms that damage of the faces does not lead to the catastrophic failure of a sandwich beam, rather it accelerates the accumulation of damage. However, this trend of damage accumulation can be used to predict the imminent failure of the sandwich beam. This is observed for all locations of damage, which is supported by the results as given in Tables 9.2 - 9.4.

In all cases of damage, the value of D reaches to unity at the complete collapse of the beam model, which is also reported by other researchers [Clark, 1997; Clark *et al.*, 1999; Kulkarni *et al.*, 2004; Mahi *et al.*, 2004]. Sensitivity analysis in this section, reveals that the proposed control method indicates the initiation and presence of small amount of accumulated damage, in the face and the core. The damage parameter is also sensitive to the interacting damage modes. The next step after characterising the cumulative damage parameter (D), is to design and develop the control system, implementing the cumulative damage model.

The proposed system is designed with capabilities to automatically initiate the analysis (like those used in Chapters 6 & 8), and activate the control system to raise the alarm, when the degree of damage in the beam specimen exceeds their threshold value. The extent of the alarm varies from low to a high level depending on their extent in the beam specimens. Hence, an additional layer of decision-making using the control method of Section 5.3 must be integrated with the real-time SHM and control system, to determine whether the degree of damage exceeded the threshold values or not. Thus, the following criteria to distinguish three phases of damage are set for the control system,

$$D \leq D_{low} \qquad => Safe \text{ "}No\ Alarm\text{"}, \tag{9.1}$$

$$D_{low} < D \leq D_{high} \quad => Moderate\ damage, \text{ "}Sound\ warning\ Alarm\text{"}, \tag{9.2}$$

$$D > D_{high} \qquad => Severe\ damage, \text{ "}Stop\ Testing\text{"}. \tag{9.3}$$

The values of D_{low} and D_{high} are the threshold values for the first and the second phase of damage respectively. Their values for the damaged beam specimens must be determined, using the numerical characterisation of the control system, which is presented in this section.

Based on the discussion of the results in this section, the values of D_{low} and D_{high} for the beam specimens are set to be 0.70 and 0.80 respectively. D_{low} is determined by assuming only the core shear degradation in the first phase of the damage. For determination of D_{high}, it is assumed that the face has started to loose its stiffness, which accelerates the damage process leading to a complete failure of the sandwich beam specimen, as discussed in this section. The software layer implementing the control system is then integrated with the system, using the framework presented in Sub-section 9.3.4.

9.4 Testing of the system

This section has two following objectives,

- To validate that the capabilities of the designed components are same, as envisaged during their design.

- To demonstrate that these components perform as one cohesive system, as envisaged in the system architecture.
- To identify the novel applications of the grid technologies, in the development of a real-time structural health monitoring and control system.

All testings in this section, are performed by using the computers having the specifications as listed in Table 9.5.

Table 9.5: Specifications of the machines and softwares used in testing.

Machine	Laboratory's computer	e-Science computer	Pacifica
Operating system	Windows XP Professional	Windows XP Professional	Linux
CPU	Pentium 4	Pentium 4	12-processor Xeon
RAM(MB)	512	512	
Database	Oracle10g	Oracle 10g	NA
Java version	1.4.2	1.4.2	NA
Measurement studio	7	NA	NA
Matlab version	NA	NA	6.5.1

9.4.1 Data acquisition

In this sub-section, the data acquisition system, designed in Sub-section 9.3.2, is tested by using the experimental set-up used in Chapter 8. For this purpose, the beam specimen was clamped on the set-up, as shown, in Fig. 8.4 and excited by using the random excitation technique. The objectives of this testing are as follows,

- Verify the design methodology used for the data acquisition system in Sub-section 9.3.2,
- Test the capabilities of the system for high-speed data acquisition from many accelerometers, like the one shown in Section 8.2,
- Upload the measured data to the local database system.

The data acquisition system and the local database server, designed in Sub-section 9.3.2, is installed in the same machine for similicity in the design. The specifications of the machine for the testing purpose is given in Table 9.5. Installation of the local

database server on the same machine requires a large memory, thus more overhead to run the system.

In order to reduce the overhead of the system, the data acquisition system is configured to scan only two accelerometers for measurements. One accelerometer is fixed on the shaker whereas second on the beam specimen. Accelerometer on the beam specimen measures the responses of the specimen under the cyclic load applied by the shaker. This applied cyclic load is measured by the accelerometer fixed on the shaker. These two measurements are used to obtain the FRF of the beam specimen as outlined in Section 7.4. Responses of the beam specimen and shaker are referred as the output responses and input forces in the FFT alogorithm described in Appendix F. The geometrical and mechanical properties of beam specimen is same as those used in Chapter 7. However, the damage mode introduced in the specimen is delamination between the face and core. This scheme provides opportunities to verify the capabilities of the data acquisition system and its integration, with the overall system. It is observed that the data acquisition system was able to achieve the objective identified in this chapter, by acquiring the accelerometers' readings of a certain time duration and uploading to the local database server. Their functionalities were validated, by comparing the plot of, the power spectral density obtained from the in-built data acquisition system, with those obtained from the data stored in the local database server, as shown in Figs. 9.9 and 9.8 respectively. It is observed that these two plots are exactly the same, which means that the data used to obtain these plots are also the same. This clearly indicates that all readings were uploaded to the local database server and the integrity of unique identifier were maintained.

9.4.2 Data management

In the previous sub-section, the functioning of the data acquisition system was validated for uploading the measured data to the local database server, in real-time. The next stage is to test the data management system, designed in Sub-section 9.3.3, for transfer of these data to the remote data management system. The objectives of the data management system are to perform basic data management tasks, such as providing easy and efficient search in the dataset and backups, as well as, an advanced task of ensuring that the real-time data is available to the user. These functionalities add one step further towards the automation in a real-time structural health monitoring and control system to achieve the desired characteristics, as outlined in Section 2.6.

The reliability of the data management system is verified by testing the beam specimens, using the procedures used in Chapter 8. In order to identify the responses of the selected beam specimen, each beam specimen is given an unique identifier by defining a column, named `spcid` in the table `list`. Hence, an unique value of `spcid` is set for the beam specimen before its testing. For each testing, the measurements are acquired by the data acquisition system designed in Sub-section 9.4.1 and transferred to the data management system. Each measurement also has their time-stamp to give an unique identifier, which also serves the purpose of identifying the measurement at that particular time or between the selected time duration. It is verified that all measurements are received by the data management system from the beam specimens, in near real-time. These claims will be validated in Sub-section 9.4.4 after verifying the capabilities to extract the stored data, in Sub-section 9.4.3.

9.4.3 Query support

One of the main characteristics outlined in Section 2.6, is the formal query support for the accelerometers' readings, stored in the data management system. SQL provides an easy and efficient way to access these data stored in the data management system, for their subsequent analysis. Use of SQL enables a user to retrieve data using different criteria such as specimen ID, time-period, which can also be embedded in a Java program.

From the user perspective, there are two major classes of queries that are executed frequently. In the first query, the accelerometers' readings are queried according to the specimen ID (`spcid` to retrieve the accelerometer's reading for the specimen). This query runs several times until all the required data are retrieved. The second type of query retrieves accelerometers' readings for a specified period of time when a large dataset for a particular specimen are available. These queries are performed by using the SQL command `SELECT` for the above criteria. Since, the number of measurement channels are limited, measurements from only two accelerometers are used for the analysis. The SQL command to query the data for specimen (`spcid`) i.e. **DEL1** is as follows,

```
SELECT channel00, channel01 FROM list ORDER BY measuredtime
WHERE spcid=DEL1
```

Similarly, the SQL command to query the dataset for a specified period of time for the selected specimen is as follows,

```
SELECT channel00, channel01 FROM list ORDER BY measuredtime
```

```
WHERE spcid=DEL1 AND measuredtime > time1 AND measuredtime
< time2
```

The data obtained by these embedded commands in a Java program, are stored in a temporary file for analysis, to calculate the FRF like one in Section 8.3. After completion of analysis, this temporary file is deleted from the computer.

9.4.4 Data analysis and validation

In this sub-section, the computational system designed in Sub-section 9.3.4, is tested by analysing the data stored in the data management system. It is aimed to test the automated computation in the system for the structure, like those used in Chapters 6 and 8. The automated computation may start automatically by the system or by a user/event.

For validation of the system designed in Section 9.3, the measurements obtained from the disbonded sandwich beam specimen, shown in Fig. 9.7, are used. The fabricated beam specimen is excited by the random excitation technique, using the same set-up used in Chapter 8. The extent of disbond is 40.00 *mm* at mid-span, as shown in Fig. 9.7. The accelerometers' readings for this beam specimen is retrieved from the data management system, by using the SQL command embedded in the Java program. These retrieved data are saved in the temporary file, which is then transferred to the computational resource (`pacifica`), by using GridFTP for their analysis and using an archived executable `MATLAB` code to obtain the FRF of the beam specimen. The objective of this analysis is to validate the claims made in previous sub-sections, i.e. all data are transferred from the laboratory and can be queried in order of measured time(`measuredtime`). This is validated, by comparing the calculated FRF with the FRF plot obtained from the in-built analyser, from the system attached with the shaker in Figs. 9.8 and 9.9 respectively. It can be observed that these two plots match exactly with each other, which implies that the same data set were used for these calculations, thus validating the claims made in the design and testing of the system.

Here, this process was initiated by the user by following the sequence shown in Fig. 9.4.

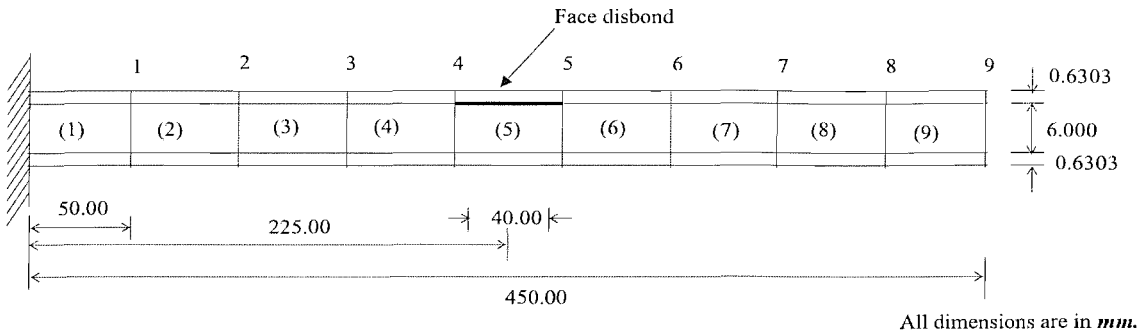

Figure 9.7: Geometrical dimensions of the beam specimen for disbond located at mid-span.

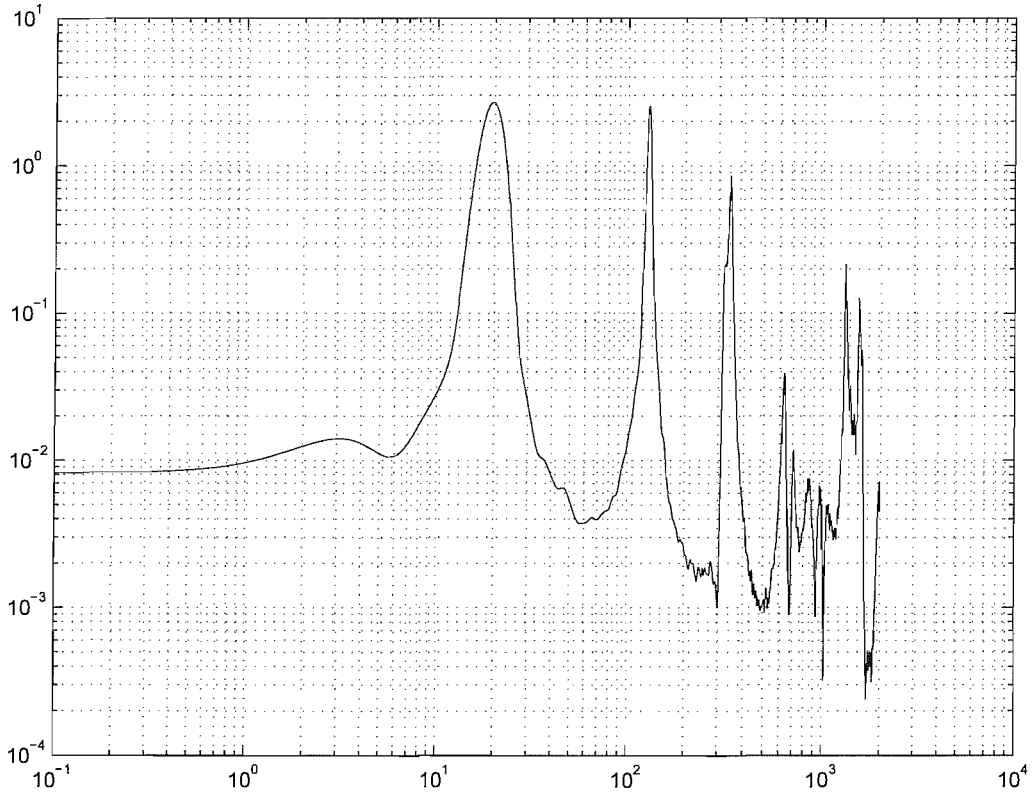

Figure 9.8: Plot of Power spectral density for disbonded beam specimen.

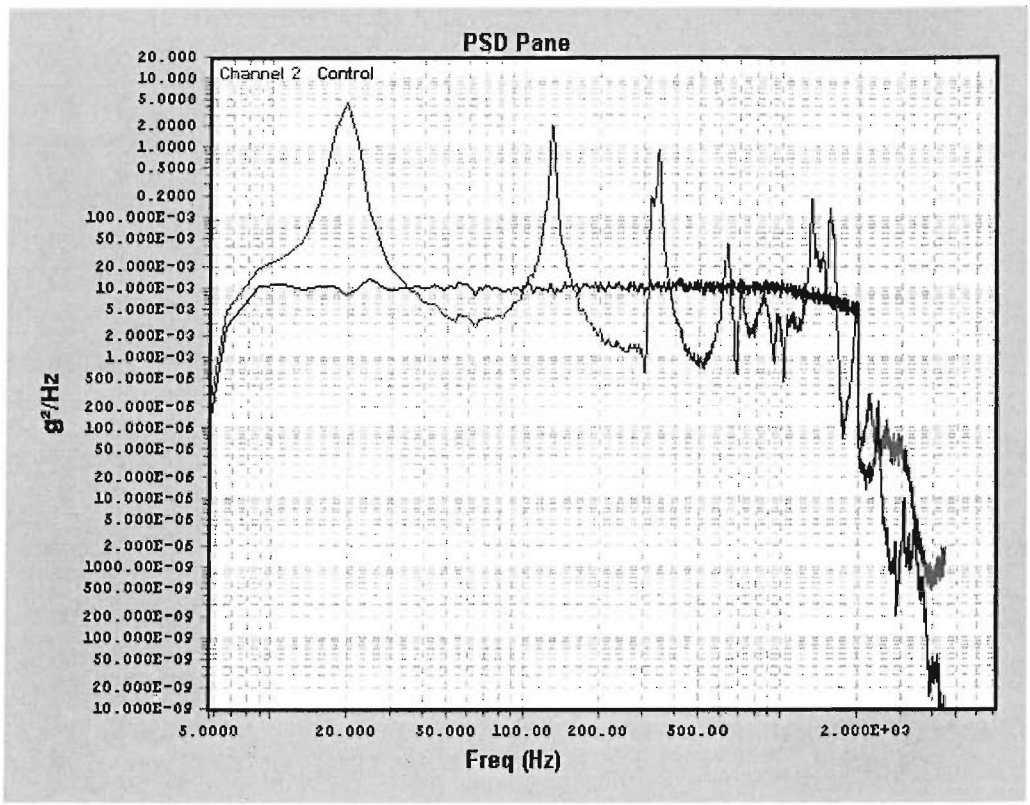

Figure 9.9: Plot of Power spectral density for disbonded beam specimen from controller attached to shaker.

9.5 Recommendations for Implementation of control system

One of the objective of this work is to provide design recommendations and guidelines, for the implementation of a real-time structural health monitoring and control system, by using the grid technologies. In previous sections of this chapter, a system architecture connecting different components was developed and implemented. Due to the limitations of the data acquisition system, measurements from only few of the accelerometers on the structure were obtained, which constrained their damage identification. In this section, the recommendation and guideline for implementation of the control system is presented.

The basic theory behind the control system characterised in Sub-section 9.3.5, was to determine the threshold values (D_{low} & D_{high}) of the damage parameter (D). The tested and validated computational system in Section 9.4, could be used to analyse the measurements as shown in Section 8.2, which are used as inputs in the damage identification method. The results obtained from the damage identification method, i.e., location, extent and level of damage are then processed, to obtain the cumulative damage parameter (D), by using the theory presented in Section 5.3. Then, the value of D will be compared with those of the threshold values (D_{low} and D_{high}) to raise the alarm, as per level defined in Sub-section 9.3.5. The code required to implement this logic could be stored and executed in the computational resource (`pacifica`). The flowchart is shown in Fig. 9.10. The code required to execute the steps of the flowchart could be implemented by using Java programming language and Java CoG toolkit, like those in Sub-section 9.3.4.

9.6 Potential Applications

In this section, the potential application scenarios are identified to illustrate how the system, designed in Section 9.2, can be used for structural health monitoring and control purposes in practice. These application scenarios are envisaged to harness the capabilities of the real-time structural health monitoring and control system.

9.6.1 Real-time damage assessment

Real-time damage assessment of a structure is the prime application of the system. This objective requires the availability of the vibration measurements from the sensors, by using the system tested in Sub-section 9.4.1 and stored in the data management

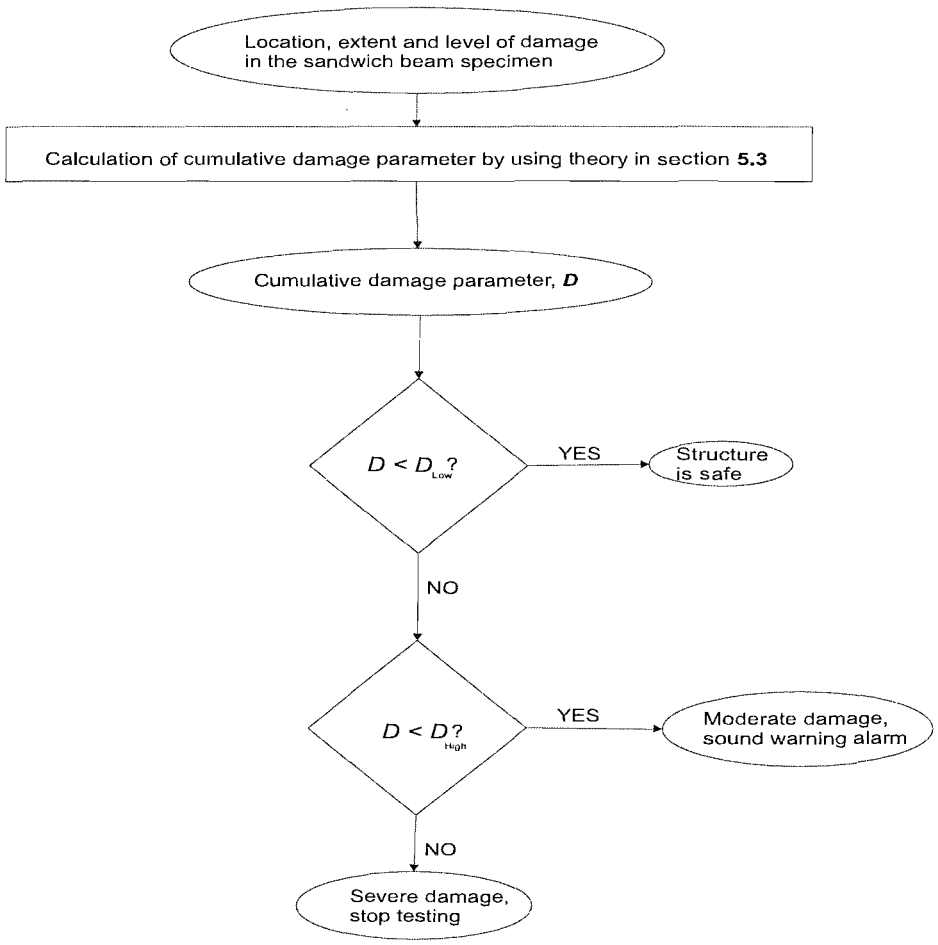

Figure 9.10: Process and steps of the control system.

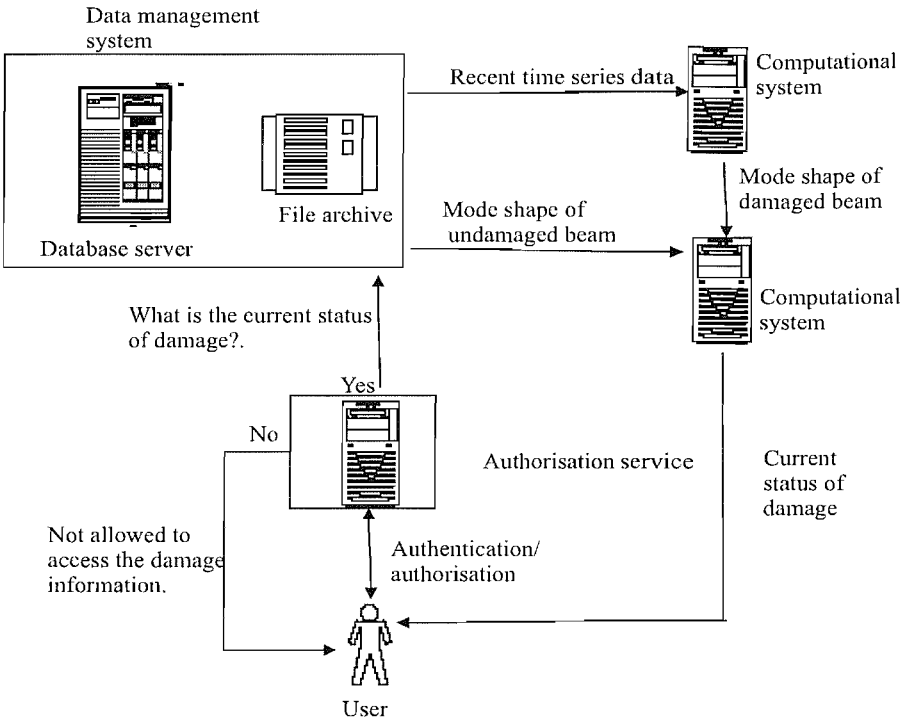

Figure 9.11: An envisaged application scenario for the real-time damage assessment.

system, tested in Sub-section 9.4.2. These measurements would be then analysed as per procedure in Fig. 7.3, by using the computational system tested in Sub-section 9.4.4. These data can be used by the validated damage identification method, to predict the current state of damage in the structure. The analysis code required to perform the same can be integrated with the system, by using the methodology in Sub-section 9.3.4 and could be executed periodically or could be user/event driven. These obtained damage results could be uploaded to the data management system, by using Java CoG as shown in Section 3.4, for future use.

9.6.2 Damage propagation monitoring

One of the most common usage scenario would be monitoring initiation and propagation of damage in a structure. The importance of monitoring the same for prediction of catastrophic failure of a sandwich structure, is highlighted in Section 2.1. In this application, an user with authorisation to assess the structural health information,

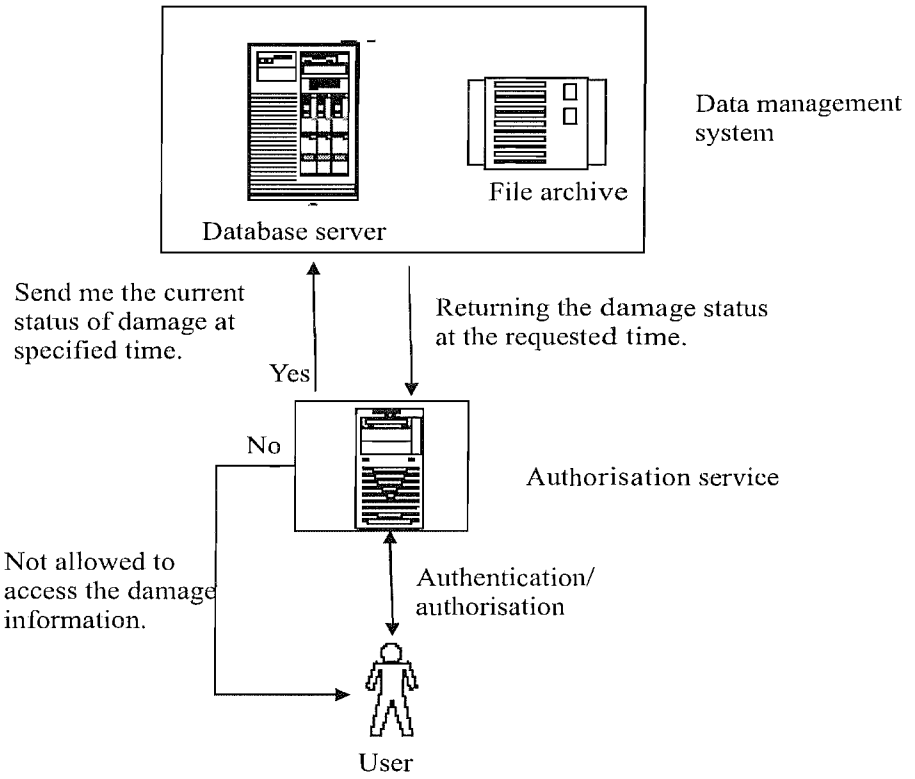

Figure 9.12: An envisaged application scenario for the damage monitoring.

would be able to retrieve all the stored information from the data management system, which could be updated after receiving results obtained in Sub-section 9.6.1. Data management system could be updated periodically or could be user/event driven.

It is envisaged that an user authorised to access the damage information, stored in the data management system can follow the steps shown in Fig. 9.12, to monitor the damage propagation.

9.6.3 Active control

Recommendations given in Section 9.5 could be implemented, to integrate the control system with the real-time structural health monitoring and control system. The integration methodology could be similar to those used in Sub-section 9.3.4, for, the calculation steps as shown in Fig. 9.10. Based on the real-time damage assessment results, the control system would determine the criticality of damage using the control method characterised in Sub-section 9.3.5, which would then alert the user for

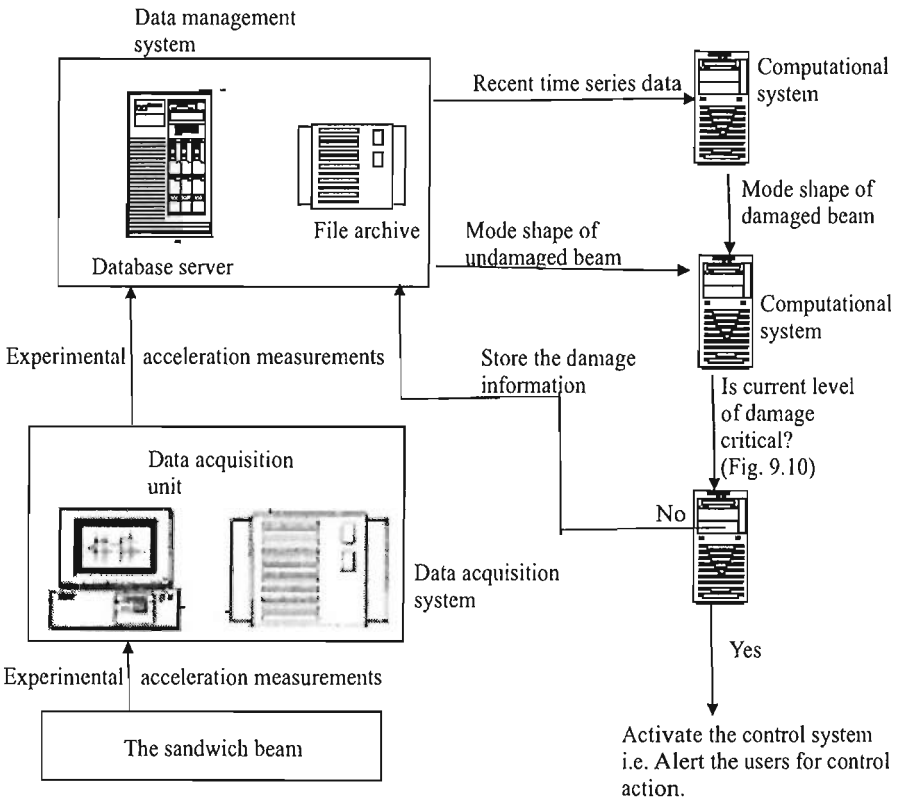

Figure 9.13: An envisaged application scenario for the active control.

any probable critical damage. This requires the comparison of the cumulative damage parameter (D) with those threshold values defined for the critical level of damage (D_{low} and D_{high}). The inputs in the system for this purpose, would be the damage identification results, like those obtained in Chapters 6 and 8. Thus, the control system could be used in the real-time structural health monitoring and control system, to identify the propagation of damage into critical damage and alert the users, if required. The mechanism of the proposed control system is shown in Fig. 9.13, which could be implemented in the system.

9.7 Conclusions

This chapter discussed the design, implementation and testing of the real-time structural health monitoring and control system, which can incorporate the calculations used in Chapters 6 and 8. This was realised by using the tools from grid technologies as discussed in Chapter 3. The study in this chapter proves the feasibility of using grid technologies for deployment of the system in practice. It was observed that the data acquisition system measuring data at high sampling frequency, involving many accelerometers, was unable to achieve the target. This is attributed to a large amount of data and their processing requirements, which the system was unable to handle. However, the required sampling frequency for a real structure is much lower than that used in this chapter. Hence, the system can perform well for a real-structure having many sensors.

Chapter 10

Conclusions and Future Work

A vibration-based damage identification method for a sandwich beam, by using changes in elemental modal strain energy was developed and validated with the experimental data. This method was verified for various damage cases in the sandwich beam by using numerical simulations. Changes in the elemental modal strain energy, were derived from the variations in the vibration reponses of the sandwich beam, which were obtained from the numerical simulations and the experimental testings. Further, a system architecture was developed, by using toolkits based on grid technologies for a real-time structural health monitoring and control system, to transfer and process the experimental measurements in real-time. Components of this system were designed, implemented and tested by using the experimental measurements. Finally, this chapter draws conclusions from the numerical and the experimental work presented in this thesis and presents the recommendations for future work, to improve the system. The following are the key contributions provided by this work,

Key Contributions

- A thorough investigation of the damage identification method was conducted to study its effectiveness for the location, the extent and the level of damage in the composite sandwich beam.
- An integrated design of components for a real-time structural health monitoring and control system is presented by using grid technologies, which is currently not available in the published literature.

Numerical Results

1. Complete derivation of the damage identification method upto Level 3, by using changes in the modal strain energies was presented for the sandwich beam. (Section 5.2)

2. First published work for verification of damage identification method, based on the changes in modal strain energies for simulated damage cases, by using the natural frequencies and mode shapes of the sandwich beam. (Section 6.6).

3. First published work for the damage identification in a sandwich beam with interactive damage modes and their identification. (Section 6.6)

4. Sensitivities of the damage identification method for the location, the extent and the level of damage in the sandwich beam. (Section 6.6)

5. Derivation of a criteria to define the severity of damage for a sandwich beam, which is also used for control purposes. (Section 5.3)

6. Characterisation of the control method by using numerical simulation for various simulated damage cases. (Sub-section 9.3.5).

Experimental Results

1. First published work validating the damage identification method (Level 3), based on the changes in elemental strain energies, by using the experimental measurements obtained from the sandwich beam specimens, with single and multiple damages. (Chapter 8)

2. Innovative application of grid technologies for the development of data management and computational system, in a real-time structural health monitoring and control system. (Section 9.3)

3. Innovative application of database technology for implementing real-time transfer of experimental measurements, from the laboratory to the remote data management system. (Sub-sections 9.3.2 and 9.4.1)

General Contributions

- Recommendations for the potential applications of a real-time structural health monitoring and control system (Section 9.6).

- Review of structural health monitoring system, its limitations and desirable characteristics. (Sections 2.6 and 2.7)

- Thorough review of grid technologies and their application in solving engineering problems. (Chapter 3)

10.1 Conclusions

This thesis presented a numerical and experimental study of the vibration-based damage identification method, as a basis for structural health monitoring of sandwich beams. For this purpose, an extensive literature review was presented to identify the achievements and limitations of the previous work, on damage identification and structural health monitoring system, followed by development of the presented methods in this thesis. An extensive study by using numerical simulations was undertaken, to investigate the sensitivity of the damage identification method, for various damage cases. Further, this method was validated with experimental measurements obtained from testings of the sandwich beam specimens.

The first part of this study, concentrated on the development of accurate finite element model for the sandwich beam, used for generation of its vibration responses. Subsequently, this model was used to create the damaged beam model, by changing the local stiffness in the face and the core of the undamaged model. These beam models were used to generate the natural frequencies and mode shapes of the sandwich beam. Good correlations were found between the analytical results and the numerical results for the undamaged beam model. This model was then used to compare the mode shapes of the undamaged and damaged sandwich beam model, to study their sensitivities towards the location and the extent of the damage. It was observed that the mode shapes show sensitivities towards the damage but were unable to locate the damage.

Theoretically, the presence of damage alters the vibration responses of the damaged sandwich beam model, which in turn changes the elemental modal strain energies. These changes were used to derive the damage identification method. The effectiveness of this method was verified, by using the numerical simulations of the sandwich beam, for various simulated damage cases, including interactive damage types.

After developing the damage identification method, the first four natural frequencies and mode shapes of the sandwich beam model, were used as inputs for predicting the existence, the location, the extent and the level of the damage. For this purpose, various damage cases at three different locations in the beam model were considered, to study the sensitivity of the method for different damage locations and extents. The

obtained results were then compared with those of the simulated damage cases. It was found that the damage in the beam model was located accurately, but predictions of the extent showed slight deviation from those of the simulated values of the damage cases.

Similar sandwich beam specimens, with and without face delamination, were then fabricated by resin infusion process and vaccum bagging technique. They were cut in the geometrical dimensions similar to those of the numerical study. Face delamination was introduced in the beam specimens by placing a teflon sheet, between the face and the core during fabrication, at two locations and removing the part of face above the resultant disbond. Their geometrical dimensions were then measured at various points of the beam specimens and averaged to obtain the geometrical dimensions. Their mechanical properties were determined by using the experimental technique and the rule of mixture. These sandwich beam specimens were tested to measure their vibration responses, by using accelerometers under frequency sweep excitation. The experimental natural frequencies agreed well with the natural frequencies of the numerical simulations. The "blind experimental tests" were also conducted on the sandwich beam specimens with an artificially introduced damage. Nine accelerometers were fixed at regular intervals along the centre line of the beam specimen. Their experimental measurements were then used to obtain their first four mode shapes, which were used in conjunction with the natural frequencies to predict the location, the extent and the level of the damage in the beam specimens. Hence, experimental validation of the damage identification method was achieved by using their first four natural frequencies and mode shapes.

After experimental validation of the damage identification method, a multi-disciplinary approach was applied for the development of a real-time structural health monitoring and control system. A system architecture connecting different components such as sensors, communications, data management, algorithm and control system was developed. The integration of the control system required the development of a control method that could use the results obtained from the damage identification method, to predict the severity of damage in the sandwich beams. The control method was characterised by using numerical simulations for various simulated damage cases. Many components were implemented by using the toolkits based on grid technologies and their testing revealed their successful implementation, as they performed intended functions. Recommendations were provided for implementation of the control system and its integration with the system.

10.2 Future work

Much work still remains before a real-time structural monitoring and control system can be relied upon practice. This is not an indication of a lack of effort its their development. Rather, it reflects the fact that the methodology developed in this work, is a transitional stage from theory to implementation and needs further investigation. Hence, this work provides the beginning of a new application of grid technologies, for development of a real-time structural health monitoring and control system. The damage identification method requires additional experimental testings and the possibilities for improvements are numerous, in both damage identification method and real-time structural health monitoring and control system. This section summarises some suggestions for further investigation.

- **Additional experimental testings**

  The future work should focus on continued experimental testings, with more damage types, at more locations, in order to assess the performance of the damage identification method in practice. The performance of the method for varying damage extent/size of the damaged area will also be useful to determine the sensitivity and the robustness of the method. Investigation of the damage modes that can be identified is equally important.

- **Application of the technique to real structures**

  The damage identification method was validated with the experimental data, obtained from the testings in controlled laboratory environment, with artificially introduced damage. However, there is a need to validate this method for real structures, which are subjected to dynamic and uncertain environments.

- **Implementation of the control system**

  After integrating the sensors, the data management system and the computational resources by using the grid technologies based toolkits, it is equally important to integrate the control system with them. Testing the integration of the control system will be an important part of a successful programme. Most directly, remote control and access of data from sensors via wireless connection needs much attention.

- **Implementation of wireless monitoring**

  In recent years, there has been a rapid development in the field of wireless monitoring. Development and deployment of a wireless monitoring system can be useful for an external environment and does not require continuous supervision. The data obtained from the wireless system could be easly integrated into a real-time structural health monitoring and control system.

- **Data transfer across the National Grid**

  Another future direction for the current work, is to use the methodology to extend the system for real-time transfer of data, from the laboratory to a remote data management system, outside of the university network. For this purpose, the data storage system connected to the National Grid Service may be used. Real-time transfer of data can be achieved by using the *Oracle streaming technology*, which was also used in this work. This implementation will further improve the system presented in this thesis.

References

ADAMS, R.D., CAWLEY, P. & PYE, C.J. (1978). A vibration technique for non-destructively assessing the integrity of structures. *Journal of Mechanical Engineering Science*, **20**, 93–100. 2.4.1, 2.4, 2.5

AKTAN, A.E., CATBAS, F.N., GRIMMELSMAN, K.A. & TSIKOS, C.J. (2000). Issues in infrastructure health monitoring for management. *Journal of Engineering Mechanics*, **126**, 711–724. 2.3

ALLEN, H.G. (1969). *Analysis and Design of Structural Sandwich Panels.* Pregamon Press Ltd., London. 5.1.1

ALVANDI, A. & CREMONA, C. (2006). Assessment of Vibration-based Damage Identification techniques. *Journal of Sound and Vibration*, **292**, 179–202. 2.4.3

ANANTHANARAYAN, A., BALACHANDRAN, R., GROSSMAN, R., GU, Y., HONG, X., LEVERA, J. & MAZZUCCO, M. (2003). Data webs for earth science data. *Parallel Computing*, **29**, 1363–1379. 3.5

ARMON, D., BEN-HAIM, Y. & BRAUN, S. (1994). Crack detection in beams by rank-ordering of eigenfrequency shifts. *Mechanical Systems and Signal Processing*, **8**, 81–91. 2.4.1

AVERY, P. (2002). Data grids : A new computational infrastructure for data-intensive science. *Philosphical Transactions : Mathematical, Physical and Engineering Sciences*, **360**, 1191–1209. 3.5

BANKS, H.T., INMAN, D.J., LEO, D.J. & WANG, Y. (1996a). An Experimentally Validated Damage Detection Theory in Smart Structures. *Journal of Sound and Vibration*, **191**, 859–880. 6.3

BANKS, H.T., INMAN, D.J., LEO, D.J. & WANG, Y. (1996b). An experimentally validated damage detection theory in smart structures. *Journal of Sound and Vibration*, **191**, 859–880. 2.4.2, 2.4

BEATTIE, A.G. (1998). An Acoustic Emission Test for Aircraft Halon 1301 Fire Extinguisher Bottles. Tech. Rep. DOT/FAA/AR-97/9, Federal Aviation Administration, Office of Aviation Rsearch. 2.3.3

BESTER, J., FOSTER, I., KESSELMAN, C., TEDESCO, J. & TUECKE, S. (1999). A Data movement and Access Service for Wide Area Computing Systems. In *Proceedings of the 6^{th} Workshop on Input/Output in Parallel and Distributed Systems*, Atlanta, USA. 3.4

BOLLER, C. (2000). Next Generation Structural Health Monitoring and its Integration into Aircraft Design. *International Journal of Systems Science*, **31**, 1333–1349. 2.5.1

BURMAN, M. & ZENKERT, D. (1997). Fatigue of foam core sandwich beams - 1: Undamaged specimen. *International Journal of Fatigue*, **19**, 551–561. 2.1, 2.1, 2.1

BUTLER, R., ENGERT, D., FOSTER, I., KESSELMAN, C., TUECKE, S. & WELCH, V. (2000). Design and Deployment of a National-Sacle Authentication Infrastructure. *IEEE Computer*, **33**, 60–66. 3.4

CARNEIRO, S.H.S. (2000). *Model-Based Vibration Diagnostic of Cracked Beams in the Time Domain*. Ph.D. thesis, Virginia Polytechnic Institute and State University. 6.6.2

CAWLEY, P. & ADAMS, R.D. (1979). The location of defect in structure from measurements of natural frequencies. *Journal of Strain Analysis*, **14**, 49–57. 2.4.1, 2.4, 2.5

CHANCE, J., TOMLINSON, G.R. & WORDEN, K. (1994). A simplified approach to the numerical and experimental modeling of the dynamics of a cracked beam. In *Proceedings of the 12^{th} International Modal Analysis Conference*, 778–785. 2.4.1

CHERVENAK, A., DEELMAN, E., KESSELMAN, C., ALLCOCK, B., FOSTER, I., NEFEDOVA, V., LEE, J., SIM, A., SHOSHANI, A., DRACH, B., WILLIAMS, D. & MIDDLETON, D. (2003). High-performance remote access to climate simulation data : A challenge problem for data grid technologies. *Parallel Computing*, **29**, 1335–1356. 3.5

CHONDROS, T.G. & DIMAROGONAS, A.D. (1980). Identification of cracks in welded joints of complex structures. *Journal of Sound and Vibration*, **69**, 531–538. 2.4.1, 2.5

CLARK, S.D. (1997). *Long Term Behaviour of FRP Structural Foam Cored Sandwich Beam*. Ph.D. thesis, University of Southampton. 2.1, 2.1, 2.2, 5.3, 5.3, 9.3.5

CLARK, S.D., SHENOI, R.A. & ALLEN, H.G. (1999). Modelling fatigue behaviour of sandwich beam under 2-step and block-loading regimes. *Composite Science and Technology*, **59**, 471–486. (document), 2.3, 2.1, 2.2, 5.3, 5.3, 9.3.5

COOK, R.D., MALKUS, D.S. & PLESHA, M.E. (1989). *Concepts and Applications of Finite Element Analysis*. John Wiley and Sons, 3rd edn. 5.1.2

CoreCell© (2003). *Technical Data Sheet*. ATC Chemical Corporation, Accessed on 5th September 2003. 7.1

CORNWELL, P., DOEBLING, S.W. & FARRAR, C.R. (1999). Application of the strain energy damage detection method to plate-like structures. *Journal of Sound and Vibration*, **224**, 704–719. 2.4.2, 2.4.3, 2.4, 2.5, 5.2.4

COULOURIS, G., DOLLIMORE, J. & KINDBERG, T. (2001). *Distributed Systems : Concept and Design*. Addison Wesley, 3rd edn. (document), 3.1.1, 3.2

CUNHA, J. & PERREUX, D. (1998). Method for Damage Evaluation of Laminated Composite Materials by using Model Updating Techniques in Dynamics. *Journal of Engineering Materials and Technology – Trans. ASME*, **120**, 256–260. 2.4

CYRAN, M. & LANE, P. (2003). Oracle Database Concepts, $10g$ Release 1. Tech. rep., Oracle Corporation, A white Paper. 9.3.3

DAI, J. & HAHN, H.T. (2004). Fatigue analysis of sandwich beams using a wear-out model. *Journal of Composite Materials*, **38**, 581–589. 2.2

DAWOOD, T., SHENOI, R.A., VERES, S.M., SAHIN, M. & GUNNING, M.J. (2003). Damage detection in a sandwich composite beam using wavelet transforms. In *The SPIE Smart Structures and Materials Symposium*, vol. 5049, 5049–5088. 2.4.1, 2.5, 2.6, 2.5.1, 2.7.1

DAWOOD, T.A., SHENOI, R.A., VERES, S.M. & SAHIN, M. (2004a). Low level damage characterisation in frp sandwich beams using a the lipschitz exponent. In C. Boller & W.J. Staszewksi, eds., *Proceeding of the Second European Workshop Structural Health Monitoring*, 661–668, Munich, Germany. 2.4.1, 2.5, 2.6, 2.5.1, 2.7.1, 8.3

DAWOOD, T.A., SHENOI, R.A., VERES, S.M., SAHIN, M. & GUNNING, M.J. (2004b). Damage characterisation in frp sandwich beams using a wavelet based multifractal approach. In C. Boller & W.J. Staszewksi, eds., *Proceeding of the Second European Workshop Structural Health Monitoring*, 653–660, Munich, Germany. 2.4.1, 2.5, 2.6, 2.5.1, 2.7.1, 8.3

DOEBLING, S.W., FARAR, C.R., PRIME, M.B. & SHEVTZ, D.W. (1996). Damage identification in structures and mechanical systems based on change in the vibration characteristics : A detailed literature review. Tech. Rep. LA-13070-MS, Las Alamos National Laboratory. 2.4, 2.4.3, 2.5.1, 2.7.1

DOEBLING, S.W., HEMEZ, F.M., PETERSON, L.D. & FARHAT, C. (1997). Improved damage location accuracy using strain energy-based mode selection criteria. *AIAA Journal*, **35**, 693–699. 2.4.2, 2.4

DOEBLING, S.W., FARRAR, C.R. & PRIME, M.B. (1998). A summary of vibration based damage identification methods. *The Shock and Vibration Digest*, **30**, 91–105. 2.4.1, 2.7.1, 5.2.4

EWINS, D. (2000). *Modal Testing : Testing and Practice*. Wiley, Newyork. 7.4

FAGERBERG, L. (2004). Wrinkling and Compression Failure Transition in Sandwich Panels. *Journal of Sandwich Structures and Materials*, **6**, 129–144. (document), 2.1, 2.6

FARRAR, C.R. & JAUREGUI, D.A. (1998a). Comparative study of damage identification algorithms applied to a bridge : 1. experiments. *Smart Materials and Structures*, **7**, 704–719. 2.4.2, 2.4.3, 2.4

FARRAR, C.R. & JAUREGUI, D.A. (1998b). Comparative study of damage identification algorithms applied to a bridge : 2. numerical study. *Smart Materials and Structures*, **7**, 720–731. 2.4.2, 2.4.3

FARRAR, C.R., HEMEZ, F., PARK, G., ROBERTSON, A.N., SOHN, H. & WILLIAMS, T.O. (2003). A coupled approach to developing damage prognosis solution. In *Proceedings of the 5^{th} International Conference on Damage Assessment of Structures(DAMAS2003)*, 289–306, University of Southampton, Southampton, U.K. 2.4.3

FLETCHER, R. (1987). *Practical Methods of Optimization*. Wiley-Interscience, New York, USA, 2nd edn. 5.2.4

FOSTER, I. (2002a). The grid : A new infrastructure for 21st century science. *Physics Today*, **42**, 42. (document), 3.2.1, 3.3

FOSTER, I. (2002b). *What is the Grid? A Three Point Checklist*. Argonne National Laboratory & University of Chicago. 3.2, 3.2

FOSTER, I. & KESSELEMAN, C., eds. (1999). *The Grid : Blueprint for a New Computing Infrastructure*. Morgan Kauffman. 3

FOSTER, I., KESSELMAN, C. & TUECKE, S. (2001). The anatomy of the grid : Enabling scalable virtual organisations. *International Journal of High Performance Computing Applications*, **15**, 200–222. 3.2, 3.2.2

FRISWELL, M.I., PENNY, J.E.T. & WILSON, D.A.L. (1994). Using vibration data and statistical measures to locate damage in structures. *International Journal of Analytical and Experimental Modal Analysis*, **9**, 239–254. 2.4.1

GAGEL, A., FIEDLER, B. & SCHULTE, K. (2006). On modelling the mechanical degradation of fatigue loaded glass-fibre non-crimp fabric reinforced epoxy laminates. *Composites Science and Technology*, **66**, 657 – 664. 6.3

GAO, Z. (1994). A cumulative damage model for fatigue life of composite laminates. *Journal of Reinforced Plastics and Composites*, **13**, 128–141. 2.2

GIURGIUTIU, V., ZAGRAI, A. & BAO, J.J. (2002). Piezoelectric Wafer Embedded Active Sensors for Aging Aircraft Structural Health Monitoring. *Structural Health Monitoring*, **1**, 41–61. 2.5

GODIN, N., HUGUET, S., GAERTNER, R. & SALMON, L. (2004). Clustering of Acoustic Emission Signals Collected during Tensile Tests on Unidirectional glass/polyester Composite using Supervised and Unsupervised Classifiers. *NDT & E International*, **37**, 253–264. 2.3.3

GORANSON, U.G. (1997). Jet transport structures performance monitoring. In *Proceeding of International Workshop on Structural Health Monitoring*, 3–17, California, USA. 2.5

GRONDEL, S., ASSAAD, J., DELEBARRE, C. & MOULIN, E. (2004). Health Monitoring of a Composite Wingbox Structure. *Ultrasonics*, **42**, 819–824. 2.3.3

GULAMALI, M.Y., LENTON, T.M., YOOL, A., PRICE, A.R., MARSH, R.J., EDWARDS, N.R., VALDES, P.J., WASON, J.L., COX, S.J., KRZNARIC, M., NEWHOUSE, S. & DARLINGTON, J. (2003). GENIE : Delivering e-Science to the Environmental Scientist. In *UK- e-Science All Hand Meeting*, 145–152, Nottingham, U.K. 3.5

HALL, S.R. (1999). The Effective Management and Use of Structural Health Data. In *Proceedings of the 2nd International Workshop on Structural Health Monitoring*, 265–275, Stanford, USA. 1, 2.5, 3.6

HAMEY, C.S., LESTARI, W., QIAO, P. & SONG, G. (2004). Experimental Damage Identification of Carbon/Epoxy Composite Beams using Curvature Mode Shapes. *Structural Health Monitoring*, **3**, 333–353. 2.4.1, 2.4

HAMMING, R.W. (1989). *Digital filters*. Prentice-Hall International Edition, Englewood Cliffs, NJ. 2.5.2

HASHIN, Z. (1985). Cumulative damage theory for composite materials : Residual life and residual strength methods. *Composite Science and Technology*, **23**, 1–19. 2.2, 2.2

HOSCHEK, W., JAEN-MARTINEZ, J., SAMAR, A., STOCKINGER, H. & STOCKINGER, K. (2000). Data Management in an International Data Project. In *First IEEE/ACM International Workshop*, Banglore, India. (document), 3.6, 3.5

HOUSNER, G.W. & BRADY, A.G. (1963). Natural periods of vibrations of buildings. *Journal of the Engineering Mechanics Division, Proceedings of ASCE*, **89**, 31–65. 2.4.1

HU, H., WANG, B.T., LEE, C.H. & SU, J.S. (2006). Damage detection of surface cracks in composite laminates using modal analysis and strain energy method. *Composites Science and Technology*, **74**, 399–405. 2.4.2

HUGUET, S., GODIN, N., GAERTNER, R., SALMON, L. & VILLARD, D. (2002). Use of Acoustic Emission to Identify Damage Modes in Glass Fibre Reinforced Polyester. *Composites Science and Technology*, **62**, 1433–1444. 2.3.3

HUNT, S.R. & HEDBEN, I.G. (2000). Validation of the eurofighter typhoon structural health and usage monitoring system. In *European COST F3 Conference on System Identification and Structural Health Monitoring*, 743–753, Madrid, Spain. 2.5

IGLESIAS, M.J. & PALOMINO, A. (2000). SHMS, A Good Chance to Gain Experience to Optimise the Aircraft Structural Capability. In *European COST F3 Conference on System Identification and Structural Health Monitoring*, 753–771, Madrid, Spain. 2.5

IRRETIER, H. (1993). Crack detection in composite driving shaft by experimental modal analysis. In *ASME - 14^{th} Biennial Conference on Mechanical Vibration and Noise*, 47–54, Albuquerque, New Mexico. 2.4.1

IRRETIER, H., BELZ, J. & REUTTER, F. (1993). On the crack detection in composite driving shaft by frequency and damping tests. In *The Institute of Physics Stress Analysis Group Conference on Modern Practice in Stress and Vibration Analysis*, 109–122. 2.4.1

ISLAM, A.S. & CRAIG, K.C. (1994). Damage Detection in Composite Structures using Piezoelectric Materials. *Smart Materials and Structures*, **3**, 318–328. 2.4

JACKSON, T., AUSTIN, J., FLETCHER, M. & JESSOP, M. (2003). Delivering a Grid Enabled Distributed Aircraft Maintenance Environment (DAME). In *Proceeding of the UK e-Science All Hands Meeting*, Nottingham, UK. 3.5

JOHNSTON, W.E. (2002). Computational and data grids in large-scale science and engineering. *Future Generation Computer Systems*, **18**, 1085–1100. 3.5

JR, V.L., PEREIRA, J.A. & WEBBER, H.I. (1997). Using model updating technique to train neural network for fault detection. In *Proceedings of ASME Design Engineering Technical Conference*, Sacramento, California. 2.4.1

KABASHIMA, S., OZAKI, T. & TAKEDA, N. (2000). Damage detection of satellite structures by optical fiber with small diameter. In *Smart Structures and Materials 2000: Smart Structures and Integrated Systems, Proceedings of SPIE*, vol. 3985, 343–351. 2.5

KAM, T.Y. & LEE, T.Y. (1992). Detection of cracks in structure using modal test data. *Engineering Fracture Mechanics*, **42**, 381–387. 2.4.2

KEAHEY, K., FREDIAN, T., PENG, Q., SCHISSEL, D.P., THOMPSON, M., FOSTER, I., GREENWALD, M. & MCCUNE, D. (2002). Computational grids in action : the national fusion collaboratory. *Future Generation Computer Systems*, **18**, 1005–1015. 3.5

KESAVAN, A., DEIVASIGAMANI, M., JOHN, S. & HERSZBERG, I. (2006). Damage detection in t-joint composite structures. *Composite Structures*, **75**, 313–320. 2.4.1

KESSELMAN, C., BUTLER, R., FOSTER, I., FUTRELLE, J., MARCUSIU, D., GULIPALLI, S., PEARLMAN, L. & SEVERANCE, C. (2003). Neesgrid system architecture version 1.1. Tech. rep., The George E. Brown, Jr. Network for Earthquake Engineering Simulation (NEES). 3.5

KIM, H.S. & MELHEM, H. (2004). Damage Detection of Structures by Wavelet Analysis. *Engineering Structures*, **26**, 347–362. 2.4.1, 2.5

KIM, H.Y. (2003). Vibration-based Damage Identification Using Reconstructed FRFs in Composite Structures. *Journal of Sound and Vibration*, **259**, 1131–1146. 2.4, 2.5, 2.6

KIM, J.T., RYU, Y.S., CHO, H.M. & STUBBS, N. (2003). Damage Identification in Beam-type Structures : Frequency-based Method vs Mode-shape-based Method. *Engineering Structures*, **25**, 57–67. 5.2.4

KOTTAPALLI, V.A., KIREMIDIJIAN, A.S., LYNCH, J.P., CARRYER, E., KENNY, T.W., LAW, K.H. & LEI, Y. (2003). Two-tier Wireless Sensor Network Architecture for Structural Health Monitoring. In *SPIE 10th Annual International Symposium on Smart Structures and Materials*, San Diego, CA, USA. 2.5

KULKARNI, N., MAHFUZ, H., JEELANI, S. & KARLSSON, L.A. (2003). Fatigue crack growth and life prediction of foam core sandwich composites under flexural loading. *Composite Structures*, **59**, 499–505. (document), 2.1, 2.1, 2.5

KULKARNI, N., MAHFUZ, H., JEELANI, S. & CARLSSON, L.A. (2004). Fatigue Failure Mechanism and Crack Growth in Foam Core Sandwich Composites under Flexural Loading. *Journal of Reinforced Plastics and Composites*, **23**, 83–94. 9.3.5

KYRIAZOGLOU, C., PAGE, B.H.L. & GUILD, F.J. (2004). Vibration Damping for Crack Detection in Composite Laminates. *Composite Part A- Applied Science and Manufacturing*, **35**, 945–953. 2.4

LéOTOING, L., DRAPIER, S. & VAUTRIN, A. (2002). Nonlinear Interaction of Geometrical and Material Properties in Sandwich Beam Instabilities. *International Journal of Solids and Structures*, **39**, 3717–3739. 2.1

LASZEWSKI, G.V., FOSTER, I., GAWOR, J. & LANE, P. (2001). A Java Commodity Grid Kit. *Concurrency and Computation : Practice and Experience*, **13**, 643–662. 3.4, 9.3.4

LASZEWSKI, G.V., GAWOR, J., LANE, P., REHN, N. & RUSSELL, M. (2002). Features of the Java Commodity Grid Kit. *Concurrency and Computation : Practice and Experience*, **14**, 1045–1055. (document), 3.5, 3.4

LEE, B.L. & LIU, D.S. (1994). Cumulative damage of fiber-reinforced elastomer under fatigue loading. *Journal of Composite Materials*, **28**, 1261–1286. 2.2

LEE, B.T., SUN, C.T. & LIU, D. (1987). An Assessment of Damping Measurement in the Evaluation of Integrity of Composite Beams. *Journal of Reinforced Plastics and Composites*, **6**, 114–125. 2.4

LIFSHITZ, J.M. & ROTEM, A. (1969). Determination of Reinforcement Unbonding of Composite by a Vibration Technique. *Journal of Composite Materials*, **3**, 412–423. 2.4.1

LIU, G.R. & CHEN, S.C. (2001). Flaw Detection in Sandwich Plate based on Time-harmonic Response Using Genetic Algorithm. *Computer Methods in Applied Mechanics and Engineering*, **190**, 5505–5514. 2.5, 2.6

LIU, G.R. & CHEN, S.C. (2002). A Novel Technique for Inverse Identification of Distributed Stiffness Factor in Structures. *Journal of Sound and Vibration*, **254**, 823–835. 2.5, 2.6

LU, Q., REN, G. & ZHAO, Y. (2002). Multiple Damage Location with Flexibility Curvature and Relative Frequency Change for Beam Structures. *Journal of Sound and Vibration*, **253**, 1101–1114. 2.4.1, 2.7.1

LUO, H. & HANAGUD, S. (1997). An Integral Equation for Changes in the Structural Dynamics Characteristics of Damaged Structures. *Internation Journal of Solids and Structure*, **34**, 4557–4579. 6.3

LYNCH, J.P., SUNDARAJAN, A., LAW, K.H., KIREMIDJIAN, A.S. & CARRYER, E. (2002a). Power-Efficient Data Management for a Wireless Structural Monitoring System. In *Proceedings of the 4^{th} International Workshop on Structural Health Monitoring*, Stanford, USA. 2.5

LYNCH, J.P., SUNDARAJAN, A., LAW, K.H., KIREMIDJIAN, A.S., KENNY, T. & CARRYER, E. (2002b). Computational Core Design of a Wireless Structural Health Monitoring System. In *Proceedings of Advances in Structural Engineering and Mechanics*, Pusan, Korea. 2.5

MAHI, A.E., FAROOQ, M.K., SAHRAOUI, S. & BEZAZI, A. (2004). Modelling the Flexural Behaviour of Sandwich Composite Materials Under Cyclic Fatigue. *Material and Design*, **25**, 199–208. 5.3, 5.3, 9.3.5

MANNAN, M.A. & RICHARDSON, M.H. (1990). Detection and location of structural cracks using frf measurements. In *Proceedings of the 8^{th} International Modal Analysis Conference*, vol. 1, 652–657. 2.4.2

MARTIN, A., HUDD, J., WELLS, P., TUNNICLIFFE, D. & DAS GUPTA, D. (1999). Development and Comparison of Low Profile Piezoelectric Sensors for Impact and Acoustic Emission (AE) Detection in CFRP Structures. In *Proceedings of the 5^{th} International Conference on Damage Assessment of Structures (DAMAS1999), Dublin, Ireland*, 102–111. 2.5.1

MEIROVITCH, L. (1986). *Elements of Vibration Analysis*. McGraw-Hill Book Company, 2nd edn. 5.2.2

MINER, M.A. & CALIF, S.M. (1945). Cumulative damage in fatigue. *Journal of Applied Mechanics*, **Part A**, 159–164. 2.2

NéMETH, Z. & SUNDERAM, V. (2003). Characterizing Grids : Attributes, Definitions, and Formalisms. *Journal of Grid Computing*, **1**, 9–23. (document), 3.4

NAG, A., MAHAPATRA, D. & GOPALAKRISHNAN, S. (2002). Identification of Delamination in a Composite Beam using a Damaged Spectral Element. *Structural Health Monitoring*, **1**, 105–125. 2.4

NOURY, P.M., SHENOI, R.A. & SINCLAIR, I. (1998). On mixed-mode fracture of sharp crack-shaped notches in pvc foam. *International Journal of Fracture*, **92**, 131–151. 2.1

OH, B.H. & JUNG, B.S. (1998). Structural Damage Assessment with Combined Data of Static and Modal Data. *Journal of Structural Engineering-ASCE*, **124**, 956–965. 2.4.1, 2.4

OKAFOR, A.C., CHANDRASHEKHRA, K. & JIANG, Y.P. (1996). Delamination Prediction in Composite Beams with Built-in Piezoelectric Deviced using Modal Analysis and Neural Network. *Smart Materials and Structures*, **5**, 338–347. 2.4

OKAFOR, A.C., OTIENO, A.W., DUTTA, A. & RAO, V.S. (2001). Detection and Characterisation of High-Velocity Impact Damage in Advanced Composite Plates Using Multi-sensing Techniques. *Composite Structures*, **54**, 289–297. 2.3.3

OSTACHOWICZ, W. & KRAWCZUK, M. (2001). On Modelling of Structural Stiffness Loss due to Damage. In *Proceedings of the 4^{th} International Conference on Damage Assessment of Structures (DAMAS2001) Cardiff, England*, 191–199, U.K. 5.2.1, 6.3

PANDEY, A.K. & BISWAS, M. (1994). Damage Detection in Structure Using Change in Flexibility. *Journal of Sound and Vibration*, **169**, 3–17. 2.4.1, 2.4.3, 2.4, 2.5

PANDEY, A.K., BISWAS, M. & SAMMAN, M.M. (1991). Damage detection from change in curvature mode shapes. *Journal of Sound and Vibration*, **145**, 321–332. 2.4.1, 2.4.3, 2.4, 2.5

PARK, S., STUBBS, N., BOLTON, R., CHOI, S. & SIKORSKY, C. (2001). Field Verification of the Damage Index Method in a Concrete Box-girder Bridge via Visual Inspection. *Computer-Aided Civil and Infrastructure Engineering*, **16**, 58–70. 2.4.2, 2.4, 2.5

PETERSON, S.T., MCLEAN, D.I., SYMANS, M.D., POLLOCK, D.G., COFER, W.F., EMERSON, R.N. & FRIDELY, K.J. (2001a). Application of Dynamic System Identification to Timber Beams. I. *Journal of Structural Engineering-ASCE*, **127**, 418–425. 2.4.2, 2.4

PETERSON, S.T., MCLEAN, D.I., SYMANS, M.D., POLLOCK, D.G., COFER, W.F., EMERSON, R.N. & FRIDELY, K.J. (2001b). Application of Dynamic System Identification to Timber Beams. II. *Journal of Structural Engineering-ASCE*, **127**, 426–432. 2.4.2, 2.4

PRESS, W.H., TEUKOLSKY, S.A., VETTERING, W.T. & FLANNERY, B.P. (1992). *Numerical Recipes in C*. Cambridge University Press, 2nd edn. 2.5.2

PRICE, A.R., XUE, G., YOOL, A., LUNT, D.J., LENTON, T.M., WASON, J.L., POUND, G.E., COX, S.J. & TEAM, G. (2004). Tuning GENIE Earth System Model Components using a Grid Enabled Data Management System. In *Proceeding of the UK e-Science All Hands Meeting*, 593–600, Nottingham, UK. 3.5

RAMIREZ-JIMENEZ, C.R., PAPADAKIS, N., REYNOLDS, N., GAN, T.H., PURNELL, P. & PHARAOH, M. (2004). Identification of Failure Modes in Glass/polypropylene Composites by Means of the Primary Frequency Content of the Acoustic Emission Event. *Composites Science and Technology*, **64**, 1819–1827. 2.3.3

RATCFLIFFE, C.P. & BAGARIA, W.J. (1998). Vibration Technique for Locating Delamination in a Composite Beam. *AIAA Journal*, **36**, 1074–1077. 2.4.1, 2.4

RATCLIFFE, C.P. (1997). Damage Detection Using a Modified Laplacian Operator on Mode Shape Data. *Journal of Sound and Vibration*, **204**, 505–517. 2.4.1, 2.5

RENARD, J. & THIONNET, A. (2006). Damage in composites : From physical mechanisms to modelling. *Composites Science and Technology*, **66**, 642 - 646. 2.7.1, 6.4

RICLES, J.M. & KOSMATKA, J.B. (1992). Damage detection in elastic structures using vibratory residual forces and weighted sensitivity. *AIAA Journal*, **30**, 2310–2316. 2.4.2

RIZOS, P.F., ASPRAGATHOS, N. & DIMAROGONAS, A.D. (1990). Identification of Crack Location and Magnitude in a Cantilever Beam from the Vibration Modes. *Journal of Sound and Vibration*, **138**, 381–388. 2.4.1, 2.5

ROBERTSON, A.N., FARRAR, C.R. & SOHN, H. (2003). Singularity Detection for Structural Health Monitoring Using Holder Exponents. *Mechanical Systems and Signal Processing*, **17**, 1163–1184. 2.4.1, 2.5

ROSE, C.R., MOORE, D.F., JR, N.F.K. & RANKIN, C.R. (2002). Finite Element Modeling of the Bickling Response of Sandwich Panels. In *43rd AIAA/ASME/ASCE/AHS/ASC Structures, Structural Dynamics, and Material Conference*, AIAA 2002–1517, Denver, Colorado. 2.1

RUCKA, M. & WILDE, K. (2006). Application of continuous wavelet transform in vibration based damage detection method for beams and plates. *Journal of Sound and Vibration*, **297**, 536–550. 2.4.1

RYTTER, A. (1993). *Vibration Based Inspection of Civil Engineering Structures*. Ph.D. thesis, Department of Building Technology and Structural Engineering, Aalborg University, Denmark. 2.4

RYTTER, A. & KIRKEGAARD, P. (1997). Vibration Based Inspection Using Neural Networks. In *Proceedings of DAMAS'97*, 97–108, University of Sheffield, UK. 2.4.1, 2.5

SAHIN, M. & SHENOI, R.A. (2003a). Quantification and Localisation of Damage in Beam-like Structures by Using Artificial Neural Networks with Experimental Validation. *Engineering Structures*, **25**, 1785–1802. 2.4.1, 2.5, 2.5.1

SAHIN, M. & SHENOI, R.A. (2003b). Vibration Based Damage Identification in Beam-like Composite Laminates by Using Artificial Neural Networks. *Journal of Mechanical Engineering Science*, **217**, 661–676. 2.4.1, 2.4, 2.5, 2.5.1

SAINSBURY, M.G. & ZHANG, Q.J. (1999). The galerkin element method applied to the vibration of damped sandwich beams. *Computers and Structures*, **71**, 239–256. (document), 5.1.2, 5.3

SALKIND, M.J. (1972). Fatigue of composites. composite materials: Testing and design (2nd conference). In *ASTM STP*, vol. 472, 143–169. 1.1

SAMPAIO, R.P.C. (2000). More insight into some frequency-response function methods for damage detection. In *Proceedings of the 18th International Modal Analysis Conference*, 681–189. 2.4.2, 2.4.3

SANTOS, J.V.A.D., SOARES, C.M.M., SOARES, C.A.M. & PINNA, H.L.G. (2000). A damage identification numerical model based on the orthogonal conditions and least square techniques. *Computers and Structures*, **78**, 283–291. 2.4.1, 2.4, 2.5

SHI, Z.Y. & LAW, S.S. (1998). Structural Damage Localization from Modal Strain Energy Change. *Journal of Sound and Vibration*, **218**, 825–844. 2.4.2, 2.5, 2.7.1, 5.2.1, 5.2.3, 5.2.3

SHI, Z.Y., LAW, S.S. & ZHANG, L.M. (2000). Structural Damage Detection from Modal Strain Energy Change. *Journal of Engineering Mechanics*, **126**, 1216–1223. 2.4.2, 2.4, 2.5, 2.7.1, 5.2.3, 5.2.3, 6.6.1

SHI, Z.Y., LAW, S.S. & ZHANG, L.M. (2002). Improved Damage Quantification from Elemental Modal Strain Energy Change. *Journal of Engineering Mechanics*, **128**, 521–529. 2.4.2, 2.4, 2.5, 2.7.1, 5.2.3, 5.2.3, 6.6.1

SOHN, H., FARRAR, C.R., HEMEZ, F.M., SHUNK, D.D., STINEMATES, D.W. & NADLER, B.R. (2003). A Review of Structural Health Monitoring Literature : 1996-2001. Tech. Rep. LA-13976-MS, Las Alamos National Laboratory. 2.4.3, 2.5.1, 2.7.1

SONG, W., KEANE, A.J., ERES, M.H., POUND, G.E. & COX, S.J. (2003). Two Dimensional Airfoil Optimisation using CFD in a Grid Computing Environment. *Lecturer Notes in Computer Science*, **2790**, 525–532. 3.5

SPENCER, B.F., ELNASHAI, A., NAKATA, N., SALIEM, H., YANG, G., FUTRELLE, J., GLICK, W., MARCUSIU, D., RICKER, K., FINHOLT, T., HORN, D., HUBBARD, P., KEAHEY, K., LIMING, L., ZALUZEC, N., PEARLMAN, L. & STAUFFER, E. (2004). The most experiment : Earthquake engineering on the grid. Tech. Rep. TR-2004-41, The George E. Brown, Jr. Network for Earthquake Engineering Simulation (NEES). 3.5

STASZEWSKI, W.J. (2000). Advanced Data Pre-processing for Damage Identification based on Pattern Recognition. *International Journal of Systems Science*, **31**, 1381–1396. 2.5.2

STASZEWSKI, W.J. (2002). Intelligent Signal Processing for Damage Detection in Composite Materials. *Composites Science and Technology*, **62**, 941–950. 2.5.2, 2.6

STEEVES, C.A. & FLECK, N.A. (2004). Collapse Mechanisms of Sandwich Beams with Compiste Faces and a Foam Core Loaded in Three Point Bending Part I : Analytical Models and Minimum Weight Design. *International Journal of Mechanical Sciences*, **46**, 561–583. 2.1

STUBBS, N. & KIM, J.T. (1996). Damage Localization in Structure Without Baseline Modal Parameters. *AIAA Journal*, **34**, 1644–1649. 5.2.4

STUBBS, N. & OSEGUEDA, R. (1990a). Global damage detection in solids - experimental verification. *International Journal of Analytical and Experimental Modal Analysis*, **5**, 81–97. 2.4.1

STUBBS, N. & OSEGUEDA, R. (1990b). Global damage nondestructive evaluation in solids. *International Journal of Analytical and Experimental Modal Analysis*, **5**, 67–79. 2.4.1

SURGEON, M. & WEVERS, M. (1999). Modal Analysis of Acoustic Emission Signals from CFRP Laminates. *NDT & E International*, **32**, 311–322. 2.3.3

SWAMIDAS, A.S.J. & CHEN, Y. (1995). Monitoring crack growth through change of modal parameters. *Journal of Sound and Vibration*, **2**, 325–343. 2.4.1

TALIA, D. (2002). The Open Grid Services Architecture : where the Grid meets the web. *Internet Computing, IEEE*, **6**, 67–71. 3.5

TALREJA, R. (1994). *Damage Mechanics of Composite Materials, Composite Materials Series*, vol. 9. Elsevier, Amsterdam. 6.3

TEUGHELS, A., MAECK, J. & ROECK, G.D. (2002). Damage Assessment by FE model updating using Damage Functions. *Computers and Structures*, **80**, 1869–1879. 2.4.2, 2.4, 2.5

THOMSON, R.S., KHAN, M.Z.S. & MOURITZ, A.P. (1998). Shear properties of a sandwich composite containing defects. *Composite Structures*, **42**, 107–118. 2.1

THYAGARAJAN, S.K., SCHULZ, M.J. & PAI, P.F. (1998). Detecting Structural Damage Using Frequency Response Functions. *Journal of Sound and Vibration*, **210**, 162–180. 2.4.2, 2.4, 2.5

TIMOSHENKO, S., YOUNG, D.H. & W. WEAVER, J. (1974). *Vibration Problems in Engineering*. John Wiley and Sons, 4th edn. 5.1.1

TODOROKI, A., OMAGARI, K., SHIMAMURA, Y. & KOBAYASHI, H. (2006). Matrix crack detection of cfrp using electrical resistance change with integrated surface probes. *Composites Science and Technology*, **66**, 1539–1545. 2.4.1

TRIANTAFILLOU, T.C. & GIBSON, L.J. (1987). Failure mode maps for foam core sandwich beams. *Material Science and Engineering*, **95**, 37–53. 2.1

URBANO, R. (2003). *Oracle Streams Concepts and Administration, 10g*. Oracle Corporation. 9.3.3

VADAKKE, V. & CARLSSON, L.A. (2004). Experimental Investigation of Compression Failure Mechanisms of Compression Failure Mechanisms of Composite Faced Foam Core Sandwich Specimens. *Journal of Sandwich Structures and Materials*, **6**, 327–342. (document), 2.4, 2.1

VALDES, S.H.D. & SOUTIS, C. (1999). Delamination Detection in Composite Laminates from Variation of Their Modal Characteristics. *Journal of Sound and Vibration*, **228**, 1–9. 2.4.1

VALDES, S.H.D. & SOUTIS, C. (2000). Delamination Detection in Composite Laminates from Variation of Their Modal Characteristics. *Journal of Low Frequency Noise Vibration and Active Control*, **19**, 27–33. 2.4

VINSON, J.R. (1999). *The Behaviour of Sandwich Structures of Isotropic and Composite Materials*. Technomic Publishing Company, Lancaster. 5.1.2

WAHAB, M.M.A. & ROECK, G.D. (1999). Damage Detection in Bridge Using Modal Curvature : Application to A Real Damage Scenario. *Journal of Sound and Vibration*, **226**, 217–235. 2.4

WANG, Y.Y., LIU, K.Y. & LIU, G.R. (1996). Detection of Flaws in Sandwich Plates. *Composite Structures*, **34**, 409–418. 2.5, 2.6, 6.3

WEI, G., ZHENG, Y. & ZHANG, J. (2004a). Grid service-based parallel finite element analysis. *Lecturer Notes in Computer Science*, **3032**, 123–130. 3.5

WEI, Z., YAM, L.H. & CHENG, L. (2004b). Detection of Internal Delamination in Multi-layer Composites using Wavelet Packets Combined with Modal Parameter Analysis. *Composite Structures*, **64**, 377–387. 2.3.8, 2.4

WELCH, V., FOSTER, I., KESSELMAN, C., MULMO, O., PEARLMAN, L., TUECKE, S., GAWOR, J., MEDER, S. & SIEBENLIST, F. (2004). X.509 Proxy Certificates for Dynamic Delegation. In *3rd Annual PKI Research and Development Workshop*. 3.3.2

WEST, W.M. (1984). Illustration of the use of modal assurance criterion to detect structural changes in an orbiter test specimen. In *Proceedings of the Air Force Conference on Aircraft Structural Integrity*, 1–6. 2.4.1

WEVERS, M. (1997). Listening of the Sound of Materials : acoustic Emission for the Analysis of Materials Behaviour. *NDT & E International*, **30**, 99–106. 2.3.3

WORDEN, K. & DULIEU-BARTON, J.M. (2004). An Overview of Intelligent Fault Detection in Systems and Structures. *Structural Health Monitoring*, **3**, 85–98. 3.6

WORDEN, K. & FIELLER, N.R.J. (1999). Damage Detection Using Outlier Analysis. *Journal of Sound and Vibration*, **229**, 647–667. 2.4.2, 2.5

WORDEN, K. & MANSON, G. (2003a). Experimental validation of a structural health monitoring methodology : Part i. novelty detection on a laboratory structure. *Journal of Sound and Vibration*, **259**, 323–343. 2.4.1

WORDEN, K. & MANSON, G. (2003b). Experimental validation of a structural health monitoring methodology : Part ii. novelty detection on a gnat aircracft. *Journal of Sound and Vibration*, **259**, 345 – 363. 2.4.1

WORDEN, K. & MANSON, G. (2003c). Experimental validation of a structural health monitoring methodology : Part iii. damage location on an aircraft wing. *Journal of Sound and Vibration*, **259**, 365 – 385. 2.4.1

WORDEN, K., MANSON, G. & ALLMAN, D.J. (2001). An Experimental Appraisal of the Strain Energy Damage Location Method. In *Proceeding of the 4^{th} International Conference on Damage Assessment of Structures(DAMAS2001)*, 35–46, Cardiff, Wales, U.K. 2.4.2, 2.4, 2.5

WU, C.L. & SUN, C.T. (1996). Low Velocity Impact Damage in Composite Sandwich Beams. *Composite Science and Technology*, **34**, 21–27. 2.1

WU, H.W., MU, B. & WARNEMUENDE, K. (2003). Failure Analysis of FRP Sandwich Bus Panel by Finite Element Method. *Composite Part B: Engineering*, **34**, 51–58. 5.1.2

WU, Y.J., SHI, X.Z. & ZHUANG, T.G. (2000). Fusion of Wavelet Packets and Neural Network In Detection of Composites. *AIAA Journal*, **38**, 1063–1069. 2.4.1, 2.4

YAM, L.H., LEUNG, T.P., LI, D.B. & XUE, K.Z. (1996). Theoretical and experimental study of modal strain analysis. *Journal of Sound and Vibration*, **191**, 251–260. 2.4.1

YAM, L.H., YAN, Y.J. & JIANG, J.S. (2003a). Identification of Complex Crack Damage for Honeycomb Sandwich Plate Using Wavelet Analysis and Neural Networks. *Smart Materials and Structures*, **12**, 661–671. 2.5, 2.6

YAM, L.H., YAN, Y.J. & JIANG, J.S. (2003b). Vibration-based Damage Detection for Composite Structures Using Wavelet Transform and Neural Network Identification. *Composite Structures*, **60**, 403–412. 2.4.1, 2.6

YAN, Y.J. & YAM, L.H. (2004). Detection of Delamination Damage in Composite Plates using Energy Spectrum of Structural Dynamic Responses Decomposed by Wavelet Analysis. *Computers and Structures*, **82**, 4–5. 2.4, 6.3

YANG, J.N. & JONES, D.L. (1980). Effect of load sequence on the statistical fatigue life of composites. *AIAA Journal*, **18**, 1525–1531. 2.2

YANG, Q.W. & LIU, J.K. (2006). A coupled method for structural damage identification. *Journal of Sound and Vibration*, **296**, 401–405. 2.4.1

YOO, S.H., KWAK, H.K. & KIM, B.S. (1999). Detection and location of a crack in a plate using modal analysis. In *Proceedings of the 17th International Modal Analysis Conference*, vol. 2, 1902–1908. 2.4.1

YUEN, M.M. (1985). Numerical study of the eigenparameters of a damaged cantilever. *Journal of Sound and Vibration*, **103**, 301–310. 2.4.1, 6.3

YUN, C.B. & BAHNG, E.Y. (2000). Substructural identification using neural networks. *Computers and Structures*, **77**, 41–52. 2.4.1, 2.5

ZAK, A., KRAWCZUK, M. & OSTACHOWICZ, W. (1999). Vibration of a laminated composite plate with closing delamination. In *Proceedings of the 5th International Conference on Damage Assessment of Structures (DAMAS1999), Dublin, Ireland*, 17–26. 2.5.1

ZENKERT, D. (1995). *An Introduction to Sandwich Construction*. Engineering Materials Advisory Services Ltd, London. (document), 2.2, 2.1, 5.1.1, 5.1.2, 6.1, 6.3, A, B.1, B.2

ZHANG, Z. & AKTAN, A.E. (1995). The Damage Indices for Constructed Facilities. In *Proceedings of IMAC*, vol. 13, 1520–1529. 2.4.3

ZIMMERMAN, D.C. (1999). Looking into the crystal ball : The continued need for multiple viewpoints in damage detection. In *Proceedings of the 5^{th} International Conference on Damage Assessment of Structures (DAMAS1999), Dublin, Ireland*, 76–90. 2.5.1

ZIMMERMAN, D.C. & KAOUK, M. (1994). Structural damage detection using a minimum rank update theory. *Journal of Vibration and Acoustics*, **116**, 222–231. 2.4.2

ZIMMERMAN, D.C., KIM, H.M., BARTKOWICZ, T.J. & KAOUK, M. (2001). Damage detection using expanded dynamic residuals. *Journal of Dynamic Systems, Measurement, and Control*, **123**, 699–705. 2.4.2, 2.4, 2.5

Appendix A

Design of the proposed beam specimen

The materials available for fabrication of the beam specimens are as follows,

- E-glass stitched fibre ($0^o/90^o$)
- PVC foam core of thickness 6.00 mm

For thin behaviour of the sandwich beam, Zenkert [Zenkert, 1995] proposed the relationship between the thickness of the face and depth of the sandwich beam. This relationship is as follows,

$$\frac{d}{t_f} > 5.77 \tag{A.1}$$

Using Eqn. A.1, the thickness of each face(t_f) is calculated, which gives the value of thickness less than 1.06 mm for the available core thickness, i.e., 6 mm. Hence, there is a need to calculate the thickness of each layer in the face of beam specimen, made of stitched E-glass fibre impregnated in epoxy resin. Estimated thickness of the laminate made of one layer of stitched glass fibre impregnated in epoxy resin is given by the following relationship,

$$t_{f,e} = \frac{w_f}{\rho_f} + \frac{w_{matrix}}{\rho_{matrix}}, \tag{A.2}$$

where $t_{f,e}$ is the estimated thickness of laminate made of one layer of stitched glass fibre. In Eqn. A.2, w_f and w_{matrix} are the aerial density of glass fibre and matrix respectively. ρ_f and ρ_{matrix} are the density of glass fibre and matrix respectively.

Density of glass fibre and matrix are 2500 kg/m^3 and 1148.7 kg/m^3 respectively. Aerial density of the stitched glass fibre is obtained by its weight and area.

Weight of stitched glass fibre = 2.0464 gm.

Area of stitched glass specimen = 50 $\times 10^{-3}$ m $\times$ 50$\times 10^{-3}$ m = 2.50 $\times$ 10^{-3} m^2

Hence, the aerial density of the laminate (w_f) is calculated equal to 0.818 kg/m^2. Aerial density of matrix (w_{matrix} is calculated from the weight fraction of matrix and its density. It is assumed that weight fraction of matrix in laminate is 0.65.

Aerial density of matrix, w_{matrix} = 0.65 $\times$ w_f = 531.7 kg/m^2

Aerial densities and densities of the glass fibre and matrix can be substituted in the relationship given by Eqn. A.2 to obtain estimated thickness of each face ($t_{f,e}$), which gives the value of $t_{f,e}$ equal to 0.8142 mm. Since, t_f can not be more than 1.06 mm, hence only two layers of stitched glass fibre will be used for fabrication of the sandwich beam specimens. After fabrication, the thickness of faces are measured at many points and these values are averaged to obtain the thickness. The value of thickness is 0.6303 mm, which is used for numerical simulations.

Appendix B

Determination of the Mechanical Properties

B.1 Volume fractions and density calculations

In the present work, the mechanical properties are calculated using the *rule of mixture* formulae [Zenkert, 1995]. The volume and weight fractions are the primary factors, influencing the mechanical properties of composites. The fractions are defined as the relative proportion of the fibre and the matrix in a composite materials. Weight fractions are easier to obtain; whereas, volume fractions are convenient for theoretical calculations. Thus, it is desirable to identify the values of fractions used in the manufacturing of the sandwich beam.

For the sake of completeness, the volume fraction calculations are reproduced. The GFRP laminate sample of dimension $40mm \times 38mm \times 0.63mm$ was selected for the test and, was weighted.

Mass of the sample laminae, $m_{composite} = m_{fibre+matrix} = 1.296\ gm$

Volume of the sample laminae, $V_{composite} = 40 \times 38 \times 0.63 = 957.6\ mm^3$

Using the mass and volume of sample laminae, density of laminae can be calculated by using formulae,

Density of the laminae, $\rho_{face} = \frac{m_{composite}}{V_{composite}} = \frac{1.296 \times 10^{-3}}{957.6 \times 10^{-9}} = 1353.92$ kg/m^3

Density of the E-glass fibre, ρ_{fibre}=2500kg/m^3

Density of the matrix, $\rho_{resin-after\ cure} = 1148$ kg/m^3

Substituting the above values of densities of laminae, glass fibre and resin can be used in the *rule of mixture* formula to calculate density,

Density of the laminae, $\rho_{face} = \nu_{fibre} \times \rho_{fibre} + \nu_{matrix} \times \rho_{resin-after-cure}$

Using the above equation, volume fractions can be calculated and their values are as follows,

Fibre volume fraction , $\nu_{fibre} = 0.54$

Matrix volume fraction , $\nu_{matrix} = 0.46$

B.2 Stiffness parameter calculation

The longitudinal Young's modulus of the face is estimated by using the *rule of mixture* formulae given for bi-directional laminate by Zenkert[Zenkert, 1995]. This formulae evaluates the longitudinal Young's modulus of the laminates and given as,

$$E_1 = 0.5 \times \nu_{fibre} \times E_{fibre} + \nu_{matrix} \times E_{matrix}. \tag{B.1}$$

The volume fractions, ν_{fibre} and ν_{matrix}, calculated in Section B.1 are used in Eqn. B.1 to evaluate E_f. Young's modulus of the E-glass fibre and the matrix are taken from manufacturer's data sheets and, these are $69.00GPa$ and $3.28GPa$ respectively. Substituting these values in Eqn. B.1,

$$E_f = 0.5 \times 0.54 \times 69.00 + 0.46 \times 3.28 = 20.14\, GPa. \tag{B.2}$$

Thus, the value obtained for E_f is used for the numerical analysis.

Appendix C

Computer codes

C.1 FORTRAN code for elemental matrices generation

In this sub-section, the steps, formulae and computer code used to calculate the contribution of elemental bending (K_b) stiffness and shearing stiffness (K_S) into the elemental stifness (K) matrix and elemental mass matrix are presented. Fig. C.1 shows the steps for calculation of abovementioned matrices followed by the computer code implementing these steps. The compute code uses the formulation presented in section . Eqns. 5.19 and 5.23 are used to calculate the contribution of elemental bending and stiffness matrix into elemental stiffness matrix. Eqn. 5.27 is used for calculation of elemental mass matrix.

```
c Computer code to generate elemental matrices
double precision kb(8,8),ks(8,8),k(8,8),k1(8,8),m(8,8),ef,ifa,bf,tf,af
double precision ac,tc,el,fc,h,ml,mf,l,df,dc
dimension ni(5)
open(unit=14,file='mech_prop.dat',status='OLD')
read(14,*) ef,gc,df,dc
close(unit=14)
c      "ef" is the Young Modulus of face sheet
c      "gc" is the Shear Modulus of core
c   File "geo_prop.dat" file contains all Geometrical Properties
open(unit=15,file='geo_prop.dat',status='OLD')
read(15,*) l,bf,tf,tc,nelm
close(unit=15)

c   "df" and "dc" are the DENSITY of face and core respectively
```

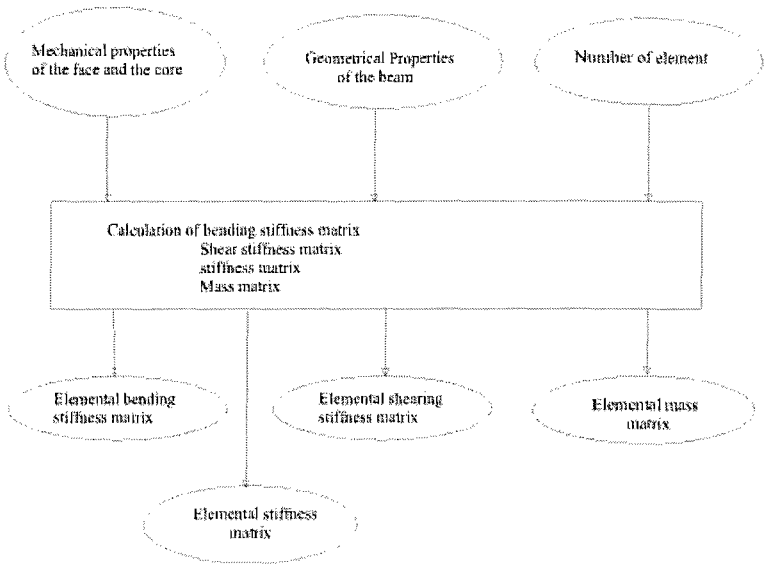

Figure C.1: Flow chart for generation of elemental matrices.

```
c   "nelm" is the Number of Element in the FE Model
c "el" is the length of element
el=l/nelm
c  "af" is the area of face
af=bf*tf
c "a" is the distance between the neutral axis of beam and neutral axis
c of face
a=(tc+tf)/2
c "ifa" is the moment of area of the face
ifa=bf*(tf**3)/12
c "h" is the distance centre to centre distance between faces
h=tc+tf
ac=bf*tc

mf=df*af
c "ml" is the mass per unit area of beam
ml=2*mf+dc*ac
```

```
fc=gc*ac*el/(tc**2)
do i=1,8
do j=1,8
k(i,j)=0
kb(i,j)=0
ks(i,j)=0
k1(i,j)=0
m(i,j)=0
enddo
enddo

c Elemental bending stiffness matrix calculated by
c Using equation
kb(1,1)=2*12*ef*ifa/(el**3)
kb(2,1)=2*6*ef*ifa/(el**2)
kb(2,2)=2*4*ef*ifa/el
kb(3,3)=ef*af/el
kb(4,4)=kb(3,3)
kb(5,1)=-kb(1,1)
kb(5,2)=-kb(2,1)
kb(5,5)=kb(1,1)
kb(6,1)=kb(2,1)
kb(6,2)=2*2*ef*ifa/el
kb(6,5)=-kb(2,1)
kb(6,6)=kb(2,2)
kb(7,3)=(-ef*af/el)
kb(7,7)=kb(3,3)
kb(8,4)=-kb(3,3)
kb(8,8)=kb(3,3)

c Elemental shearing stiffness matrix calculated by
c Using equation

ks(1,1)=fc*1.2*h*h/(el**2)
ks(2,1)=fc*0.1*h*h/el
```

```
ks(2,2)=fc*2*h*h/15
ks(3,1)=-fc*0.5*h/el
ks(3,2)=fc*h/12
ks(3,3)=fc*0.3333333333
ks(4,1)=-ks(3,1)
ks(4,2)=-ks(3,2)
ks(4,3)=-fc*0.333333333
ks(4,4)=fc*0.3333333333
ks(5,1)=-ks(1,1)
ks(5,2)=-ks(2,1)
ks(5,3)=ks(4,1)
ks(5,4)=ks(3,1)
ks(5,5)=ks(1,1)
ks(6,1)=fc*0.1*h*h/el
ks(6,2)=-fc*(h*h/30)
ks(6,3)=-ks(3,2)
ks(6,4)=ks(3,2)
ks(6,5)=-ks(2,1)
ks(6,6)=ks(2,2)
ks(7,1)=ks(3,1)
ks(7,2)=-ks(3,2)
ks(7,3)=fc*0.1666666667
ks(7,4)=-fc*0.166666666
ks(7,5)=-ks(3,1)
ks(7,6)=ks(3,2)
ks(7,7)=fc*0.333333333
ks(8,1)=-ks(3,1)
ks(8,2)=ks(3,2)
ks(8,3)=-fc*0.166666666
ks(8,4)=fc*0.1666666666
ks(8,5)=ks(3,1)
ks(8,6)=-ks(3,2)
ks(8,7)=-fc*0.3333333333
ks(8,8)=fc*0.33333333333
```

```
do j=1,8
do i=1,j
ks(i,j)=ks(j,i)
enddo
enddo

c Elemental mass stiffness matrix calculated by
c Using equation

m(1,1)=(13*ml*el)/35
m(2,1)=11*ml*el*el/210
m(2,2)=(ml*el**3)/105
m(3,3)=mf*el/3
m(4,4)=m(3,3)
m(5,1)=9*ml*el/70
m(5,2)=13*ml*el*el/420
m(5,5)=m(1,1)
m(6,1)=-(13*ml*el*el)/420
m(6,2)=-(ml*el**3)/140
m(6,5)=-m(2,1)
m(6,6)=m(2,2)
m(7,3)=mf*el/6
m(7,7)=m(3,3)
m(8,4)=m(7,3)
m(8,8)=m(4,4)

do j=1,8
do i=1,j
kb(i,j)=kb(j,i)
ks(i,j)=ks(j,i)
m(i,j)=m(j,i)
enddo
enddo

do i=1,8
```

```
do j=1,8
c  Add elemental bending stiffness (kb) and shearing stiffness(ks)
c matrix to obtain elemental stiffness matrix using equation
k(i,j)=kb(i,j)+ks(i,j)
enddo
enddo

c  "el_stiff.dat" stores elemental stiffness matrix
open(unit=9,file='el_stiff.dat',status='OLD')
c  "el_k_stiff.dat" stores elemental bending stiffness matrix
open(unit=1,file='el_k_stiff.dat',status='OLD')
c  "el_s_stiff.dat" stores elemental shearing stiffness matrix
open(unit=2,file='el_s_stiff.dat',status='OLD')
c  "el_mass.dat" stores elemental mass matrix
open(unit=19,file='el_mass.dat',status='OLD')
do i=1,8
do j=1,8
write(1,*) kb(i,j)
write(2,*) ks(i,j)
write(9,*) k(i,j)
write(19,*) m(i,j)
enddo
enddo
close(unit=9)
close(unit=1)
close(unit=2)
close(unit=19)
stop
end
```

C.2 FORTRAN code for stiffness matrix assembly of undamaged beam

The elemental matrices, generated by computer code in Sub-section C.1, are used to assemble the global stiffness and mass matrix of the undamaged sandwich beam

models. This is performed in various steps as shown in Fig. C.2. The computer codes, given in this section, implement these steps for generation of the global stiffness matrices.

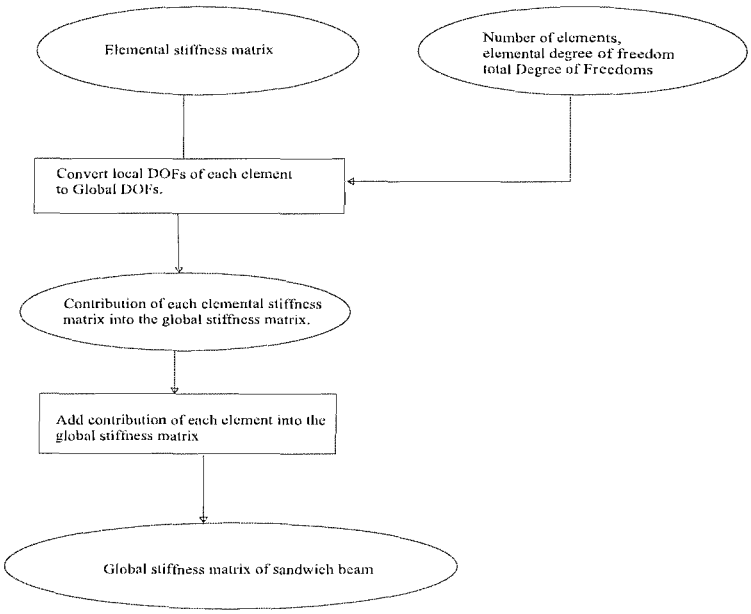

Figure C.2: Steps for assembly of global stiffness matrix of the undamaged sandwich beam.

```
c Fortran code to assemble stiffness matrix for
undamaged sandwich beam
double precision sst(500,8,8),ssk(4000,4000),sk_k(8,8),sk_s(8,8),sk(8,8)
double precision sst_k(500,8,8),sst_s(500,8,8)
double precision ss(500,8,8)
dimension ni(5)
open(unit=11,file='info.dat',status='OLD')
do i=1,5
read(11,*) ni(i)
enddo
close(unit=11)
```

```
ngdof=ni(3)
ieldof=ni(4)
ndof=ni(5)
nelm=ni(1)

do k=1,nelm
do i=1,ieldof
do j=1,ieldof
sst(k,i,j)=0.0
sst_k(k,i,j)=0
sst_s(k,i,j)=0
enddo
enddo
enddo

c Reading Elemental Bending and Shear Stiffness matrix

open(unit=6,file='el_stiff.dat',status='OLD')
open(unit=1,file='el_k_stiff.dat',status='OLD')
open(unit=2,file='el_s_stiff.dat',status='OLD')
do i=1,ieldof
do j=1,ieldof
read(6,*) sk(i,j)
read(1,*) sk_k(i,j)
read(2,*) sk_s(i,j)
enddo
enddo
close(unit=6)
close(unit=1)
close(unit=2)

c Convert Local DOFs of each element to
c  global DOFs
do i=1,nelm
do j=1,ieldof
```

```
do k=1,ieldof
sst(i,j,k)=sk(j,k)
sst_k(i,j,k)=sk_k(j,k)
sst_s(i,j,k)=sk_s(j,k)
ss(i,j,k)=sst_k(i,j,k)+sst_s(i,j,k)
enddo
enddo
enddo

do i=1,ndof
do j=1,ndof
ssk(i,j)=0
enddo
enddo

c Add contribution of each element to form
global stiffness matrix
do k=1,nelm
do i=1,ieldof
do j=1,ieldof
ig=ndof*(k-1)+i
jg=ndof*(k-1)+j
ssk(ig,jg)=ssk(ig,jg)+ss(k,i,j)
enddo
enddo
enddo
open(unit=19,file='global_stiffness.dat',status='OLD')
do i=1,ngdof
do j=1,ngdof
write(19,*) ssk(i,j)
enddo
enddo
close(unit=19)
write(*,*) 'Assembly of Stiffness Matrix over'
stop
```

```
end
```

C.3 FORTRAN code for stiffness matrix assembly of damaged beam

The elemental matrices, generated by the computer code in Sub-section C.1 and damage location and extents, are used to generate the stiffness and mass matrix of the damaged sandwich beam model. This is performed in various steps as shown in Fig. C.3 and implemented in the computer code given in this section.

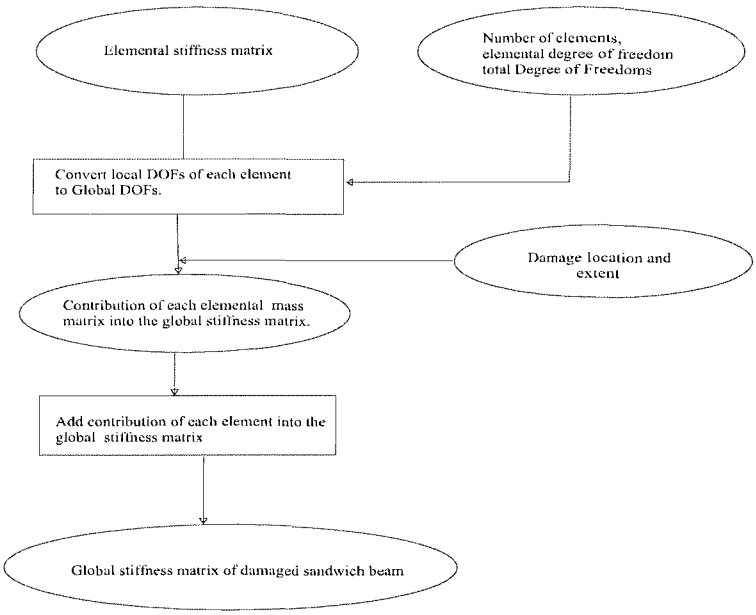

Figure C.3: Steps for assembly of global stiffness matrix of the damaged sandwich beam.

```
double precision sst(500,8,8),ssk(4000,4000),sk_k(8,8),sk_s(8,8),sk(8,8)
double precision fc_k(500),fc_s(500),sst_k(500,8,8),sst_s(500,8,8)
double precision ss(500,8,8)
dimension ni(5)

open(unit=11,file='info.dat',status='OLD')
```

```
do i=1,5
read(11,*) ni(i)
enddo
close(unit=11)
c "ngdof" is total DOFs, "ieldof" is DOFs each element
ngdof=ni(3)
ieldof=ni(4)
ndof=ni(5)
c "nelm" is number of elements
nelm=ni(1)

open(unit=21,file='op_dam_kb_extent.dat',status='OLD')
open(unit=22,file='op_dam_ks_extent.dat',status='OLD')
do i=1,nelm
c "fc_k(i)" is the % damage in the face of ith element
read(21,*) fc_k(i)
c "fc_s(i)" is the % damage in the core of ith element
read(22,*) fc_s(i)
enddo
close(unit=21)
close(unit=22)
do k=1,nelm
do i=1,ieldof
do j=1,ieldof
sst(k,i,j)=0.0
sst_k(k,i,j)=0
sst_s(k,i,j)=0
enddo
enddo
enddo

c Reading Elemental Bending and Shear Stiffness matrix

open(unit=6,file='el_stiff.dat',status='OLD')
open(unit=1,file='el_k_stiff.dat',status='OLD')
```

```
open(unit=2,file='el_s_stiff.dat',status='OLD')
do i=1,ieldof
do j=1,ieldof
read(6,*) sk(i,j)
read(1,*) sk_k(i,j)
read(2,*) sk_s(i,j)
enddo
enddo
close(unit=6)
close(unit=1)
close(unit=2)

do i=1,nelm
do j=1,ieldof
do k=1,ieldof
sst(i,j,k)=sk(j,k)
c Including damage in the face of the ith element into
c Global stiffness matrix
sst_k(i,j,k)=fc_k(i)*sk_k(j,k)
c Including damage in the core of the ith element into
c Global stiffness matrix
sst_s(i,j,k)=fc_s(i)*sk_s(j,k)
ss(i,j,k)=sst_k(i,j,k)+sst_s(i,j,k)
enddo
enddo
enddo

do i=1,ndof
do j=1,ndof
ssk(i,j)=0
enddo
enddo

c Assembelly of matrix starting now
do k=1,nelm
```

```
do i=1,ieldof
do j=1,ieldof
ig=ndof*(k-1)+i
jg=ndof*(k-1)+j
ssk(ig,jg)=ssk(ig,jg)+ss(k,i,j)
enddo
enddo
enddo
open(unit=19,file='d_global_stiffness.dat',status='OLD')
do i=1,ngdof
do j=1,ngdof
write(19,*) ssk(i,j)
enddo
enddo
close(unit=19)
stop
end
```

C.4 FORTRAN code for mass matrix assembly

The elemental mass matrix generated by computer code in Sub-section C.1 are used to generate the global mass matrix the sandwich beam. This is performed in various steps as shown by Fig. C.4 followed by the computer code used.

```
double precision sst(500,8,8),ssk(4000,4000),sk(8,8)
dimension ni(5)
double precision stemp
open(unit=6,file='el_mass.dat',status='OLD')
open(unit=11,file='info.dat',status='OLD')
open(unit=19,file='global_mass.dat',status='OLD')
do i=1,5
read(11,*) ni(i)
enddo
close(unit=11)
ngdof=ni(3)
ieldof=ni(4)
```

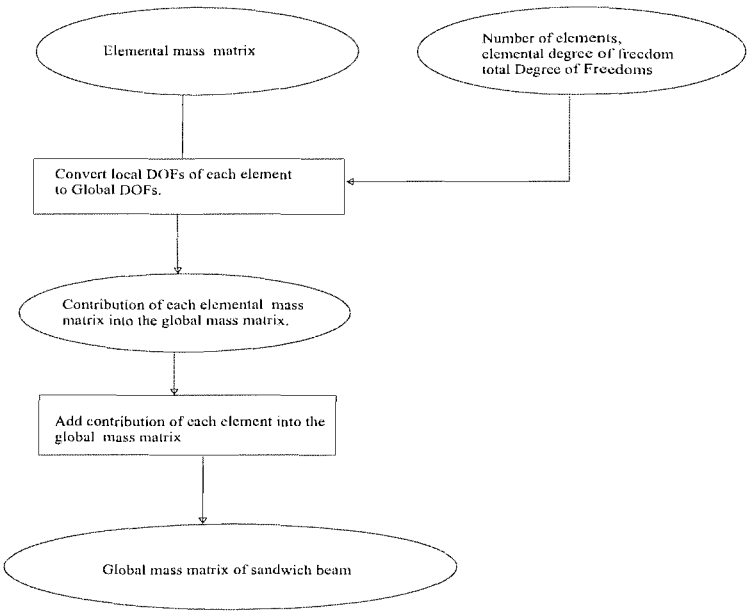

Figure C.4: Steps for assembly of global mass matrix of the undamaged sandwich beam.

```
ndof=ni(5)
nelm=ni(1)

do k=1,nelm
do i=1,ieldof
do j=1,ieldof
sst(k,i,j)=0.0
enddo
enddo
enddo
c Reading elemental mass matrix

do i=1,ieldof
do j=1,ieldof
read(6,*) sk(i,j)
enddo
enddo

do i=1,nelm
do j=1,ieldof
do k=1,ieldof
sst(i,j,k)=sk(j,k)
enddo
enddo
enddo

do i=1,ndof
do j=1,ndof
ssk(i,j)=0
enddo
enddo
c Assembelly of matrix starting now
do k=1,nelm
do i=1,ieldof
do j=1,ieldof
```

```
ig=ndof*(k-1)+i
jg=ndof*(k-1)+j
ssk(ig,jg)=ssk(ig,jg)+sst(k,i,j)
enddo
enddo
enddo

do i=1,ngdof
do j=1,ngdof
write(19,*) ssk(i,j)
enddo
enddo
close(unit=19)
close(unit=6)
close(unit=11)

stop
end
```

C.5 MATLAB code for free vibration analysis

This section presents the steps for the calculation of the natural frequencies and the mode shapes of the sandwich beam, using the global stiffness and global mass matrix. These matrices are calculated in Sections C.2 and C.3 for the undamaged and damaged sandwich beam respectively.

```
ffi=fopen('info.dat','r');
ffr=fopen('frequency.dat','w');
fundam=fopen('disp.dat','w');
[ni]=fscanf(ffi,'%f',[5]);
ng=ni(3); % Number of global DOFs
nmode=5; % Number of modes to extract
fstf=fopen('global_stiffness.dat','r');
%"stf" is the global stiffness matrix
[stf]=fscanf(fstf,'%f',[ng,ng]);
fms=fopen('global_mass.dat','r');
```

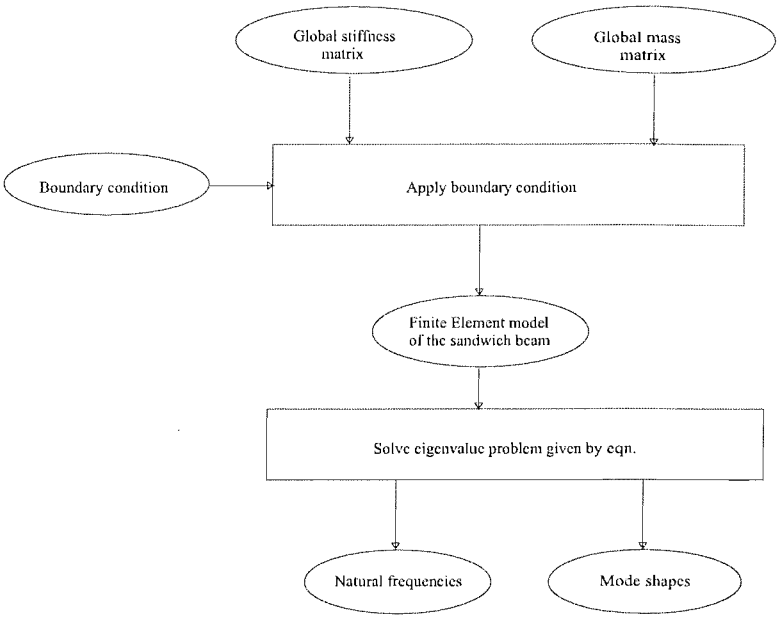

Figure C.5: Steps for free vibration analysis of a sandwich beam.

```
%"ms" is the global stiffness matrix
[ms]=fscanf(fms,'%f',[ng,ng]);
% Apply Boundary condition
st1=stf(5:ng,5:ng); % Stiffness matrix after boundary condition
ms1=ms(5:ng,5:ng); % Mass matrix after applying boundary condition
[v,d]=eig(st1,ms1); % Solve eigen values problem
[s,k]=sort(diag(d));
phi=v(:,k); % Extract mode shapes in ascending order of mode
s=sort(eig(st1,ms1));
eg=sqrt(s); % natural frequencies in rad/sec
nf=eg/(2*pi); % natural frequencies in Hz
for i=1:nmode
fprintf(ffr,'%6.8f\n',eg(i));
end
for i=1:nmode
for j=1:(ng-4)
modeshape(j+4,i)=phi(j,i);
```

```
end
end
for i=1:nmode
for j=1:ng
fprintf(fundam,'%3.9f\n',modeshape(j,i));
end
end

fclose(ffi);
fclose(ffr);
fclose(fundam);
```

Appendix D

Software for design of data acquisition system

D.1 Parameters for data acquisition

```
private void Start_Click(object sender, System.EventArgs e)
{
try
{

waveformGraph1.ClearData();
NoChannels=System.Convert.ToInt16(deviceTB.Value);
axCWAI1.Device =1;// System.Convert.ToInt16(deviceTB.Value);
axCWAI1.Channels.RemoveAll();
// int i;
string channel;
for(i=0;i<NoChannels;++i)
{
// string channel;
channel=i.ToString();
axCWAI1.Channels.Add(channel, 10, -10, 0, 0);

// axCWAI1.Channels.Add(ch_1, 10, -10, 0, 0);
}
/*
/ Specify the number of scans to acquire, or, in the case of a continuous
```

```
/ acquisition, the number of scans to return with each AcquiredData event.
*/
axCWAI1.NScans =System.Convert.ToInt32(numberScansTB.Value);
NoScans=System.Convert.ToInt32(numberScansTB.Value);
// Specify the scan rate (i.e. # of scans to acquire per second)
axCWAI1.ScanClock.Frequency = System.Convert.ToInt64(frequencyTB.Value);
SampleFr=System.Convert.ToInt64(frequencyTB.Value);
// Configure the antialias filter
//*************************************************
int device1 = 1;//System.Convert.ToInt16(deviceTB.Value); NI-DAQPad 6020E
CWAIParameterNames paramName = CWAIParameterNames.cwaiFilterSetting;
string channelString = "1";//ChannelStr.Text;
CWDAQParameterOperations operation = CWDAQParameterOperations.cwdaqParameterSet;
float floatIn = 5000;//System.Convert.ToSingle(filtersettingTB.Value);   //100 kHz
CWAIParameterValues valueIn = CWAIParameterValues.cwaiVolts;
string stringIn = "";
bool boolIn = false;

object deviceOut = null;
object valueOut =  null;
object floatOut = null;
object stringOut = null;
object boolOut = null;

axCWDAQTools1.AIParameter(device1, paramName,
channelString, operation,
floatIn, valueIn, stringIn,
boolIn, ref deviceOut,
ref valueOut,ref floatOut,
ref stringOut,ref boolOut);
//*************************************************


iStatus = axCWAI1.Configure();  // Configure the DAQ device and begin the acquisiti
iStatus = axCWAI1.Start();
```

```
inAcquisition = true;
}
catch(Exception Ex)
{
MessageBox.Show(Ex.Message.ToString());
}

}
```

D.2 Code for data acquisition

```
private void axCWAI1_AcquiredData(object sender,
       AxCWDAQControlsLib._DCWAIEvents_AcquiredDataEvent e)
{
string table="list1";

try
{
int nTotByte,nEachByte,n,nf;
float [,] dataF = (Single[,])e.scaledData; // Size of dataF is NoChannles X
n=dataF.GetLength(1); //  no of scans
nf=dataF.GetLength(0);
DateTime dateTime = DateTime.Now;
TimeSpan duration = dateTime - refDate;
timeDiff=duration.TotalMilliseconds;
double[] x=new double[n];
double[] data= new double[n];
float[] dataD01 = new float[n];
float[] dataD02 = new float[n];
double[] dataG0= new double[n];

nTotByte=Buffer.ByteLength(dataF);
nEachByte=(nTotByte/NoChannels)-1;

Buffer.BlockCopy(dataF,0,dataD01,0,nEachByte); // 1st channel
```

```
Buffer.BlockCopy(dataF,4*n,dataD02,0,nEachByte); // 2nd channel


Array.Copy(dataD01, dataG0,n-1); // 1st channel
//Array.Copy(dataD1, dataG1,n-1); // 2nd channel
waveformGraph1.PlotY(dataG0);

InsertToDataBase(table,dataD01,dataD02);
}
catch(System.Runtime.InteropServices.COMException ex)
{
MessageBox.Show(ex.Message.ToString());
axCWAI1.Reset();
}
}
```

D.3 Function to upload data

```
private void InsertToDataBase(String table,float[] value1,float[] value2)
{
/* Method for inserting data into Oracle Database
 * This method can be used to store data from a channel to oracle data base.
 * 1. "table"  is the name of Table where data for a particular channel
 *     are stored.
 * va is an array containing data for certain period  */
int i,n=value1.Length-1;
double[] id= new double[n];

for(i=0;i<n;++i)
{
id[i]=timeDiff+i*1000/SampleFr;
}

//float v1,v2;
int t=1;
```

```
String ConnectStr="User Id=manojk;Password=naval;Data Source=lab;";

OracleConnection conn=new OracleConnection(ConnectStr);
conn.Open();
OracleCommand cmd1= new OracleCommand("",conn);
cmd1.CommandText="Test_Arraybind";
cmd1.CommandType=CommandType.StoredProcedure;
cmd1.ArrayBindCount=n;

OracleParameter timePar = new OracleParameter();
timePar.ParameterName="timeName";
timePar.DbType=DbType.Double;
timePar.Value=id;
timePar.Direction=ParameterDirection.Input;

OracleParameter valuePar1 = new OracleParameter();
valuePar1.DbType=DbType.Double;
valuePar1.Value=value1;
valuePar1.Direction=ParameterDirection.Input;

OracleParameter valuePar2 = new OracleParameter();
valuePar2.ParameterName="valueName2";
valuePar2.DbType=DbType.Double;
valuePar2.Value=value2;
valuePar2.Direction=ParameterDirection.Input;

cmd1.Parameters.Add(valuePar1);
cmd1.Parameters.Add(valuePar2);
cmd1.Parameters.Add(timePar);
try
{
cmd1.ExecuteNonQuery();
}
catch(Exception e)
{
```

```
MessageBox.Show(e.Message.ToString());
}

conn.Close();

}
```

Appendix E

Steps and computer code for damage identification

In this chapter, sequence of the steps required for damage identification of the composite sandwich beam using the method developed in Chapter 5 are pictorially shown in Fig. 5.4. The correlation of the equations developed in Section 5.2 with the steps in Fig. E.1 and the computer code used for damage identification are highlighted throughout the flowchart and computer code written in MATLAB.

```
f_k_st=fopen('el_k_stiff.dat','r');
f_s_st=fopen('el_s_stiff.dat','r');
fddis=fopen('disp.dat','r');
funda=fopen('intactdisp.dat','r');
fid=fopen('info.dat','r');
ffr=fopen('frequency.dat','r');
fvr=fopen('virgin_fr.dat','r');
%
nmode=5; % Number of modes used

[eig]=fscanf(ffr,'%f',[nmode]); % Natural frequencies of undamaged beam
[veig]=fscanf(fvr,'%f',[nmode]);% Natural frequencies of damaged beam
[ni]=fscanf(fid,'%i',[6]);

ng=ni(3); % Number of global DOFs in FE model
nelm=ni(1); % Number of elements
ieldof=ni(4); % Number of DOFs per element
```

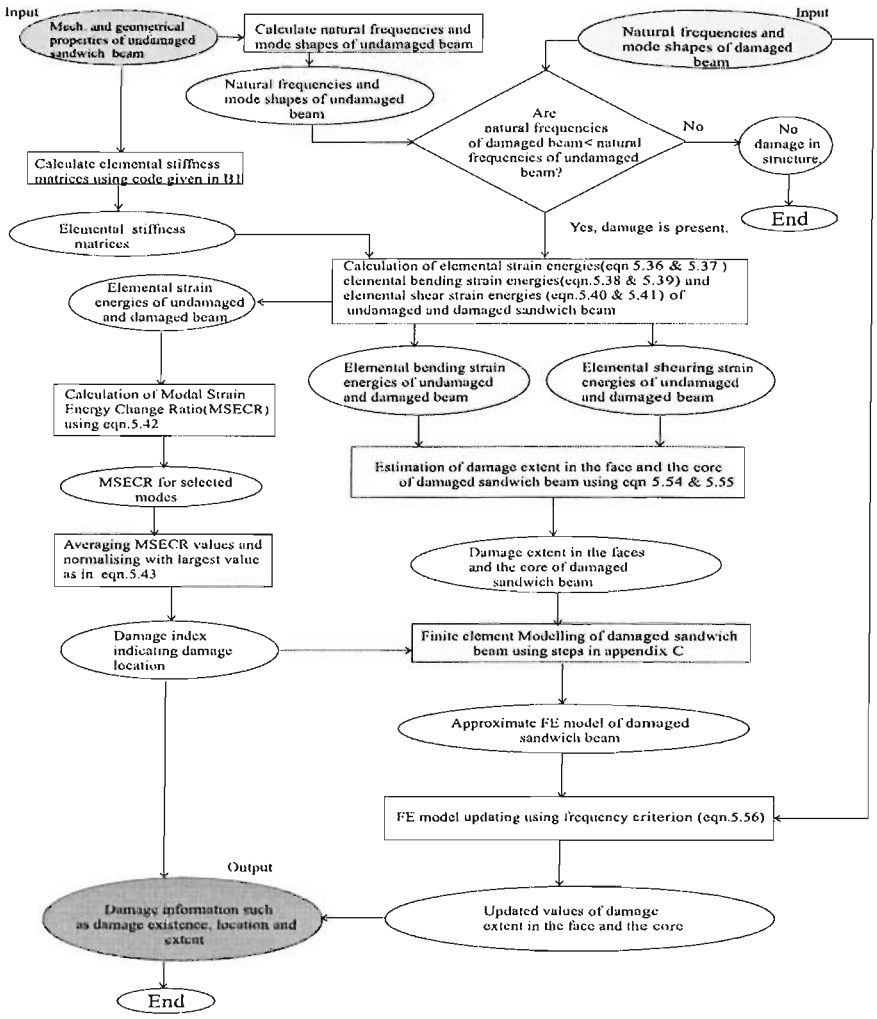

Figure E.1: Flow chart for proposed damage identification method.

```
[s_st]=fscanf(f_s_st,'%f',[n,n]); % Elemental shearing stiffness
  % matrix of undamaged sandwich beam
[k_st]=fscanf(f_k_st,'%f',[n,n]); % Elemental bending stiffness
  % matrix of undamaged sandwich beam
[dis]=fscanf(fddis,'%f',[ng,nmode]); % Mode shapes of damaged beam
[unddis]=fscanf(funda,'%f',[ng,nmode]); % Mode shapes of
% undamaged sandwich beam
stf=k_st+s_st; % Elemental stiffness matrix of undamaged sandwich beam

for nm=1:nmode
for i=1:nelm
nmin=4*(i-1);

for j=1:ieldof
damelmode(i,j)=dis(nmin+j,nm); % Contribution of ith element in the
       % jth mode shapes of damaged sandwich beam
undamelmode(i,j)=unddis(nmin+j,nm);% Contribution of i th element in the
   % j th mode shapes of undamaged sandwich beam
end
% Modal strain energy of i th undamaged beam element calculated using eqn.
mse(nm,i)=(undamelmode(i,:)*stf*undamelmode(i,:)');
% Modal shearing strain energy of i th
% undamaged beam element calculated using eqn.
mse_ks(nm,i)=(undamelmode(i,:)*s_st*undamelmode(i,:)');
% Modal bending strain energy of i th
% undamaged beam element calculated using eqn.
mse_kb(nm,i)=(undamelmode(i,:)*k_st*undamelmode(i,:)');
% Modal strain energy of i th damaged beam element calculated using eqn.
msed(nm,i)=(damelmode(i,:)*stf*damelmode(i,:)');
% Modal shearing strain energy of i th
% damaged beam element calculated using eqn.
msed_ks(nm,i)=(damelmode(i,:)*s_st*damelmode(i,:)');
% Modal bending strain energy of i th
% damaged beam element calculated using eqn.
```

```
msed_kb(nm,i)=(damelmode(i,:)*k_st*damelmode(i,:)');
% Calculation of Modal Strain Energy Change using eqn
msec(nm,i)=(msed(nm,i)-mse(nm,i));
% Calculation of Modal Strain Energy Change ratio using eqn
msecr(nm,i)=msec(nm,i)/(mse(nm,i));
end
end

for i=1:nmode
maxm=max(abs(msecr(i,:))); % Maximum value of MSECR in i th mode
for j=1:nelm
smsecr(i,j)=abs(msecr(i,j)/maxm); % Normalisation w.r.t. to "maxm"
  % in i th mode
end
end
for i=1:nelm
sm(i)=sum(smsecr(:,i));
end
smax=max(sm);
sms=sm/smax; % Normalised damage index for damage localisation

for i=1:nmode
for j=1:nelm

msed_f(i,j)=msed(i,j)/eig(i);
msed_kb_f(i,j)=msed_kb(i,j)/eig(i);
msed_ks_f(i,j)=msed_ks(i,j)/eig(i);
mse_f(i,j)=mse(i,j)/veig(i);
mse_kb_f(i,j)=mse_kb(i,j)/eig(i);
mse_ks_f(i,j)=mse_ks(i,j)/eig(i);
end
end
for i=1:nmode
eg(i)=eig(i);
end
```

```
dn=sum(eg(:));
vn=sum(veig(:));
for i=1:nelm

smsed(i)=sum(msed_f(:,i));
smsed_kb(i)=sum(msed_kb_f(:,i));
smsed_ks(i)=sum(msed_ks_f(:,i));
smse(i)=sum(mse_f(:,i));
smse_kb(i)=sum(mse_kb_f(:,i));
smse_ks(i)=sum(mse_ks_f(:,i));

r_msed(i)=smsed(i)/dn;
r_msed_kb(i)=smsed_kb(i)/dn;
r_msed_ks(i)=smsed_ks(i)/dn;
r_mse(i)=smse(i)/vn;
r_mse_ks(i)=smse_ks(i)/vn;
r_mse_kb(i)=smse_kb(i)/vn;
end
ex_kb=r_mse_kb./r_msed_kb;
ex_ks=r_mse_ks./r_msed_ks;

for i=1:nelm
if(ex_kb(i)>1)
ex_kb(i)=1;
end
if(ex_ks(i)>1)
ex_ks(i)=1;
end
end

d_ex_kb=1-ex_kb;     % Estimation of damage extent in
   % face using eqn.
d_ex_ks=1-ex_ks;     % Estimation of damage extent in
   % the core using eqn.
f1st_st_kb=fopen('sev_1_step_kb.dat','w');
```

```
f1st_st_ks=fopen('sev_1_step_ks.dat','w');
for i=1:nelm
fprintf(f1st_st_kb,'%f \n',d_ex_kb);
fprintf(f1st_st_ks,'%f \n',d_ex_ks);
end

in_guess(1,:)=(ex_kb); % Set initial guesses for face damage
in_guess(2,:)=(ex_ks); % set initia guesses for core damage

disp(' Please wait : Optimising damage extent values');

opton=optimset('MaxFunEvals',20000,'MaxIter',20000);
%  Model updating using equation and steps given in appendix
[opt_ext,fval]=fminsearch('frequency_error_criteria',in_guess,opton,nmode);
fr_op_kb=opt_ext(1,:); % Fractional residual stiffness of face
fr_op_ks=opt_ext(2,:); % Fractional residual stiffness of core

for i=1:nelm
% if fractional residual stiffness is more than 1,
% keep it equal to 1
if(fr_op_kb(i)>1.00)
fr_op_kb(i)=1;
end

if(fr_op_ks(i)>1.00)
fr_op_ks(i)=1;
end
end

d_face=1-fr_op_kb;
d_core=1-fr_op_ks;

fclose(funda);
fclose(fddis);
fclose(fstiff);
```

```
fclose(ffr);
fclose(fid);
```

Appendix F

Fast Fourier Transformation

Fast Fourier Transform (FFT) is an analysis for transforming data from the time domain to the frequency domain. FFT is the discrete fourier transform of a block of time signal. It represents the frequency spectrum of the time signal, which have complex signal meaning that has both magnitude and phase information. One model of a linear system is a frequency for which relationship between the output spectrum ($X(\omega)$), input spectrum ($F(\omega)$) and Transfer function ($H(\omega)$) is shown in Fig. F.1.

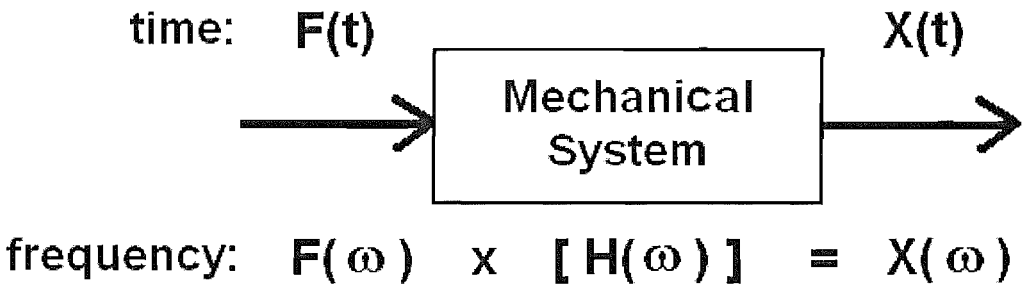

Figure F.1: Block diagram of an FRF.

The physical interpretation of the FRF is that a sinusoidal input force, at a frequency ω, will produce a sinusoidal output responses at the same frequency. The output amplitude by will be multiplied H(ω), and the phase, between output and input. The FRF describes the dynamic properties of a system independent of the signal type for the measurement. Hence, FRF is equally applicable to all types of excitations. Steps required to calculate FRF are shown by Fig. F.2. **XPS** and **APS** in Fig. F.2 are

acronymes for *Cross Power Spectrum* between input & output signal and *Auto Power Spectrum* of the input signal respectively.

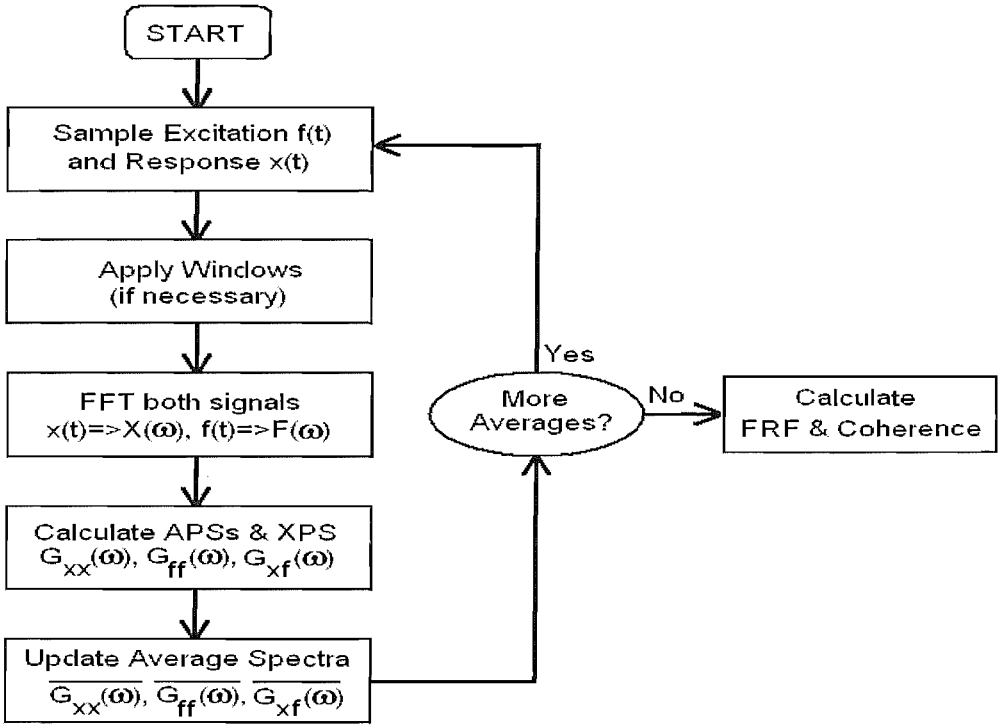

Figure F.2: Steps for calculation of FRF.

Response spectrum matrices $G_{XX}(\omega)$, $G_{ff}(\omega)$ and $G_{Xf}(\omega)$ as required at different steps in Fig. F.2 are given by following equations,

$$G_{XX}(\omega) = \left\{X(\omega).X(\omega)^T\right\} \tag{F.1}$$

$$G_{ff}(\omega) = \left\{F(\omega).F(\omega)^T\right\} \tag{F.2}$$

$$G_{Xf}(\omega) = \left\{X(\omega).F(\omega)^T\right\} \tag{F.3}$$

Transfer function $H(\omega)$ shown in Fig. F.1 uses the responses spectrum given by Eqn. F.1 - F.3 as per steps shown in Fig. F.2.

Appendix G

Acceleration conversion

The proposed damage identification algorithm requires displacement mode shapes of the intact and the damaged sandwich beam. In Section 7.4, it is planned to measure the acceleration values, which need to be converted in the displacements.

G.1 Acceleration-displacement relationship

The relationship between acceleration and displacement functions are linked through a velocity function. This is based on the principle that the integral of the acceleration function is equal to the velocity function over the same period of time. Mathematically, it can be expressed as,

$$\int a(t)dt = v(t). \tag{G.1}$$

Eqn. G.1 can also be written as,

$$\frac{dv}{dt} = a(t) \tag{G.2}$$

The integral of a function is also interpreted as the area under the integrating function as shown in Fig. G.1. It is to be noted that the area up to time T_i does not equal the velocity V_i but the difference of V_i and V_0.

The same procedure can be used to determine the displacement function where velocity function is integrated to obtain displacements over the same period of time and shown mathematically by eqn. G.3.

$$\int v(t)dt = u(t) \tag{G.3}$$

$$\frac{du}{dt} = v(t) \tag{G.4}$$

Graphically, its similar to that of acceleration and velocity and shown in Fig. G.1.

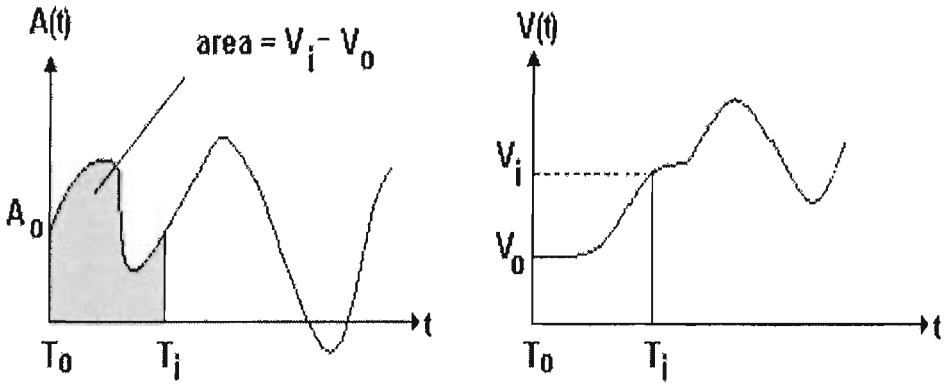

Figure G.1: Relationship between acceleration and velocity.

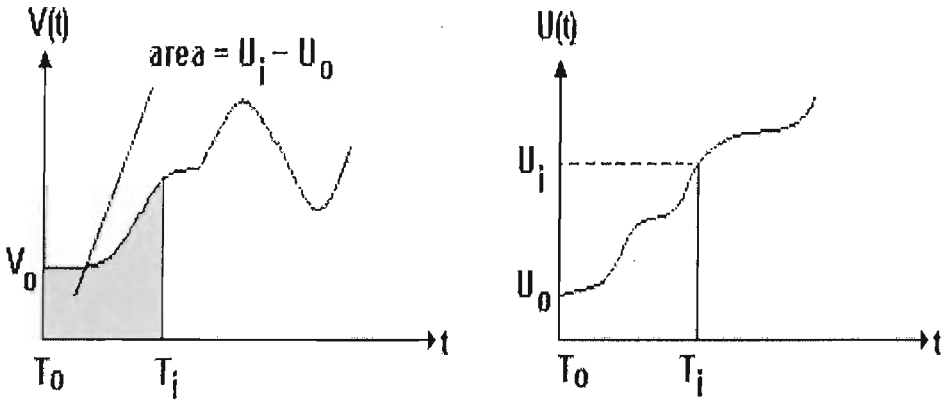

Figure G.2: Relationship between velocity and displacement.

G.2 Integration scheme

In practice, the acceleration functions obtained in a vibration analysis is discrete in nature because of accelerometers sample the measurements at some specified rate of sampling frequency. Thus, there is always missing values in between two consecutive samples. The acceleration values obtained will be a set of points resembling as a continuous function as shown in Fig. G.2. Thus, some assumptions must be made to about the missing values between tow consecutive samples. There are several integration methods with different assumptions are available, which will be described in this section.

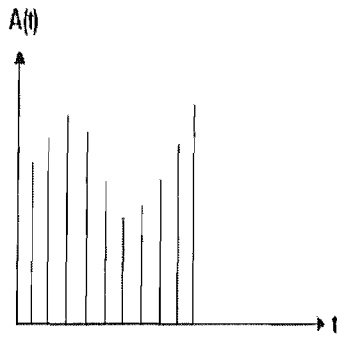

Figure G.3: Discrete acceleration function.

G.2.1 Zero-order hold

The simplest assumption that can be made is to assume that the signal retains the level dictated by the previous sample. Other terms for this procedure include the Staircase and the Boxcar method.

Applying the zero-order hold for the integration of an acceleration function will yield,

$$v_i = v_{i-1} + a_{i-1}T. \tag{G.5}$$

Similarly, displacements are obtained by,

$$d_i = (v_i - a_{i-1}T)T + d_{i-1} \tag{G.6}$$

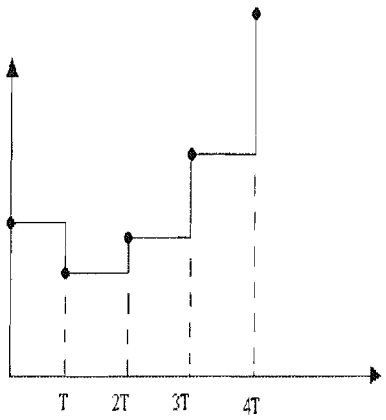

Figure G.4: Zero-order hold.

G.2.2 Midpoint rule

This method is very similar to the zero-order hold, except that it assumes the average value between the points as the horizontal interpolation. The main difference between the two methods is midpoint's dependency on the later known value, which will be common in most other interpolations mode. The same set of points, using the midpoint rule, is shown in Fig. G.2.2.

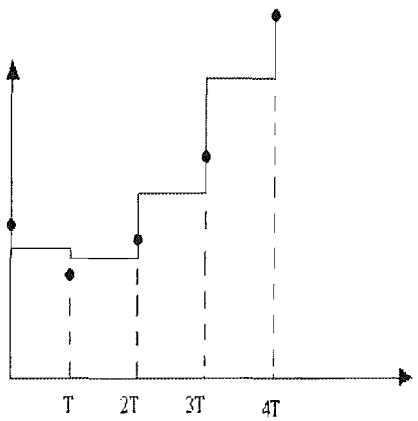

Figure G.5: Midpoint rule.

This method yields velocity and displacements as,

$$v_i = v_{i-1} + \frac{(a_i + a_{i-1})T}{2} \tag{G.7}$$

$$d_i = d_{i-1} + v_{i-1}T + \frac{(a_i + a_{i-1}T^2}{4} \tag{G.8}$$

G.3 Central difference method

This method is based on the finite difference approximation of the time derivative of displacement. Instead of beginning with the acceleration function, we begin with the displacement and derive accelerations. Graphically, this method is shown in Fig. G.3.

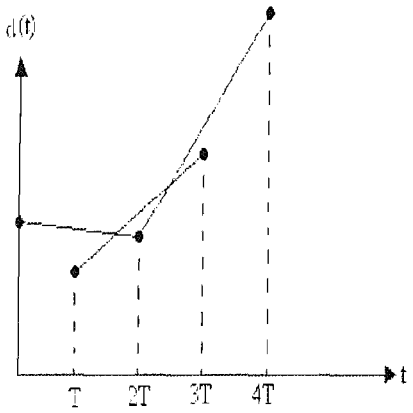

Figure G.6: Central difference method.

Applying this procedure yields velocity function and acceleration function as follow,

$$v_i = \frac{d_{i+1} - d_{i-1}}{2T}, \tag{G.9}$$

$$a_i = \frac{d_{i+1} - 2d_i + d_{i-1}}{T^2}. \tag{G.10}$$

This procedure is suitable for obtaining accelerations for the given displacement values. Eqn. G.10 can be solved for displacements in terms of accelerations by using a time shift.

$$d_i = a_{i-1}T^2 + 2d_{i-1} - d_{i-2} \tag{G.11}$$

The advantage of this method is that it bypasses velocity, but requires some additional assumptions at the beginning of the iteration. Here, the iteration can only begin at the third displacement value. Hence, this requires knowing the displacements at the first and second time positions. If the structure is at rest when the iteration

begins; then, assuming a zero value may not affect results significantly. Neverthless, it is up to the analyst to decide the precision of calculations.